

PHOTOACTIVE CONJUGATED POLYELECTROLYTES AND CONJUGATED
POLYELECTROLYTE DENDRIMERS

By

SEOUNG HO LEE

A DISSERTATION PRESENTED TO THE GRADUATE SCHOOL
OF THE UNIVERSITY OF FLORIDA IN PARTIAL FULFILLMENT
OF THE REQUIREMENTS FOR THE DEGREE OF
DOCTOR OF PHILOSOPHY

UNIVERSITY OF FLORIDA

2010

© 2010 Seoung Ho Lee

To my family

ACKNOWLEDGMENTS

Foremost, I would like to express my deep and sincere gratitude to my advisor Professor Kirk S. Schanze. My Ph.D. study and research could not have been finished without him who not only served as my supervisor but also encouraged and challenged me throughout my academic program. His guidance helped me in all the time of research and writing of this thesis. I could not have imagined having a better advisor and mentor for my Ph.D. study.

Besides my advisor, I would like to thank the rest of my thesis committee: Professors Lisa McElwee-White, Daniel R. Talham, Eric Enholm, and Elliot Douglas, for their encouragement, insightful comments, and hard questions. I warmly thank Professors John R. Reynolds and Valeria D. Kleiman for their valuable advice and friendly help, especially for kindness in writing a letter of recommendation. Their extensive discussions around my work and interesting explorations in operations have been very helpful for this study.

My former and current colleagues supported me in my research work. I want to thank them for all their help, support, interest, and valuable hints. Especially I am very much obliged to Dr. Key-Young Kim, Dr. Xiaoyong Zhao, Dr. John Peak, Dr. Yan Liu, Dr. Yongjun Li, and Dr. Jerret Vella. I also want to thank Dr. Hui Jiang and Dr. Eunkyung Ji for all discussions about the life as well as projects. I wish to thank Dr. Zhen Fang and Dr. Fude Feng for their guidance and extensive discussions in my researches. Julia Keller and Abigail Shelton were of great helps in difficult times. They looked closely at the thesis for English style and grammar, correcting both and offering suggestions for improvement. I warmly thank Dr. Anand Parthasarathy, Dr. Chen Liao, Emine Demir, Zhuo Chen, Aaron Eshbaugh, Dongping Xie, Randi Price, Amanda

Sylvester, Danlu Wu, and Cheer Yang for their valuable advice and friendship. During my researches I have collaborated with Sevnur Kömürlü in Dr. Kleiman group. I would like to show my gratitude to her for sharing her knowledge in photochemistry.

This thesis would not have been possible without the love and support of my family. I owe my deepest gratitude to my parent. They always encourage and understand me to continue my education abroad.

Finally, as always, my biggest thanks are due to my wife Sangmi without whose love and understanding my works could never have been completed. Additionally, I would like to share this pleasure with my son, Junseo.

TABLE OF CONTENTS

	<u>page</u>
ACKNOWLEDGMENTS.....	4
LIST OF TABLES.....	10
LIST OF FIGURES.....	11
ABSTRACT	17
 CHAPTER	
1 INTRODUCTION	21
Conjugated Polyelectrolytes	21
Synthetic Methodology	23
Functional Group Effects on Aggregation.....	25
Linear functional group effects	26
Branched functional group effects.....	27
Amplified Quenching of Conjugated Polyelectrolytes	30
Stern-Volmer fluorescence quenching	30
Molecular wire effect	31
Applications of Conjugated Polyelectrolytes to Sensors.....	33
Conjugated Polyelectrolyte Dendrimers.....	37
Dendrimers.....	37
Architecture of Conjugated Dendrimers	38
Synthetic Approaches	40
Divergent approach.....	41
Convergent approach	42
Water-Soluble Dendrimers	43
Water-Soluble Conjugated Dendrimers.....	45
Scope of the Present Study	46
 2 WATER-SOLUBLE CONJUGATED POLYELECTROLYTES WITH BRANCHED POLYIONIC SIDE CHAINS: SYNTHESIS, CHARACTERIZATION, AND OPTICAL PROPERTIES	 50
Results and Discussion.....	52
Synthesis and Characterization.....	52
Precursor polymers.....	54
Hydrolysis of precursor polymers.....	56
¹ H NMR spectroscopy.....	56
Optical Properties.....	58
pH-Dependent Aggregation.....	65
Fluorescence Lifetime Spectroscopy.....	69
Summary and Conclusions	73

Experimental.....	75
Materials.....	75
Instrumentation and Methods.....	75
Synthetic Procedures.....	76
3 HIGHLY EFFICIENT MERCURY (II) ION SENSOR BASED ON CONJUGATED POLYELECTROLYTE-RHODAMINE COMBINATION SYSTEM	84
Results and Discussion.....	85
Synthesis.....	85
Optical Properties.....	86
Application to Hg ²⁺ ion Sensor	87
Selectivity.....	87
Sensitivity.....	89
Sensing Mechanism	90
Comparison of Sensitivity between S-Rho/PPE System and S-Rho	92
Summary and Conclusions	93
Experimental.....	93
Materials.....	93
Instrumentation and Methods	94
Synthetic Procedures	94
4 PHOTOPHYSICAL PROPERTIES OF PYA4 AGGREGATE AND ITS APPLICATION TO PYROPHOSPHATE SENSOR BASED ON TURN-ON SYSTEM.....	96
Results and Discussion.....	99
Synthesis.....	99
Characterization of PyA4.....	100
Quenching with Metal Ions	104
Application to Pyrophosphate (PPi) Sensing	109
Selective and sensitive detection of PPi	109
Real-time ALP assay	112
Plausible mechanism	113
Summary and Conclusions	114
Experimental.....	114
Materials.....	114
Instrumentation and Methods	115
Synthetic Procedure	115
5 PHOTOPHYSICS AND ENERGY TRANSPORT IN CONJUGATED POLYELECTROLYTE DENDRIMERS	118
Results.....	120
Synthesis and Characterization.....	120
Synthesis of precursors	120
Hydrolysis of precursor	122

Geometric structure of CPE-Ds.....	123
Geometric Properties: CPE-Ds' Size.....	124
Dynamic light scattering (DLS).....	124
Atomic force microscopy (AFM).....	126
Optical Properties.....	127
UV-Vis & fluorescence spectroscopy.....	127
Fluorescence quantum yield.....	132
Fluorescence lifetime studies.....	134
Fluorescence excitation spectroscopy.....	136
Concentration dependent fluorescence studies.....	136
Fluorescence Quenching of CPE-Ds by DOC, DODC, and DOTC.....	137
Summary and Conclusions.....	140
Experimental.....	141
Materials.....	141
Instrumentation and Methods.....	142
Synthetic Procedures.....	142
6 DESIGN, SYNTHESIS, AND PHOTOPHYSICAL STUDIES OF THIENYL GROUP EXTENDED CONJUGATED POLYELECTROLYTE DENDRIMERS	149
Results and Discussion.....	152
Synthesis and Characterization.....	152
Optical Properties.....	155
UV-Vis absorption spectroscopy.....	155
Fluorescence spectroscopy.....	157
Fluorescence quantum yield.....	158
Fluorescence lifetimes.....	158
Chromophore/Dendrimer Aggregation.....	163
Concentration dependent fluorescence.....	163
Fluorescence excitation spectroscopy.....	163
Dynamic light scattering (DLS).....	164
Fluorescence Quenching of Th-G-n with MV ²⁺	165
FRET from Th-G-3 to Cyanine Dyes.....	167
Summary and Conclusions.....	170
Experimental.....	170
Materials.....	170
Instrumentation and Methods.....	171
Synthetic Procedures.....	172
7 CONCLUSIONS	179
Branched Polyionic Effect on Aggregation.....	179
Mercury (II) ion and Pyrophosphate ion Sensors.....	180
Conjugated Polyelectrolyte Dendrimers.....	181

APPENDIX

A	CONJUGATED POLYELECTROLYTES WITH BRANCHED POLYCATIONIC SIDE CHAINS.....	182
B	NMR SPECTRA.....	183
	LIST OF REFERENCES	188
	BIOGRAPHICAL SKETCH.....	195

LIST OF TABLES

<u>Table</u>	<u>page</u>
2-1 Structures of conjugated polyelectrolytes with branched polyionic side chains and GPC analyses for their precursor polymers.	53
2-2 UV-Vis absorption and photoluminescent properties of CPEs containing branched carboxylate or ammonium side chains.....	58
2-3 Fluorescence lifetimes (τ_i , ns) and relative amplitudes (RA, %) for PPE-Ar-^bCO₂⁻ in MeOH, basic (pH = 9.0), and acidic (pH = 4.5) conditions ^a	70
4-1 K_{sv} ^a and $[Q]_{90}$ ^b for Cu ²⁺ ion quenching of PyA4 in H ₂ O and MeOH.....	107
5-1 UV-Vis absorption and photoluminescent properties of CPE-Ds (CH ₃ OH and H ₂ O) and their precursors (THF)	127
5-2 Fluorescence lifetimes (τ_i , ns) ^a and relative amplitudes (RA, %) for CPE-Ds (CH ₃ OH and H ₂ O) and their precursors (THF).	134
5-3 K_{sv} ^a and $[Q]_{90}$ ^b of CPE-Ds with cyanine dyes in H ₂ O.	138
6-1 UV-Vis absorption and photoluminescent properties of Th-G-n (CH ₃ OH and H ₂ O(pH 8.0)) and their precursors (THF)	157
6-2 Fluorescence lifetimes (τ_i , ns) and relative amplitudes (RA, %) for Th-PG-n and Th-G-n in THF, CH ₃ OH, and H ₂ O (pH = 8.0) solutions. ^a	159
6-3 K_{sv} ^a of Th-G-n with methyl viologen (MV ²⁺) in CH ₃ OH and H ₂ O.....	165
6-4 K_{sv} ^a of CPE-Ds with cyanine dyes in H ₂ O.....	169
A-1 Fluorescence lifetimes (τ_i , ns) and relative amplitudes (RA, %) for PPE-Ar-^bNH₃⁺ in MeOH, basic (pH = 9.5), and acidic (pH = 4.5) conditions ^a	182

LIST OF FIGURES

<u>Figure</u>	<u>page</u>
1-1 Example of conjugated polyelectrolytes with various ionic side chains.	21
1-2 Structure of water-soluble conducting polymer (PT 1 and PT 2).	22
1-3 Various aromatic units.	22
1-4 Example of two different methods for the synthesis of CPEs (a) direct polymerization of monomers with ionic functional groups; (b) precursor route using monomers of organic functional groups.	23
1-5 Various functional groups.	25
1-6 Absorption and fluorescence spectra of PPE-SO₃⁻	26
1-7 Structures of P1 , P2 and P3	28
1-8 UV-Vis absorption (left) and fluorescence spectra (right) of P1-P3	29
1-9 Schematic illustration of quenching effect in conjugated polymers with receptor and their fragment via energy migration to a receptor site occupied by PQ²⁺	32
1-10 Quenching mechanism of “Molecular wire” effect in conjugated polymers with receptors.	33
1-11 Structure of cationic conjugated polyelectrolyte.	34
1-12 Schematic representation for the use of a cationic water-soluble CP with a specific PNA-C* optical reporter probe to detect a complementary ssDNA sequence.	35
1-13 (a) Structure of PPE , (b) fluorescence intensity changes; A: PPE -papain, B: all 10 metals added to PPE -papain complex, C: Same without Hg²⁺ ion, and (c) qualitative interpretation of the Hg²⁺ ion-induced agglutination.	36
1-14 Structure of D-22 (3 rd generation).	38
1-15 Space-filling models of phenylacetylene tridendrons D-4 , D-10 , D-22 , D-46 , and D-94	39
1-16 Synthetic diagram of divergent approach.	41
1-17 Synthetic diagram of convergent approach.	42

1-18	Schematic representation showing the structural similarity between the traditional Hartley micelle model and a dendrimer.....	44
1-19	(a) Representative structure of conjugated polyelectrolyte dendrimer (CPE-D). (b) CPE-Ds paired with guest molecules.	45
2-1	Synthesis of 8	52
2-2	Structure of <i>bis</i> -ethynylene substituted Ph, BTd, and TBT; synthesis of monomers (1 and 2).	54
2-3	Polymerization through precursor route.....	55
2-4	¹ H NMR spectra of (a) monomer 1 , (b) PPE-Ph-^bCO₂^tBu , and (c) PPE-Ph-^bCO₂⁻	57
2-5	(a) Relative absorption and (b) fluorescence emission spectra of PPE-Ph-^bCO₂⁻ , PPE-BTD-^bCO₂⁻ , and PPE-TBT-^bCO₂⁻	58
2-6	(a) Visual and (b) Fluorescence colors of A: PPE-Ph-^bCO₂⁻ , B: PPE-BTD-^bCO₂⁻ , and C: PPE-TBT-^bCO₂⁻	59
2-7	Excitation spectra of (a) PPE-Ph-^bCO₂⁻ at 430 and 500 nm; (b) PPE-BTD-^bCO₂⁻ at 550 and 700 nm; (c) PPE-TBT-^bCO₂⁻ at 650 and 800 nm.	59
2-8	(a) Relative absorption and (b) fluorescence emission spectra of PPE-Ph-^bNH₃⁺ and PPE-BTD-^bNH₃⁺ in MeOH, MeOH/H ₂ O (1/1, v/v), and H ₂ O.....	61
2-9	Fluorescence emission spectra of precursors of branched anionic CPEs in THF; [PPE-Ar-^bCO₂⁻] = 5 μM; Ar = Ph, BTd, and TBT.	65
2-10	Absorption and fluorescence emission spectra of (a, b) PPE-Ph-^bCO₂⁻ and (c, d) PPE-Ph-^bNH₃⁺ as pH changes in aqueous solution.	66
2-11	Absorption and fluorescence emission spectra of (a, b) PPE-BTD-^bCO₂⁻ and (c, d) PPE-BTD-^bNH₃⁺ as pH changes in aqueous solution.....	67
2-12	(a) Absorption and (b) fluorescence emission spectra of PPE-TBT-^bCO₂⁻ as pH changes in aqueous solution.....	68
3-1	Structure of PPE-^bCO₂⁻ , S-Rho 1 , and S-Rho 2	85
3-3	(a) Fluorescence spectra of PPE-^bCO₂⁻ (0.1 μM), PPE-^bCO₂⁻ (0.1 μM)/ S-Rho 1 (1 μM), and S-Rho 1 (1 μM); (b) fluorescence intensity changes of PPE-^bCO₂⁻ (0.1 μM)/ S-Rho 1 (1 μM) upon the addition of various amounts of Hg ²⁺	87
3-4	Fluorescence changes of S-Rho 1/PPE-^bCO₂⁻ system in H ₂ O/DMSO (99/1, v/v) upon the addition of various metal ions.	88

3-5	Stern-Volmer plots of S-Rho 1/PPE-^bCO₂⁻ (●) and S-Rho 2/PPE-^bCO₂⁻ (▲) (PPE: 0.1 μM and Rhodamine derivatives 1 μM) titrated with Hg ²⁺ ion.	89
3-6	Fluorescence changes of S-Rho 2/PPE-^bCO₂⁻ system upon the addition of various metal ions.....	90
3-7	Plausible sensing mechanism.	90
3-8	Fluorescence of FRET donor (PPE-^bCO₂⁻) and absorption of FRET acceptors (S-Rho 1-Hg²⁺ complex and S-Rho 2-Hg²⁺ complex).	91
3-9	Fluorescence intensity changes of S-Rho 1 upon the addition of various amounts of Hg ²⁺ ion.....	92
3-10	Titration profile ΔI as a function of [Hg ²⁺].	92
4-1	Structure of PyA4	98
4-2	Synthesis of PyA4	99
4-3	UV/Vis (left) and fluorescence emission (right) spectra of PyA4 in various solutions.	101
4-4	Fluorescence excitation and emission spectra of PyA4 (5 μM) in 20 mM HEPES buffer at pH 7.5.....	102
4-5	Fluorescence emission spectra of PyA4 in 20 mM HEPES buffer at pH 7.5....	102
4-6	¹ H NMR spectra of PyA4 in (a) D ₂ O/CD ₃ OD (3/1, v/v) and (b) DMSO- <i>d</i> ₆ ; * denotes solvent peak.....	103
4-7	(a) Fluorescence emission spectra of PyA4 solutions with increasing concentration (1-10 μM) in 20 mM HEPES buffer solutions at pH 7.5; (b) ratio of excimer to monomer with increasing concentration (1-100 μM).	104
4-8	(a) Fluorescence emission changes of PyA4 (5 μM) upon the addition of various metal ions (30 μM); (b) Titration of PyA4 (5 μM) with Cu ²⁺ ions (0-20 μM); Inset: ratio of excimer to monomer.	105
4-9	Stern-Volmer plots of PyA4 (5 μM) titrated with Cu ²⁺ ions in 20 mM HEPES buffer at pH 7.5; Excitation at 456 nm, fluorescence intensity was monitored at 497 and 640 nm.....	105
4-10	Stern-Volmer plots of PyA4 (1, 5, and 10 μM) titrated with Cu ²⁺ ions in MeOH and pure H ₂ O.....	106
4-11	Titration of (a) PyA4 (5 μM) and (b) PyE4 (5 μM) with Cu ²⁺ ions in MeOH.	108

4-12	Fluorescence emission changes of PyA4 (5 μM) - Cu^{2+} (20 μM) at 640 nm upon the addition of anions (50 μM).	109
4-13	(a) Titration of PyA4 (5 μM)- Cu^{2+} (20 μM) with PPI (1-30 μM) in 20 mM HEPES buffer at pH 7.5; (b) Titration profile with I/I_0 ratio represented by the intensity at 640 nm.	110
4-14	(a) Titration of PyA4 (5 μM)- Cu^{2+} (30 μM) with PPI (10-100 μM) in 100 mM HEPES buffer at pH 7.5.....	111
4-15	Fluorescence intensity changes of (a) PyA4 (b) PyA4 - Cu^{2+} complex, and (c) PyA4 - Cu^{2+} with PPI in 20 mM HEPES buffer at pH 7.5.....	111
4-16	Real-time ALP assay using PyA4 (5 μM)- Cu^{2+} (20 μM) and PPI (30 μM) in 20 mM HEPES buffer at pH 7.5, 37.0 $^{\circ}\text{C}$	113
4-17	Plausible mechanism of sensing process.....	113
5-1	Structure of CPE-Ds (G-1 , G-2 and G-3).....	119
5-2	Synthesis of 5 , 7 , and 8	120
5-3	Synthesis of PG-1 , PG-2 , and PG-3	121
5-4	Hydrolysis of branched side chains.	122
5-5	Space-filling model of G-1 , G-2 , and G-3 generated by using MM2 molecular mechanics in Chem 3D Pro (version 10.0).	123
5-6	GPC data of precursor of CPE-Ds (PG-1 , PG-2 , and PG-3); polystyrene standards in THF.	124
5-7	Hydrodynamic radii obtained from dynamic light scattering (DLS) for G-1 (black), G-2 (red), and G-3 (blue) in H_2O	125
5-8	AFM images of (a) G-1 , (b) G-2 , and (c) G-3	126
5-9	UV-Vis absorption and fluorescence spectra of CPE-Ds (G-1 , G-2 , and G-3) and their precursors (PG-1 , PG-2 , and PG-3) in CH_3OH , H_2O , and THF, respectively.....	129
5-10	UV-Vis absorption spectra of G-1 in CH_3OH and H_2O	130
5-11	UV-Vis absorption and fluorescence spectra of CPE-Ds (G-1 , G-2 , and G-3) and their precursors (PG-1 , PG-2 , and PG-3).	131
5-12	Fluorescence quantum yields changes of G-1 , G-2 , and G-3 at the pH 3-9....	133

5-13	Fluorescence excitation spectra of (a) G-1 at 380, 400, and 450 nm, (b) G-2 at 400, 450, and 500 nm, and (c) G-3 at 450, 500, and 550 nm in H ₂ O.	136
5-14	Fluorescence emission spectra of (a) G-1 , (b) G-2 , and (c) G-3 with increasing concentration in H ₂ O.	136
5-15	Structure of cyanine dyes (DOC, DODC, and DOTC).	137
5-16	Fluorescence emission spectra of (a) cyanine dyes only (DOC, DODC, and DOTC: 1.0 μ M) and G-3 titrated with (b) DOC, (c) DODC, and (d) DOTC in H ₂ O, pH 8.0.	139
5-17	Stern-Volmer plots of G-3 ; fluorescence quenched by cyanine dyes in H ₂ O. ...	140
6-1	Structure of CPE-Ds (Th-G-1 , Th-G-2 , and Th-G-3).	151
6-2	Synthesis of (a) focal points and (b) a core unit.....	152
6-3	Synthesis of precursors of CPE-Ds ((a) Th-PG-1 , (b) Th-PG-2 , and (c) Th-PG-3).....	153
6-4	Hydrolysis of branched side chains.	154
6-5	UV-Vis absorption and Fluorescence spectra of CPE-Ds (Th-G-1 , Th-G-2 , and Th-G-3) and their precursors (Th-PG-1 , Th-PG-2 , and Th-PG-3).	156
6-6	Fractional amplitude changes of fluorescence lifetimes of Th-G-1 in (a) CH ₃ OH and (d) H ₂ O, Th-G-2 in (b) CH ₃ OH and (e) H ₂ O, and Th-G-3 in (c) CH ₃ OH and (f) H ₂ O.....	161
6-7	Fluorescence emission spectra of (a) Th-G-1 , (b) Th-G-2 , and (c) Th-G-3 with increasing concentration in H ₂ O.....	163
6-8	Fluorescence excitation spectra of (a) Th-G-1 at 400 and 500 nm, (b) Th-G-2 at 400 and 500 nm, and (c) Th-G-3 at 450 and 500 nm in H ₂ O.....	163
6-9	Hydrodynamic radii obtained from dynamic light scattering (DLS) for (a) Th-G-1 , (b) Th-G-2 , and (c) Th-G-3 in H ₂ O.....	164
6-10	Stern-Volmer plots of Th-G-n (a) CH ₃ OH and (b) H ₂ O; fluorescence was quenched by methyl viologen (MV ²⁺).....	165
6-11	Structure of cyanine dyes (DOC, DODC, and DOTC).	167
6-12	Fluorescence of FRET donor (Th-G-3) and absorption of FRET acceptors (cyanine dyes).	167

6-13	Fluorescence emission spectra of (a) cyanine dyes only (DOC, DODC, and DOTC) and Th-G-3 titrated with (b) DOC, (c) DODC, and (d) DOTC in H ₂ O pH 8; [Th-G-3] = 1.0 μM; [dye quencher] = 0 ~ 0.3 μM.....	168
6-14	Stern-Volmer plots of Th-G-3 in H ₂ O; fluorescence quenched by cyanine dyes: DOC,DODC, and DOTC.	169
A-1	(a) Visual and (b) Fluorescence colors of A: PPE-Ph-^bNH₃⁺ and B: PPE-BTD-^bNH₃⁺ ; [PPE-Ar-^bNH₃⁺] = 30 μM in H ₂ O.	182
B-1	¹ H NMR (300 MHz, CDCl ₃) spectrum of S-Rho 1 (chapter 3).	183
B-2	¹ H NMR (300 MHz, CDCl ₃) spectrum of S-Rho 2 (chapter 3).	183
B-3	¹ H NMR (300 MHz, CDCl ₃) spectrum of PyE4 (chapter 4).	184
B-4	¹ H NMR (300 MHz, D ₂ O/CD ₃ OD (3/1, v/v)) spectrum of PyA4 (chapter 4).	184
B-5	¹ H NMR (300 MHz, CDCl ₃) spectrum of PG-1 (chapter 5).....	185
B-6	¹ H NMR (300 MHz, CDCl ₃) spectrum of PG-2 (chapter 5).....	185
B-7	¹ H NMR (300 MHz, CDCl ₃) spectrum of PG-3 (chapter 5).....	186
B-8	¹ H NMR (300 MHz, CDCl ₃) spectrum of Th-PG-1 (chapter 6).	186
B-9	¹ H NMR (300 MHz, CDCl ₃) spectrum of Th-PG-2 (chapter 6).	187
B-10	¹ H NMR (300 MHz, CDCl ₃) spectrum of Th-PG-3 (chapter 6).	187

Abstract of Dissertation Presented to the Graduate School
of the University of Florida in Partial Fulfillment of the
Requirements for the Degree of Doctor of Philosophy

PHOTOACTIVE CONJUGATED POLYELECTROLYTES AND CONJUGATED
POLYELECTROLYTE DENDRIMERS

By

Seoung Ho Lee

December 2010

Chair: Kirk S. Schanze
Major: Chemistry

In this dissertation, we primarily focus on the fundamental investigation of the photophysical properties of conjugated polyelectrolytes (CPEs) and conjugated polyelectrolyte dendrimers (CPE-Ds). Also, applications to the selective and sensitive pyrophosphate ions and mercury (II) ion sensors are explored.

First, for CPEs, various aromatic moieties including phenyl (Ph), 2,1,3-benzothiadiazole (BTD), and 4,7-bis(2'-thienyl)-2,1,3-benzothiadiazole (TBT) units have been incorporated into the polymer backbones. The photophysical properties of CPEs with branched polyionic side chains were investigated in CH₃OH and H₂O solutions by UV-Vis absorption, steady-state fluorescence, and lifetime spectroscopy. The different arylene units in the backbone led to variation of the HOMO-LUMO energy, resulting in distinctive absorption and fluorescence spectra. Branched polyionic side chains in the conjugated polyelectrolyte give rise to less aggregation even in aqueous solution, leading to higher quantum yields compared to the similar CPEs with linear side chains.

Second, we also used the CPE with branched polyionic side chains as a mercury (II) ion sensor. Conjugated polyelectrolyte (CPE)/Rhodamine derivative combination system was designed as a Hg²⁺ ion sensor with high selectivity and sensitivity. CPE

exhibited highly efficient quenching effect by the Hg^{2+} ion complexed rhodamine derivative via energy and/or charge transfer. The combination system displayed improved sensory response for the Hg^{2+} ion complex compared to a unitary CPE or rhodamine-based sensor.

Third, a fluorescence chemosensor bearing four sodium carboxylates linked to tetra-phenylacetylene substituted pyrene, **PyA4**, has been designed and developed. **PyA4** displays self-assembly behavior with strong intermolecular excimer emission in aqueous buffer solution. Fluorescence changes upon the addition of various metal ions show that **PyA4** has high selectivity for the Cu^{2+} ion over other metal ions tested via fluorescence suppression, i.e. 98.5% fluorescence quenching. We found that more excimer quenching in aqueous solution may be caused by energy migration through the aggregates of **PyA4** if the delocalized excited state of the pyrene stack is mobile as in the case of conjugated polymer. That is, the molecular aggregation controls exciton transport and amplified quenching phenomena. This system, the Cu^{2+} ion complexed to the **PyA4**, acts as a highly selective and sensitive fluorescent sensor for pyrophosphate, showing fluorescence enhancement which leads to 98% fluorescence recovery. For the bioanalytical applications, the activity of alkaline phosphatase (ALP) was successfully monitored by real-time turn-off assay.

Fourth, we have prepared three generation of CPE-Ds (**G-1**, **G-2**, and **G-3**). The phenylacetylene units are connected at the *meta*-position, and their interior hydrophobic focal point is surrounded by the geometrically increased hydrophilic carboxylate end-groups as the generation increases. GPC analysis of the ester precursors, **PG-1**, **PG-2**, and **PG-3**, clearly demonstrates the monodisperse nature of these macromolecular

structures; the three-dimensional structures of CPE-Ds show more spherical shape as the generation increases (**G1** → **G2** → **G3**). Also, AFM images and DLS data suggests that **G-2** and **G-3** in H₂O show intra-dendrimer interactions rather than *inter-dendrimer* aggregation. The photophysical properties of CPE-Ds revealed that *intra-dendrimer* interaction becomes stronger in aqueous solution with increasing generation, showing a red-shift in fluorescence spectra. The pH dependent quantum yields provide information for the state of aggregate of CPE-Ds, in which *inter-dendrimer* aggregate states of **G-1** exist while **G-2** and **G-3** shows *intra-dendrimer* aggregation at very low pH (pH = 3). More detail geometric structure of CPE-Ds is investigated by fluorescence lifetime measurement. Fluorescence quenching of **G-3** is observed in the presence of cyanine dyes (DOC, DODC, and DOTC). The quenching is independent on the chain length of cyanine dyes. Also, it is attributed to degree of energy transfer, showing different fluorescence enhancement of cyanine dyes.

Finally, conjugated polyelectrolyte dendrimers (**Th-G-1**, **Th-G-2**, and **Th-G-3**) containing thienyl (Th) groups in the conjugated backbone have been newly designed and synthesized. The modified convergent approach was used on the dendrimer synthesis. The thienyl π -extended conjugated backbone allowed a low energy UV-Vis absorption and fluorescence emission. As the generation increases (**Th-G-1** → **Th-G-2** → **Th-G-3**), intra-dendrimer aggregation is more pronounced, resulting in more red-shifted fluorescence spectra in aqueous solution. Structural peculiarity of the thienyl group induced the lack of inter-dendrimer aggregation in aqueous solution. Dynamic light scattering (DLS) and fluorescence excitation results revealed that even the first generation (**Th-G-1**) not allows *inter-dendrimer* aggregation. The fluorescence

quenching efficiency of Th-G-n for methyl viologene (MV^{2+}) was more significant with increasing generation (**Th-G-1** < **Th-G-2** < **Th-G-3**) in H_2O , and very efficient quenching was observed in **Th-G-3**. In addition, quenching was more significant in H_2O than CH_3OH . Effective fluorescence enhancement of cyanine was observed by the energy transfer effect from **Th-G-3**.

CHAPTER 1 INTRODUCTION

Conjugated Polyelectrolytes

Conjugated polyelectrolytes (CPEs) are water-soluble conjugated polymers (CPs) having ionic functional groups such as sulfonate (SO_3^-), carboxylate (CO_2^-), phosphate (PO_3^{2-}), and alkyl ammonium (NR_3^+). Such ionic functional groups make the CPs soluble in aqueous solution or other polar solvents.¹⁻² Some examples of CPEs are shown in Figure 1-1. These CPEs are of great interest because they provide a number of features including not only high conductivity, charge transport, and π -electron polarization seen in organic conjugated polymers, but also environment-friendly processing, applications to biological system, and amphiphilic properties.^{1,3-7}

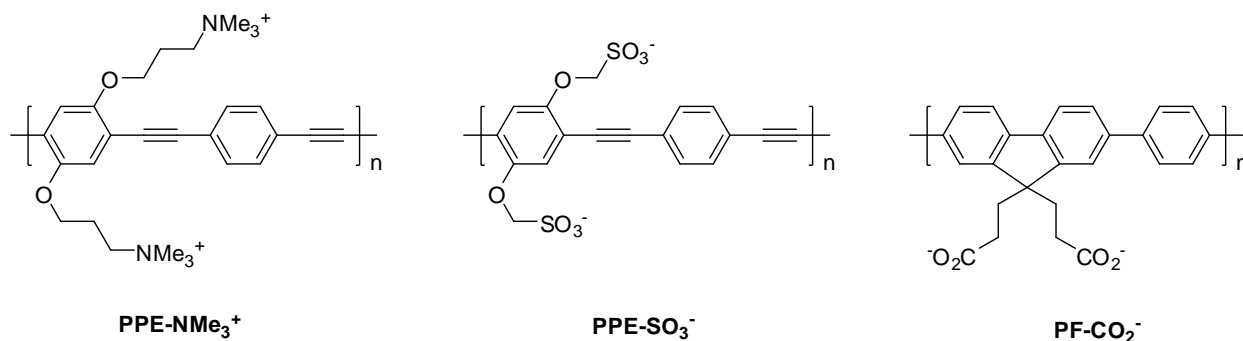


Figure 1-1. Example of conjugated polyelectrolytes with various ionic side chains.

Due to such unique properties of CPEs, the researches on conjugated polyelectrolytes have attracted considerable attention, and much effort has been devoted to the development of versatile CPEs. Since Wudl and Heeger et al. reported the results of a pioneering study in 1987, in which water-soluble conducting polymers of 3-(2-sulfonatoethyl)-substituted (**PT 1**) and 3-(4-sulfonatobutyl)-substituted (**PT 2**) polythiophene were prepared by electropolymerization (Figure 1-2),⁸ presently, extensive researches have been performed by many scientists over the world to

develop highly efficient optoelectronic applications using CPEs. In addition, because their photophysical properties can be easily modified by external stimulus, it is considered and developed to be used as sensory materials to detect chemicals (chemosensors) or bioactive species (biosensors) in aqueous media.⁹

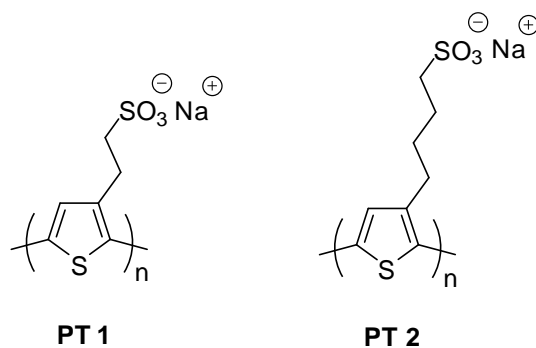


Figure 1-2. Structure of water-soluble conducting polymer (**PT 1** and **PT 2**).

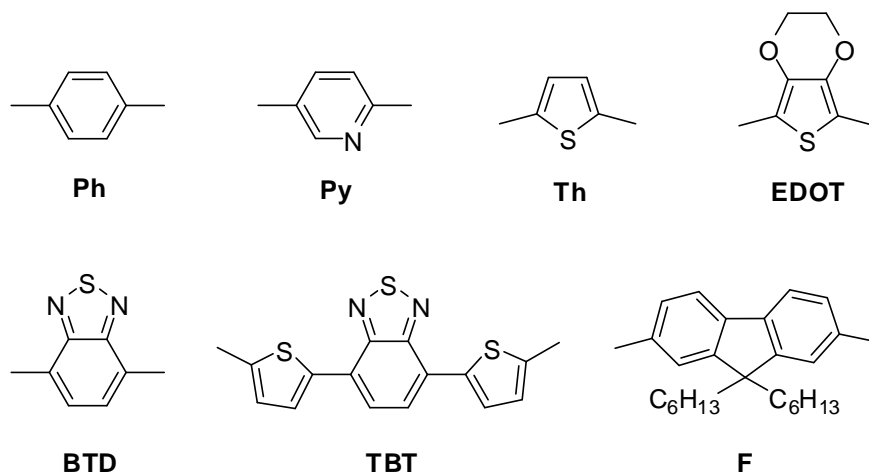


Figure 1-3. Various aromatic units.

Systematic modification of both CPEs' backbone and functional groups is required for the effective and advanced applications. As a component of CPEs' backbone, variable aromatic units such as phenyl (Ph), pyrrole (Py), thiophene (Th), 3,4-ethylenedioxythiophene (EDOT), 2,1,3-benzothiadiazole (BTB), fluorene (F), and their combinations are incorporated into polymer backbones.¹⁰⁻¹¹ Various aromatic units are presented in Figure 1-3. Also, several cationic and anionic or bulky ionic side chains are

available for efficient doping in the film or as a receptor for chemical or biomolecules as well as overcoming the solubility problems.¹⁰

Synthetic Methodology

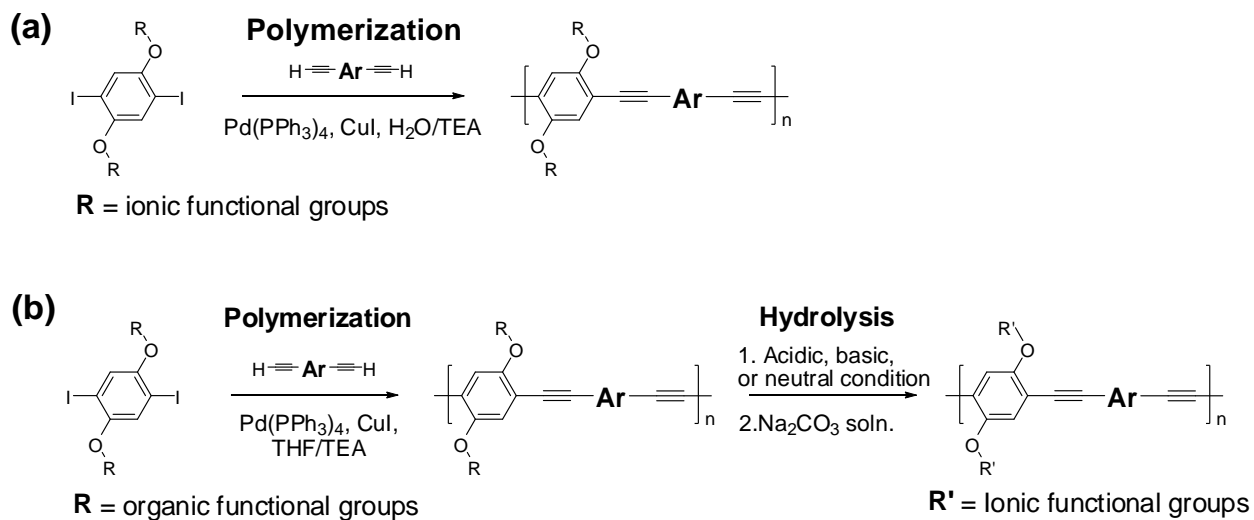


Figure 1-4. Example of two different methods for the synthesis of CPEs (a) direct polymerization of monomers with ionic functional groups; (b) precursor route using monomers of organic functional groups.

There are mainly two pathways to synthesize water-soluble conjugated polyelectrolytes: one is direct polymerization of conjugated monomer having ionic side chains in aqueous solution or polar solvents (Figure 1-4a); the other is through precursor route in organic solvents (Figure 1-4-b). The former way is simple and fast, but it is limited to estimate polymer size. In addition, electrostatic repulsions between ionic side chains prevent effective polymerization of monomers in aqueous solution or polar solvents. On the other hand, the latter way is relatively protracted because it requires more synthetic steps. Nevertheless, precursor route is frequently used in CPEs synthesis because of its easiness to understand conjugated polymers' characteristics. Indeed, gel permeation chromatography (GPC) measurement of the precursors of CPEs provides useful information such as the number of monomer units and polydispersity

(PDI) of the conjugated polymer. Furthermore, their NMR spectra and UV-Vis & fluorescence spectral data afford comparable information for CPEs after the precursor is converted to water-soluble one.

There are many methodologies for the extension of conjugated backbone in CPs. Among them, transition-metal-catalyzed cross-coupling reactions can easily be considered and widely used nowadays. Stille,¹² Heck,¹³ Suzuki,¹⁴ and Sonogashira¹⁵ coupling reactions are typical examples. Also, plenty of newly developed coupling reactions were explored during the last decades: most of these reactions are used without amine or become simplified. It is very interesting that all coupling reactions can be performed in aqueous solution while many general reactions are affected by extremely small amount of oxygen or water. Instead, oxygen is more able to disrupt the coupling reaction. This is attributed that the coupling reactions occur with unsaturated metal complexes that do not have 18 valence electrons. The empty coordination sites of the unsaturated metal ions are usually very reactive with oxygen from the air. In addition, The widely used palladium catalyst, tetrakis(triphenylphosphine)palladium(0), for the coupling reaction is usually prepared in two steps from Pd(II) precursors. The Pd(0) is easily oxidized to relatively stable Pd(II). In fact, Pd(0)-stabilizing ligands such as triphenylphosphine are frequently used.

While CPEs as a result of direct polymerization of monomers with ionic side chains are soluble in water or highly polar solvents, most important issue after polymerization using precursor routes is how organic soluble side chains can be modified to ionic states to dissolve them in aqueous or highly polar solvents. So, many organic-soluble functional groups are designed as it can be easily transformed to ionic side groups

through hydrolysis or other hydrolyzing processes. Some example of functional groups that can be readily converted to ionic groups by hydrolysis process is present in Figure 1-5. These functional groups are hydrolyzed by base, acid, or metal catalyzed process. However, choosing the appropriate method is critical because some may disturb the conjugated backbone during the process. Therefore, attaching functional groups should be systematically designed, considering conjugated backbone.

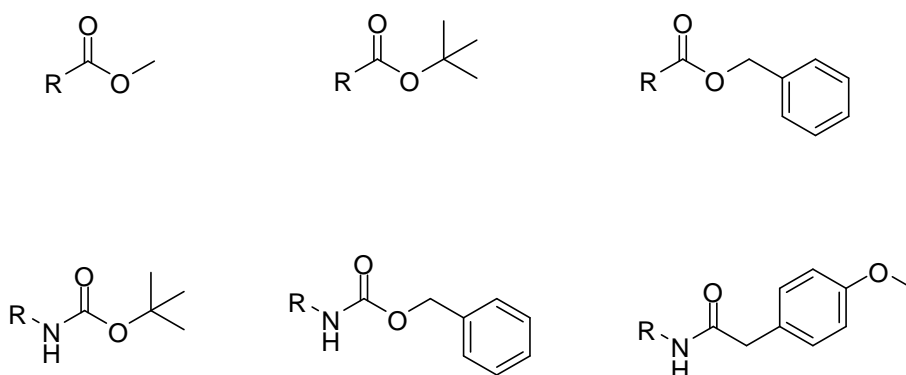


Figure 1-5. Various functional groups.

Functional Group Effects on Aggregation

The solvent induced aggregation of conjugated polyelectrolytes in solutions has been extensively explored through UV-Vis absorption and fluorescence spectral changes in poor solvents or good solvents. Because the hydrophobic backbone and hydrophilic side chain of CPEs induce aggregation in aqueous solution, their photophysical properties can be affected by solvent environment. Also, such aggregation is more significant in the presence of oppositely charged species such as metal ions, anions, and fluorescence dyes. While the aggregation frequently brings the positive effects such as highly efficient response for analytes sensing, it also induces low quantum yield, low solubility, and complex sensing behaviors. As a result, to

promote or prevent such aggregation, linear or branched side chains can be incorporated on the conjugated backbone.

Linear functional group effects

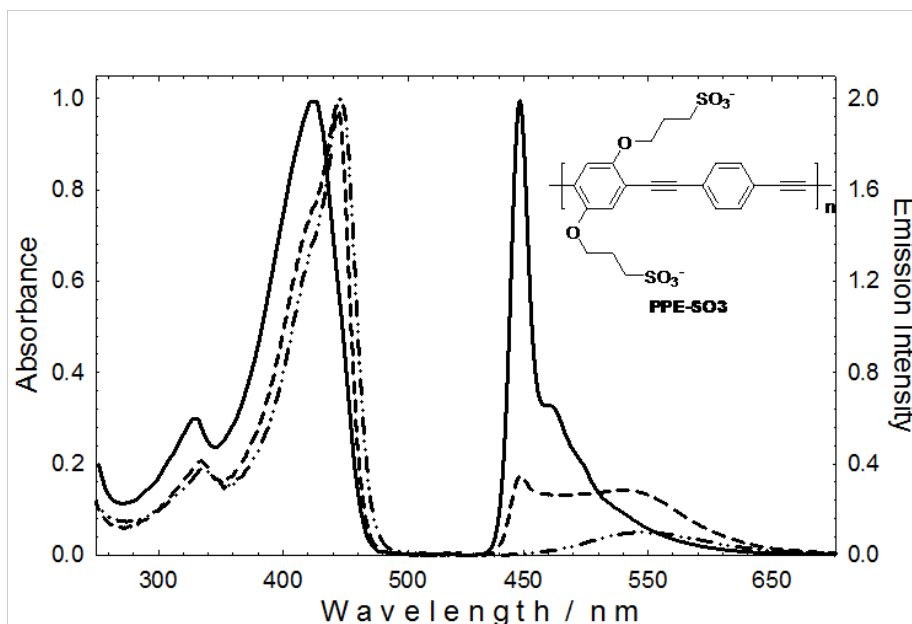


Figure 1-6. Absorption (left) and fluorescence (right) spectra of **PPE-SO₃⁻** in CH₃OH (—), 1/1 CH₃OH/H₂O (-----), and H₂O (-·-·-). Figure was taken from Tan et al.¹⁶

Conjugated polyelectrolytes with linear side chains tend to aggregate in aqueous solution because of the hydrophobic effect. In addition, when conjugated backbones approach closely, electrostatic repulsions between side chains are not significant as much as it prevents aggregation. In our previous work, solvent-induced aggregation of **PPE-SO₃⁻** was observed as the water ratio increase against CH₃OH.¹⁶ As seen in inset of Figure 1-6, its functional group is relatively a linear (non-bulky) type side chain.

As seen in Figure 1-6, both the absorption and fluorescence properties of **PPE-SO₃⁻** are very similar to those exhibited in CH₃OH where the polymer chains exist as an unaggregated state.¹⁷ Therefore, the aggregation of **PPE-SO₃⁻** can be minimized in CH₃OH. The absorption spectra in H₂O were bathochromically shifted with increasing

water ratio, showing narrow absorption spectra. The most significant change is that strong and narrow fluorescence spectra in CH₃OH become weak and broad one with bathochromic shift. Consequently, both features in UV-Vis and fluorescence spectra prove that **PPE-SO₃⁻** in water is strongly aggregated, but it exists in monomeric state in CH₃OH.

Such aggregation of CPEs having linear side chains was also found in several other CPEs having cationic or anionic linear side chains. Another previous work shows polymer aggregation in water solution, in which various aromatic units such as pyridine (Py), thiophene (Th), 3,4-ethylenedioxythiophene (EDOT), and 2,1,3-benzothiadiazole (BTD) are incorporated into conjugated backbone, containing anionic sulfonate (R-SO₃⁻) or cationic *bis*-alkylammonium (R-N⁺-R-N⁺-R) as the side chains.¹⁰ It is believed that both anionic (**PPE-Ar-SO₃⁻**) and cationic (**PPE-Ar-(4⁺)**) polymers are well dissolved in CH₃OH, but in water. Their amphiphilic character induces polymer aggregation driven by the hydrophobic effect.

Branched functional group effects

Incorporation of bulky functional group can effectively modulate the degree of aggregation in aqueous solutions. Recently, Huang et. al., reported that fluorine-containing poly(arylene ethynylene)s with bulky amino functionalized side groups exhibit a gradually decreased degree of aggregation as the number of functional group becomes larger in aqueous solution, resulting in increased quantum yield.¹⁸

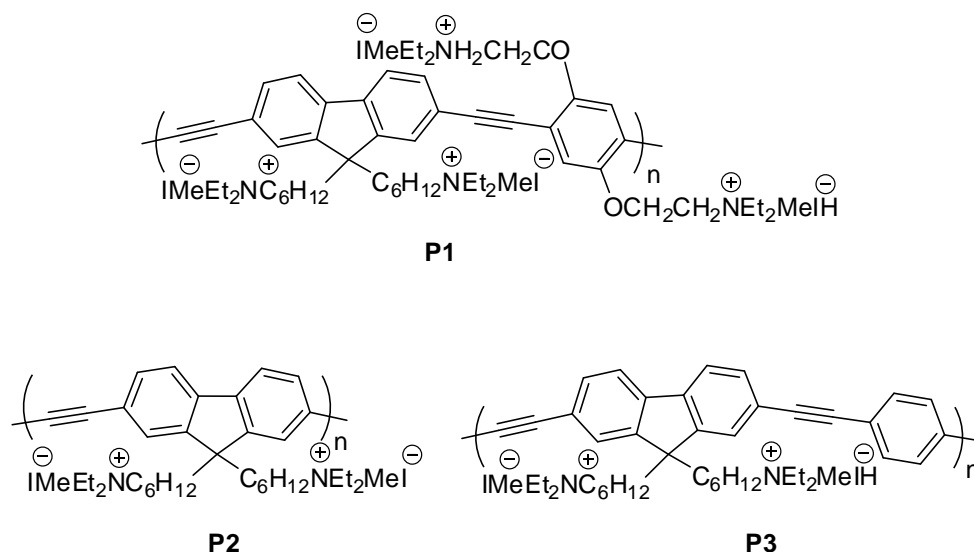


Figure 1-7. Structures of **P1**, **P2** and **P3**.

The structures of water-soluble fluorene-containing poly(arylene ethynylene)s are presented in Figure 1-7. The structure of **P1** is spatially more functionalized compared to the other **P2** and **P3**, and their steric congestion decreases from **P1** to **P3**. UV-Vis absorption and fluorescence spectra were monitored in CH₃OH, H₂O, and a mixture of the two solvents. As seen in Figure 1-8, with an increased volume fraction of H₂O in the solvent, **P1** shows very subtle wavelength changes in the UV-Vis absorption and fluorescence spectra except for the decreased intensity induced by nonradiative decay in polar solvent. These spectra are almost similar to its organic soluble precursor in THF. This observation suggests that the solution behavior of **P1** in H₂O may be similar with its precursor in THF, resulting in minimal aggregation. **P2**, however, exhibited bathochromic shift in UV-Vis absorption and fluorescence spectra, and their intensities are reduced. These spectral changes are further pronounced in **P3**. **P2** and **P3** show similar behaviors as seen in the result of CPEs with linear side chains. These results support that degree of aggregation gradually increases from **P1** to **P3** in aqueous solution.

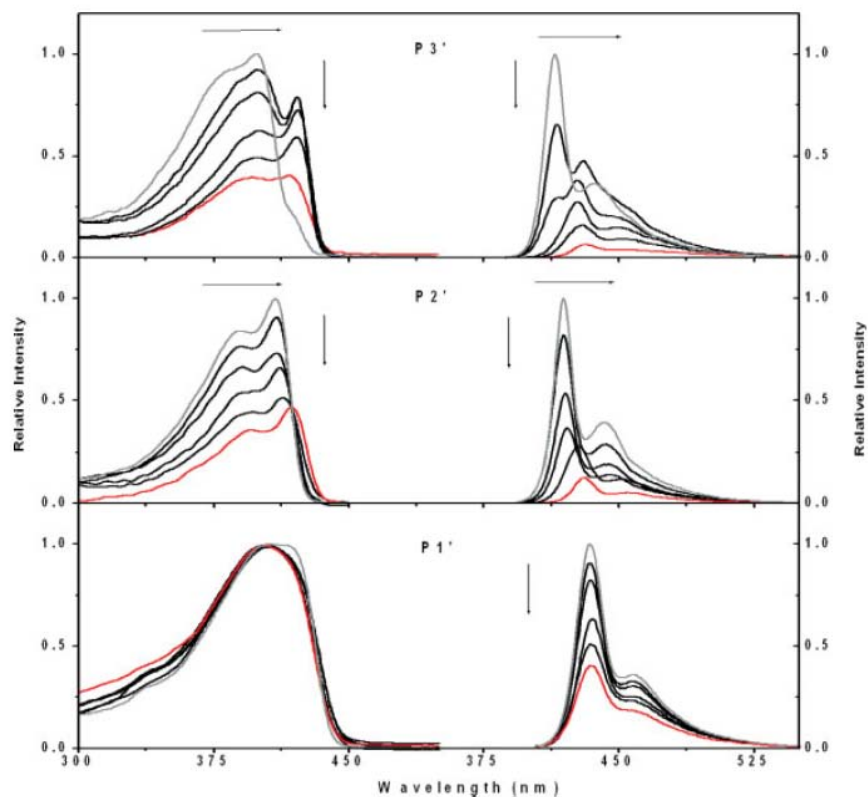


Figure 1-8. UV-Vis absorption (left) and fluorescence spectra (right) of **P1-P3** in pure CH₃OH (gray line), in pure H₂O (red line), and in mixtures of the two solvents at different compositions (black lines; 8/2, 7/3, 5/5, and 2/8 CH₃OH/H₂O from the top to the bottom). Figure was taken from Huang et al.¹⁸

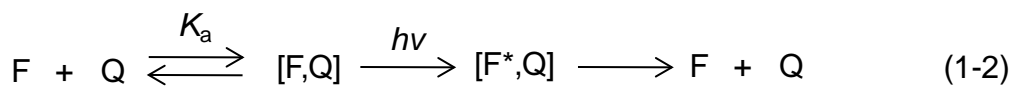
More evidence regarding degree of aggregation from **P1** to **P3** was proposed with the fluorescence lifetimes in H₂O. For **P1** in CH₃OH and H₂O, similar short-lived component ($\tau = 0.35$ ns/CH₃OH and $\tau = 0.32$ ns/H₂O) were observed with single-exponential fluorescence lifetime. These lifetimes are also very similar to that observed for its organic soluble precursor in THF. These observations suggested that aggregation of **P1** is negligible in H₂O as observed in UV-Vis and fluorescence spectra. For **P2** and **P3** in CH₃OH, on the other hand, long-lived component ($\tau_2^{p2} = 1.11$ ns and $\tau_2^{p3} = 0.94$ ns) with around 7% amplitude, while fast decay components are predominant with $\tau_1^{p2} = 0.35$ ns (94%) and $\tau_1^{p3} = 0.28$ ns (93%), respectively. These observations suggested

that the degree of aggregation of **P2** and **P3** are extremely small in CH₃OH. In water, however, the contribution of fast decay components ($\tau_1^{P2} = 0.33$ ns and $\tau_1^{P3} = 0.17$ ns) decreased and long-lived components ($\tau_2^{P2} = 0.96$ ns and $\tau_2^{P3} = 1.46$ ns) increased, contributing to 23% (**P2**) and 41% (**P3**). This increased contribution of long-live decay supports that degree of aggregation increase as the functional groups are less congested.

Amplified Quenching of Conjugated Polyelectrolytes

One of the major features of CPEs is amplification of the fluorescence quenching when the quenchers are bound to them. This property, which is referred to as superquenching or amplified quenching, has attracted much interest because of its usefulness in biological applications. This efficient quenching effect is induced via energy migration through entire conjugated backbone of CPEs, and the polymers provide very effective conduits for energy migration over long distances.

Stern-Volmer fluorescence quenching



$$I_0/I = 1 + K_{sv}[Q] \quad (1-3)$$

Fluorescence quenching arises by the interaction between fluorophore and quenchers, in which the quenching can be dynamic or static quenching. The dynamic quenching (Eq. 1-1) is induced by diffusive encounters while static quenching (Eq. 1-2) takes place as a result of complex formation. In equation 1-1, F* is an excited-state fluorophore, Q is a quencher, and k_q is the bimolecular quenching rate constant. Also,

K_a is the association constant for the ground-state complex formation [F,Q] in equation 1-2. The kinetics of these process follow the Stern-Volmer¹⁹ equation (Eq. 1-3), where I_0 is the intensity without a quencher, I is the intensity with a quencher. In the case of purely dynamic quenching, K_{sv} is equal to $k_q\tau_0$, where τ_0 is the fluorescence lifetime of F^* . Since the excited state is quenched by a collision with a quencher (Q), the lifetime is reduced by the addition of quencher. On the other hand, K_{sv} is equal to association constant, K_a , for purely static quenching. The quenching is not affected by the diffusion rate of the quencher, and the fluorescence lifetime is also independent for the quencher. This SV plot is frequently used to determine the difference between materials in the quantitative quenching. If either static or dynamic quenching is dominant, the slope of the SV plot becomes a linear. However, the two processes are competitive in most cases, resulting in nonlinear SV data.

Molecular wire effect

The amplified quenching was first explored by Swager and co workers.²⁰ The fluorescence chemosensor using the molecular wire approach showed enhanced sensory response.²¹ To evaluate this concept, the fluorescence quenching of cyclophane-containing polymer was compared to that of a low molar mass model (monomer unit of cyclophane-containing polymer) (Figure 1-9). Interestingly, greatly enhanced quenching of cyclophane-containing polymer was monitored while the model compound showed moderate quenching effect in the presence of methyl viologen (MV^{2+}) which is a well known electron transfer quenching agent. As seen in Figure 1-9, the comparison of the conjugated system to an isolated fluorescence receptor illustrated how amplified quenching is processed in both systems. In a mono-receptor system, the fluorescence is quenched only for the receptor forming complex with methyl viologen. In

a molecular wire system, however, fluorescence quenching effect occurs throughout entire polymer even though only a part of polymer units is occupied by the quencher. Therefore, the electronic properties of conjugated polymers provide amplified response for analytes through the efficient energy migration to occupied receptor sites.

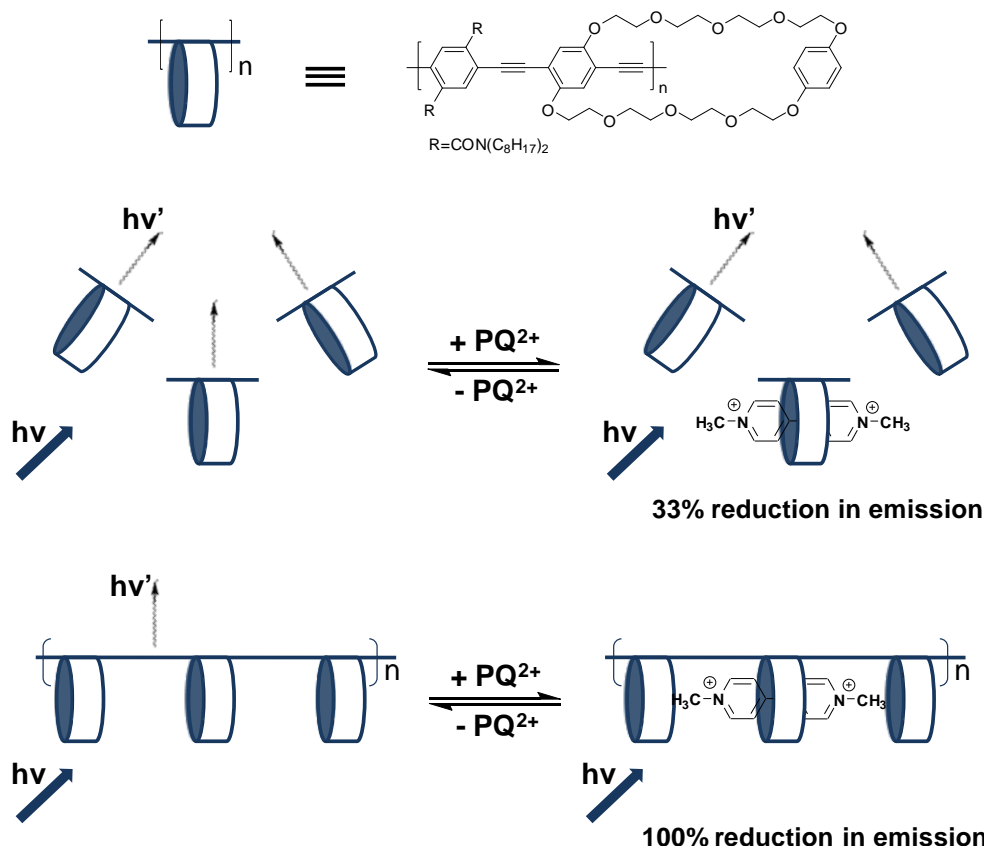


Figure 1-9. Schematic illustration of quenching effect in conjugated polymers with receptor and their fragment via energy migration to a receptor site occupied by PQ^{2+} . Figure was taken from Swager et al.²⁰

The amplified quenching efficiency in the conjugated polymer is attributed to the molecular wire effect. That is, the extended electronic communication and transport by conjugated polymer chain induce efficient fluorescence quenching. As shown in Figure 1-10, excited electron (a bound electron-hole) is generated on the polymer backbone upon the absorption of light, and it moves very rapidly along the chain. The conjugated

polymer acts as a conduit for exciton. The fluorescence is quenched when the exciton gets into proximity with the polymer repeat unit which contains a quencher occupied receptor. The extremely efficient exciton migration in the excited state leads to quenching of many repeat units in polymer chains, resulting in amplified quenching for the quencher or analytes.

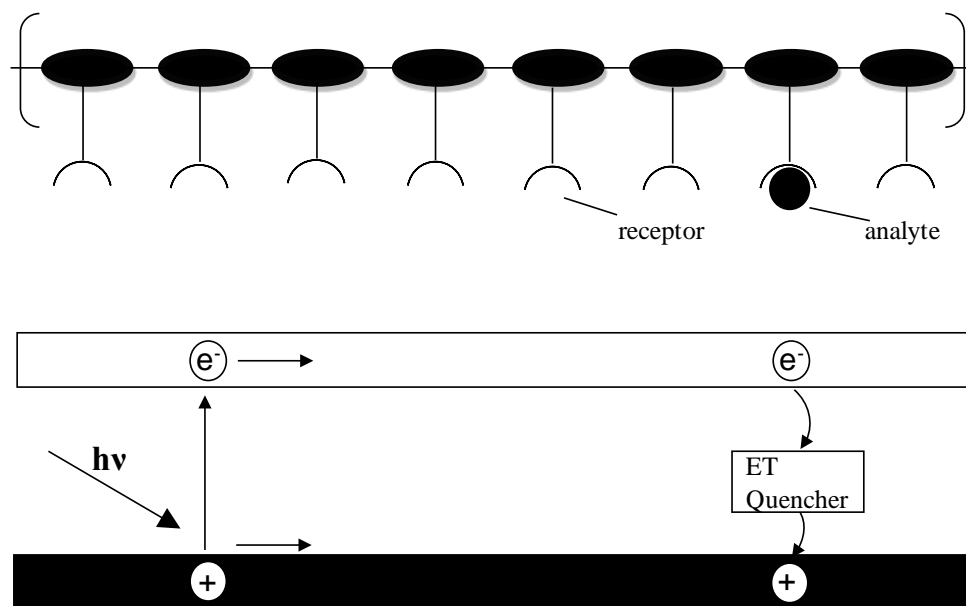


Figure 1-10. Quenching mechanism of “Molecular wire” effect in conjugated polymers with receptors. Figure was taken from Swager et al.²¹

Applications of Conjugated Polyelectrolytes to Sensors

Fluorescence is a widely used and rapidly expanding method in chemical and biological sensing. Sensor should selectively recognize the guest molecules, and sensitively translate its recognition to signal. Sensing behaviors display their signal through changes in intensity, wavelength, energy transfer, and fluorescence lifetime. So, to improve the sensitivity, such fluorescence signal should be readily perturbed by external stimuli. From this point of view, conjugated polymers (CPs) are one of the most efficient sensors because of their extraordinary sensitivity for the guest molecule

sensing, which is a remarkable advantage of CP-based sensors compared to the sensors using small molecules.²²⁻²⁶ Intra or inter-molecular energy migration provides very efficient sensing response to even minor perturbation.

Recently, water-soluble conjugated polymers have attracted intensive attention as a very efficient optical chemical sensor due to their use in analysis and detection of the guest molecules in environmental and biological setting.

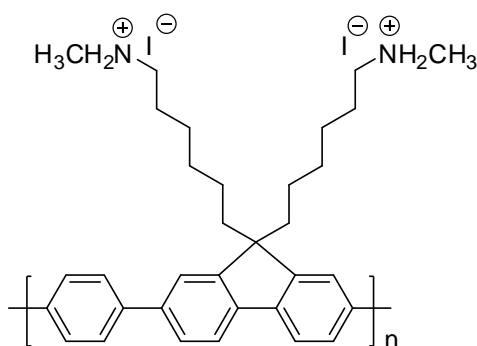


Figure 1-11. Structure of cationic conjugated polyelectrolyte.

It is reported that cationic water-soluble conjugated polymer (CCP) responds to single stranded DNA (ssDNA) in the presence of peptide nucleic acids (PNAs) labeled with a fluorescein at the 5' position where the energy transfer occurs from CCP to fluorescein dye.²⁷ Poly(9,9-bis(6'-N,N,N-trimethylammonium)-hexyl)-fluorene phenylene containing iodide counter anions (Figure 1-11), CCP, was used as a donor for fluorescence resonance energy transfer (FRET), and fluorescein dye on the 5'-position of PNAs (PNA-C*) acts as an energy acceptor. As seen in Figure 1-12, no electrostatic interaction between CCP and PNA-C* are observed in the initial solution.

Complementary ssDNA hybridizes with the PNA, and it forms a complex with CCP, resulting in a decrease in the average CCP-C* distance (Route A). This complex allows FRET from CCP to fluorescein dye on PNA. However, when a ssDNA does not match

the PNA sequence, hybridization does not take place (Route B). In this case, No FRET occurs.

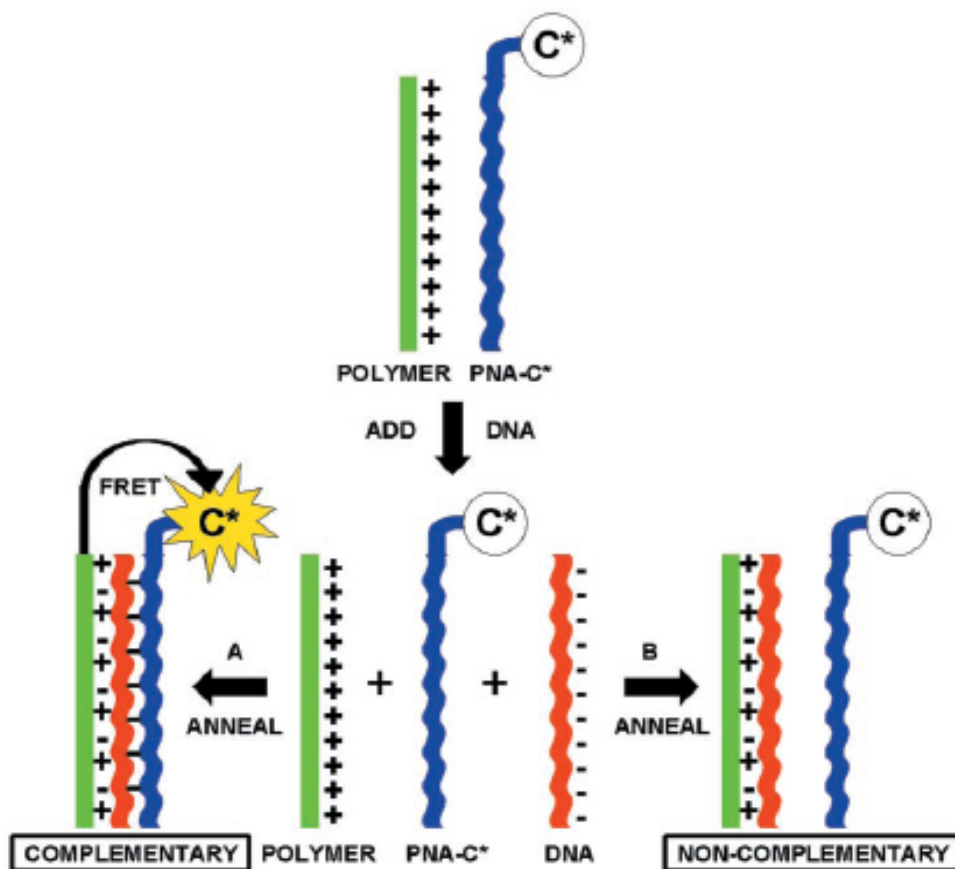


Figure 1-12. Schematic representation for the use of a cationic water-soluble CP with a specific PNA-C* optical reporter probe to detect a complementary ssDNA sequence. Figure was taken from Bazan et al.²⁷

To improve the sensory response, frequently, two or more combinations of polymers and/or receptors are used. Bunz et al. also reported that poly (para-phenyleneethynylene) (**PPE**)-papain system effectively detects Hg^{2+} ion with high sensitivity compared to **PPE**.²⁸ Figure 1-13a shows the structure of **PPE** containing carboxylate side chains (R-CO_2^-), which is water-soluble. The addition of Hg^{2+} ion leads to the weak fluorescence quenching of **PPE** in PIPES (piperazine-1,4-bis(2-

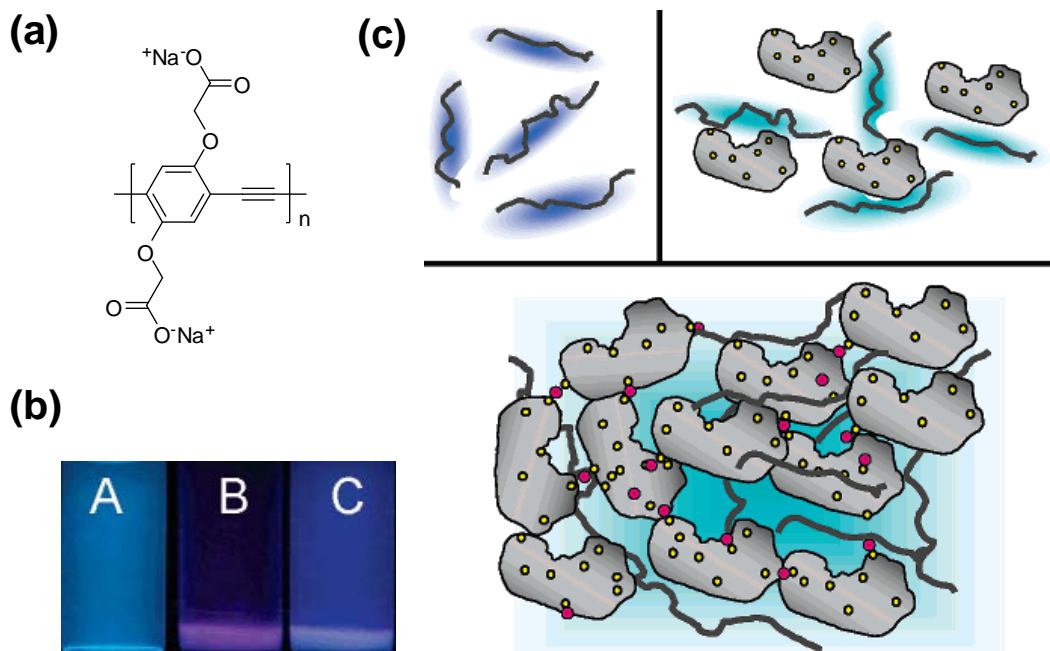


Figure 1-13. (a) Structure of **PPE**, (b) fluorescence intensity changes; A: **PPE**-papain complex, B: all 10 metals added to **PPE**-papain complex, C: Same without Hg^{2+} ion, and (c) qualitative interpretation of the Hg^{2+} ion-induced agglutination of the **PPE**-papain complex; top left: **PPE** alone, top right: electrostatic complex from **PPE**-papain, bottom: the addition of Hg^{2+} ion to **PPE**-papain leads to its precipitation by cross-linking of the papain molecules through Hg^{2+} ion. Figure was taken from Bunz et al.²⁸

ethanesulfonic acid)) buffer at pH 7.2. On the other hand, the detection of Hg^{2+} ion by **PPE**-papain complex system was more efficient than either **PPE** or papain alone. **PPE**-papain complex (A) shows blue color fluorescence as shown in Figure 1-13b. Its fluorescence was quenched in the presence of various divalent metal ions including Hg^{2+} ion (B). However, the fluorescence quenching was not observed upon the addition of other metal ions without Hg^{2+} ion (C). Figure 1-13c proposed mechanism of action for this Hg^{2+} ion sensing. Positively charged papain slightly quenched the fluorescence of **PPE**. The addition of Hg^{2+} ion, however, caused precipitation because all of the chain of **PPE** incorporated into **PPE**- Hg^{2+} -papain agglutinate, and its solution was fully quenched.

Conjugated Polyelectrolyte Dendrimers

Dendrimers

Dendrimers are highly branched macromolecules that can be subdivided into three architectural components: a central core, interior branches, and surface functional groups. Since the dendrimer was firstly synthesized by Vögtle in 1978,²⁹ it has been disclosed by Denkewalter at Allied Corporation in 1981, Tomalia at Dow Chemical in 1983 and in 1985,³⁰ Newkome in 1985,³¹ and in 1990 Fréchet introduced a convergent synthesis.³² In spite of short historical background, dendrimer has been rapidly developed as new research area and attracted great scientific interest because of their unique molecular architecture. At present, the global trend for dendrimer researches is shifted to their properties and potential application from the research related to the synthesis.

The word dendrimer by Tomalia in 1980 is derived from the Greek words Dendron (tree) and meros (part) because this type of molecule resembles a tree. Dendrimer is symmetric and monodisperse molecules and synthesized through a stepwise repetitive reaction sequence, which gives rise to different generations of the dendrimers. In addition, their structure is mainly divided into three parts: core, branches, and end groups. Such distinguished frameworks induce relatively rigid conformation in terms of size and shape compared to linear polymers.³³ Furthermore, geometrically increased number of end groups with increasing generation affect to the surface functionality of the dendrimer, i.e. changing the end groups leads to distinct characteristics of dendrimer. Also, appropriately designed high generation dendrimers display a distinctive interior that is sterically encapsulated by external end groups, enabling applications as unimolecular container molecules.³⁴ Such structural features enable the

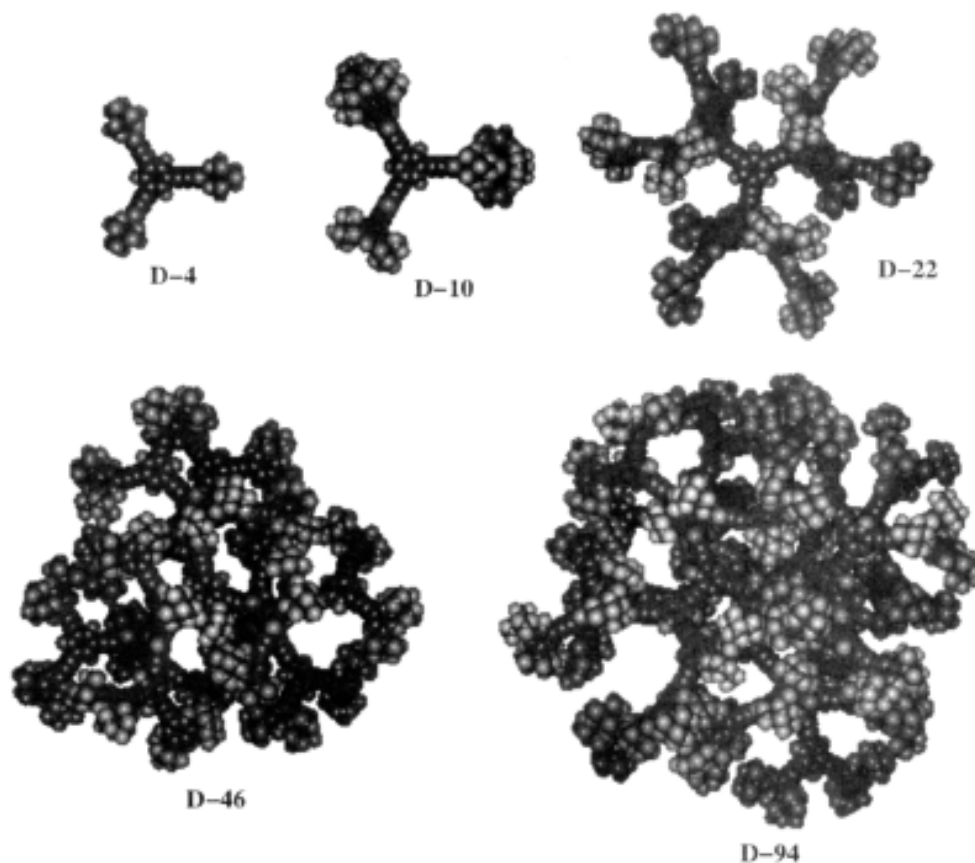


Figure 1-15. Space-filling models of phenylacetylene tridendrons **D-4**, **D-10**, **D-22**, **D-46**, and **D-94**. Figure was taken from Moore et al.³⁶

One of the characteristics of dendrimers is the presence of numerous peripheral end groups that all converge to a single core. Such plentiful end groups induce a three-dimensional globular architecture of dendrimers, which has limited degrees of conformational flexibility. Figure 1-15 shows the space-filling models of the five members of the conjugated phenylacetylene dendrimers. This series also shows more spherical shape as the generation increases. The structure of D-96 has a diameter of approximately 5.5 nm.³⁶ Consequently, such structures define the concept of a shape-persistent macromolecules.

Synthetic Approaches

Similar to synthesis of conjugated polyelectrolytes, the reactions used in preparation of phenylacetylene dendrimers are activation process of protected terminal acetylene and its palladium catalyzed cross-coupling reaction with aryl halides in the presence of a catalytic amount of copper (I) iodide. As a protecting group of the terminal acetylene, the trimethylsilyl (TMS) group is an excellent masking group which is the most common protecting group on the terminal acetylene group. Necessarily, various protecting groups such as triisopropylsilyl (TIPS), *tert*-butyldimethylsilyl (TBDMS), and *tert*-butyldimethylsilyloxymethyl (TOM) are available when the reaction needs selective activation for regioselective substitutions or appropriate reaction conditions. These protecting groups are readily removed by acid or fluoride salts (such as NaF, TBAF, HF-Py, or HF-NEt₃). For the cross-coupling reaction, typically two kinds of catalysts can be employed: palladium complexes and a halide salt of copper (I). Several palladium (0) complexes such as *tetrakis*(triphenylphosphine)palladium (0) and *bis*(dibenzylideneacetone)palladium (0) as well as palladium (II) complex, *bis*(triphenylphosphine)palladium (II) chloride, are available in this reaction. These catalysts activate the aryl halides by oxidative addition into carbon-halogen bond. Also, another catalyst, copper (I) halides, forms aryl-alkyne-Cu complex with terminal alkyne, in which complex formation is promoted by base such as amines (usually diisopropylamine or triethylamine). Finally both activated species generate new carbon-carbon bonds.

Based on above coupling reaction, various approaches are considered for the combination of phenylacetylene building blocks. Among various synthetic methodologies for dendrimer synthesis, two major approaches known as divergent and

convergent methods have been developed and widely used as foremost means.

Although desired dendrimers can be generated by either one approach, the reactions have to be considered by many factors including the solubility, separation from byproducts, and costs.

Divergent approach

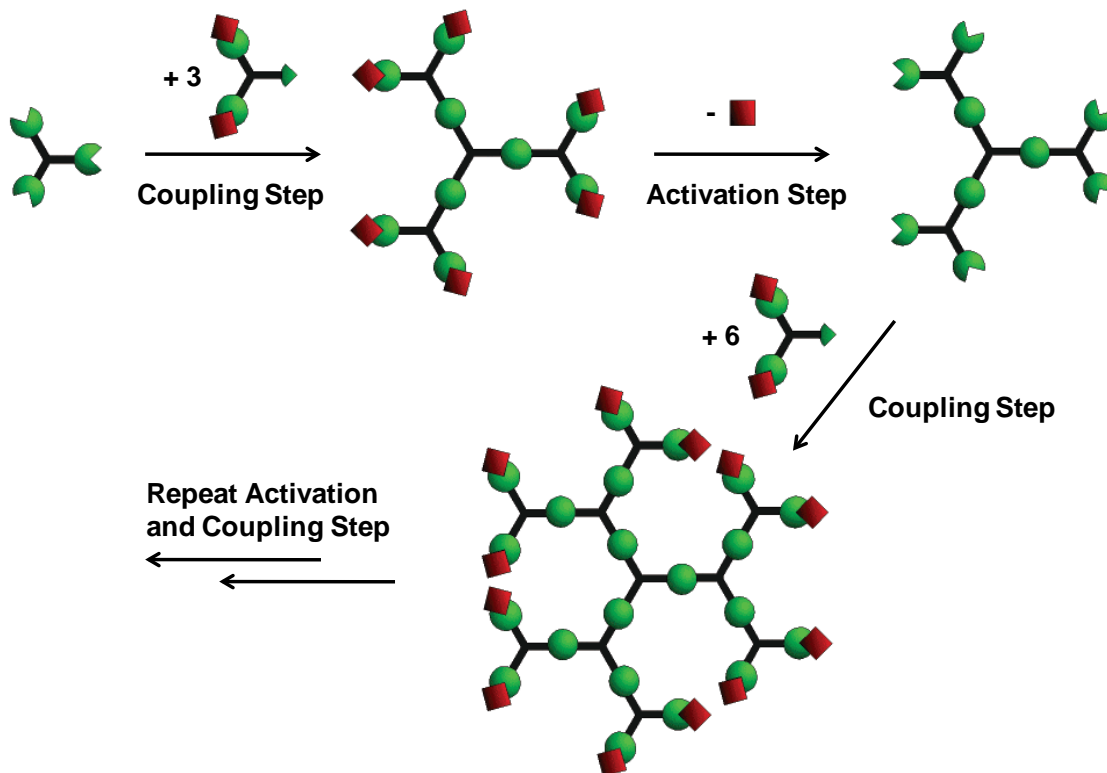


Figure 1-16. Synthetic diagram of divergent approach. Figure was taken from Fréchet et al.³⁷

The original divergent method is developed by Newkome and Tomalia, which involves conjunction of repeat units on a core. Figure 1-16 shows stepwise synthetic cartoon for divergent approach. The sequential repetitions of coupling and activation process induce continuous outward of branches with a number of functional groups on the periphery of the dendrimer. Additional coupling and activation steps lead to an geometric increase in the number of branches, providing the abundant reactive site for

the end-groups. Finally, functionalized end-groups are incorporated into each reactive site to have unique properties.

Remarkable advantage of the divergent approach is less steric effect in growth of the dendrimer size, which also induce improved yields in growth of dendrimer size. However, this method is limited by the factor that many functional groups should be incorporated at higher generation. This may cause increase of the possibility of molecular imperfection with increasing generation. Poor solubility also makes dendrimer synthesis difficult. Furthermore, it is difficult to selectively substitute the end-groups for exclusive functionality in use.

Convergent approach

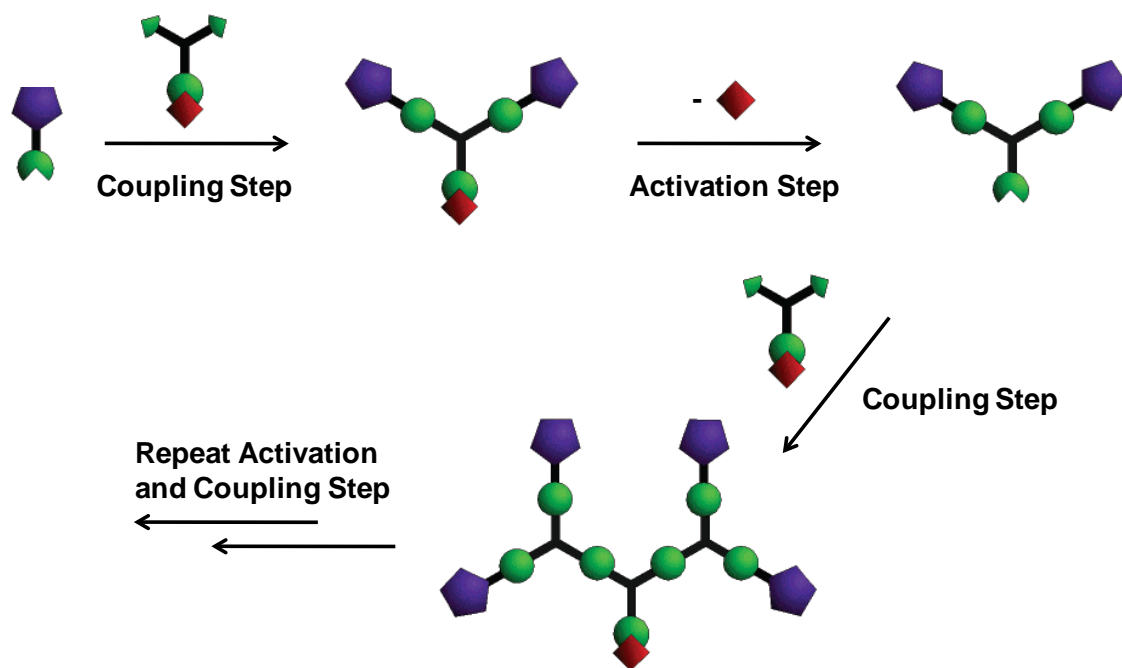


Figure 1-17. Synthetic diagram of convergent approach. Figure was taken from Fréchet et al.³⁷

The convergent approach was first reported by Hawker and Fréchet in 1989-1990. As seen in Figure 1-17, the growth of dendrimer initiates inward from the exterior by coupling end groups to each branch of the monomer. This coupling reaction creates a

single functional group located at the focal point, displaying wedge-shaped dendritic fragment. After activation of this dendron, continuous accumulation on an additional monomer units leads to a higher generation dendron. After repetition of this process for desired dendrimer, the dendrons can be incorporated into a core unit, affording a multi-functionalized dendrimer. It should be noted that this convergent method is absolutely comparable to its divergent counterpart because only a few reactive sites are involved in this reaction.

This approach proffers distinctive features such as involvement of one or two reactive sites for growth, easy organization of end group functionality, and uncomplicated purification and characterization of intermediates. That is, it provides greater control in synthetic and structural manipulation than the divergent method. Such distinct features enable their functionality to be selectively and strategically modified throughout the molecules. One limitation of this approach is that attaching the dendrons on the core is less straight-forward than the divergent method because of steric congestion, causing poor yield. Nevertheless, it is the most attractive that well-defined unsymmetrical dendrimers can be producible with this approach. Also, advanced convergent approaches such as double-stage convergent method have been developed to overcome such shortcoming, in which flexible multifunctional dendritic core is employed in the final step of the synthesis.³⁶

Water-Soluble Dendrimers

Water-soluble dendrimers are dendrimers having either positively or negatively charged ionic solubilizing groups as an end groups. Their entire structures also are very similar in both size and shape to that of the Hartley micelle model as seen in Figure 1-18.³⁸ That is, both models have spherical structure with hydrophobic interior and

hydrophilic exterior. In fact, such similarity between Hartley micelle and unimolecular micelle has been demonstrated by several groups.^{31,34,38-40} The critical difference between these micelles is that water-soluble dendrimer is a single molecule incapable of disintegration while the formation of traditional micelle relies on the external surroundings. For instance, the traditional micelles are affected by a variety of factors such as pH changes, ionic strength, solvent polarity, concentration, and temperature. On the other hand, the elemental structures of water-soluble dendrimers in solution are independent on such exterior environments. Namely, water-soluble dendrimers retain their structure unless covalent bonds are physically destroyed.

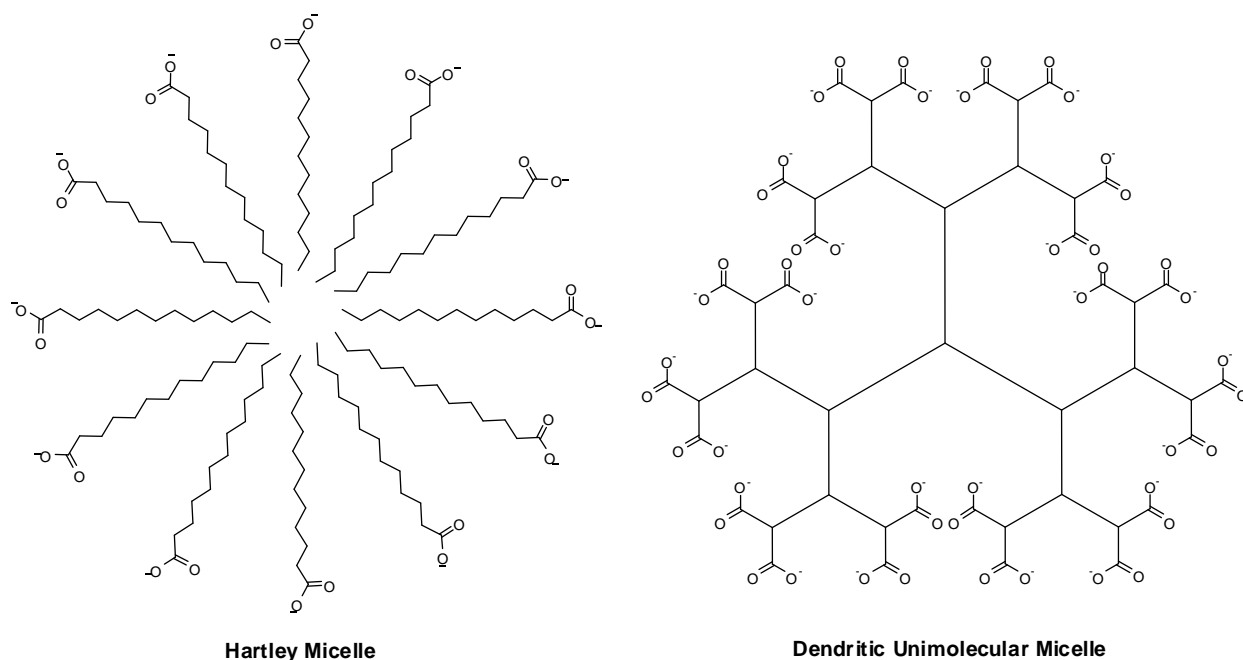


Figure 1-18. Schematic representation showing the structural similarity between the traditional Hartley micelle model and a dendrimer. Figure was taken from Moore et al.³⁸

Such water-soluble dendrimers have recently attracted intensive attention because of their amphiphilic characteristic.⁴¹⁻⁴⁵ Because of the presence of charged groups, the properties of these dendrimers are strongly affected by the electrostatic interactions on

the dendrimer surface and by the hydrophilic effect in interior branches. Also, although little attention is paid to the aggregation behavior of such amphiphilic dendrimers, their higher generation exists as a single molecule capable of molecular inclusion. Such feature is of use to the application such as the drug delivery, molecular encapsulation, charge transport, and sensor.⁴⁶

Water-Soluble Conjugated Dendrimers

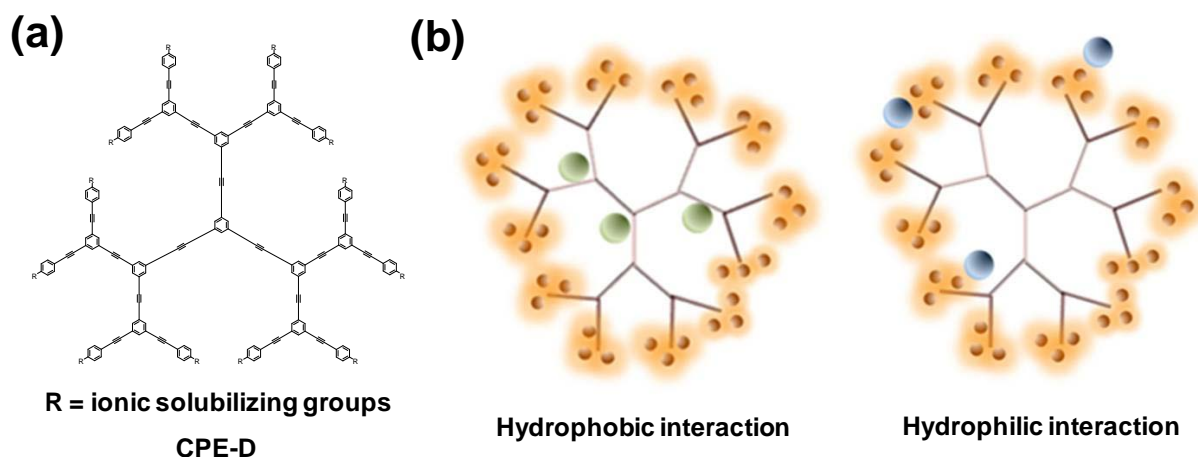


Figure 1-19. (a) Representative structure of conjugated polyelectrolyte dendrimer (CPE-D). (b) CPE-Ds paired with guest molecules; (left) hydrophobic species is closed to the dendrimer core and (right) hydrophilic species resides in dendrimer periphery.

Conjugated polyelectrolyte dendrimers (CPE-Ds) are a new class of the water soluble dendrimers carrying ionic solubilizing groups, and their back bones are conjugated with phenylacetylene units (Figure 1-19a). The most remarkable feature of these CPE-Ds is the shape-persistence. In the case of common non-conjugated dendrimers with amphiphilic feature, their conformations are found to shrink or change size with changing external environment because they are physically flexible systems. Unlike such non-conjugated systems, however, CPE-Ds retain their certain stiffness because of the rigid backbone. Another unique feature of conjugated dendrimers is that their hydrophobic backbone consists of all-hydrocarbon without hetero atoms, which

makes the interior more hydrophobic than other systems containing hetero atoms including oxygen and nitrogen. Such characteristics of the CPE-D might provide some unusual properties. It is possible that relatively more rigid and hydrophobic characteristics provide proper geometric structure to the specific molecules and form stable complex with analytes. In addition, amphiphilic feature allows two different binding modes, so that both hydrophilic species and hydrophobic molecules can affect its photophysical properties or sensing response (Figure 1-19b). Furthermore, we may expect that CPE-Ds having higher net density throughout entire conjugated backbone provide outstanding platforms for energy or electron transport as seen in conjugated polyelectrolytes (CPEs). For this distinctive dendrimer, not many researches have been investigated and developed. Only one example is documented by Moore and co workers, in which synthesis and synthetic characterization are reported.

Scope of the Present Study

The purpose of the present study is to investigate and elucidate the photophysical properties of conjugated polyelectrolytes (CPEs) and conjugated polyelectrolyte dendrimers (CPE-Ds). In this dissertation, CPEs and CPE-Ds are newly designed and synthesized and their characterizations are well described. Their photophysical properties are studied by the spectroscopic analysis such as UV-Vis absorption, fluorescence, and fluorescence lifetime spectroscopy. Also, AFM images and Dynamic Light Scattering (DLS) measurement are used to define their aggregation property. Finally their unique photophysical properties are developed as a metal or biomolecular sensor.

In Chapter 2, branched polyionic side chain effects on the conjugated polymers are examined and compared to linear side chains. Since conjugated polyelectrolytes

having linear side chains show aggregation propensity in aqueous solution, their prospective applications are sometimes limited by low quantum yield, low solubility, and unexpected or complicated solution behavior induced by aggregation. To prevent polymer aggregation, relatively bulky polyionic side chains are incorporated to polymer backbone. Comparisons between CPEs having linear or branched polyionic side chains are studied by UV-Vis absorption, fluorescence, and lifetime spectroscopy in CH₃OH and H₂O solutions. Aggregation dependent on size of aromatic units in conjugated backbone is also explored.

In Chapter 3, CPE based Hg (II) ion sensor is described. In CPE based sensory system, PPE with branched polyionic side chains retaining less aggregation in aqueous solution is used as a signaling moiety and a rhodamine derivative acts as a Hg (II) ion receptor. This system shows high selectivity and sensitivity for Hg (II) ion upon the addition of various metal ions. Such sensing response was identified by fluorescence intensity changes. Also, plausible sensing mechanism is provided, in which a spiro-type rhodamine derivative undergoes ring-opening by complexation with Hg (II) ion, providing a positive charge on the nitrogen atom. This result leads to the strong electrostatic binding with anionic carboxylate of PPE, resulting in fluorescence quenching of PPE by the effective energy transfer.

In Chapter 4, water-soluble conjugated pyrene bearing phenylacetylene units with carboxylate side chains (**PyA4**) was synthesized, and it is applied to a pyrophosphate (PPi) sensor. Photophysical properties and solution behaviors of **PyA4** were studied in CH₃OH and H₂O solutions by fluorescence spectroscopy. Selectivity for Cu²⁺ ion over other metal ions and its quenching mechanism were explained by

comparison of Stern-Volmer plots in CH₃OH and H₂O solutions. **PyA4**-Cu²⁺ complex as a PPI sensor was also studied by fluorescence intensity changes upon addition various anions. Furthermore, the activity of alkaline phosphatase (ALP) was monitored by the real-time turn-off assay.

In Chapter 5, novel water-soluble conjugated polyelectrolyte dendrimers (CPE-Ds) were synthesized by the convergent method, where the branched carboxylate ionic groups were incorporated as an end group. Structural configuration of each CPE was characterized by the computational modeling, AFM, and dynamic light scattering (DLS). GPC analysis provides a mono-dispersity which one of the notable characteristics of the dendrimers. Because of higher electrostatic repulsion between the branched polyionic side chains and more spherical type with generation, little or no aggregation is expected at higher generation. Such properties of CPE-Ds are characterized by UV-Vis absorption, fluorescence, and lifetime spectroscopy. Quenching and energy transfer effect from CPE-Ds to the cyanine dyes (DOC, DODC, and DOTC) were studied with fluorescence measurement and Stern-Volmer Plot.

In Chapter 6, we developed systematically water-soluble conjugated polyelectrolyte dendrimers containing thienyl (Th) groups in the center of conjugated backbone, which were obtained by hydrolysis process using basic condition to dissolve them in aqueous solution. The photophysical properties were carefully studied in CH₃OH and H₂O solutions using UV-Vis absorption and fluorescence spectroscopy. Intra-dendrimer energy transfer from phenyl units to aromatic unit including thienyl (Th) and 2,1,3-benzothiadiazole (BTD) was observed. Lifetime spectroscopy provides more

detail photophysical properties of Th-CPE-Ds in CH₃OH and H₂O solutions. More efficient quenching or energy transfer effect was observed at the higher generation.

CHAPTER 2

WATER-SOLUBLE CONJUGATED POLYELECTROLYTES WITH BRANCHED POLYIONIC SIDE CHAINS: SYNTHESIS, CHARACTERIZATION, AND OPTICAL PROPERTIES

Over the past several decades conjugated polyelectrolytes (CPEs) have attracted considerable attention and become one of the versatile polymeric materials in optoelectronic devices⁴⁷ and biochemical²⁶ detection research because they have the exceptional features, such as high fluorescence quantum yield, unique solution behavior, ability to interact electrostatically with other oppositely charged species, and extraordinary high sensitivity to fluorescence quenchers due to exciton migration.^{21,48-51} Particularly, high sensitivity to quenchers is amplified in aggregated states because exciton migration occurs through not only intrachain but also interchain processes when quencher ions are bound to polymer aggregates.^{16,52-53} However, in spite of such potential advantages of CPEs, their solution processing is sometimes limited by a low quantum yield, low solubility, and unexpected sensing behavior induced by a strong propensity to self-assemble into aggregates in aqueous solutions.^{11,18,54-55}

For this reason, much effort has been devoted to retaining non-aggregated state or increasing fluorescence quantum yield in aqueous media by variation of solvent polarity, pH, and ionic strength.⁵⁶⁻⁵⁸ In previous studies, however, conditions that are required for non-aggregation of polymers were not sufficient to maintain non-aggregated states or could not be qualified for detecting analytes in biological settings. Furthermore, fluorescence quantum yield showed relatively small enhancement in such conditions.⁵⁷ Nevertheless, several photochemical sensors have been developed to take advantage of aggregation between water-soluble CPEs modulated by addition of analytes, which are based on electron transfer or energy transfer.^{16,52-53,59-61} For example, Bazan et al.

observed that significant enhancement of fluorescence emission in polymer aggregates is due to shielding effect of the emitters from water contacts.⁶² This result may encourage development of highly sensitive chemical sensors even in various experimental conditions.

According to previous studies, the aggregation occurs by a hydrophobic interaction of the polymer backbones and/or an electrostatic interaction between side chains of polymer in certain conditions.^{10,58} Furthermore, it is not surprising that such aggregation is also related to the solubility of polymers.^{11,18,54-55} To overcome this drawback in aqueous solutions, recently, Swager reported that introducing relatively bulky fluorophore into the CPEs' backbone induce less aggregation because its backbone is a less planar and linear shaped.⁵⁴

Therefore, we hypothesized that attaching crowded and bulky ionic functional groups could be an effective way of reducing hydrophobic interaction by increased electrostatic repulsion between polymers as well as it would increase polymer's solubility in aqueous solution. Moreover, another distinctive advantage of these CPEs having branched polyionic side chains is three-dimensional structure of a receptor, which can provide appropriate geometric cavity to the specific biomolecule and form stable complex with analytes.⁶³⁻⁶⁴ This might increase their selectivity to the target molecules. In addition, we may expect that highly dense charges in a receptor can enhance binding of the anion, cation or biomolecule. Consequently, these structural advantages with a sensible optical characteristic which can be easily perturbed by external stimuli would show a potential possibility as an effective fluorescence sensor in highly sensitive bioassays.

Results and Discussion

Synthesis and Characterization

In this study, we report the synthesis of water-soluble CPEs having branched polyionic side chains (bulky functional groups) as shown in Table 1. As a polymer repeat unit, phenyl (Ph), 2,1,3-benzothiadiazole (BTD), or 4,7-Bis(2'-thienyl)-2,1,3-benzothiadiazole (TBT) units have been introduced into polymer backbone, and negatively or positively charged water-soluble branched polyionic side chains that can structurally hinder the aggregation of the polymer chains were also incorporated to the conjugated polymer backbones, thereby suppressing self-quenching of their excited state.

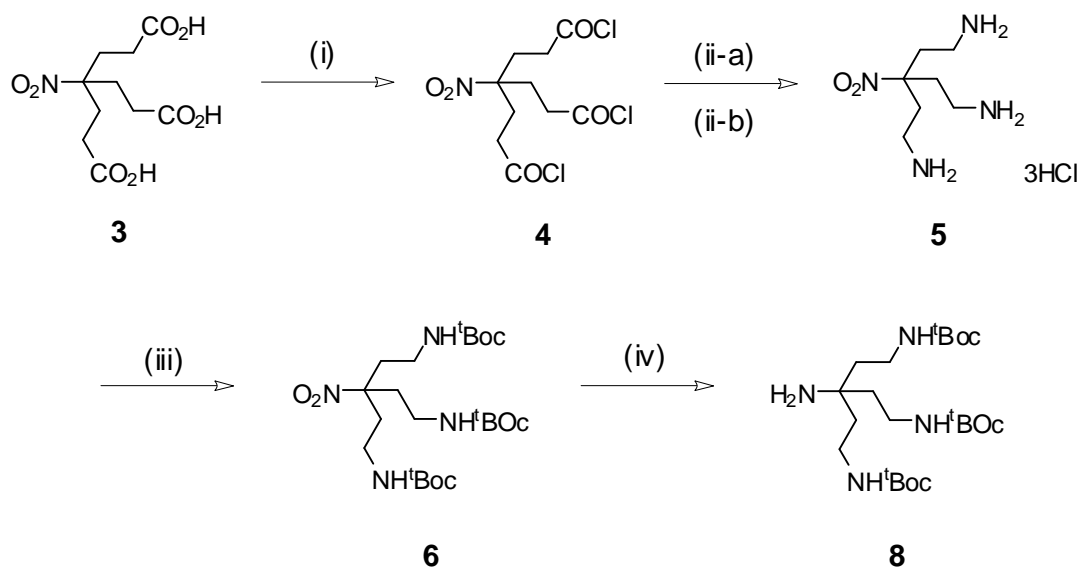
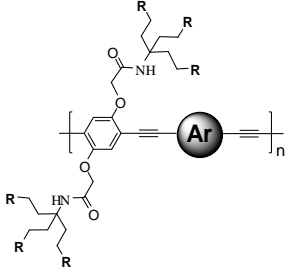

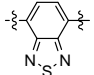
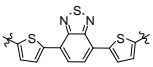

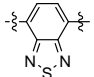


Figure 2-1. Synthesis of **8** (i) SOCl_2 , DMF, reflux for 2 hrs.; (ii-a) $(\text{CH}_3)_3\text{SiN}_3$, dioxane, 80 °C for 2 hrs.; (ii-b) acetone, HCl (12 N), 50 °C for 1 hr.; (iii) Boc_2O , Et_3N , CH_3CN , reflux for 7 hrs.; (iv) T-1 Raney nickel, EtOH, H_2 , 100 psi, 70 °C for 36 hrs.

Table 2-1. Structures of conjugated polyelectrolytes with branched polyionic side chains and GPC analyses for their precursor polymers.

Structure	Acronym	R	Ar	Precursor polymers (GPC) ^a		
				M _n (kDa)	M _w (kDa)	PDI
 <p>R = CO₂⁻ or NH₃⁺</p>	PPE-Ph- ^b CO ₂ ⁻	CO ₂ ⁻		33.2	112.0	3.00
	PPE-BTD- ^b CO ₂ ⁻	CO ₂ ⁻		11.7	16.3	1.40
	PPE-TBT- ^b CO ₂ ⁻	CO ₂ ⁻		16.8	37.8	2.26
	PPE-Ph- ^b NH ₃ ⁺	NH ₃ ⁺		24.1	105.6	4.40
	PPE-BTD- ^b NH ₃ ⁺	NH ₃ ⁺		12.3	44.7	3.60

^a Estimated by GPC (THF), polystyrene standards.

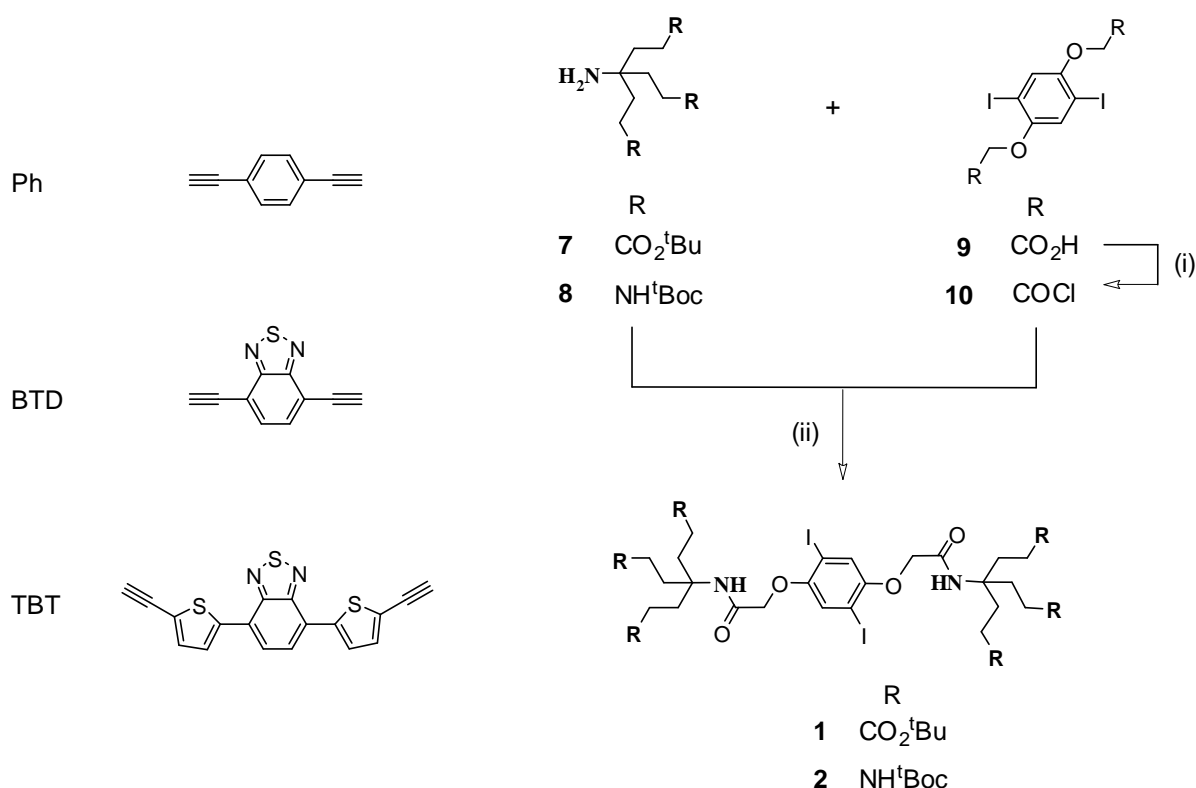


Figure 2-2. Structure of *bis*-ethynylene substituted Ph, BTB, and TBT; synthesis of monomers (1 and 2) (i) SOCl_2 , DMF, reflux for 2 hrs; (ii) TEA, DCM, 25 °C for 24 hrs.

Precursor polymers

For the synthesis of monomers **1** and **2**, anionic bulky functional group **7** and compound **9** were prepared in a good yield as described in the literature,^{11,18,54-55} and cationic bulky functional group **8** was first prepared as depicted in Figure 2-1. Starting from commercially available 4-(2-carboxyethyl)-4-nitroheptanedioic acid (**3**), it was converted to 4-(3-chloro-3-oxopropyl)-4-nitroheptanedioyl dichloride (**4**) in an excellent yield by treating with thionyl chloride (SOCl_2). The latter was then reacted with trimethylsilyl azide to give 3-(2-aminoethyl)-3-nitropentane-1,5-diamine•HCl salt (**5**) in 81% yield. After reacting with 3 equivalents of di-*tert*-butyldicarbonate, compound **6** was obtained in 85% yield. The nitro group in compound **6** was then hydrogenated (60 °C,

100 psi) in the presence of T-1 Raney nickel⁶⁵ to give compound **8** in 93% yield. For the aromatic monomer synthesis, *bis*-ethynylene substituted aromatic units (Ph, BTB, and TBT) were easily synthesized with an excellent yield as described in literatures (Figure 2-2 left).^{16,52-53} Figure 2-2 shows the synthetic route of monomers **1** and **2** which are protected with butyloxycarbonyl (Boc) groups (after deprotection, side chains of **1** and **2** will be negatively and positively charged, respectively). Compound **9** was converted to **10** by chlorination using SOCl₂, which was purified by precipitation with mixture of heptane/toluene (10/1, v/v). Then, reactions of **10** with **7** or **8** afforded monomers **1** and **2** in 76% and 50% yield, respectively. The purity of these monomers was proven by ¹H and ¹³C NMR spectroscopy, elemental analysis, and mass spectrometry.

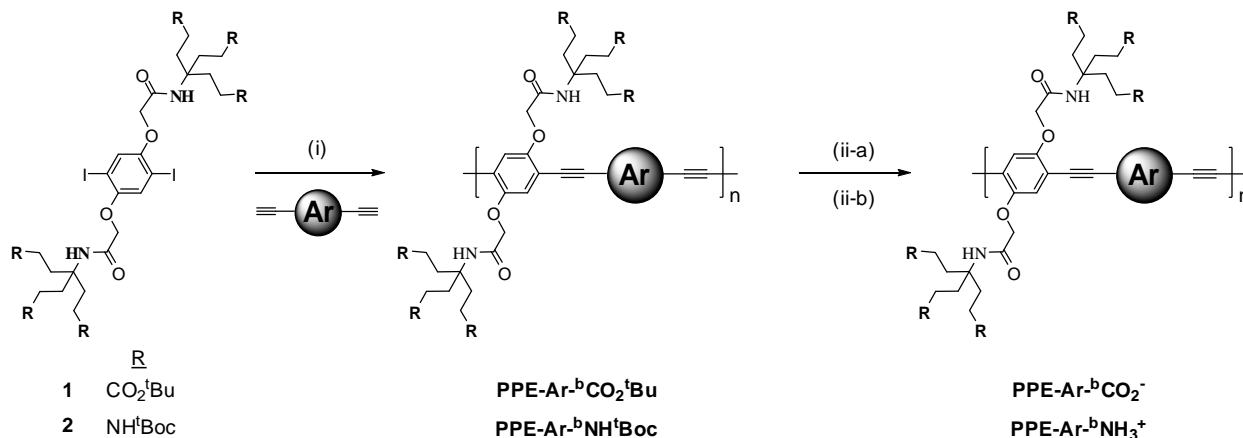


Figure 2-3. Polymerization through precursor route; Ar = Ph, BTB and TBT. (i) Pd(PPh₃)₄, CuI, THF/TEA (3/1, v/v); (ii-a) Ph and BTB: TFA/DCM for anionic polymer, HCl/DMSO for cationic polymer; TBT: ZnBr₂, DCM/H₂O, (ii-b) sat. Na₂CO₃ aqueous solution for anionic polymer, 4 N HCl, dioxane for cationic polymer.

The precursor route for the polymerization was carried out in organic solutions in order to prevent less polymerization by electrostatic repulsion of ionic charged functional groups during polymerization in aqueous media, and the polymer molecular weight was estimated by GPC analysis. As shown in Figure 2-3, all precursor polymers

were synthesized by Sonogashira coupling of a stoichiometric amount of the monomers (**1** or **2**) and a diacetylene aromatic unit using $\text{Pd}(\text{Ph}_3)_4$ and CuI as catalysts in a mixture of THF/TEA (3/1, v/v) with yield of 50-80%. After the reaction was stirred at 60 °C for 24 hours, the organic soluble precursors were isolated as solids and purified by repeated precipitation from THF solution into methanol or hexane. Each polymer was characterized by ^1H NMR spectroscopy. By GPC analysis using polystyrene standards, the number average molecular weight (M_n), weight average molecular weight,¹⁰ and polydispersity of each polymer were listed in Table 2-1.

Hydrolysis of precursor polymers

While the hydrolysis of both precursors for anionic and cationic CPEs was easily accomplished in acidic conditions (TFA/DCM for anionic polymer, HCl/DMSO for cationic polymer), in the case of a CPE having TBT as an aromatic unit, which can be decomposed by acid or basic conditions, mild condition using zinc bromide and water was carried out.⁶⁶ The residues were treated with saturated Na_2CO_3 solution and then purified by dialysis method using 12 kD molecular-weight-cutoff (MWCO) dialysis membranes. The water soluble branched polycationic and anionic side chains attached CPEs were obtained as solids in 90~100% yield.

^1H NMR spectroscopy

Figure 2-4 shows representative ^1H NMR spectra of monomer **1**, the precursor polymer **PPE-Ph-^bCO₂^tBu**, and the water-soluble polymer **PPE-Ph-^bCO₂⁻** (where superscript “b” stands for branched polyionic side chains). Comparison between the spectra of monomer **1** and **PPE-Ph-^bCO₂^tBu** reveals that there is only one new resonance peak at $\delta = 7.58$ ppm, which is assigned to the aromatic protons of 1,4-

phenylene on the polymer backbone. The *tert*-butyl protons appear as a strong singlet at $\delta = 1.42$ ppm in the spectra of monomer **1** and **PPE-Ph-^bCO₂^tBu**.

After hydrolysis, the ¹H NMR spectroscopy of **PPE-Ph-^bCO₂⁻** was accomplished in a mixture of DMSO-*d*₆/D₂O (1/1, v/v). No signals were observed in the 1.4 ~ 1.5 ppm range, indicating that the *tert*-butyl groups were cleaved with an excellent yield (> 95%). The absorption band changes corresponding to carbonyl group in IR spectra also support disappearance of *tert*-butyl groups after deprotection process. The similar phenomenon was also found in other deprotected polymers in which more than 95% of the peak of *tert*-butyl groups disappeared in ¹H NMR and IR spectra.

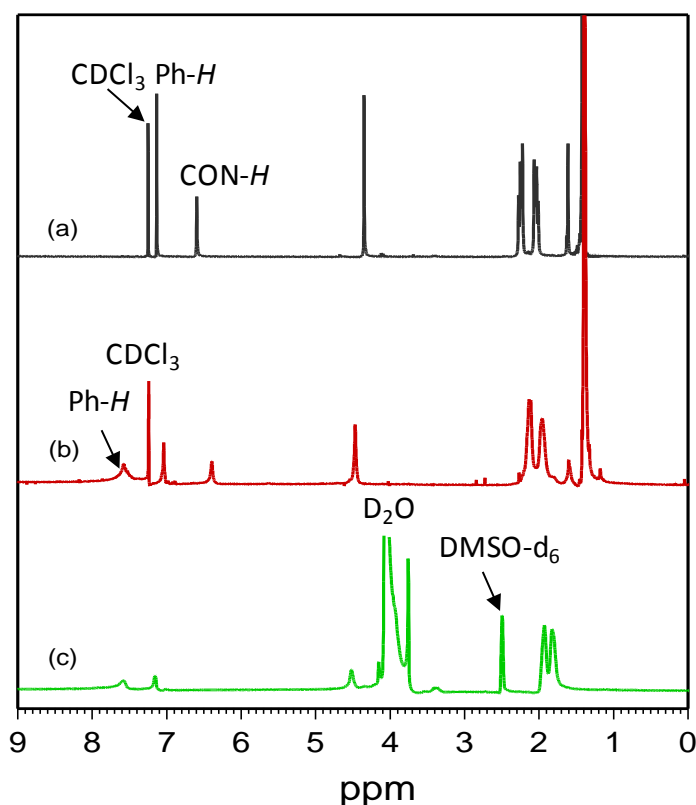


Figure 2-4. ¹H NMR spectra of (a) monomer **1**, (b) **PPE-Ph-^bCO₂^tBu**, and (c) **PPE-Ph-^bCO₂⁻**.

Optical Properties

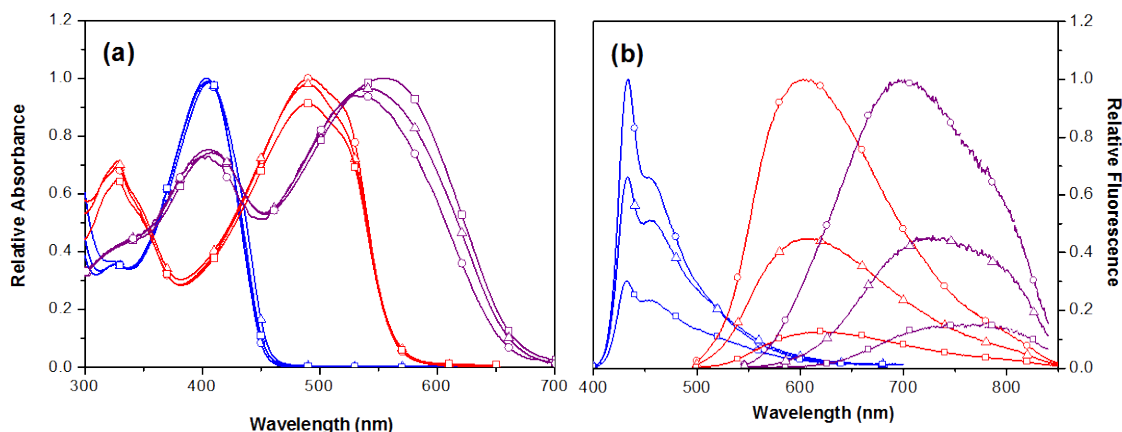


Figure 2-5. (a) Relative absorption and (b) fluorescence emission spectra of **PPE-Ph-^bCO₂⁻** (blue), **PPE-BTD-^bCO₂⁻** (red), and **PPE-TBT-^bCO₂⁻** (purple) in MeOH (○), MeOH/H₂O (1/1, v/v) (Δ), and H₂O (□); [**PPE-Ar-^bCO₂⁻**] = 5 μM.

Table 2-2. UV-Vis absorption and photoluminescent properties of CPEs containing branched carboxylate or ammonium side chains.

	MeOH			H ₂ O		
	$\lambda_{\max}^{\text{abs}}/\text{nm}$	$\lambda_{\max}^{\text{em}}/\text{nm}$	Φ_{PL}	$\lambda_{\max}^{\text{abs}}/\text{nm}$	$\lambda_{\max}^{\text{em}}/\text{nm}$	Φ_{PL}
PPE-Ph- ^b CO ₂ ⁻	403	433	0.31 ^a	404	432	0.12 ^a
PPE-BTD- ^b CO ₂ ⁻	491 530 (sh)	605	0.04 ^b	490 530 (sh)	623	0.007 ^b
PPE-TBT- ^b CO ₂ ⁻	529	698 780 (sh)	0.028 ^b	536	741 780 (sh)	0.004 ^b
PPE-Ph- ^b NH ₃ ⁺	402	432	0.45 ^a	405	432	0.13 ^a
PPE-BTD- ^b NH ₃ ⁺	493	604	0.04 ^b	489 530 (sh)	620	0.004 ^b

^a Coumarin 102 in EtOH as the standard, $\Phi_{\text{FL}}=0.95$. ^b Ru(bpy)₃Cl₂ in H₂O as standard, $\Phi_{\text{FL}}=0.036$ (degassed).

The photophysical properties of CPEs having branched polyanionic and cationic side chains were investigated by UV-Vis spectroscopy and steady state fluorescence measurement in MeOH, MeOH/H₂O (1/1, v/v), and H₂O. Figure 2-5 shows systematically red-shifted UV-Vis absorption and fluorescence spectra of both branched

anionic and cationic side chains attached polymers in the order Ph < BTD < TBT in all solutions (MeOH, MeOH/H₂O (1/1, v/v), and H₂O), respectively. Figure 2-6 illustrates the visual and fluorescence colors of branched anionic side chains attached CPEs as variation of the HOMO-LUMO band gap of the polymers; visual and fluorescence color: pale yellow, bright blue for **PPE-Ph^bCO₂⁻**; red, bright red for **PPE-BTD^bCO₂⁻**; purple, dark purple for **PPE-TBT^bCO₂⁻** (for **PPE-Ar^bNH₃⁺**, see Figure A-1 in the Appendix A).

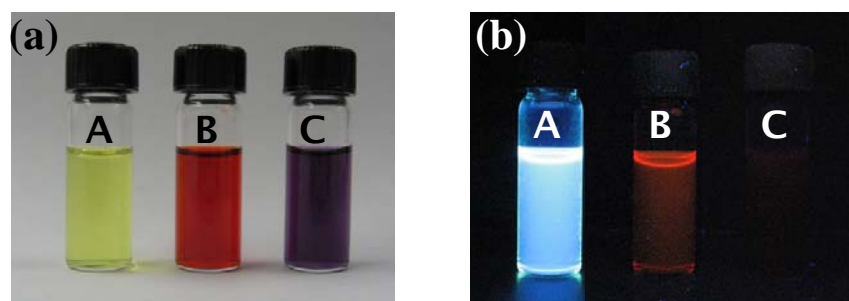


Figure 2-6. (a) Visual and (b) Fluorescence colors of A: **PPE-Ph^bCO₂⁻**, B: **PPE-BTD^bCO₂⁻**, and C: **PPE-TBT^bCO₂⁻**; [**PPE-Ar^bCO₂⁻**] = 30 μ M in H₂O.

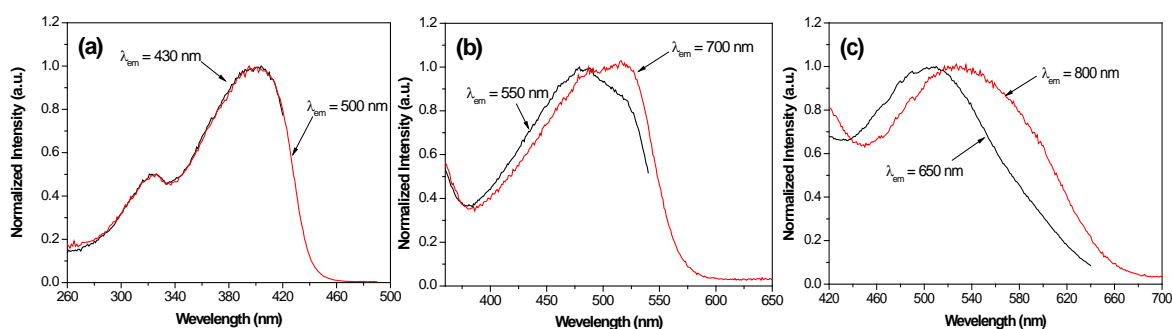


Figure 2-7. Excitation spectra of (a) **PPE-Ph^bCO₂⁻** at 430 and 500 nm; (b) **PPE-BTD^bCO₂⁻** at 550 and 700 nm; (c) **PPE-TBT^bCO₂⁻** at 650 and 800 nm; [**PPE-Ar^bCO₂⁻**] = 5 μ M in MeOH.

In MeOH, **PPE-Ph^dCO₂⁻** exhibited an absorption maximum at 403 nm and a fluorescence emission maximum at 433 nm, and its counterpart CPE, **PPE-Ph^bNH₃⁺**, showed almost similar wavelength maximum ($\lambda_{\text{abs}} = 402$ nm and $\lambda_{\text{em}} = 432$ nm) in both spectra (see Table 2-2). These wavelength maxima in the UV-Vis absorption spectra

were hypsochromically shifted (around 15 to 22 nm shifted) compared to that of **PPE-CO₂⁻** or **PPE-SO₃⁻** which has the same conjugated backbone but has linear side chains (less bulky than branched side chains).^{10,67-68} Since the degree of polymerization (DP) for both **PPE-Ph-^bCO₂⁻** and **PPE-Ph-^bNH₃⁺** is larger than 10 (approximately 20 arylene ethynylene units), we believe that the coplanarity of the CPEs' backbone was disturbed by the increased electronic repulsion between the branched side chains compared to that in **PPE-CO₂⁻** in MeOH, resulting in hypsochromic shift in the UV-Vis absorption spectra. In fluorescence emission spectra, however, there is a negligible wavelength difference between **PPE-Ph-^bCO₂⁻**, **PPE-Ph-^bNH₃⁺** and **PPE-CO₂⁻**. This lack of energy difference in the fluorescence emission indicates that regardless of the state of the CPEs' backbone, singlet excitons migrate to the lowest energy level in the excited state by an energy transfer process. Similar to branched polyionic side chains attached PPE-Ph series, in MeOH, UV-Vis absorption maxima of **PPE-BTD-^bCO₂⁻** ($\lambda_{\text{max}}^{\text{abs}} = 491 \text{ nm}$) and **PPE-BTD-^bNH₃⁺** ($\lambda_{\text{max}}^{\text{abs}} = 493 \text{ nm}$) respectively showed around 23 and 21 nm hypsochromic shifts compared to that of **PPE-BTD-SO₃⁻**, while the emission spectra of **PPE-BTD-^bCO₂⁻** ($\lambda_{\text{max}}^{\text{em}} = 605 \text{ nm}$) and **PPE-BTD-^bNH₃⁺** ($\lambda_{\text{max}}^{\text{em}} = 604 \text{ nm}$) displayed similar wavelength maxima to **PPE-BTD-SO₃⁻** or **PPE-BTD-(4+)**.¹⁰ These observations support the fact that the polymer's optical properties are mainly determined by the structure of the π -conjugated backbone. Unfortunately, for **PPE-TBT-^bCO₂⁻** we could not compare the optical properties to its counterpart having linear side chains even though this polymer is structurally different from others: there is longer distance between phenyl groups caused by introducing large size of TBT in **PPE-TBT-^bCO₂⁻**, which may reduce the electronic repulsion between branched side chains. However, as seen in Figure 2-5

we could observe the wavelength maximum at 698 with the shoulder band around 780 nm in the fluorescence spectrum, thereby indicating that even in MeOH solution there is already a small fraction of aggregated chains which differ from other branched side chains attached CPEs having Ph or BTD backbones. Although we could not observe the “shoulder like” band in UV spectrum, in MeOH its excitation spectra ($\lambda_{em} = 650$ nm and $\lambda_{em} = 800$ nm) clearly showed that aggregates exist in the ground state (Figure 2-7c). On the other hand, no big difference was observed in the excitation spectra of **PPE-Ph-^bCO₂⁻** ($\lambda_{em} = 430$ nm and $\lambda_{em} = 500$ nm) and **PPE-BTD-^bCO₂⁻** ($\lambda_{em} = 550$ nm and $\lambda_{em} = 700$ nm) as seen in Figure 2-7a and 2-7b, respectively. This implies little or no aggregation in the ground state.

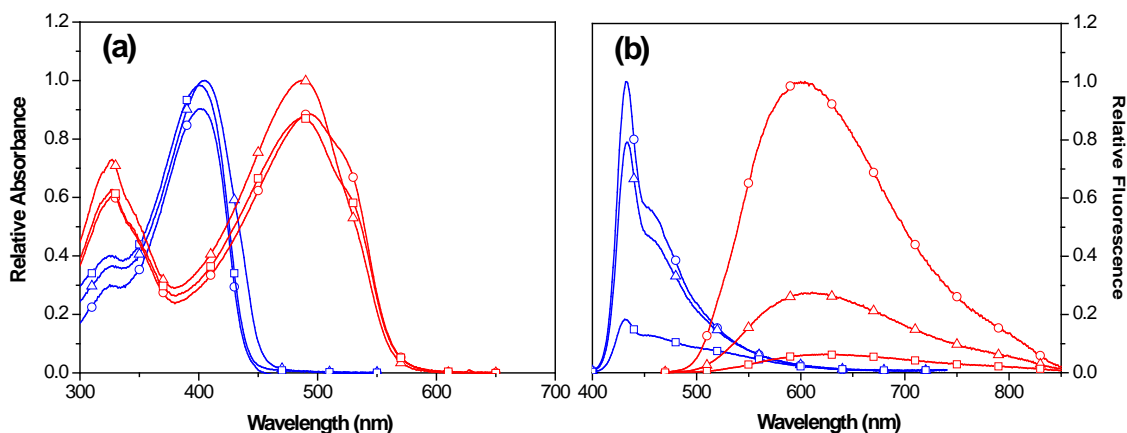


Figure 2-8. (a) Relative absorption and (b) fluorescence emission spectra of **PPE-Ph-^bNH₃⁺** (blue) and **PPE-BTD-^bNH₃⁺** (red) in MeOH (○), MeOH/H₂O (1/1, v/v) (Δ), and H₂O (□); [**PPE-Ar-^bNH₃⁺**] = 5 μM.

The effect of branched side chains has been widely investigated through the UV-Vis absorption and fluorescence emission changes in the presence of a relatively poor solvent to a good solvent (MeOH, MeOH/H₂O (1/1, v/v), and H₂O). In our previous studies, **PPE-SO₃⁻** and **PPE-CO₂⁻**, CPEs with linear anionic side chains, revealed strongly solvent dependent optical properties.^{10,68} In MeOH, the UV-Vis absorption and

fluorescence emission spectra displayed structurally analogous spectra with precursor polymer which exists as an unaggregated or less aggregated monomeric state. On the other hand, in aqueous solution it is believed that both polymers are strongly aggregated, showing a relatively red-shifted UV-Vis absorption spectrum with a shoulder band and an “excimer like” band in fluorescence emission spectra; this was concluded as the result of coplanarization of the backbones induced by strong aggregation.⁶⁹ As seen in Figure 2-5 and 2-8, however, **PPE-Ph-^bCO₂⁻** and **PPE-Ph-^bNH₃⁺** showed subtle wavelength changes in both UV/Vis absorption and fluorescence emission spectra as increasing volume fraction of H₂O. It is only observed that the fluorescence quantum yield is moderately reduced. In addition, we could not find any shoulder band which **PPE-SO₃⁻** and **PPE-CO₂⁻** revealed in the UV-Vis absorption spectra. Moreover, the shapes of all the spectra were almost similar to those of their precursor polymer (Figure 2-9). This observation suggests that unlike CPEs which have linear side chains, **PPE-Ph-^bCO₂⁻** and **PPE-Ph-^bNH₃⁺** is possibly less aggregated even in H₂O solution because of their torsional strains induced by electrostatic repulsion between branched side chains.

For branched side chains attached CPEs having BTB unit, **PPE-BTD-^bCO₂⁻** and **PPE-BTD-^bNH₃⁺** reveal slightly decreased absorption spectra as increasing H₂O ratio, and their fluorescence emission was gradually diminished and a little bit bathochromically shifted (18 and 16 nm, respectively). According to previous report, it is well known that tight π - π stacking or aggregation gives rise to a huge red-shift (>30 nm) in both absorption and fluorescence emission spectra.^{17,70} Our research group reported a similar result that **PPE-BTD-SO₃⁻** showed more than 40 nm red-shifted absorption and

fluorescence emission maxima.¹⁰ In addition, another previous studies revealed that relatively modest red-shifts (<20 nm) in both UV-Vis absorption and fluorescence spectra might be caused by the planarization of the conjugated backbone.¹⁸ In present study, however, negligible wavelength changes were observed in UV-Vis absorption spectra. These observations suggest that **PPE-BTD-^bCO₂⁻** and **PPE-BTD-^bNH₃⁺** disfavor strong aggregation in aqueous solution which is attributed to electrostatic repulsion as seen in branched side chains attached CPE-Ph series. Also, the red-shift in fluorescence spectra is possibly due to the intramolecular charge transfer (ICT) effect between Ph (donor) and BTB (acceptor) in the excited state. It is notified that such solvatochromism is typical in donor-acceptor type molecule.⁷¹ Accordingly, we propose that the branched side chains attached CPEs having BTB backbones may retain their monomeric characteristics in aqueous solution as a result of minimal polymer π - π aggregation. This less aggregation of CPEs having Ph or BTB conjugated backbones is also supported by comparison of the quantum yield with CPEs having linear side chains (Table 2- 2). The quantum yields of the branched side chains attached CPEs were relatively higher (1.3 ~ 21-fold) than those of CPEs having linear side chains in both MeOH and H₂O. Furthermore, the increase of quantum yield of CPEs was stronger in H₂O. Such increased quantum yield might be due to less aggregation caused by electrostatic repulsion between branched side chains.^{10,67-68}

In contrast to branched side chains attached CPEs with Ph or BTB, the UV/Vis absorption and fluorescence spectra of **PPE-TBT-^bCO₂⁻** were significantly shifted to the red region by 29 nm and 43 nm, respectively, with increasing volume fraction of H₂O as seen in Figure 2-5. In addition, its fluorescence intensity was gradually decreased and

the shoulder band was relatively enforced at 780 nm which became the fluorescence maximum in aqueous solution. These might be ascribed to the following possible two reasons: first, the charge-transfer character in the excited state led to bathochromical shift in fluorescence spectra as H₂O fraction increases. It is well known that the BTB group acts as a strong electron acceptor while phenyl- π -thiophene is electron donor, which gives rise to charge separation in the excited state, and this charge separation is more pronounced in **PPE-TBT-^bCO₂⁻** than phenyl-BTB system (e.g. **PPE-BTB-^bCO₂⁻** and **PPE-BTB-^bNH₃⁺**) in high polar solvent.⁷² Second, the shoulder broad band at 780 nm is presumably “exciplex like” band induced by hydrophobic inter-chain interaction between Ph and TBT groups. The bathochromic shift with increased volume fraction of H₂O in absorption spectrum also supports the aggregation characteristic of **PPE-TBT-^bCO₂⁻**.¹⁶ It is possible that longer distance between phenyl groups caused by introducing TBT may reduce the electronic repulsion between branched side chains. Also, the incorporation of TBT group increases the hydrophobic character of the polymer. The similar result was found in our previous research in which **PPE-CO₂⁻** having cofacial factor (additional phenyl group between side functional group substituted phenyl units) displayed alternative type aggregation, showing dominant excimer-like emission in the fluorescence spectrum over **PPE-CO₂⁻** without additional phenyl group.^{58,68,73} Therefore, on the basis of spectral changes of the branched side chains attached CPE series having Ph, BTB, and TBT, we propose that less aggregation is dominant in the case of aromatic units (Ph and BTB) in relatively small size while affordable hydrophobic interaction induced by cofacial factors (e.g. TBT-Ph system) is more considerable in polymer aggregation.

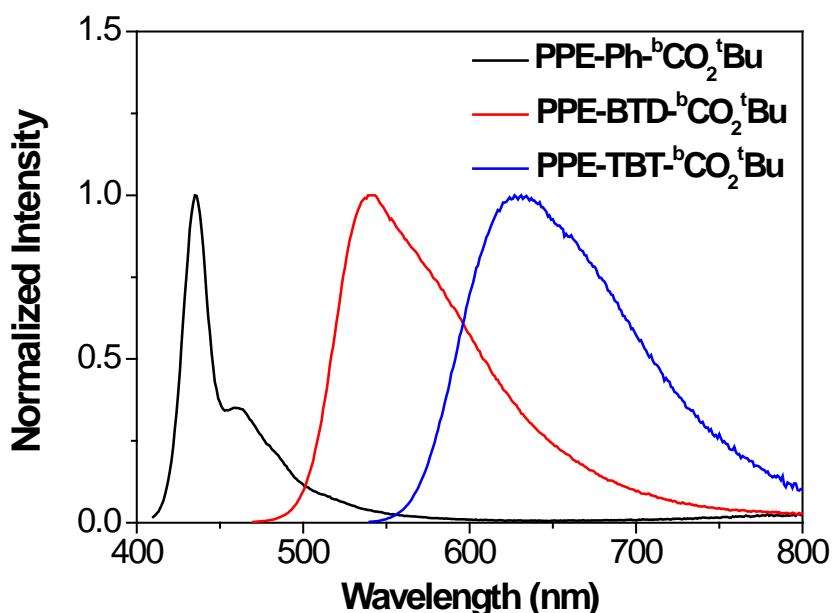


Figure 2-9. Fluorescence emission spectra of precursors of branched anionic CPEs in THF; [PPE-Ar-^bCO₂⁻] = 5 μM; Ar = Ph (black), BTD (red), and TBT (blue).

pH-Dependent Aggregation

In several previous investigations of water soluble anionic CPEs, low pH induced different levels of aggregation and energy transfer behavior as a result of the decreased electronic repulsion between side chains caused by the protonation of anionic charged functional group, while the cationic ones react the opposite way.^{40,58,62} So, we believe that controlling pH of the solution would influence the optical properties of CPEs having branched anionic or cationic side chains. We observed that **PPE-Ar-^bCO₂⁻** and **PPE-Ar-^bNH₃⁺** reveal strongly pH dependent optical properties in the UV-Vis absorption and fluorescence emission spectra. The pH of aqueous solution was adjusted with HCl and/or NaOH using a pH meter. These conditions encouraged their aggregation or disaggregation, controlling the repulsion of charged side chains.

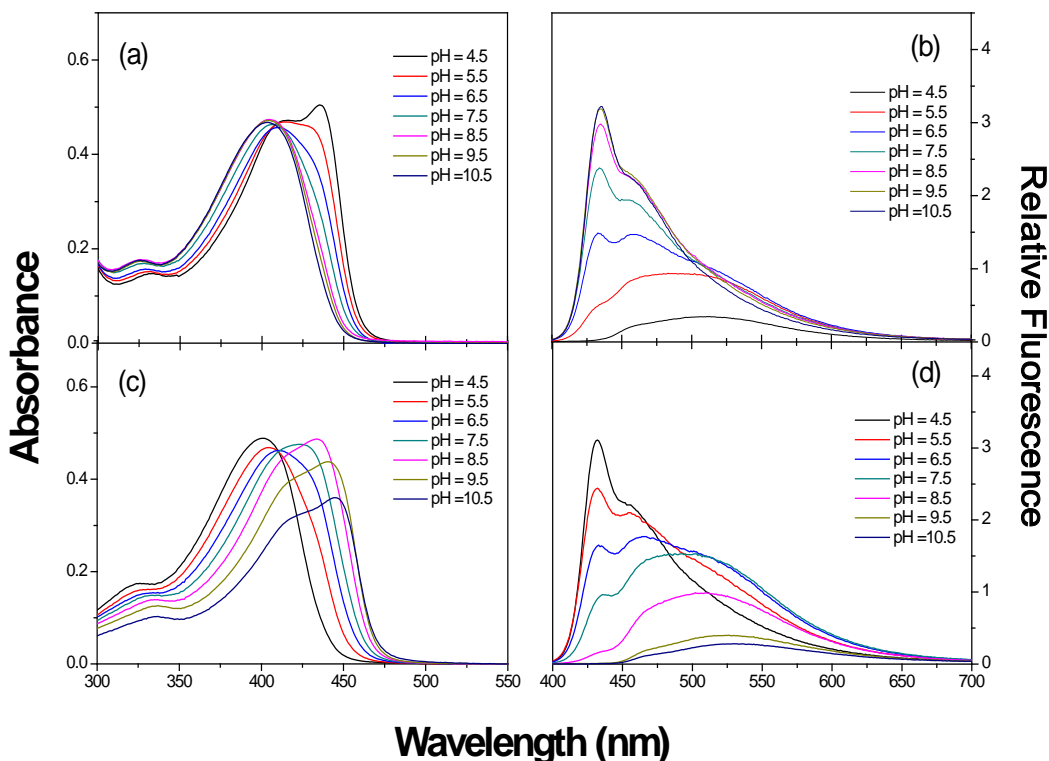


Figure 2-10. Absorption and fluorescence emission spectra of (a, b) **PPE-Ph-^bCO₂⁻** and (c, d) **PPE-Ph-^bNH₃⁺** as pH changes in aqueous solution; [**PPE-Ph-^bCO₂⁻** or **^bNH₃⁺**] = 5 μ M.

Figure 2-10 shows the absorption and emission spectra of **PPE-Ph-^bCO₂⁻** and **PPE-Ph-^bNH₃⁺** in aqueous solution as a function of pH. At pH 10.5 the absorption spectra of **PPE-Ph-^bCO₂⁻** showed one band maximized at 404 nm and the emission showed a well-defined emission at 435 nm. As the pH decreases, its absorption spectra showed bathochromic shift with strong shoulder band at 435 nm and the fluorescence emission displays “excimer like” band at 515 nm (pH 4.5) concomitant with fluorescence quenching. Based on many research groups’ reports about these characteristics, we conclude that these optical behaviors imply the aggregation of CPE in acidic conditions (pH 4.5).^{58,62} This is ascribed to conformational change of CPE backbone. As pH decreases from 10.5 to 4.5, phenylene ethynylene groups tend to be less twisted in

CPE backbone because electrostatic repulsion between the protonated carboxylate side chains could be minimized. Moreover, the de-solvation effect of the neutral and hydrophobic CPE leads to the planarization of the conjugated backbone.

It is also very important to note that the series of absorption spectra define an isosbestic point at 410 nm, suggesting that the pH-induced change is between two distinct types of chromophores, which are probably the neutral and charged segments. Unlike **PPE-Ph-^bCO₂⁻**, positively charged CPE, **PPE-Ph-^bNH₃⁺**, showed opposite tendency. That is, we found aggregation behavior of **PPE-Ph-^bNH₃⁺** at high pH (pH 10.5) and it retains monomeric characteristic at low pH (pH 4.5). Especially, in this CPE, we found that a significant decrease occurs in the UV-Vis absorption spectra when the pH reaches around 9.5. This probably indicates that CPE is slightly precipitated at this point.

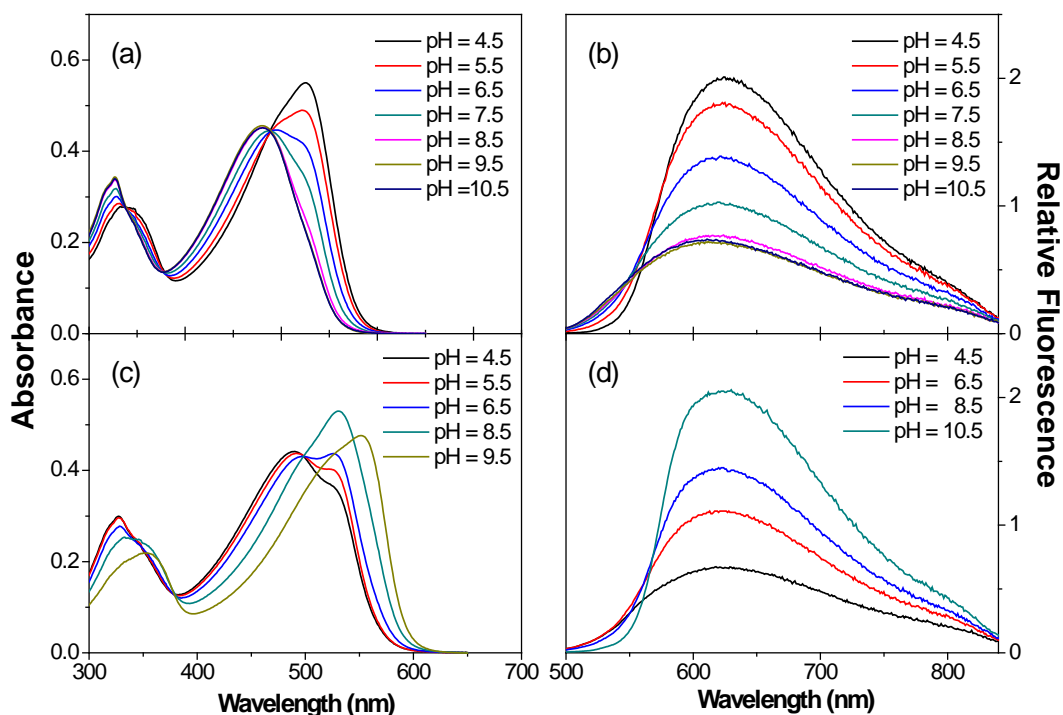


Figure 2-11. Absorption and fluorescence emission spectra of (a, b) **PPE-BTD-^bCO₂⁻** and (c, d) **PPE-BTD-^bNH₃⁺** as pH changes in aqueous solution; [**PPE-Ar-^bCO₂⁻** or **^bNH₃⁺**] = 5 μ M.

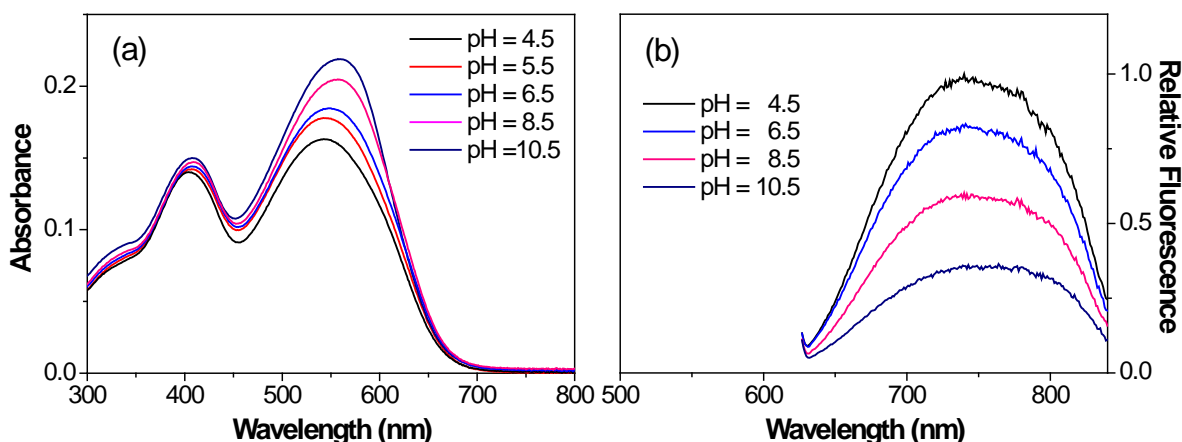


Figure 2-12. (a) Absorption and (b) fluorescence emission spectra of **PPE-TBT-^bCO₂⁻** as pH changes in aqueous solution; [**PPE-TBT-^bCO₂⁻**] = 5 μM.

The pH dependent absorption and emission changes of **PPE-BTD-^bCO₂⁻** and **PPE-BTD-^bNH₃⁺** are shown in Figure 2-11. In the absorption spectra, similar changes to **PPE-Ph-^bCO₂⁻** and **PPE-Ph-^bNH₃⁺** were observed. However, unexpected behavior compared to CPEs having Ph backbone was observed in the emission spectra. The emission band of **PPE-BTD-^bCO₂⁻** was narrow and gradually increased in intensity when the pH decreased. At pH = 4.5, more than 3-fold enhancement of fluorescence emission intensity was observed at 640 nm (Figure 2-11b). This phenomenon was also found by Bazan et al., in which aggregated CPEs having BTD and fluorine-phenylene units as a conjugated backbone caused fluorescence intensity enhancement. This is due to the result of shielding effect from water within the aggregate structure.⁶² Interestingly, we found that the similar appearance was also observed in the fluorescence emission spectra of **PPE-BTD-^bNH₃⁺** under basic conditions (pH = 10.5) (Figure 2-11d). This observation makes it clear that the fluorescence enhancement of aggregated CPEs is not due to the photophysical changes of the CPEs' backbone affected by acidic or basic conditions. As a result, we propose that one possible reason

for this enhancement in fluorescence intensity may be less water contact effect of conjugated backbone induced by aggregation as suggested previously in Bazan and co-workers' report.⁶² Like CPEs having BTB units, when the BTB group was replaced by a TBT unit, **PPE-TBT-^bCO₂⁻** showed a bathochromic shift in the UV/Vis absorption spectra and displayed fluorescence enhancement as the pH decreases from 10.5 to 4.5 as seen in Figure 2-12. In addition, the enhancement of fluorescence intensity was similar to those of CPEs having a BTB unit. However, the UV/Vis absorption spectrum exhibited hypsochromic shift by 16 nm. For this observation, we propose that the blue shift in acidic condition was likely a result of the slightly increased torsional conformation of the monomeric units when **PPE-TBT-^bCO₂⁻** approaches closely, but it is true that the aggregation obviously controls considerable emission efficiency.

Fluorescence Lifetime Spectroscopy

To gain more insight into the photophysical properties of the CPEs with branched polyionic side chains, pH dependent behaviors of branched side chains attached CPEs were studied by a fluorescence lifetime measurement based on the solvent polarity and pH changes. As seen in Table 2-3, all the CPEs showed relatively complicated multi-exponential lifetimes, which is attributed to the existence of non-specific interaction between CPEs and/or to unexpected results caused by the polydispersity in the polymer chain length. Therefore, we focus on the highly dominant fluorescence lifetime decays over contribution of amplitudes. For two CPEs having cationic side chains, the fluorescence lifetime decays under acidic or basic conditions showed almost opposite tendencies to their anionic counterpart (see Table A-1 in the Appendix A). Therefore, we only present lifetime results for CPEs having anionic carboxylate side chains.

Table 2-3. Fluorescence lifetimes (τ_i , ns) and relative amplitudes (RA, %) for **PPE-Ar-^bCO₂⁻** in MeOH, basic (pH = 9.0), and acidic (pH = 4.5) conditions^a

Compd.	MeOH			H ₂ O, pH 9.0			H ₂ O, pH 4.5		
	τ_i (ns) ^b	RA (%)		τ_i (ns)	RA (%)		τ_i (ns)	RA (%)	
PPE-Ph- ^b CO ₂ ⁻		430 nm	500 nm		430 nm	500 nm		430 nm	500 nm
	$\tau_1 = 0.21$	32	17	$\tau_1 = 0.08$	55	36	$\tau_1 = 0.25$	94	54
	$\tau_2 = 0.52$	64	70	$\tau_2 = 0.23$	42	52	$\tau_2 = 1.30$	5	24
	$\tau_3 = 1.76$	3	11	$\tau_3 = 1.29$	2	6	$\tau_3 = 4.57$	<1	22
	$\tau_4 = 4.67$	<1	<2	$\tau_4 = 4.19$	<1	<6			
	χ^2	0.977	1.068	χ^2	1.016	1.112	χ^2	1.173	1.042
PPE-BTD- ^b CO ₂ ⁻	τ_i (ns)	600 nm	650 nm	τ_i (ns)	600 nm	650 nm	τ_i (ns)	600 nm	650 nm
	$\tau_1 = 0.27$	34	28	$\tau_1 = 0.17$	92	93	$\tau_1 = 0.25$	58	59
	$\tau_2 = 0.92$	48	47	$\tau_2 = 1.11$	6	4	$\tau_2 = 0.92$	41	39
	$\tau_3 = 2.38$	18	25	$\tau_3 = 5.10$	<2	<3	$\tau_3 = 5.20$	1	<2
	χ^2	1.105	1.143	χ^2	1.112	1.273	χ^2	1.243	1.153
PPE-TBT- ^b CO ₂ ⁻	τ_i (ns)	650 nm	700 nm	τ_i (ns)	700 nm	>700 nm	τ_i (ns)	700 nm	>700 nm
	$\tau_1 = 0.12$	17	68	$\tau_1 = 0.14$	87	86	$\tau_1 = 0.16$	75	81
	$\tau_2 = 1.05$	51	23	$\tau_2 = 0.75$	1	10	$\tau_2 = 0.62$	6	15
	$\tau_3 = 3.55$	32	9	$\tau_3 = 3.46$	12	4	$\tau_3 = 3.25$	19	<4
	χ^2	1.234	1.185	χ^2	1.099	1.080	χ^2	1.223	1.054

^aData were collected by global fitting Algorithm. ^bTypical limits of error on τ_i are less than $\pm 3\%$.

At pH 9.0, **PPE-Ph-^bCO₂⁻** featured relatively wavelength independent fluorescence decays, and two fast components ($\tau_1 = 80$ and 230 ps) were dominant (RA > 88%) when the emission decays were monitored at 430 or 500 nm, which were very similar to that observed in MeOH ($\tau_1 = 210$ and $\tau_2 = 520$ ps), but the lifetimes at pH 9.0 were faster than those in MeOH. On the other hand, the lifetimes became wavelength-dependent at pH 4.5, in which short-lived lifetime ($\tau_1 = 250$ ps) is over 90% at 430 nm whereas at 500nm, the relative amplitude of long-lived lifetimes ($\tau_2 = 1.30$ ns and $\tau_3 = 4.57$ ns) become 46%. These observations support the fact that the aggregation of **PPE-Ph-^bCO₂⁻** is minimized at pH 9.0 with repulsion between side chains but is more pronounced in acidic condition (pH 4.5). The similar results of lifetime changes were found in the studies on the aggregation of CPEs having linear side chains, in which the lifetimes were wavelength-dependent, and the amplitude of the long-lived component ($\tau > 3$ ns) became larger in aqueous solution.¹⁰

For **PPE-BTD-^bCO₂⁻**, when emission decay was monitored at 600 or 650 nm, relatively short-lived lifetimes ($\tau_1 = 270$ and $\tau_2 = 920$ ps) was over 75% in MeOH. Also, lifetime decay of $\tau_1 = 170$ ps was mostly dominant (> 90 %) at pH 9.0, which is likely due to rapid decay of the charge transfer state in the polar solvent. These results propose that less aggregation occurs in both MeOH and basic conditions (pH = 9.0). At pH 4.5, however, when the lifetime components were compared to those at pH 9.0, the amplitudes of $\tau_1 = 250$ ps decreased from around 90 to 60% while those of 920 ps, which is also relatively short-lived lifetime, increased from around 5 to 40% at both 600 and 650 nm. Also, although the amplitude is very small, long-lived lifetime ($\tau_3 = 5.20$ ns) exists (around 1%). In addition, we found that these lifetimes reveal wavelength-

independent tendencies. This increased amplitude of $\tau_2 = 920$ ps is attributable to the distinctive characteristic of **PPE-BTD-^bCO₂⁻** via fluorescence enhancement in low pH conditions, and small amplitude of $\tau_3 = 5.20$ ns is probably due to the presence of very weak fluorescence of “exciplex like” emission in aggregate states.¹⁰ The similar results for **PPE-TBT-^bCO₂⁻** were obtained in aqueous solution (pH 4.5 and 9.0, respectively). Interestingly, the wavelength dependent lifetime decay was observed in MeOH. At short wavelength (monitored at 650 nm), large amplitude of long-lived component ($\tau_3 = 3.55$ ns) was observed ($\tau_3 > 30\%$) whereas short-lived component ($\tau_1 = 120$ ps) was less than 20 %. In comparison with CPEs having Ph and BTD, **PPE-TBT-^bCO₂⁻** is in strong donor-acceptor structure which may produce long-lived charge transfer state in the excited state of the CPE. In this regard, this charge transfer state should return to the ground state very slowly.⁷⁴ However, when monitored at 700 nm, short-lived component ($\tau_1 = 120$ ps) became dominant (around 68%) and contribution of long-lived one ($\tau_3 = 3.55$ ns) decreases to less than 10%. This result indicates that even in MeOH aggregation of **PPE-TBT-^bCO₂⁻** exists at the long wavelength ranges (> 700 nm), which comes from rapid quenching effect of the interchain exciton. We could find similar phenomenon in lifetime results of precursor polymer (**PPE-TBT-^bCO₂^tBu**) where lifetime from non-aggregated state of **PPE-TBT-^bCO₂^tBu** showed a large fraction (around 80%) of the long-lived component ($\tau = 2.33$ ns) in THF. Furthermore, we could not find large fraction of short-component ($\tau < 1$ ns) at entire wavelength, indicating that no aggregation exists in THF. In other words, **PPE-TBT-^bCO₂⁻** is slightly aggregated in MeOH, showing the short-lived component at all wavelength.

Summary and Conclusions

In this Chapter, we have prepared a new class of CPEs with Ph, BTB, or TBT aromatic units featuring branched anionic ($R-^b\text{CO}_2^-$) or cationic ($R-^b\text{NH}_3^+$) side chains. The polymerization was carried out with a precursor route in a mixture of THF and Triethylamine using Sonogashira coupling reaction. Hydrolysis of the precursor polymers was completed in either acidic condition for Ph and BTB units or mild condition using $\text{ZnBr}_2/\text{H}_2\text{O}$ for a TBT unit, which was followed by a solubilization process into water solution using saturated Na_2CO_3 solution for the anionic polymers and 4 N HCl solution for the cationic polymers. Varying the structure of arylene units in conjugated backbones caused the variation of the HOMO-LUMO band gap of the polymers, showing clearly different visual and fluorescence colors. The photo-physical properties data suggested that the branched anionic and cationic CPEs with Ph and BTB backbones show less aggregation in aqueous solution, resulting in higher quantum yields than all other CPEs with linear side chains. However, **PPE-TBT- $^b\text{CO}_2^-$** showed aggregated aspect in both MeOH and aqueous solution. Probably, this is due to less electrostatic repulsion between side chains induced by the size effect of an arylene unit of the conjugated backbone, which may cause alternative type aggregation. In this case, we observed the red-shift in UV/Vis absorption spectra, and more pronounced ICT effect in aqueous solution particularly led to the significant red-shift emission in fluorescence spectra. In addition, “exciplex type” band strongly suggested inter-chain interaction between polymer backbones. The pH dependent spectral changes of all CPEs having branched anionic or cationic side chains clearly showed their photo-physical behaviors in both acidic and basic conditions. **PPE-Ph-X** ($X = ^b\text{CO}_2^-$ or $^b\text{NH}_3^+$) showed red-shift in UV/Vis absorption spectra at either pH 4.5 for the anionic side chain

or pH 10.5 for the cationic one and displayed strong “excimer type” band with less efficient fluorescence as the polymers aggregate. On the other hand, monomeric characteristics in both UV/Vis absorption and fluorescence spectra were retained at their opposite pHs (pH = 10.5 for anionic side chain, pH = 4.5 for cationic one). For **PPE-BTD-X**, we obtained attractive result that aggregation may induce fluorescence enhancement. In addition, the similar result could be also found in the fluorescence spectra of **PPE-TBT-^bCO₂⁻**. We proposed that the aggregation of these CPEs reduces water contact of conjugated backbone via decreasing nonradioactive relaxation processes. Particularly, observed blue shift in UV/Vis absorption spectra of **PPE-TBT-^bCO₂⁻** as the pH decreases revealed the new insight that conjugated polymer backbone could be twisted form rather than co-planar one in the aggregated state.

The lifetime measurement provides concrete evidence that changing the pH of CPEs having branched side chains in aqueous solution controls the degree of aggregation. The branched anionic CPEs having Ph and BTD backbones exhibited wavelength independent lifetime and showed predominant short-lived lifetimes ($\tau < 1$ ns) in MeOH and pH 9.0. At pH 4.5, **PPE-Ph-^bCO₂⁻** revealed long-lived lifetimes ($\tau = 1.30$ and 4.57 ns) more than 68%. For **PPE-BTD-^bCO₂⁻**, the extremely long-lived lifetime ($\tau > 5.00$ ns) and dominant lifetime of 920 ps indicated that aggregated polymers exist and their fluorescence intensity increases in acidic condition, respectively. The photo-physical behaviors of **PPE-TBT-^bCO₂⁻** in acidic and basic conditions showed similar results to those of **PPE-BTD-^bCO₂⁻**. Interestingly, lifetime of **PPE-TBT-^bCO₂⁻** was wavelength dependent in MeOH. However, more amplitude long-lived lifetime ($\tau = 3.55$, 32%) of **PPE-TBT-^bCO₂⁻** is seen at short wavelength (650 nm) while more amplitude

short-lived one ($\tau = 0.12$, 68%) showed at long wavelength (700 nm). This result is believed to arise because the long-lived charge transfer state exists in this system, which causes dominant long-lived lifetime decay. Furthermore, unlike **PPE-BTD-^bCO₂⁻**, predominant short-lived lifetimes ($\tau = 0.12$, 68%) of **PPE-TBT-^bCO₂⁻** over 700 nm revealed that aggregation exists in MeOH.

Experimental

Materials

All chemicals used in the synthesis were of reagent grade and used without further purification. T-1 Raney nickel, *tert*-butylacrylate, copper iodide, 2-bromoacetic acid, thionyl chloride, 4-(2-carboxyethyl)-4-nitroheptanedioic acid, azidotrimethylsilane, di-*tert*-butyl dicarbonate, triethylamine, tetrakis(triphenylphosphine)palladium (0), and diisopropylamine were purchased from Sigma-Aldrich Chemical Company. Iodine, nitromethane, hydroquinone, and sodium carbonate were bought from Fisher Scientific Company. Zinc bromide was obtained from Acros Chemical Company. THF and DMF were purified by solvent dispensing system (SDS). Silica gel (Merck, 230-400 mesh) was used for chromatographic purification of all of intermediate and target molecules. All other chemicals and solvents were purchased from Sigma-Aldrich, Fisher Scientific, or Acros Chemical Company and used as received.

Instrumentation and Methods

NMR spectra were recorded using a Varian VXR-300 FT NMR, operating at 300 MHz for ¹H NMR and at 75 MHz for ¹³C NMR. Gel permeation chromatography (GPC) analyses were carried out on a system comprised of a Rainin Dynamax SD-200 pump, Polymer Laboratories PL gel mixed D columns, and a Beckman Instruments Spectroflow 757 absorbance detector. Polystyrene standards were used for molecular

weight calibration. UV/Vis absorption spectra were recorded using a Varian Cary 50 Spectrophotometer. Steady-state fluorescence spectra were obtained with a PTI fluorometer. Lifetime measurements were carried out using a PicoQuant FluoTime 100 Compact Fluorescence Lifetime Spectrometer. A 1 cm quartz cuvette was used for all spectral measurements.

Stock solutions (1.0 mM) of all of the CPEs were prepared in H₂O and have been stored at 0 °C. The solutions have been kept at the room temperature for one hour before use. The excessive exposure of the stock solution to the room temperature caused slight polymer aggregation in both CH₃OH and H₂O solutions: the aggregation was detected by excitation measurement at different wavelength, but no definite aggregation was observed in fluorescence emission spectra (no considerable excimer type band). However, this slight aggregation can be overcome by addition of catalytic amount of NaOH.

Fluorescence quantum yield are reported relative to known standards (coumarin 102, $\Phi = 0.95^{75}$ in EtOH; Ru(bpy)₃Cl₂, $\Phi = 0.036^{76}$ in H₂O). The pH of aqueous solution was adjusted with HCl and/or NaOH using a Corning pH meter 320.

Synthetic Procedures

Compounds **7** and **9** were prepared in a good yield as described in the literature.³

4-(3-Chloro-3-oxopropyl)-4-nitroheptanedioyl dichloride (4). A 100 mL round bottom flask was charged with 4.44 g of 4-(2-carboxyethyl)-4-nitroheptanedioic acid (**3**) (16.0 mmol) and 30 mL of thionyl chloride (SOCl₂). Two drops of DMF was added to the suspension and the mixture was then slowly heated up to reflux. After 1 hour, the solution became clear and there was no more gas evolution. The excess SOCl₂ was

removed by vacuum distillation. The yellow residue solidified after flushing with nitrogen and used without further purification. ^1H NMR (CDCl_3 , δ_{ppm}): 2.96 (t, 6H), 2.30 (t, 6H); ^{13}C NMR (300 MHz, CDCl_3 , δ_{ppm}): 172.46, 89.91, 41.29, 30.16.

3-(2-Aminoethyl)-3-nitropentane-1,5-diamine-HCl salt (5). The acid chloride (4) obtained from last step was dissolved in dioxane (30 mL) in a three-necked round bottom. Trimethylsilyl azide (6.3 mL, 48.0 mmol) was added to the solution at room temperature under argon gas. The solution was then slowly heated up to 80 °C. When there was no more gas evolution, the reaction mixture was allowed to cool down to 45 °C and then added 20 mL of acetone. Concentrated HCl (12 mL) was added to the mixture dropwise. White precipitate formed immediately following the addition. After 1 hour, the reaction mixture was allowed to cool down to room temperature. The white precipitate was collected by vacuum filtration and washed with 200 mL of cold acetone. After drying in the hood overnight, a slightly yellow solid was obtained (yield: 3.86 g, 81%). ^1H NMR (300 MHz, $\text{DMSO}-d_6$, δ_{ppm}): 8.39 (s, 9H), 2.81 (t, 6H), 2.33 (t, 6H).

Compound (6). 3-(2-Aminoethyl)-3-nitropentane-1,5-diamine-HCl salt (5) (3.0 g, 10.0 mmol) was dissolved in 100 mL of $\text{Et}_3\text{N}/\text{CH}_3\text{CN}$ (1/3, v/v). Then di-*tert*-butyl dicarbonate (10.2 g, 46.8 mmol) was added. The mixture was heated at reflux for 7 hours and then diluted with 150 mL of ethyl acetate. The mixture was washed with H_2O (250 mL \times 2). Then the aqueous phase was extracted with ethyl acetate (150 mL \times 2). The organic phase was combined and dried with anhydrous MgSO_4 . After the filtration, the solvent was removed *in vacuo*, affording a yellow oil which was solidified under vacuum (yield: 4.2 g, 86%). ^1H NMR (300 MHz, CDCl_3 , δ_{ppm}): 4.81 (s, 3H), 3.13 (m, 6H), 2.16 (t, 6H), 1.40 (s, 27H); ^{13}C NMR (75 MHz, CDCl_3 , δ_{ppm}): 155.84, 90.59, 79.63,

35.79, 35.59, 28.34; LR-MS: calcd for $C_{22}H_{42}N_4O_8$ $[M+H]^+ = 491.6$, found 491.0;

Elemental analysis: calcd for $C_{22}H_{42}N_4O_8$: C, 57.86; H, 8.63; N, 11.42. found: C, 53.78; H, 9.03; N, 11.24.

Compound (8). A solution of compound **6** (3.1 g, 6.3 mmol) in 200 mL of ethanol with T1 Raney Nickel (3.0 g) was hydrogenated at 100 psi and 70 °C for 36 hours. The catalyst was removed by filtering the reaction mixture through a bed of celite. The solvent was removed *in vacuo*, affording a slightly yellow oil, which was solidified as a fluffy white solid under vacuum (yield: 90%). 1H NMR (300 MHz, $CDCl_3$, δ_{ppm}): 5.06 (s, 3H), 3.18 (m, 6H), 1.78 (s, 2H), 1.56 (t, 6H), 1.41 (s, 27H); ^{13}C NMR (75 MHz, $CDCl_3$, δ_{ppm}): 155.99, 79.22, 52.96, 39.37, 36.14, 28.41; LR-MS: calcd for $C_{22}H_{44}N_4O_6$ $[M+H]^+ = 461.6$, found 461.0.

2,2'-(2,5-Diiodo-1,4-phenylene)bis(oxy)diacetyl chloride (10). 2,2'-(2,5-Diiodo-1,4-phenylene)bis(oxy)diacetic acid (**9**) (5.8 g, 12.0 mmol) was suspended in 30 mL of $SOCl_2$. After adding 2 drops of DMF, the reaction mixture was heated up and stirred at reflux for 2 hours. Then, the excess $SOCl_2$ was removed by vacuum distillation and the resulting off-white solid was crystallized from 200 mL of heptane/toluene (10/1, v/v), affording a slightly yellow crystalline solid (yield: 5.0 g, 80%). 1H NMR (300 MHz, $CDCl_3$, δ_{ppm}): 7.15 (s, 2H), 4.92 (s, 4H); ^{13}C NMR (75 MHz, $CDCl_3$, δ_{ppm}): 152.58, 124.41, 113.62, 86.44, 74.05.

Compound 1. Compound **7** (1.2 g, 2.9 mmol), 0.4 mL of Et_3N and 25 mL of dry CH_2Cl_2 were placed in a 50 mL round bottom flask and cooled with an ice/water bath. Then 2,2'-(2,5-diiodo-1,4-phenylene)bis(oxy)diacetyl chloride (**10**) (10.67 mg, 1.30 mmol) in 15 mL of CH_2Cl_2 was added. After 2 hours, the reaction mixture was allowed to

warm to room temperature and further stirred for 24 hours. The solvent was removed *in vacuo*, the crude product was purified by flash chromatography (silica gel, EtOAc/hexane (1/3, v/v)) to give a white solid (yield: 1.4 g, 78%). ^1H NMR (300 MHz, CDCl_3 , δ_{ppm}): 7.13 (s, 2H), 6.60 (s, 2H), 4.35 (s, 4H), 2.25 (m, 12H), 2.03 (m, 12H), 1.42 (s, 27H); ^{13}C NMR (75 MHz, CDCl_3 , δ_{ppm}): 172.19, 165.73, 151.57, 122.63, 86.29, 80.63, 68.83, 57.80, 30.17, 29.74, 28.09; HR-MS: calcd for $\text{C}_{54}\text{H}_{86}\text{I}_2\text{N}_2\text{O}_{16}$ $[\text{M}+\text{Na}]^+ = 1295.39$, found 1295.39.

Compound 2. Compound **8** (1.5 g, 3.3 mmol), 0.45 mL of Et_3N (3.2 mmol) and 30 mL of dry CH_2Cl_2 were placed in a 50 mL round bottom flask, which was cooled in an ice/water bath. To the mixture, a solution of 2,2'-(2,5-diiodo-1,4-phenylene)bis(oxy)diacetyl chloride (**10**) (0.76 g, 1.5 mmol) was added. After 2 hours, the reaction mixture was allowed to warm to room temperature and further stirred for 24 hours. The solvent was removed *in vacuo*, the crude product was purified by flash chromatography on silica gel with EtOAc/hexane (1/1, v/v) to give a colorless oil, which solidified as a white solid under vacuum (yield: 1.0 g, 50%). ^1H NMR (300 MHz, CDCl_3 , δ_{ppm}): 7.15 (s, 2H), 6.71 (s, 2H), 4.80 (s, 6H), 4.36 (s, 4H), 3.19 (m, 12H), 2.03 (m, 12H), 1.42 (s, 27H); ^{13}C NMR (75 MHz, CDCl_3 , δ_{ppm}): 166.38, 155.94, 151.61, 122.72, 86.43, 79.33, 68.71, 59.92, 35.76, 35.60, 28.39; HR-MS: calcd for $\text{C}_{54}\text{H}_{92}\text{I}_2\text{N}_8\text{O}_{16}$ $[\text{M}+\text{Na}]^+ = 1385.46$, found 1385.46.

General polymerization procedure for PPEs with branched side chains.

Monomer **1** or **2** (0.25 mmol) and 0.25 mmol of the other monomers (1,4-diethynylbenzene (Ph), 4,7-Diethynyl-2,1,3-benzothiadiazole (BTD), or 4,7-bis[2'-(5'-ethynyl)thienyl]-2,1,3-benzothiadiazole (TBT)) were dissolved in 16 mL of THF/ Et_3N

(3/1, v/v). The resulting solution was deoxygenated with argon for 15 minutes. Then Pd(PPh₃)₄ (17.3 mg, 15.0 μmol) and CuI (5.7 mg, 30.0 μmol) were added to the stirred solution under the protection of argon. The reaction mixture was then heated up to 60 ~ 65 °C and stirred for 24 hours. The viscous solution was then poured into 200 mL of methanol. The precipitate was collected by vacuum filtration and washed with methanol (200 mL). After drying under vacuum, the polymer was stored as a solid. Typical reaction yields for the polymerization are 80 ~ 90%.

Hydrolysis for PPEs with branched anionic side chains. PPEs having Ph or BTB: the organic precursor polymer (0.25 mmol) was dissolved in 20 mL CH₂Cl₂ and cooled in an ice/water bath. Trifluoroacetic acid (TFA, 20 mL) was added to the polymer solution drop-wise. Upon the completion of the addition, the reaction mixture was allowed to warm to room temperature and stirred for another 12 hours. The excess of TFA and the solvent were removed *in vacuo*; PPE having TBT: to a solution of the organic precursor polymer (0.25 mmol) in 20 mL CH₂Cl₂/DMSO (3/1, v/v), ZnBr₂ (6.0 equiv.) was added and the solution stirred for 24 hours. At this time, 20 mL of water was added and the mixture was stirred for 1 hour. The layers were separated and the organic solvent was removed *in vacuo*; the residue was treated with saturated aqueous Na₂CO₃ solution (10 mL) and stirred at room temperature for 3 hours. The solution was then poured into 200 mL of acetone. The polymer precipitate was then dissolved in water and purified by dialysis using 12 kD MWCO regenerated cellulose membranes (yield: 90 ~ 100%). The water-soluble polymers could be either stored as aqueous solutions or as solid powders.

PPE-Ph-^bCO₂^tBu. ¹H NMR (300 MHz, CDCl₃, δ_{ppm}): 7.57 (br, s, 4H), 7.04 (s, 2H), 6.39 (s, 2H), 4.47 (s, 4H), 2.13 (br, m, 12H), 1.96 (br, s, 12H), 1.39 (s, 54 H); GPC (THF, polystyrene standard): M_w = 33, 230, M_n = 101, 210, PDI = 3.00; FT-IR (ν_{max}, KBr pellet): 3403, 2978, 2935, 2205, 1731, 1692, 1532, 1512, 1484, 1456, 1410, 1393, 1368, 1312, 1282, 1256, 1214, 1154, 1101, 1051, 954, 891, 848, 758.

PPE-Ph-^bCO₂Na. ¹H NMR (300 MHz, D₂O/DMSO-*d*₆ (v/v, 1/1), δ_{ppm}): 7.58 (br, 4H), 7.16 (s, 2H). 5.25 (s, 4H); FT-IR (ν_{max}, KBr pellet): 3391, 2937, 2202, 1665, 1564, 1404, 1283, 1208, 1099, 1053, 892, 847, 675.

PPE-BTD-^bCO₂^tBu. ¹H NMR (300 MHz, CDCl₃, δ_{ppm}): 7.91 (br, s, 2H), 7.19 (s, 2H), 6.51 (s, 2H), 4.59 (s, 4H), 2.12 (br, m, 12H), 1.94 (br, s, 12H), 1.39 (br, s, 54H); GPC (THF, polystyrene standard): M_w = 16, 250, M_n = 11, 690, PDI = 1.40; FT-IR (ν_{max}, KBr pellet): 3405, 2978, 2936, 2679, 2494, 2204, 1731, 1693, 1519, 1486, 1457, 1393, 1368, 1312, 1281, 1256, 1213, 1154, 1101, 1056, 954, 847, 758, 721.

PPE-BTD-^bCO₂Na. ¹H NMR (300 MHz, D₂O/DMSO-*d*₆ (v/v, 1/1), δ_{ppm}): 7.88 (br, s, 2H), 7.22 (br, s, 2H), 4.83 (s, 4H); FT-IR (ν_{max}, KBr pellet): 3391, 2951, 2204, 1667, 1566, 1403, 1283, 1207, 1097, 1061, 838, 778, 721, 667.

PPE-TBT-^bCO₂^tBu. ¹H NMR (300 MHz, CDCl₃, δ_{ppm}): 8.10 (s, 2H), 7.95 (s, 2H), 7.51 (s, 2H), 7.08 (s, 2H), 6.45 (s, 2H), 4.55 (s, 4H), 2.24 (m, 12H), 2.08 (m, 12H), 1.38 (s, 54H); GPC (THF, polystyrene standard): M_w = 37, 817, M_n = 16, 771, PDI = 2.26.

PPE-TBT-^bCO₂Na. ¹H NMR (300 MHz, D₂O/DMSO-*d*₆ (v/v, 1/1), δ_{ppm}): 8.20 (br, 4H), 7.55 (br, 2H), 7.40 (br, 2H), 7.18 (br, 2H), 4.62 (br, 4H), 2.20 (br, 12H), 1.90 (br, 12H).

Hydrolysis for PAEs with branched cationic side chains. The organic polymer (0.25 mmol) was dissolved in 20 mL of dioxane. The polymer solution was then cooled to 0 ~ 5 °C using an ice/water bath. Concentrated HCl (7 mL, 4 N) was added to the stirred solution drop-wise. Upon the completion of the addition, the reaction mixture was allowed to warm to room temperature and stirred for another 12 hours. The polymer was then precipitated by pouring the solution into a large amount of acetone (200 mL). The precipitate was collected, washed with acetone (100 mL) and finally dried under vacuum (yield: 90 ~ 100%). The polymer was then dissolved in water and purified by dialysis using 12 kD MWCO regenerated cellulose membranes (yield: 90 ~ 100%). The water-soluble polymers could be either stored as aqueous solutions or as solid powders.

PPE-Ph-^bNH^tBoc. ¹H NMR (300 MHz, CDCl₃, δ_{ppm}): 7.61 (br, s, 4H), 7.05 (s, 2H), 6.60 (br, s, 2H), 4.92 (s, 6H), 4.46 (s, 4H), 3.09 (br, s, 12H), 1.93 (br, 2, 12H), 1.39 (s, 54H); GPC (THF, polystyrene standard): M_w = 105, 640, M_n = 24, 080, PDI = 4. 40); FT-IR (ν_{max}, KBr pellet): 3393, 2977, 1691, 1517, 1457, 1392, 1367, 1274, 1252, 1170, 1046, 866, 839, 781, 637, 601.

PPE-Ph-^bNH₃Cl. ¹H NMR (300 MHz, D₂O/DMSO-*d*₆ (v/v, 1/1), δ_{ppm}): 7.61 (br, s, 4H), 7.18 (s, 2H), 4.66 (s, 4H), 2.92 (br, s, 12H), 2.05 (br, 2, 12H); FT-IR (ν_{max}, KBr pellet): 3392, 3031, 2202, 2002, 1672, 1607, 1516, 1489, 1407, 1281, 1191, 1063, 1017, 966, 906, 842, 786, 721, 548.

PPE-BTD-^bNH^tBoc. ¹H NMR (300 MHz, CDCl₃, δ_{ppm}): 7.94 (br, s, 2H), 7.25 (br, s, 2H), 4.97 (s, 6H), 4.58 (s, 4H), 3.09 (s, 12H), 1.94 (s, 12H), 1.40 (s, 54H); GPC (THF, polystyrene standard): M_w = 44, 700, M_n = 12, 320, PDI = 3.60); FT-IR (ν_{max}, KBr pellet):

3350, 2977, 2939, 2679, 2490, 2203, 1693, 1570, 1458, 1392, 1366, 1279, 1252, 1171, 1041, 966, 892, 866, 780, 634, 564.

PPE-BTD-^bNH₃Cl. ¹H NMR (300 MHz, D₂O/DMSO-*d*₆ (v/v, 1/1), δ_{ppm}): 8.01 (br, s, 2H), 7.36 (s, 2H), 4.78 (s, 4H), 2.94 (s, 12H), 2.07 (s, 12H); FT-IR (ν_{max}, KBr pellet): 3394, 3035, 2202, 2011, 1672, 1610, 1542, 1509, 1409, 1342, 1281, 1191, 1067, 1020, 965, 893, 852, 786, 632, 563, 509.

CHAPTER 3

HIGHLY EFFICIENT MERCURY (II) ION SENSOR BASED ON CONJUGATED POLYELECTROLYTE-RHODAMINE COMBINATION SYSTEM

Mercury ion is a toxic heavy metal ion which causes serious nervous disorders such as acrodynia, Hunter-Russell syndrome, and Minamata disease. Wide availability in many areas including medicines, cosmetics, and optics gives rise to the increase of diseases related to such mercury poisoning.⁷⁷ Accordingly, during the past several decades, numerous fluorescence mercury ion sensors for selective detection have been designed and developed.⁷⁸⁻⁸⁰ Especially, a great effort has gone into the increase of its sensitivity because even extremely trace amount of mercury ion gives rise to critical issues.⁸¹⁻⁸²

Among many fluorescence sensors, conjugated polyelectrolytes (CPEs) have been extensively investigated as potential chemo- and biosensors because of their highly efficient quenching effect known as superquenching or amplified quenching.^{26,83} Such quenching effect is induced by the various interactions including biotin-avidin, antigen-antibody, and electrostatic or hydrophobic interactions. Recently, Bunz et al. reported the detection of Hg^{2+} ion using CPEs, in which biotin functionalized CPE-avidin agglutination showed highly effective quenching effect for Hg^{2+} ion complexation via not only intra-polymer but also inter-polymer exciton migration as the mercury ions are bound to carboxylate side chains of the CPE.⁸² Also, rhodamine based sensors have been extensively utilized in bio-labeling and material science because rhodamine derivatives have high fluorescence quantum efficiency and exhibit long wavelength absorption and fluorescence.^{78,84} The rhodamine derivatives with spiro-cyclic form have received increasing attention as a turn-on Hg^{2+} ion sensor with high sensitivity.^{80-81,85-90} The spiro-type rhodamine derivatives are non-fluorescent and colorless. Ring-opening

of spiro-cyclic form induced by Hg^{2+} ion complexation, however, leads to significant fluorescence enhancement.

We speculate that the positively charged rhodamine derivative- Hg^{2+} ion (**S-Rho 1**- Hg^{2+} ion) complex would form an electrostatic complex with negatively charged CPE (**PPE-^dCO₂⁻**). Also, highly favorable effect of sulfur atom on spiro-type rhodamine to complex with Hg^{2+} ion coupled with the amplified quenching effect of **PPE-^bCO₂⁻** might cause improved sensory response for Hg^{2+} ion detection. In this system, **PPE-^bCO₂⁻** is used as a signaling unit, and rhodamine acts as a receptor because of the strong thiophilic nature of Hg^{2+} ion.

Results and Discussion

Synthesis

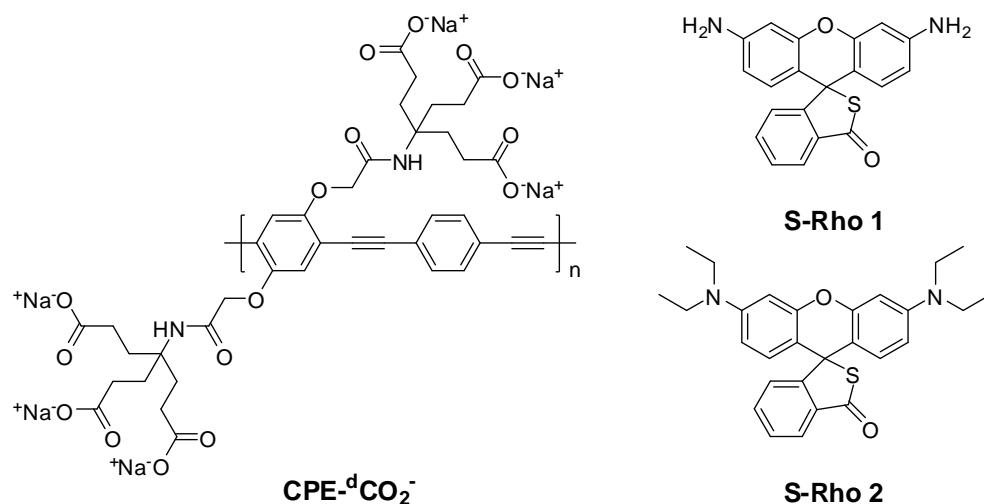


Figure 3-1. Structure of **PPE-^bCO₂⁻**, **S-Rho 1**, and **S-Rho 2**.

Figure 3-1 shows the structure of the CPE with branched polyanionic side chains (**PPE-^bCO₂⁻**) and spiro-cyclic rhodamines (**S-Rho 1** and **S-Rho 2**). As discussed in Chapter 2, the conjugated polyelectrolyte **PPE-^bCO₂⁻** was synthesized through precursor route using a Sonogashira coupling reaction. As a polymer repeat unit,

phenyl group has been introduced into polymer backbone, and negatively charged water-soluble branched side chains that can structurally hinder the aggregation of the polymer chains were also incorporated to the conjugated polymer backbones, thereby suppressing self-quenching of their excited state. As shown in Figure 3-2, **S-Rho 1** was synthesized from commercially available rhodamine 110. First, it was reacted with phosphorus oxychloride, which was then treated with excess Na₂S in saturated aqueous solution. **S-Rho 1** was obtained as a colorless powder in 48 % yield. As a reference compound, **S-Rho 2** was also prepared in a good yield as described in the literatures.⁸⁸

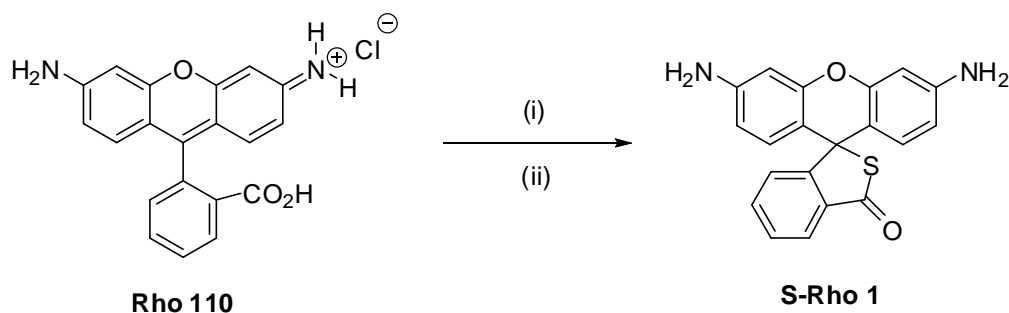


Figure 3-2. Synthesis of **S-Rho 1** (i) 1,2-dichloroethane, POCl₃, reflux, 4 hrs.; (ii) excess Na₂S saturated aqueous solution, 12 hrs.

Optical Properties

It is well known that CPEs having linear ionic chains tend to be aggregated in aqueous solution because of a hydrophobic interaction of the polymer backbones and an electrostatic interaction between side chains of polymer, showing excimer-like fluorescence at longer wavelength.¹⁰ As shown in Figure 3-3a, however, **PPE-^bCO₂⁻** shows structured fluorescence at $\lambda_{\text{max}} = 433$ nm without an excimer-like band at the longer wavelength. Unlike CPEs having linear side chains, aggregation effect of **PPE-^bCO₂⁻** which has bulky, branched polyionic functional groups is minimized because of

the electrostatic repulsion between the branched side chains. In addition, a number of ionic side chains are able to increase solubility in aqueous solution. Such features provide higher fluorescence quantum efficiency, so that less aggregated **PPE-^bCO₂⁻** gives rise to an efficient sensing signal.

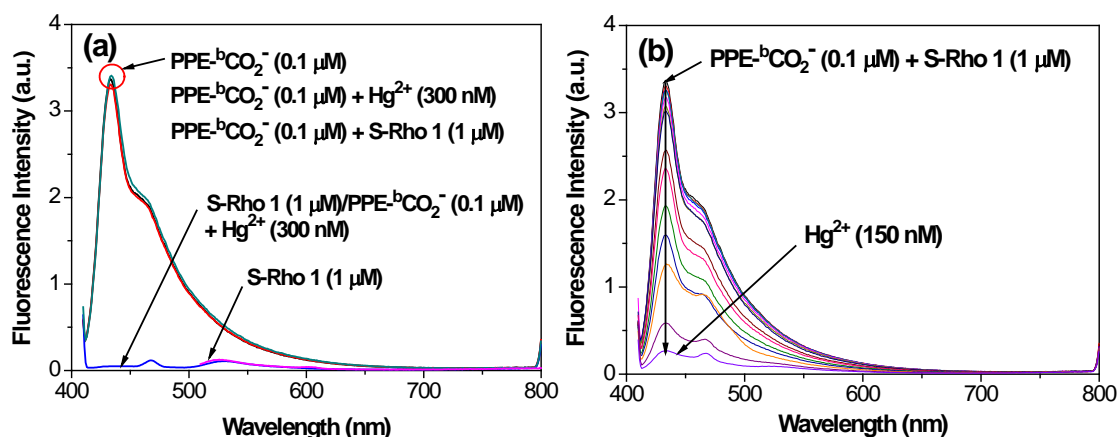


Figure 3-3. (a) Fluorescence spectra of **PPE-^bCO₂⁻** (0.1 μM) and **PPE-^bCO₂⁻** (0.1 μM)/**S-Rho 1** (1 μM) upon the addition of **Hg²⁺** ion (300 nM), and **S-Rho 1** (1 μM) in H₂O/DMSO (99/1, v/v); (b) fluorescence intensity changes of **PPE-^bCO₂⁻** (0.1 μM)/**S-Rho 1** (1 μM) upon the addition of various amounts of **Hg²⁺** ion; Excitation at 403 nm.

Application to **Hg²⁺** ion Sensor

Selectivity

Figure 3-3a shows the fluorescence intensity of **S-Rho 1** (1 μM), **PPE-^bCO₂⁻** (0.1 μM), and their mixture (**S-Rho 1/PPE-^bCO₂⁻**) in H₂O/DMSO (99/1, v/v). The addition of **S-Rho 1** (1 μM) to **PPE-^bCO₂⁻** (0.1 μM) give rise to no changes in the fluorescence spectra. Without **Hg²⁺** ion, interaction between **S-Rho 1** to **PPE-^bCO₂⁻** is negligible. The addition of **Hg²⁺** ion, however, caused the overall intensity of the emission spectra to decrease, resulting in 98.6% quenching at 433 nm upon the addition of 300 nM of **Hg²⁺** ion (Figure 3-3a). On the other hand, **PPE-^bCO₂⁻** displayed no detectable fluorescence quenching by the addition of **Hg²⁺** ion (300 μM). This implies that fluorescence change

by interaction between carboxylate side chains of **PPE-^bCO₂⁻** and Hg²⁺ ion is negligible in this concentration level. Addition of Hg²⁺ ion creates a positively charged **S-Rho 1**-Hg²⁺ ion complex by ring-opening process⁸⁰ of **S-Rho 1**, resulting in efficient fluorescence quenching of **PPE-^bCO₂⁻** via energy or charge transfer mechanism. It is evident that fluorescence quenching is “static” because of the ion-pair complex formed between negatively charged **PPE-^bCO₂⁻** and positively charged **S-Rho 1/Hg²⁺** ion complex. In contrast, the addition of other metal ions (Ag⁺, Ca²⁺, Mg²⁺, Co²⁺, Ni²⁺, Mn²⁺, Fe²⁺, Zn²⁺, Cd²⁺, Pb²⁺, Cu²⁺, Ba²⁺, and Cr³⁺) showed very subtle fluorescence intensity changes (Figure 3-4).⁹¹ Thus, the selectivity of this system for Hg²⁺ ion over other metal ions is remarkably high.

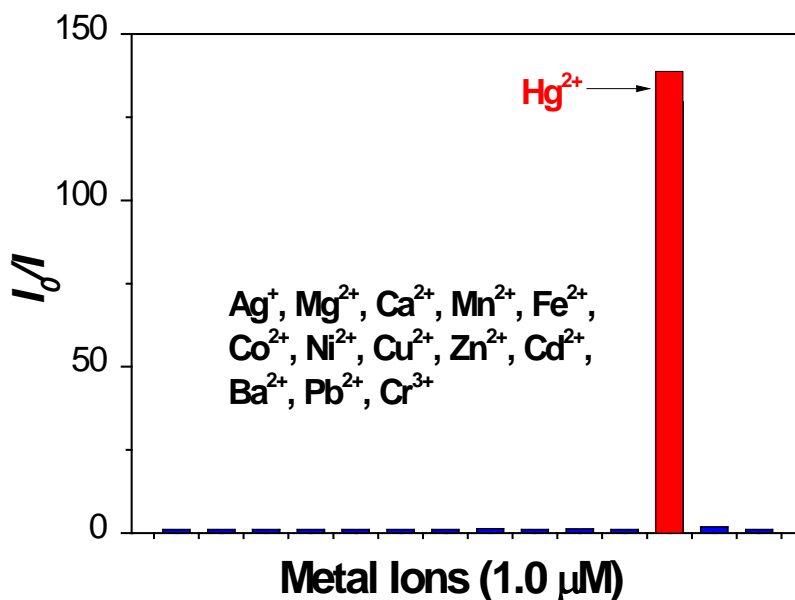


Figure 3-4. Fluorescence changes of **S-Rho 1/PPE-^bCO₂⁻** system in H₂O/DMSO (99/1, v/v) upon the addition of various metal ions; Excitation at 403 nm; fluorescence intensity was monitored at 433 nm.

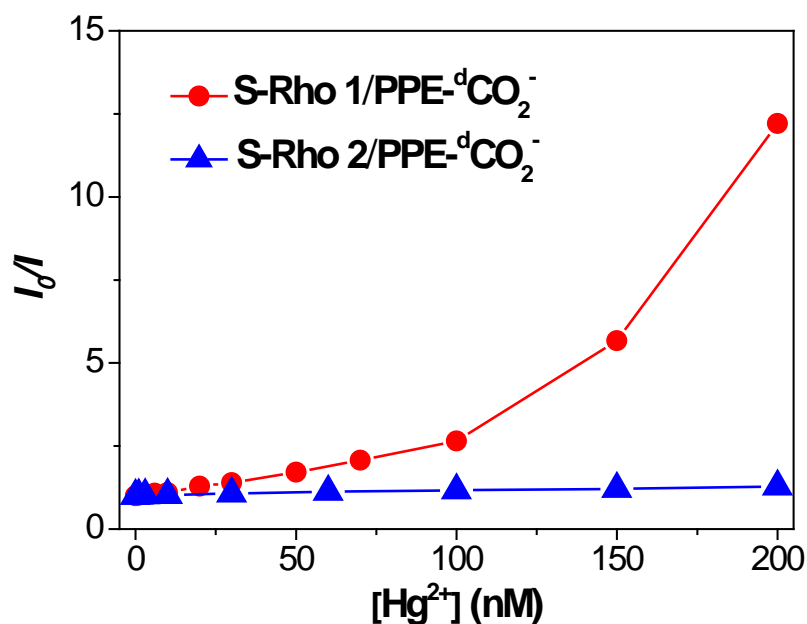


Figure 3-5. Stern-Volmer plots of **S-Rho 1/PPE-^bCO₂⁻** (●) and **S-Rho 2/PPE-^bCO₂⁻** (▲) (PPE: 0.1 μM and Rhodamine derivatives 1 μM) titrated with Hg²⁺ ion in in H₂O/DMSO (99/1, v/v); Excitation at 403 nm; Fluorescence intensity was monitored at 433 nm.

Sensitivity

Figure 3-3b shows fluorescence intensity change of **PPE-^bCO₂⁻** by the addition of Hg²⁺ ion in the presence of **S-Rho 1** in H₂O/DMSO (99/1, v/v). The Stern-Volmer¹⁹ plot was obtained at λ_{max} = 433 nm (Figure 3-5). The SV plot for such quenching effect exhibits a linear profile at very low concentration of Hg²⁺ ion, where *K*_{SV} value of 1.4 × 10⁷ M⁻¹ was obtained, which is the highest value among early reported CPE based Hg²⁺ ion sensors. This quenching profile becomes nonlinear with increasing concentration of Hg²⁺ ion, indicating amplified quenching.⁸³

It is reported the fluorescence of **S-Rho 2** is efficiently enhanced with increasing Hg²⁺ ion concentration, which implies that **S-Rho 2** can act as a good receptor for Hg²⁺ ion.⁸⁸ Unlike **S-Rho 1/PPE-^bCO₂⁻** system, nevertheless, the fluorescence of **S-Rho 2/PPE-^bCO₂⁻** system is not effectively quenched by Hg²⁺ ion as well as other metal ions

(Figure 3-6). Its SV plot is much less sloped than **S-Rho 1/PPE-^bCO₂⁻** system (Figure 3-5), in which K_{SV} value is $8.3 \times 10^5 \text{ M}^{-1}$.

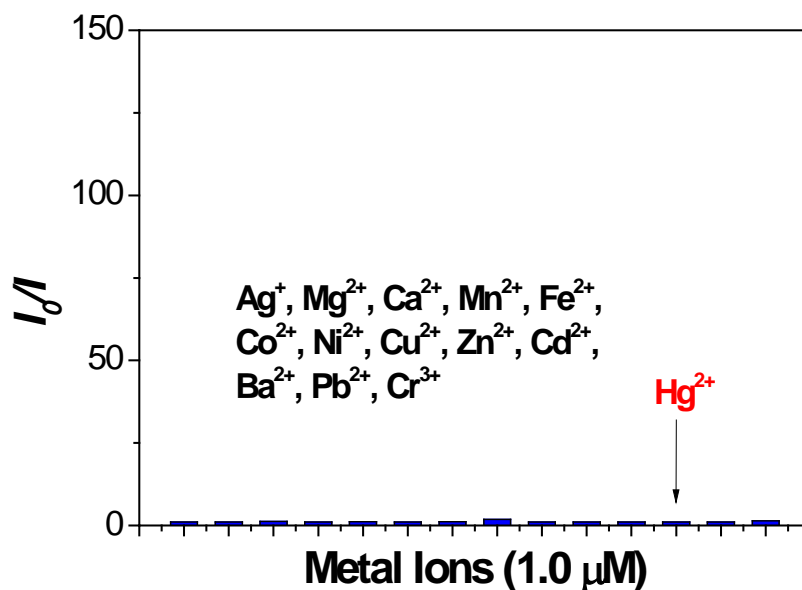


Figure 3-6. Fluorescence changes of **S-Rho 2/PPE-^bCO₂⁻** system in $\text{H}_2\text{O}/\text{DMSO}$ (99/1, v/v) upon the addition of various metal ions; Excitation at 403 nm; fluorescence intensity was monitored at 433 nm.

Sensing Mechanism

The plausible mechanism for sensing Hg^{2+} ion is displayed in Figure 3-7. A spiro-type rhodamine derivative undergoes ring-opening by complexation with Hg (II) ion, providing a positive charge on the nitrogen atom. According to the results of comparison

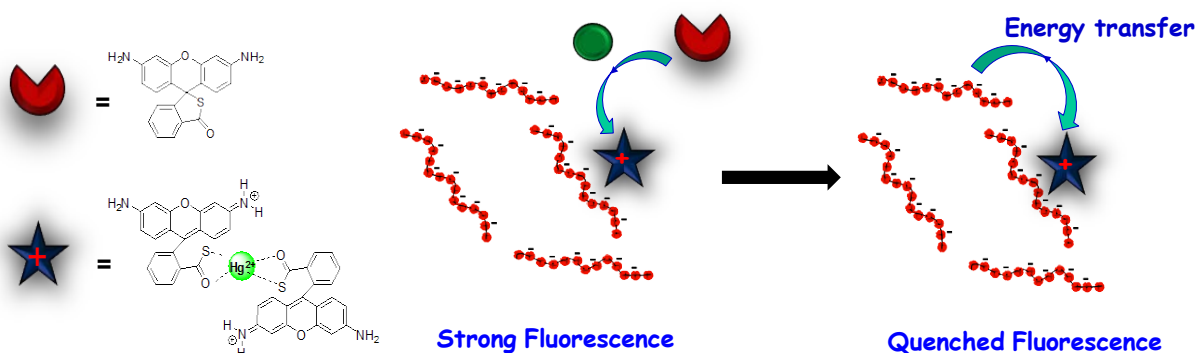


Figure 3-7. Plausible sensing mechanism.

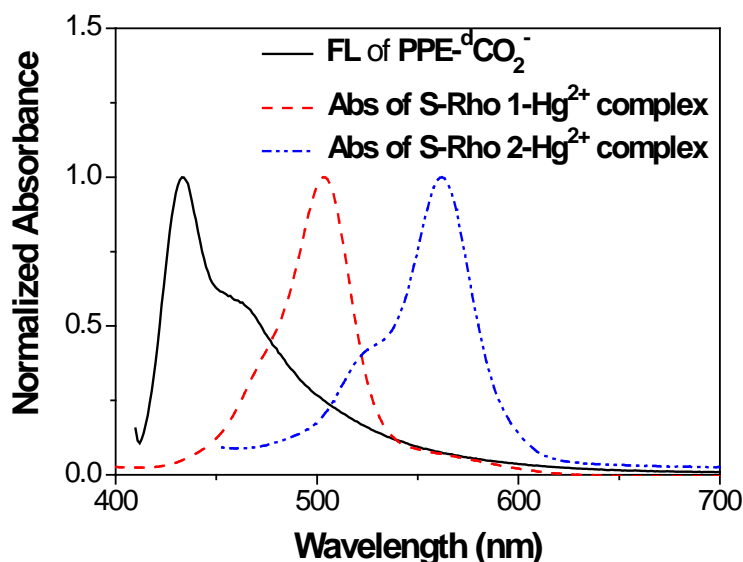


Figure 3-8. Fluorescence of FRET donor ($\text{PPE}^{\text{b}}\text{CO}_2^-$) and absorption of FRET acceptors (S-Rho 1-Hg^{2+} complex and S-Rho 2-Hg^{2+} complex).

of **S-Rho 1** and **S-Rho 2**, it is suggested that the proton on the nitrogen atom plays an important role in the complexation with carboxylate ions of $\text{PPE}^{\text{b}}\text{CO}_2^-$. Figure 3-8 shows a spectral overlap between donor fluorescence ($\text{PPE}^{\text{b}}\text{CO}_2^-$) and acceptor absorption (S-Rho 1-Hg^{2+} ion or S-Rho 2-Hg^{2+} ion complex), in which absorption of **S-Rho 2-Hg**²⁺ ion complex is less overlapped with fluorescence of $\text{PPE}^{\text{b}}\text{CO}_2^-$ than that of **S-Rho 1-Hg**²⁺. Such less overlapped bands between donor fluorescence ($\text{PPE}^{\text{b}}\text{CO}_2^-$) and acceptor absorption (S-Rho 2-Hg^{2+} ion complex) give rise to less FRET (fluorescence resonance energy transfer) effect, resulting in less efficient quenching effect in **S-Rho 2/PPE**^b CO_2^- system. With this reason it is quite understandable that efficient quenching effect is mainly due to FRET effect in **S-Rho 1/PPE**^b CO_2^- system. Unfortunately, we could not observe fluorescence increase of the acceptor (**S-Rho 1-Hg**²⁺ ion complex) by FRET effect. It is possible relatively small stoichiometric ratio of the donor ($\text{PPE}^{\text{b}}\text{CO}_2^-$) is not enough to act as an efficient fluorescence donor in this system.

Comparison of Sensitivity between S-Rho/PPE System and S-Rho

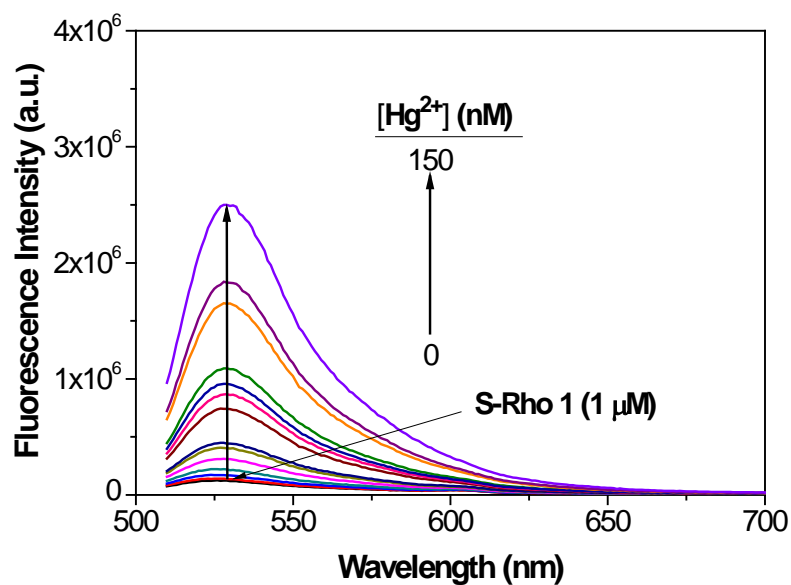


Figure 3-9. Fluorescence intensity changes of **S-Rho 1** in H₂O/DMSO (99/1, v/v) upon the addition of various amounts of Hg²⁺ ion; Excitation at 500 nm.

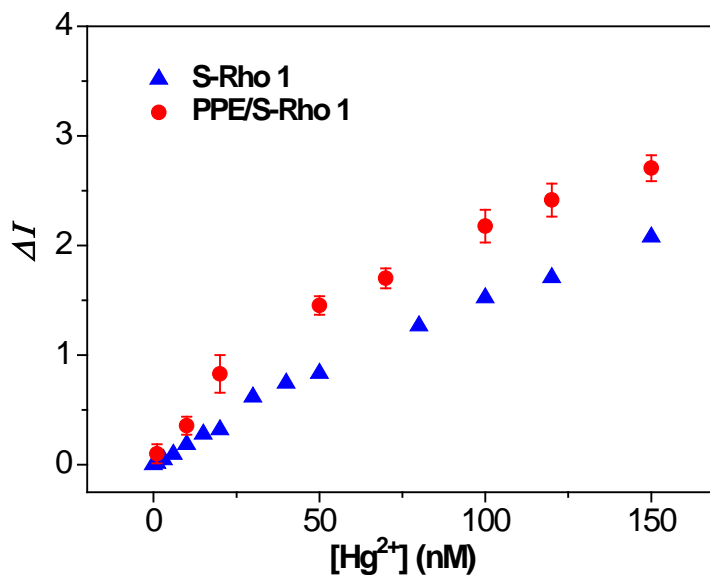


Figure 3-10. Titration profile ΔI as a function of $[\text{Hg}^{2+}]$; ΔI : $I_0 - I$ at 433 nm, excitation at 403 nm (**S-Rho 1**/**PPE-^bCO₂⁻**) and $I - I_0$ at 529 nm, excitation at 500 nm (**Rho 1**); I_0 : fluorescence emission intensity of **S-Rho 1** (1 μM)/**PPE-^bCO₂⁻** (0.1 μM) or **S-Rho 1** (1 μM), I : fluorescence emission intensity in the presence of Hg²⁺ ion.

The fluorescence response of **S-Rho 1/PPE-^bCO₂⁻** system for Hg²⁺ ion was compared to that of **S-Rho1** alone. As expected, the fluorescence intensity of **S-Rho 1** increased at $\lambda_{\text{max}} = 529 \text{ nm}$ upon addition of Hg²⁺ ion (Figure 3-9). Figure 3-10 shows fluorescence intensity changes of **S-Rho 1/PPE-^bCO₂⁻** system and **S-Rho1** alone for Hg²⁺ ion detection. Interestingly, **S-Rho 1/PPE-^bCO₂⁻** system showed larger intensity changes, which implies that **S-Rho 1/PPE-^bCO₂⁻** system is more efficient Hg²⁺ ion detector than **S-Rho1** in terms of sensitivity.

Summary and Conclusions

In this Chapter, we have devised a novel combination system for Hg²⁺ ion detection using **PPE-^bCO₂⁻** and **S-Rho 1**. The fluorescence intensity of **PPE-^bCO₂⁻/S-Rho 1** was selectively and sensitively quenched with Hg²⁺ ion over other metal ions. We demonstrated that the fluorescence energy transfer is the main factor in the fluorescence quenching. Although this **PPE-^bCO₂⁻/S-Rho 1** system is turn-off sensor, this sensor showed improved sensory response compared to the unitary rhodamine based sensor that is a widely used one with high sensitivity and strong fluorescence quantum efficiency. Thus, this result proposes that stoichiometric uses of CPEs for combination system may promote sensory response of the other sensors that are presently available.

Experimental

Materials

All chemicals used for the synthesis were of reagent grade and used without further purification. Rhodamine 110, phosphorus oxychloride, 1,2-dichloroethane, and thiourea were purchased from Sigma-Aldrich Chemical Company. THF was purified by Solvent Dispensing System (SDS). Silica gel (Merck, 230-400 mesh) was used for

chromatographic purification of all of intermediate and target molecules. All other chemicals and solvents were purchased from Sigma-Aldrich, Fisher Scientific, or Acros Chemical Company and used as received.

Instrumentation and Methods

NMR spectra were recorded using a Varian VXR-300 FT NMR, operating at 300 MHz for ^1H NMR and at 75 MHz for ^{13}C NMR. UV/Vis absorption spectra were recorded using a Varian Cary 50 Spectrophotometer. Steady-state fluorescence spectra were obtained with a PTI fluorometer. A 1 cm quartz cuvette was used for all spectral measurements.

Stock solutions (1.0 mM) of **S-Rho 1** and **S-Rho 2** was prepared in DMSO. The chloride salts of Ag^+ , Ca^{2+} , Mg^{2+} , Co^{2+} , Ni^{2+} , Mn^{2+} , Fe^{2+} , Hg^{2+} , Zn^{2+} , Cd^{2+} , Pb^{2+} , Cu^{2+} , Ba^{2+} , and Cr^{3+} ions (stock solutions = 10.0 mM in H_2O) were tested to evaluate the metal ion binding properties of **PPE-^bCO₂⁻** (stock solution = 1.0 mM in H_2O). For fluorescence measurements of combination system and **S-Rho 1**, the excitations were made at 403 nm and 500 nm, respectively.

Synthetic Procedures

Synthesis of rhodamine derivatives. Rhodamine 110 (0.20 g, 0.55 mmol) or rhodamine B base (0.5 g, 1.3 mmol) was dissolved in 20 mL of 1,2-dichloroethane. Then phosphorus oxychloride (1 mL) was added dropwise. The mixture was heated at reflux for 4 hours, and then the solvent was removed *in vacuo*. The crude acid chloride was dissolved in 5 mL of THF. After the addition of solution of thiourea and triethylamine in THF/water (20 mL/5 mL) at room temperature, the reaction mixture was stirred for overnight. The solvent was removed *in vacuo*, and then 30 mL of water was added. The

precipitate was filtered and washed 3 times with water. The crude product was purified by chromatography (silica gel, CH₂Cl₂) to give a white solid..

S-Rho 1: Yield: 48%; ¹H NMR (300 MHz, CDCl₃, δ_{ppm}): 7.84 (d, 1H), 7.50 (m, 2H), 7.16 (d, 1H), 6.66 (d, 2H), 6.38 (s, 2H), 6.27 (d, 2H), 4.77 (br, 4H); ¹³C NMR (75 MHz, CDCl₃, δ_{ppm}): 1605.0, 159.8, 157.0, 153.9, 151.8, 147.5, 134.2, 130.3, 128.4, 127.2, 122.5, 112.8, 101.5.

S-Rho 2: Yield: 72%; ¹H NMR (300 MHz, CDCl₃, δ_{ppm}): 8.85 (d, 1H), 7.51(m, 1H), 7.43(m, 1H), 7.20 (d, 1H), 6.70 (d, 2H), 6.35 (s, 2H), 6.30 (d, 2H), 3.32 (q, 8H), 1.15 (t, 12 H).

CHAPTER 4

PHOTOPHYSICAL PROPERTIES OF PYA4 AGGREGATE AND ITS APPLICATION TO PYROPHOSPHATE SENSOR BASED ON TURN-ON SYSTEM

In the past decade, many fluorescence sensors for ionic species have been designed and developed due to their use in analysis and detection of metal ions, anions, and biomolecules.^{19,92} Effective fluorescence chemosensors should selectively recognize guest molecules and easily convert the recognition event into photophysical changes with high sensitivity.⁹³ In recent years many fluorescence sensors having photophysical properties utilizing excimer/excimer formation, PET (photoinduced electron transfer), ESPT (excited state proton transfer), MLCT (metal to ligand charge transfer), and FRET (fluorescence resonance energy transfer) mechanisms have been developed.⁹⁴⁻⁹⁵ One widely used mechanism is the excimer formation of pyrenes because pyrenes display not only a well-defined monomer emission but also an efficient excimer emission: after excitation, pyrene displays fluorescence from both the excited state monomer and the excited state dimer (excimer).⁹⁶ Because excimer formation is sensitive to even subtle physical changes of the pyrene moieties induced by the environment such as metal ion binding, temperature, and use of viscous solvent, the I_e/I_m (the excimer to monomer emission intensity) changes can be an informative parameter in various sensing systems.⁹⁴

Anions play important roles in biology and the environment. As an example, pyrophosphate ion (PPi) has an important role in many biological processes such as cellular energy metabolism and regulation of enzyme activity.⁹⁷⁻⁹⁸ PPi is the product of ATP hydrolysis under cellular conditions, and many of the common enzymes, such as phosphoribosyltransferases and alkaline phosphatase, produce or consume pyrophosphate (PPi), which are also related to the enzyme activity.⁹⁸ Accordingly,

detecting variation of pyrophosphate concentration in the enzymatic conditions is a general way to monitor the enzyme's activity.

Fluorescence based pyrophosphate (PPi) sensors have attracted considerable interest, and much effort has been devoted to the development of PPi receptors or sensors,⁹⁹ since Czarnik et al.¹⁰⁰ reported the results of a pioneering study in 1994 in which an anthracene derivative bearing polyamine groups was used as a PPi sensor in 100% aqueous solutions. However, relatively few reports of the effective PPi receptors¹⁰¹ or sensors^{97,102-108} that operate in aqueous solutions were reported because most known anion sensors do not have a sufficiently strong affinity for anions in aqueous solutions, or they have a limit to convert anion recognition into a fluorescence signal.¹⁰⁹

Recently, Yoon et al. reported that a chemosensor based on Zn^{2+} ion complexed DPAs (di-2-picolylamines) with high selectivity for PPi over ATP, ADP and AMP in aqueous solution in which two fluorophores display 2+2 type intermolecular dimer formation upon PPi complexation, showing excimer type emission at 480 nm.¹⁰⁴ Fabbrizzi et al. also reported an Off-On switchable fluorescence chemosensor for effective PPi sensing with a chemosensing ensemble (CE) paradigm in which an indicator (I: fluorophore) binds to a receptor (R: a dinuclear Cu^{2+} ion macrocyclic complex) by means of non-covalent interaction, which is able to effectively detect PPi through recovery of the fluorescence emission of the displaced indicator in aqueous solutions.¹⁰⁸ In most cases, however, fluorescence emission after PPi recognition was just several fold higher than in the absence of PPi, attributable to comparatively

inefficient quenching effect in aqueous solutions when quencher is bound. Therefore, the sensitivity for detecting PPI is limited.

On the other hand, more recently it was reported that PPE-CO₂⁻-which is a conjugated polyelectrolyte (CPE) responds even at very low PPI concentration where the amplified quenching system has been introduced.¹⁰² In a molecular wire system, the exciton migrates throughout the polymer, which makes the quenching of polymer more efficient compared to single molecular system when a quencher is bound.^{16,21,59} This approach enables sensor to sensitively change the fluorescence emission when the quencher is affected by another analyte.

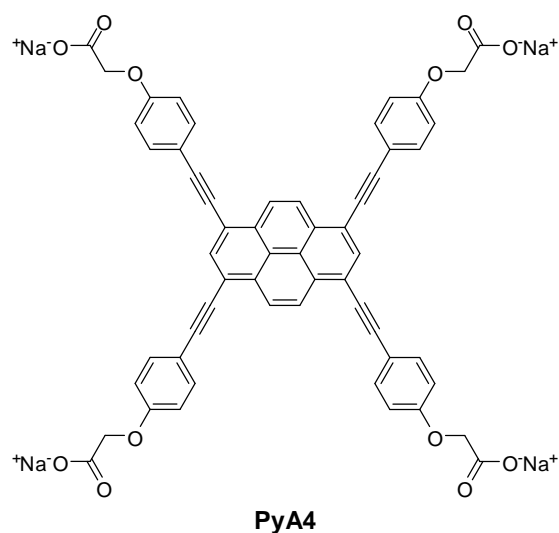


Figure 4-1. Structure of **PyA4**.

With this background in mind, here we have designed and developed an Off-On switchable fluorescence sensing system for PPI that consists of **PyA4** (Figure 4-1) and cupric (II) ions, giving sensitive fluorescence changes in 20 mM HEPES buffer.

Results and Discussion

Synthesis

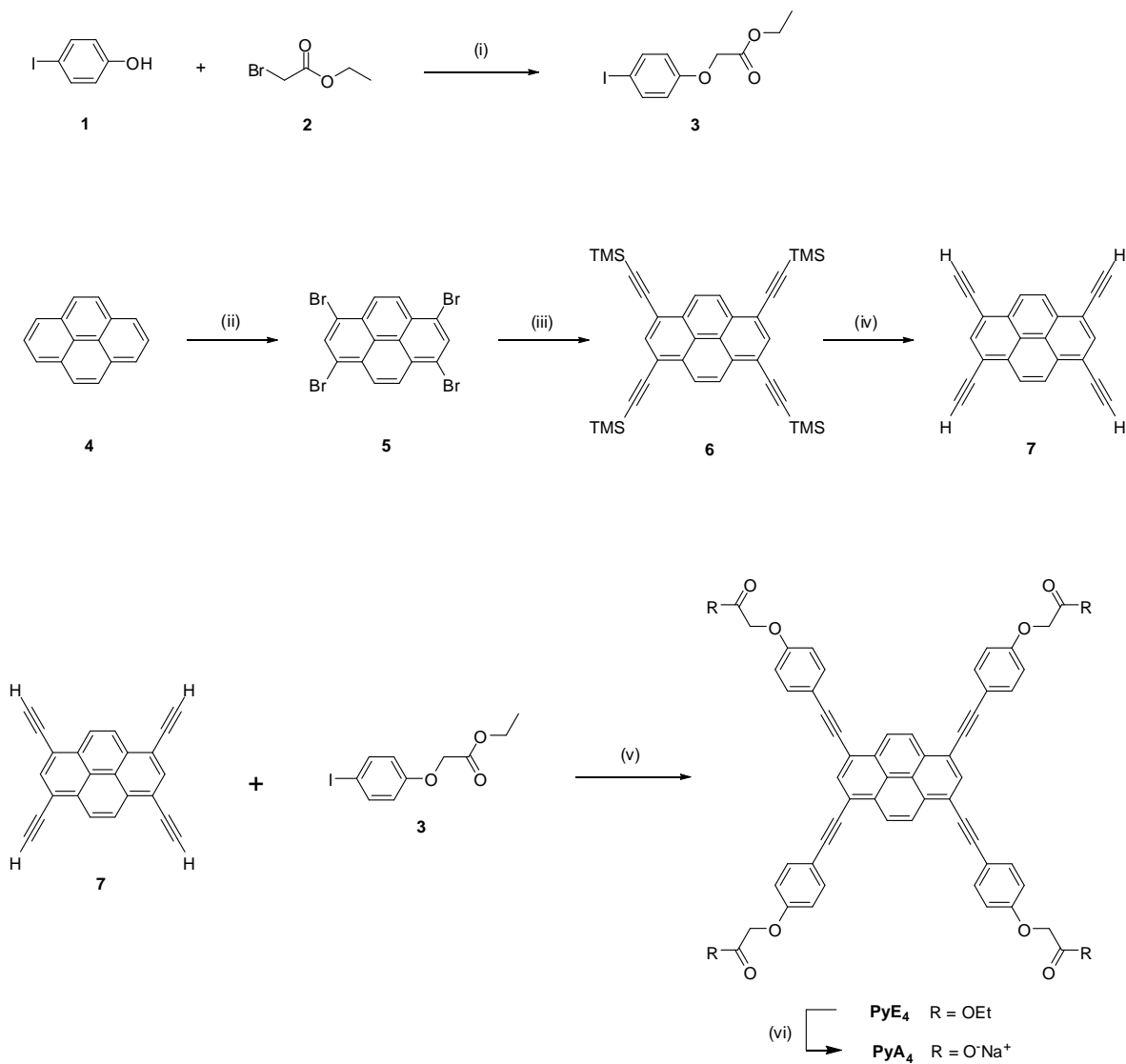


Figure 4-2. Synthesis of **PyA4** (i) K_2CO_3 , CH_3CN , reflux for 24 hrs; (ii) Br_2 , nitrobenzene, 120°C for 24 hrs; (iii) trimethylsilylacetylene, $\text{Pd}(\text{PPh}_3)_4$, CuI , THF/TEA (1/1, v/v), 70°C for 12 hrs; TBAF, THF, r.t for 1 hr; (v) **3**, $\text{Pd}(\text{PPh}_3)_4$, CuI , THF/TEA (1/1, v/v), 70°C for 12 hr; (vi) NaOH, 2-methoxyethanol, reflux for 12 hrs.

The synthetic pathway for **PyA4** is outlined in Figure 4-2. First, the starting material, 4-(ethoxycarbonylmethoxy)iodobenzene (**3**), was synthesized by the reaction of 4-iodophenol (**1**) with 1.1 equivalents of ethyl bromoacetate (**2**) in the presence of anhydrous K_2CO_3 as a base in dried CH_3CN in moderate yield. Second, commercially

available pyrene (**4**) was converted to 1,3,6,8-tetrabromopyrene (**5**) in a 94% yield through bromination using 5.0 equivalents of bromine in nitrobenzene. Then, **5** was reacted with 4.5 equivalents of trimethylsilylacetylene using a catalytic amount of $\text{Pd}(\text{PPh}_3)_2\text{Cl}_2$, PPh_3 and CuI to give a 1,3,6,8-tetrakis(trimethylsilylethynyl)-pyrene (**6**) in a 21% yield (Sonogashira coupling). After desilylation by treatment with TBAF (*n*-tetrabutylammonium fluoride) in THF for 1 hour, 1,3,6,8-tetraethynylpyrene (**7**) was obtained in a 93% yield. Using the Sonogashira coupling, **7** was then reacted with previously synthesized **3** to give the tetraphenoxymethyl ester bearing tetraethynylpyrene (**PyE4**) with yield of 55%. The hydrolysis of **PyE4** was easily accomplished by the addition of 5.0 equivalents of NaOH in 2-methoxyethanol. The further purification was followed by dialysis method using 500 D molecular-weight-cutoff (MWCO) dialysis membranes. The water soluble **PyA4** was obtained as a dark red crystalline solid in an excellent yield (83% yield).

Characterization of **PyA4**

The photophysical properties of the **PyA4** were investigated by the UV/Vis spectroscopy and by the fluorescence measurement in MeOH, DMSO, and HEPES buffer (0.02 M, pH 7.5) (HEPES=2-[4-(2-hydroxyethyl)-1-piperazinyl]ethanesulfonic acid) at 25 °C. It is well known that pyrene derivatives show excimer emission in both highly concentrated solutions and highly polar solvents, especially in water.⁹⁶ Figure 4-3 shows UV/Vis spectra (left) and fluorescence emission spectra (right) of **PyA4** in a solution of DMSO, MeOH, and 20 mM HEPES buffer. Unlike in DMSO and MeOH solutions, the absorption spectrum of **PyA4** in HEPES buffer at pH 7.5 exhibits a small shoulder band at 518 nm (Figure 4-3c). Moreover, the fluorescence emission spectrum of **PyA4** in HEPES buffer exhibits broad excimer emission at 640 nm (Figure 4-3c').

This indicates that **PyA4**'s in HEPES buffer are stacked not only in the ground state but also in the excited state. This behavior can be ascribed to intermolecular hydrophobic interaction of pyrene centered in aqueous media. In contrast, **PyA4** in DMSO and MeOH exhibited only monomer emission at around 500 nm and 480 nm, respectively, suggesting that no aggregation occurs (Figure 4-3a' and 4-3b').

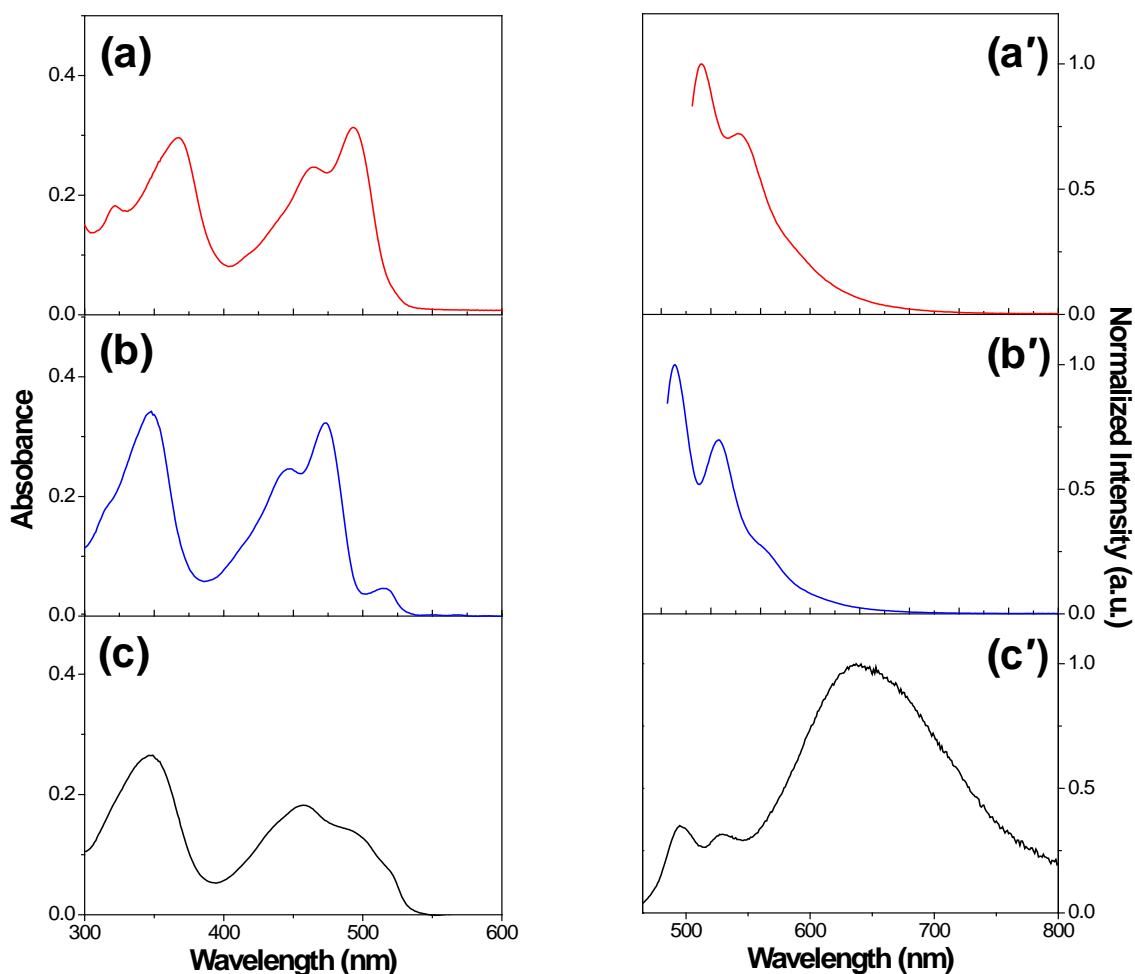


Figure 4-3. UV/Vis (left) and fluorescence emission (right) spectra of **PyA4** in various solutions. (a), (a'): DMSO; (b), (b'): MeOH; (c), (c'): 20 mM HEPES buffer at pH 7.5.

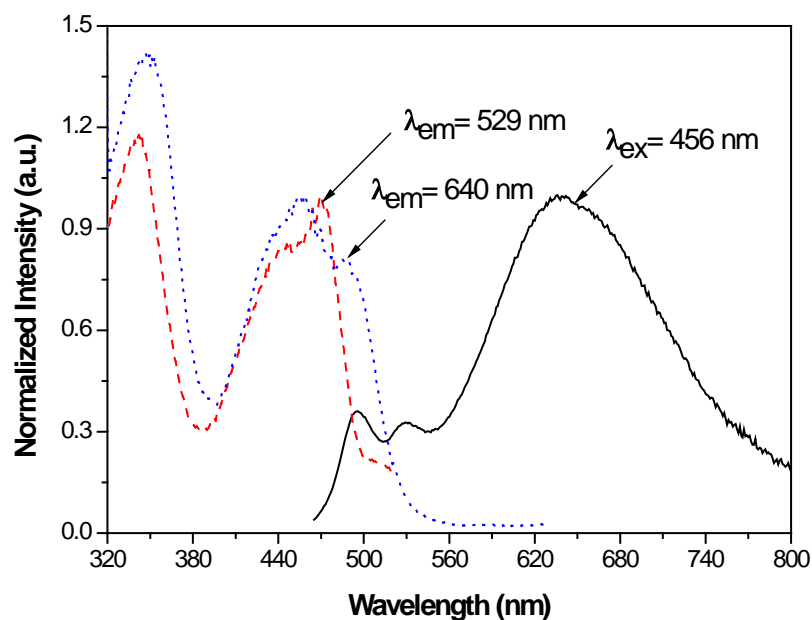


Figure 4-4. Fluorescence excitation and emission spectra of **PyA4** (5 μ M) in 20 mM HEPES buffer at pH 7.5; left: excitation spectra (red dash line, $\lambda_{em}=529$ nm and blue dot line, $\lambda_{em}=640$ nm), right: emission spectrum ($\lambda_{ex}=456$ nm).

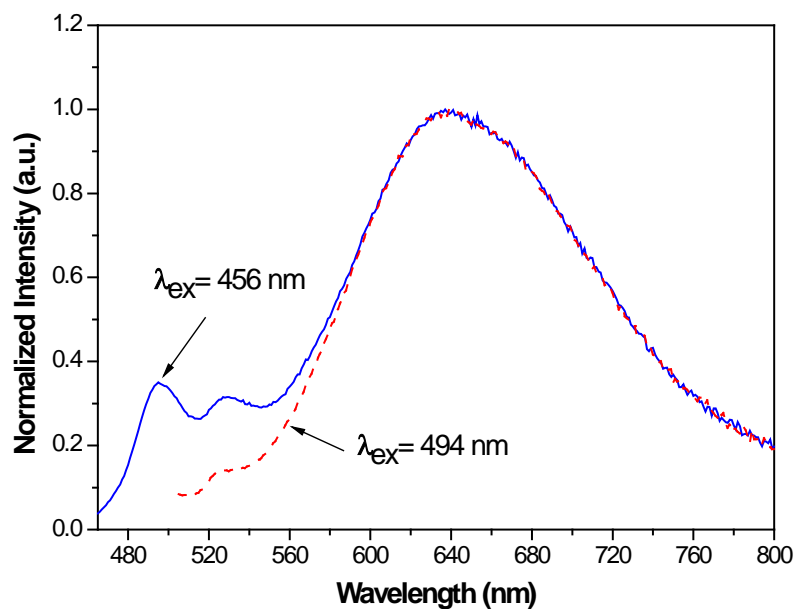


Figure 4-5. Fluorescence emission spectra of **PyA4** in 20 mM HEPES buffer at pH 7.5 (blue, $\lambda_{ex}=456$ nm and red, $\lambda_{ex}=494$ nm).

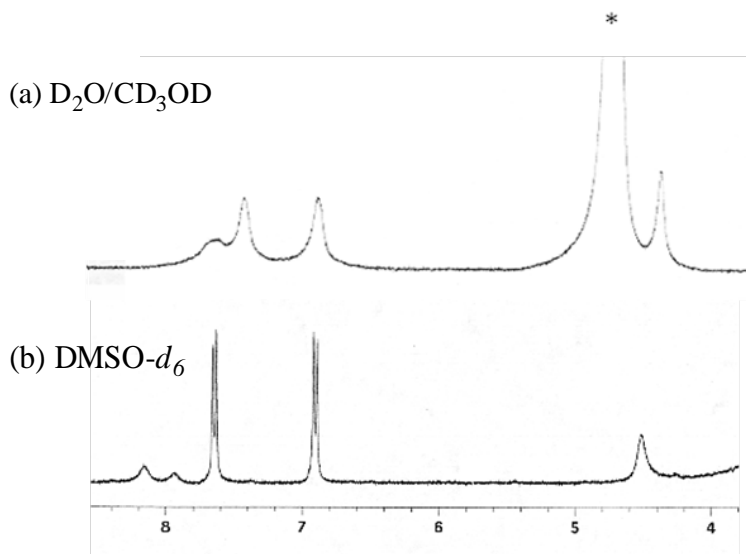


Figure 4-6. ^1H NMR spectra of **PyA4** in (a) $\text{D}_2\text{O}/\text{CD}_3\text{OD}$ (3/1, v/v) and (b) $\text{DMSO}-d_6$; * denotes solvent peak.

As shown in Figure 4-4, two distinctive excitation spectra were observed from monomer emission ($\lambda_{\text{em}}=529\text{ nm}$) and excimer emission ($\lambda_{\text{em}}=640\text{ nm}$), respectively. The excitation spectrum from the monomer part (red dashed line) shows a band which resembles the absorption spectrum of **PyA4** in DMSO and MeOH solutions. On the other hand, the excitation spectra monitoring at the excimer emission shows a shoulder band at 494 nm (blue dot line). This is attributed to direct excitation from aggregated **PyA4** in the ground state. In addition, fluorescence emission of **PyA4** shows only the excimer band when it was excited at the shoulder band (494 nm) (Figure 4-5). As a result, fluorescence excitation spectra ($\lambda_{\text{em}}=529$ and 640 nm) clearly show that two pathways for the excimer band exist: direct excitation from the aggregated ground state and excitation from the non-aggregated ground state. This ground state aggregation is also supported by ^1H NMR spectrum, in which broad peaks in $\text{D}_2\text{O}/\text{CD}_3\text{OD}$ (3/1, v/v) indicate ground state aggregation whereas peaks in $\text{DMSO}-d_6$ show relatively sharp features (Figure 4-6).

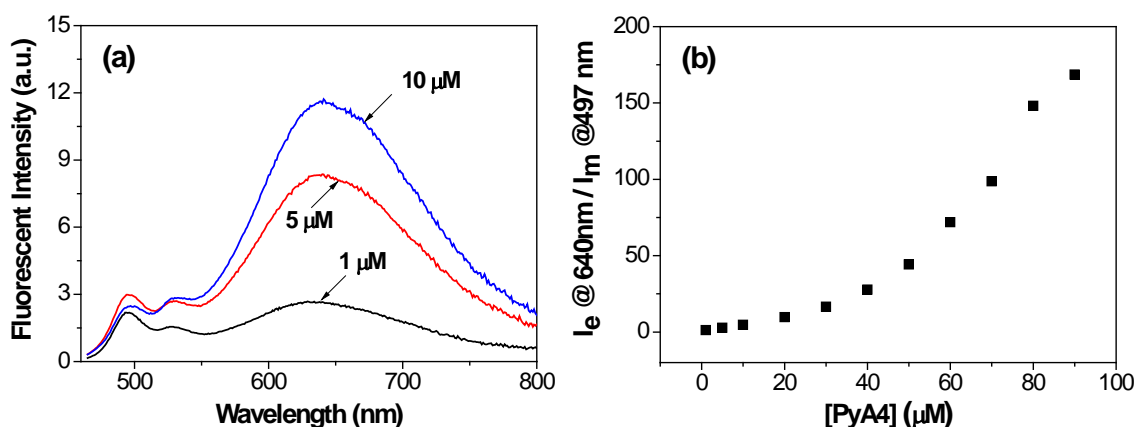


Figure 4-7. (a) Fluorescence emission spectra of **PyA4** solutions with increasing concentration (1-10 μM) in 20 mM HEPES buffer solutions at pH 7.5; (b) ratio of excimer (640 nm) to monomer (497 nm) with increasing concentration (1-100 μM); Excitation at 456 nm.

As shown in Figure 4-7a, the fluorescence spectrum ($\lambda_{\text{ex}} = 456\text{ nm}$) of **PyA4** displays a stronger excimer emission at 640 nm with increasing its concentration in HEPES buffer. Figure 4-7b shows the intensity ratio of the excimer (640 nm) to monomer (497 nm) for **PyA4** with varying concentration. The ratio increases with increasing concentration of **PyA4**, indicating that the higher the concentration of **PyA4** is, the more the aggregation occurs in HEPES buffer.

Quenching with Metal Ions

To develop a metal based **PyA4** sensor for anion, the quenching efficiency of **PyA4** was tested with many divalent metal ions: Ca^{2+} , Mg^{2+} , Co^{2+} , Ni^{2+} , Mn^{2+} , Fe^{2+} , Hg^{2+} , Zn^{2+} , Cd^{2+} , Pb^{2+} , and Cu^{2+} . **PyA4** shows a Cu^{2+} ion selectivity over other metal ions in terms of decreasing fluorescence (Figure 4-8a). The fluorescence quenching can be explained as PET⁹⁵ from **PyA4** to the Cu^{2+} ions bound to carboxylate groups when Cu^{2+} ion is bound to the carboxylate groups, which efficiently leads to the quenching in this system. As shown in Figure 4-8b, the addition of Cu^{2+} ions caused the overall

intensity of the emission spectra to decrease, resulting in 98.5% quenching at 640 nm upon the addition of Cu^{2+} ions ($20\ \mu\text{M}$).

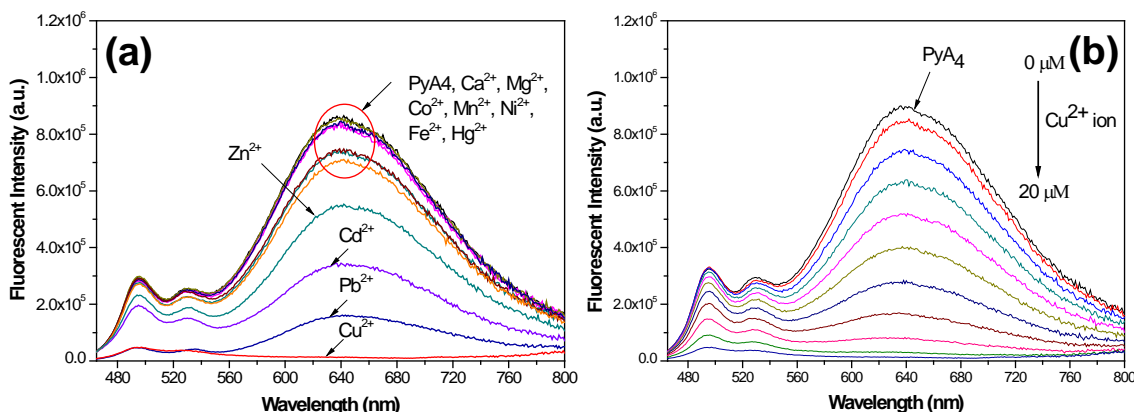


Figure 4-8. (a) Fluorescence emission changes of **PyA4** ($5\ \mu\text{M}$) upon the addition of various metal ions ($30\ \mu\text{M}$); (b) Titration of **PyA4** ($5\ \mu\text{M}$) with Cu^{2+} ions (0 – $20\ \mu\text{M}$); Inset: ratio of excimer ($640\ \text{nm}$) to monomer ($497\ \text{nm}$); Excitation at $456\ \text{nm}$ in $20\ \text{mM}$ HEPES buffer at pH 7.5 .

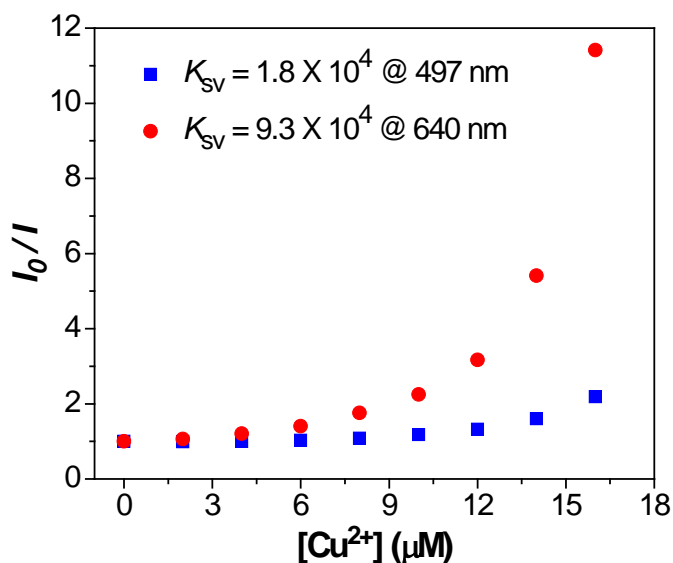


Figure 4-9. Stern-Volmer plots of **PyA4** ($5\ \mu\text{M}$) titrated with Cu^{2+} ions in $20\ \text{mM}$ HEPES buffer at pH 7.5 ; Excitation at $456\ \text{nm}$, fluorescence intensity was monitored at 497 and $640\ \text{nm}$.

Figure 4-9 shows the Stern-Volmer plots of **PyA4** (5 μM) titrated with Cu^{2+} ions in 20 mM HEPES buffer at pH 7.5. Both SV plots are linear at very low concentration of Cu^{2+} ions, but it showed upward curve at the higher concentration of Cu^{2+} ions. It is observed that more efficient quenching at excimer emission ($K_{\text{sv}} = 9.3 \times 10^4 \text{ M}^{-1}$) occurs than monomer emission ($K_{\text{sv}} = 1.8 \times 10^4 \text{ M}^{-1}$). This indicates that the excimer (the delocalized excited state) is more efficiently quenched than the monomer emission (single fluorophore component) by Cu^{2+} ions and its quenching efficiency is amplified in more aggregated states. Furthermore, this decrease is more distinguished in higher concentration of **PyA4**. This phenomenon was also found by Kool et al., in which the π -stacked pyrene system in nonconjugated polymer may cause efficient quenching as in conjugated polymer system.¹¹⁰

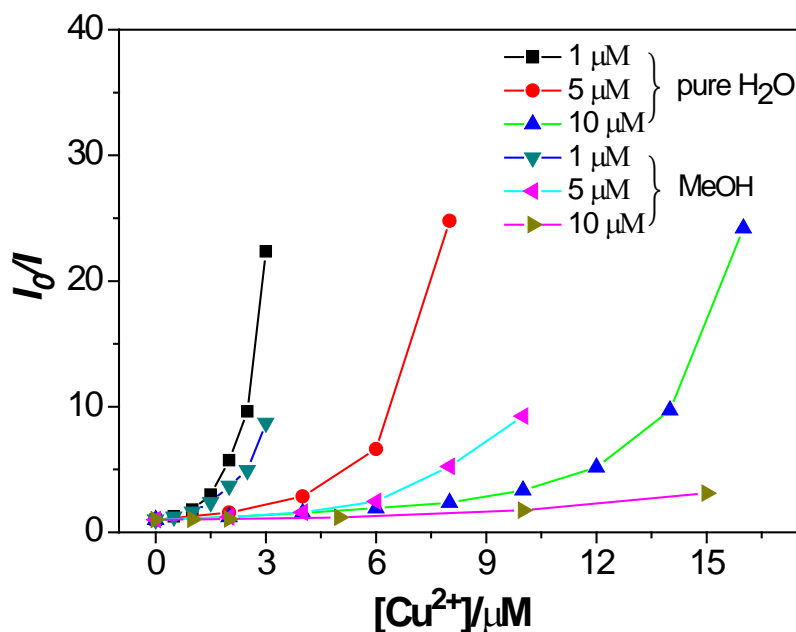


Figure 4-10. Stern-Volmer plots of **PyA4** (1, 5, and 10 μM) titrated with Cu^{2+} ions in MeOH and pure H_2O ; Excitation at 456 nm, fluorescence intensity was monitored at 491 nm in MeOH and 640 nm in pure H_2O , respectively.

Table 4-1. K_{SV} ^a and $[Q]_{90}$ ^b for Cu²⁺ ion quenching of **PyA4** in H₂O and MeOH.

[PyA4]/ μ M	$K_{SV}(H_2O) / M^{-1}$	$[Q]_{90}(H_2O)/\mu$ M	$K_{SV}(MeOH)/M^{-1}$	$[Q]_{90}(MeOH)/\mu$ M
1	9.0×10^5	≈ 2.5	8.1×10^5	> 3
5	2.8×10^5	≈ 7	1.5×10^5	> 10
10	1.7×10^5	≈ 14	7.7×10^4	> 35

^a Computed from linear fit at low quencher concentration. ^b Quencher concentration at 90% quenching.

Efficient quenching in the aggregate state was further investigated by Stern-Volmer¹⁹ quenching experiment in MeOH and pure H₂O. In both cases, fluorescence intensity was efficiently quenched by the addition of Cu²⁺ ions. The SV plots for Cu²⁺ ion quenching of **PyA4** displayed different features in MeOH and pure H₂O, respectively. As expected, in pure H₂O, the SV plot for **PyA4** (5 μ M) is linear at very low concentration of Cu²⁺ ions, but became nonlinear with increasing concentration of Cu²⁺ ions (Figure 4-10), in which K_{SV} value of $2.8 \times 10^5 M^{-1}$ was obtained. In MeOH, however, its SV plot (**PyA4** = 5 μ M) showed relatively linear at the same range of quencher concentration as in pure H₂O (K_{SV} value = $1.5 \times 10^5 M^{-1}$ in MeOH). This large K_{SV} value suggests that the quenching results from a ground state complex between **PyA4** and Cu²⁺ ions. In addition, K_{SV} values of **PyA4** (1 μ M and 10 μ M) decrease with increasing its concentration in both MeOH and pure H₂O (Table 4-1). This decrease of the K_{SV} value from 1 μ M to 10 μ M of **PyA4** is around 5-fold in pure H₂O, which is smaller compared to that in MeOH (10-fold). In other words, the decrease of K_{SV} values by the effect of concentration is less pronounced in pure H₂O. Furthermore, K_{SV} value of **PyA4** in pure H₂O is modestly larger than that in MeOH, even though there is more solvation effect in pure H₂O. Moreover, the difference of K_{SV} value in between H₂O and MeOH is more

distinctive in 10 μM than that in 1 μM . These differences reflect that **PyA4** is more efficiently quenched in aqueous solution by Cu^{2+} ions. Similar result was observed in the comparison of the relative quenching efficiencies in H_2O and MeOH . $[\text{Q}]_{90}$ values for Cu^{2+} ion in H_2O and MeOH were presented in Table 4-1. The $[\text{Q}]_{90}$ values in H_2O are lower than MeOH . Also, $[\text{Q}]_{90}$ in MeOH tracks closely with the concentration of **PyA4** whereas their difference between 1 μM and 10 μM in H_2O is less significant than MeOH . As a result, we suggest that more excimer quenching in aqueous solution may be caused by energy migration through the aggregates of **PyA4** if the delocalized excited state of the pyrene stack is mobile as in the case of conjugated polymer. However, quenching is still less efficient compared to **PPE-CO²⁻**, reflecting improved transport in CPEs.¹⁰²

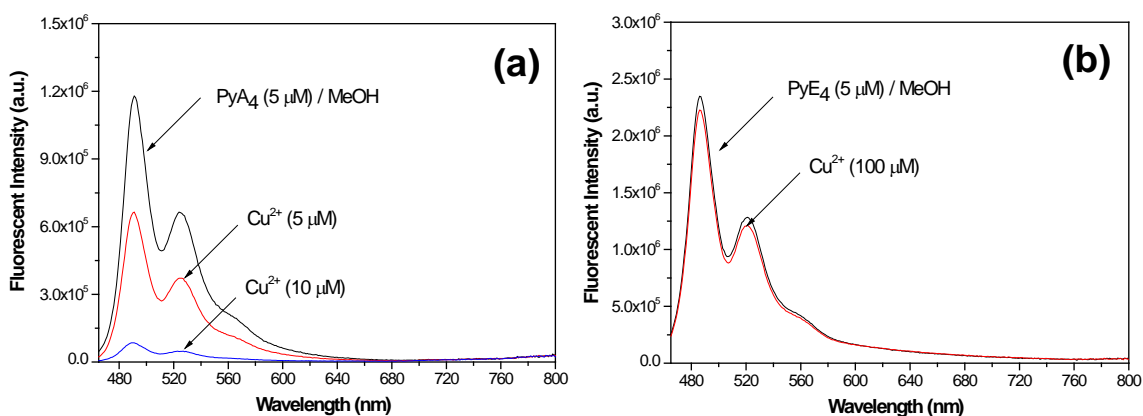


Figure 4-11. Titration of (a) **PyA4** (5 μM) and (b) **PyE4** (5 μM) with Cu^{2+} ions in MeOH ; Excitation at 456 nm.

To know the binding sites of **PyA4** in the presence of Cu^{2+} , we tested **PyE4** having tetraester groups with Cu^{2+} ion in MeOH (Figure 4-11). For **PyE4**, no remarkable changes were observed, even in spite of the addition of 200 equivalents Cu^{2+} ions. **PyA4**, on the other hand, showed significant quenching in the same media. Thus,

carboxylate groups of **PyA4** play an important role as a receptor for binding Cu^{2+} ions. Unfortunately, we cannot clearly explain the exact binding mode and ratio between **PyA4** and Cu^{2+} ions only by lack of fluorescence emission changes observed for **PyE4** upon excess amount of Cu^{2+} ions in MeOH.

Application to Pyrophosphate (PPi) Sensing

Selective and sensitive detection of PPI

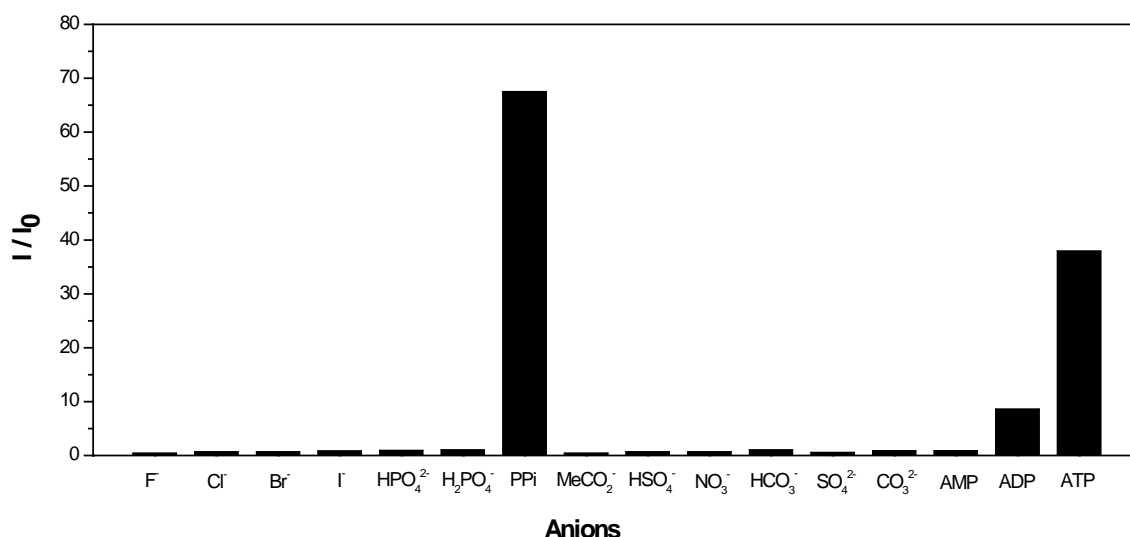


Figure 4-12. Fluorescence emission changes of **PyA4** (5 μM) - Cu^{2+} (20 μM) at 640 nm upon the addition of anions (50 μM); Excitation at 456 nm in 20 mM HEPES buffer at pH 7.5; I_0 : fluorescence emission intensity of **PyA4**- Cu^{2+} complex, I : fluorescence emission intensity in the presence of anions.

The anion binding ability of **PyA4**- Cu^{2+} (**PyA4**: 5 μM and Cu^{2+} : 20 μM) with the anions F^- , Cl^- , Br^- , I^- , H_2PO_4^- , HPO_4^{2-} , PPI, AcO^- , HSO_4^- , NO_3^- , HCO_3^- , SO_4^{2-} , CO_3^{2-} , AMP, ADP, and ATP (Sodium salts), in 20 mM HEPES buffer at pH 7.5 was investigated using fluorescence emission spectrum ($\lambda_{\text{ex}}=456 \text{ nm}$). The overall fluorescence intensity changes upon the addition of various anions (50 μM) are compared in Figure 4-12. Interestingly, the **PyA4**- Cu^{2+} system is highly selective to

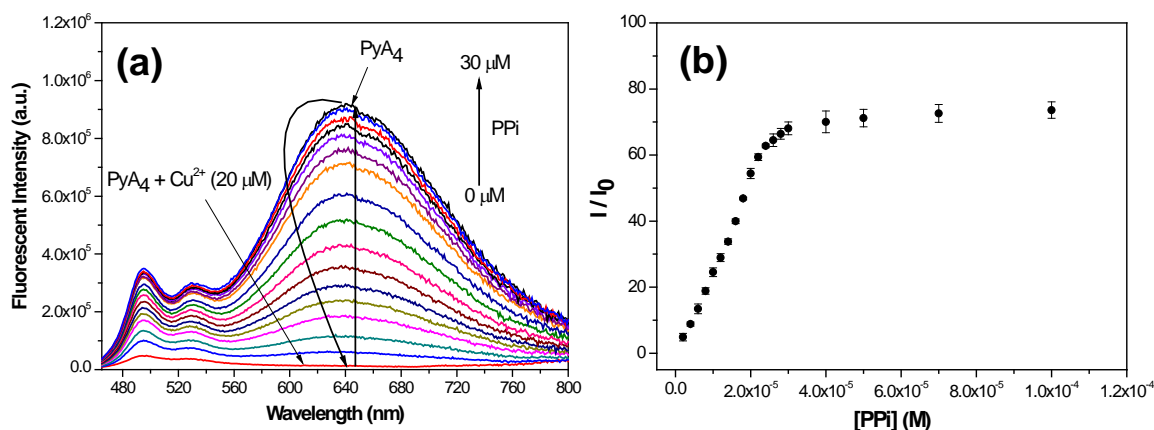


Figure 4-13. (a) Titration of **PyA4** (5 μM)- Cu^{2+} (20 μM) with PPI (1-30 μM) in 20 mM HEPES buffer at pH 7.5; (b) Titration profile with I/I_0 ratio represented by the intensity at 640 nm; I_0 : fluorescence emission intensity of **PyA4**- Cu^{2+} complex, I : fluorescence emission intensity in the presence of PPI.

PPI with a significant enhancement of excimer intensity compared to the other anions.

Figure 4-13 shows fluorescence titration results of **PyA4**- Cu^{2+} complex with PPI in 20 mM HEPES buffer at pH 7.5. Upon the addition of 20 μM PPI (which is the same concentration as Cu^{2+} ions complexed), a 54-fold enhancement of fluorescent emission intensity is observed at 640 nm, approximately 77% of the initial fluorescence of **PyA4** without Cu^{2+} ions. The analytical detection limit (ADL) for PPI is 65.6 nM at low range of quencher concentration. When 40 μM of PPI was added to a solution of the **PyA4**- Cu^{2+} complex, recovery reached approximately 99% (70-fold enhancement) of the fluorescence intensity. We believe that two oxygen anions of PPI are involved in the complexation with the divalent Cu^{2+} ion by the ratio of 1:2 (Cu^{2+} : PPI), inducing dissociation of interaction between **PyA4** and Cu^{2+} ions with recovered fluorescence. Further addition of excess PPI to **PyA4**- Cu^{2+} complex shows neither any subtle wavelength change nor remarkable emission intensity change (Figure 4-13b). This observation means that an excess amount of PPI does not affect recovered **PyA4**.

PyA4 was also tested in the high ionic strength buffer solution (100 mM HEPES solutions at pH 7.5). As seen in Figure 4-14, increasing ionic strength leads to a reduced affinity of **PyA4**-Cu²⁺ complex for PPI. Even so, it showed 91% recovery of the fluorescence intensity upon addition of 60 μ M PPI in 100 mM HEPES buffer, which is a 63-fold enhancement. Figure 4-15 shows the fluorescence intensity changes of **PyA4** upon addition of Cu²⁺ ions, the fluorescence is completely quenched (Figure 4-15b), while the further addition of PPI recovers the fluorescence intensity (Figure 4-15c).

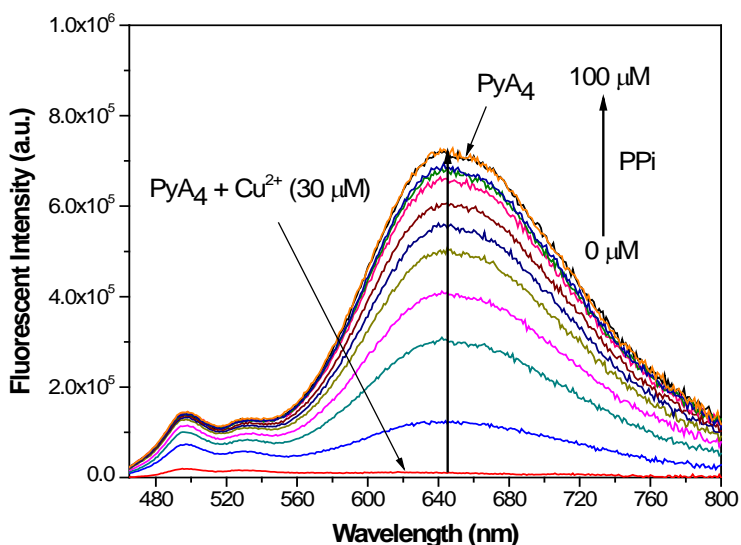


Figure 4-14. (a) Titration of **PyA4** (5 μ M)-Cu²⁺ (30 μ M) with PPI (10-100 μ M) in 100 mM HEPES buffer at pH 7.5; Excitation at 456 nm.



Figure 4-15. Fluorescence intensity changes of (a) **PyA4** (b) **PyA4**-Cu²⁺ complex, and (c) **PyA4**-Cu²⁺ with PPI; [**PyA4**]=10 μ M; [Cu²⁺]=40 μ M; [PPI]=80 μ M in 20 mM HEPES buffer at pH 7.5.

PyA4 also shows no significant changes to 50 μM of AMP (adenosine monophosphate). However, for ADP (adenosine diphosphate) and ATP (adenosine triphosphate), **PyA4**- Cu^{2+} complex shows smaller recovery compared to PPI (Figure 4-12). This is attributed to the comparatively lower anion densities on the phosphorus-oxygen of AMP, ADP, and ATP and their steric bulk when approaching to **PyA4**- Cu^{2+} complex, resulting in less effective fluorescence recovery (only 5, 15, and 50% for AMP, ADP, and ATP were recovered, respectively). This is also supported by Hong's and Febbrizzi's works in which dimetallic receptors showed higher affinity for PPI compared to ATP, Pi, and the other anions due to its relatively larger charge density.^{97,108}

Real-time ALP assay

In order to provide an insight into the bioanalytical applications of **PyA4**- Cu^{2+} system for monitoring enzyme's activity, the real-time assay of pyrophosphate hydrolysis was investigated using alkaline phosphatase (ALP) in HEPES buffer (0.02 M, pH 7.5) at 37 °C. The solution for ALP assay was prepared with 5 μM of **PyA4**, 20 μM of Cu^{2+} , and 40 μM of PPI and incubated for 10 minutes before addition of ALP. As shown in Figure 4-16, fluorescence intensity (λ_{ex} =456 nm and λ_{em} =640 nm) has gradually decreased as a function of time in the presence of ALP. As expected, this reaction is catalyzed by ALP, in which PPI is hydrolyzed to Pi. Free **PyA4** is re-associated with Cu^{2+} ion because produced Pi shows less affinity for Cu^{2+} ion, leading to the fluorescence quenching. Its quenching effect was accelerated as the ALP concentration increases. This study clearly shows that **PyA4**- Cu^{2+} system can be useful tool for not only ALP assay but also monitoring enzyme's activity involving PPI and Pi.

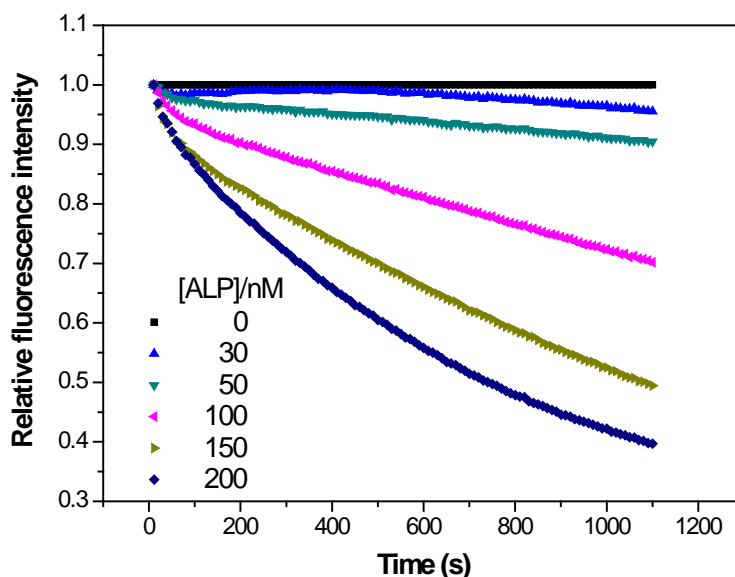


Figure 4-16. Real-time ALP assay using **PyA4** (5 μM)- Cu^{2+} (20 μM) and PPI (30 μM) in 20 mM HEPES buffer at pH 7.5, 37.0 $^{\circ}\text{C}$; Excitation wavelength = 456 nm, emission monitored = 640 nm.

Plausible mechanism

Figure 4-17 show a plausible mechanism of the entire sensing processes. Quenched fluorescence of the **PyA4** aggregates- Cu^{2+} ions complex was revived by the addition of PPI, in which PPI forms complex with Cu^{2+} ions. Hydrolysis of PPI by ALP produces re-association of **PyA4** aggregates and Cu^{2+} ions, which leads to the fluorescence-off.

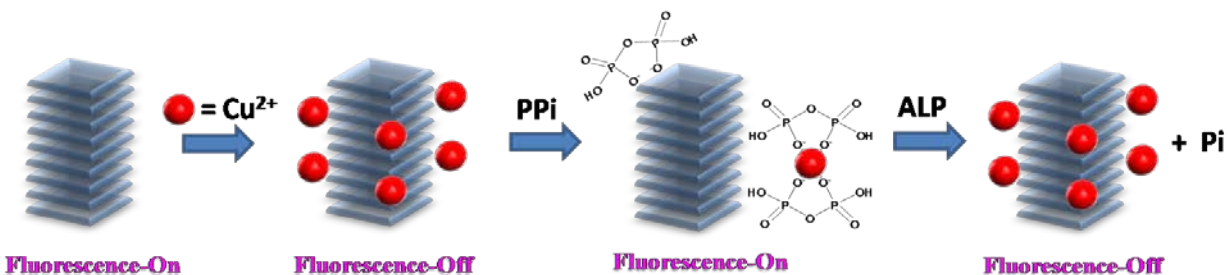


Figure 4-17. Plausible mechanism of sensing process.

Summary and Conclusions

In this Chapter, we synthesized a **PyA4** that displays self-assembly with strong excimer emission in HEPES buffer solution. **PyA4** is stacked not only in the ground state but also in the excited state in HEPES buffer. **PyA4** Fluorescence intensity of PyA4 was selectively quenched with the Cu^{2+} ion; this can be explained by the PET effect. Furthermore, the efficient quenching effect of **PyA4** in aqueous HEPES buffer can probably be explained by energy migration. This system, **PyA4**- Cu^{2+} , sensitively and selectively recognizes PPI over other anions, inducing strong fluorescence recovery by dissociation of the interaction between the **PyA4** and the Cu^{2+} ion. The real-time turn-off assay was developed to monitor ALP activity.

Experimental

Materials

All chemicals used in the synthesis were of reagent grade and used without further purification. Pyrene, 4-iodophenol, ethyl bromoacetate, bromine, copper iodide, triethylamine, *tetrakis*(triphenylphosphine)palladium (0), *tetrabutylammonium* fluoride, and diisopropylamine were purchased from Sigma-Aldrich Chemical Company. Ethynyltrimethylsilane was bought from GFC Chemical Company. Potassium carbonate was obtained from Fisher Scientific Company. THF was purified by Solvent Dispensing System (SDS). Silica gel (Merck, 230-400 mesh) was used for chromatographic purification of all of intermediate and target molecules. All other chemicals and solvents were purchased from Sigma-Aldrich, Fisher Scientific, or Acros Chemical Company and used as received.

Instrumentation and Methods

NMR spectra were recorded using a Varian VXR-300 FT NMR, operating at 300 MHz for ^1H NMR and at 75 MHz for ^{13}C NMR. UV/Vis absorption spectra were recorded using a Varian Cary 50 Spectrophotometer. Steady-state fluorescence spectra were obtained with a PTI fluorometer. A 1 cm quartz cuvette was used for all spectral measurements.

Stock solutions (1.0 mM) of **PyA4** was prepared in H_2O . The chloride salts of Ca^{2+} , Mg^{2+} , Co^{2+} , Ni^{2+} , Mn^{2+} , Fe^{2+} , Hg^{2+} , Zn^{2+} , Cd^{2+} , Pb^{2+} and Cu^{2+} ions (stock solutions = 10.0 mM in H_2O) were tested to evaluate the metal ion binding properties of PyA4 (stock solution = 1.0 mM in H_2O). The excitation was 456 nm. The sodium salts of F^- , Cl^- , Br^- , I^- , H_2PO_4^- , HPO_4^{2-} , PPi , AcO^- , HSO_4^- , NO_3^- , HCO_3^- , SO_4^{2-} , CO_3^{2-} , AMP, ADP, and ATP (stock solutions = 10.0 mM in H_2O) were used. For all fluorescence measurements, the excitation was made at 456 nm to give fluorescence intensity at 640 nm at room temperature.

Analytical detection limit (ADL) was calculated using the equation $\text{ADL} = 3\delta_{\text{bk}}/m$ ($\delta_{\text{bk}} = \delta_{\text{C=0}}/\sqrt{2}$), where $\delta_{\text{C=0}}$ is the standard deviation of the blank and m is the slope of the calibration plot.¹¹¹

Synthetic Procedure

4-(ethyloxycarbonylmethoxy)iodobenzene (3). To a solution of 4-iodophenol (**1**) (10.0 g, 45.5 mmol) in dried CH_3CN (50 mL), anhydrous K_2CO_3 (6.30 g, 45.5 mmol) was added. After stirring for 30 min, ethyl bromoacetate (**2**) (8.4 g, 50 mmol) was added to the reaction mixture. The resulting mixture was vigorously stirred at 80°C for 24 hours under argon gas. After the reaction mixture was cooled to room temperature, the solvent was removed *in vacuo*. The reaction mixture was acidified with 5 % aqueous

HCl solution (100 mL), and then extracted with CH₂Cl₂ (200 mL). The organic layer was separated and washed with water (100 mL) and dried over anhydrous MgSO₄, and the solvent was evaporated to yield a white solid. The pure product was isolated by column chromatography on silica gel using ethyl acetate:hexane (1:3) as the eluent. 61% yield; mp 58-60 °C; ¹H NMR (300 MHz, CDCl₃, δ_{ppm}): 7.55 (d, 2H, IAr-*H*_{ortho}, *J*=9.0 Hz), 6.97 (d, 2H, IAr-*H*_{meta}, *J*=9.0 Hz), 4.56 (s, 2H, ArOCH₂CO₂), 4.25 (q, 2H, CO₂CH₂CH₃, *J*=7.2 Hz), 1.27 (t, 3H, CO₂CH₂CH₃, *J*=7.2 Hz); ¹³C NMR (75 MHz, CDCl₃, δ_{ppm}): 169.4, 158.5, 139.0, 117.8, 84.5, 66.0, 62.0, 14.2.

Compounds **5**, **6**, and **7** were prepared in a good yield as described in the literatures.¹

1,3,6,8-Tetrabromopyrene (5). 94% yield. This solid product was not soluble enough in most of the common organic solvents to take a NMR spectrum. Therefore, it was identified after the Sonogashira coupling reaction with trimethylsilylacetylene.

1,3,6,8-Tetrakis(trimethylsilylethynyl)pyrene (6). 21% yield. ¹H NMR (300 MHz, CDCl₃, δ_{ppm}): 8.59 (s, 4H, pyrene-*H*), 8.30 (s, 2H, pyrene-*H*), 0.40 (s, 36H, SiCH₃).

1,3,6,8-Tetraethynylpyrene (7). 93% yield. ¹H NMR (300 MHz, CDCl₃, δ_{ppm}): 8.55 (s, 4H, pyrene-*H*), 8.31 (s, 2H, pyrene-*H*), 4.93 (s, 4H, acetylene-*H*).

1,3,6,8-Tetrakis[{4-(ethyloxycarbonylmethoxy)phenyl}ethynyl]pyrene (PyE4). To a mixture of 1,3,6,8-tetraethynylpyrene (**7**) (0.40 g, 1.34 mmol) and 4-(ethyloxycarbonylmethoxy)iodobenzene (**3**) (2.05 g, 6.70 mmol) in degassed solution of THF (10 mL) and triethylamine (10 mL), Pd(PPh₃)₄ (0.077 g, 0.067 mmol) and CuI (0.013 g, 0.067 mmol) were added. The resulting mixture was stirred at 80 °C for 12 hours under argon gas. After the reaction mixture was cooled to room temperature, the

solvent was removed *in vacuo*. The crude mixture was purified by column chromatography on silica gel using CH₂Cl₂:Hexane (3:7) as the eluent. 55% yield; mp 140-142 °C; ¹H NMR (300 MHz, CDCl₃, δ_{ppm}): 8.58 (s, 4H, pyrene-*H*), 8.30 (s, 2H, pyrene-*H*), 7.65 (d, 8H, CAr-*H*_{ortho}, *J*=8.4 Hz), 6.97 (d, 8H, CAr-*H*_{meta}, *J*=8.4 Hz), 4.68 (s, 8H, ArOCH₂CO₂), 4.33 (q, 8H, CO₂CH₂CH₃, *J*=7.2 Hz), 1.34 (t, 12H, CO₂CH₂CH₃, *J*=7.2 Hz); ¹³C NMR (75 MHz, CDCl₃, δ_{ppm}): 168.5, 158.1, 133.5, 131.5, 126.4, 122.9, 119.0, 116.8, 115.0, 94.9, 87.4, 65.6, 61.7, 14.4; APCI-TOF MS (*m/z*): [M+H]⁺ calcd for C₆₄H₅₀O₁₂, 1011.3375; found, 1011.3367.

1,3,6,8-Tetrakis[{4-(carboxymethoxy)phenyl}ethynyl]pyrene, tetrasodium salt (PyA4). To a solution of PyE4 (0.50 g, 0.51 mmol) in 2-methoxyethanol (20 mL), NaOH in water (1 mL) was added dropwise. The reaction mixture was vigorously stirred at 80 °C for 12 hours. The reaction mixture was cooled to room temperature, and then poured into a solution of methanol (300 mL) and diethyl ether (100 mL) to give the fine reddish PyA4 precipitate. Further purification of PyA4 precipitate was accomplished by dialysis using nanopure water (Millipore Simplicity water system) and a 500 D MWCO cellulose membrane. After dialysis, the water was removed *in vacuo*, which gave the crystalline product. 83% yield. ¹H NMR (300 MHz; D₂O:CD₃OD (3:1/v:v), δ_{ppm}): 7.65 (br, 6H, pyrene-*H*), 7.47 (br, 8H, OAr-*H*_{meta}), 6.95 (br, 8H, OAr-*H*_{ortho}), 4.68 (br, 8H, ArOCH₂CO₂); ESI MS (*m/z*): [M-H]⁻ calcd for C₅₆H₃₄O₁₂, 898.21; found, 898.00.

CHAPTER 5

PHOTOPHYSICS AND ENERGY TRANSPORT IN CONJUGATED POLYELECTROLYTE DENDRIMERS

Since dendrimers have received considerable attention as a potential candidate for optical devices,¹¹²⁻¹¹³ light harvesting systems,⁴¹ and medical applications,^{45,114} there is a growing interest in the synthetic methodology and development of new functional materials.^{37,45} Dendrimers are highly branched three-dimensional globular architectures and mono-disperse macromolecules, which are structurally distinct from classical linear polymers.³⁴ Also, because of such distinguished frameworks, their structures in solution are relatively rigid compared to linear polymers that vary in the size and shape depending on the solvent.³³ Furthermore, the number of dendrimer end-groups increases exponentially as the generation increases. Such end-groups in dendrimers can be interfaced between the inside of dendrimers and external materials. Therefore, their functionality is readily modulated by tuning the end-groups. In addition, their interior is encapsulated by external end-groups, which enable one to have two distinctive properties in one molecule.³³ Such unique structure may prevent inherent problems shown in traditional polymers, such as unexpected behavior induced by aggregation and/or large polydispersity (PDI). These extraordinary features can be utilized in light-harvesting system, gene and drug delivery system.

Over the past several decades, numerous types of dendritic systems have been developed, and their electronic properties have also been studied.^{37,45,115-116} As one of the dendritic systems, phenylacetylene dendrimers connected at *meta*-position have been synthesized by Moore and co-workers. Such fully conjugated dendrimers have a higher net density throughout entire dendrimer.¹¹⁷ In addition, electronic communication

between chromophores can lead to extended electronic states and coherent transfer¹¹⁸⁻¹²⁰ or enhanced through-bond energy transfer.¹²¹

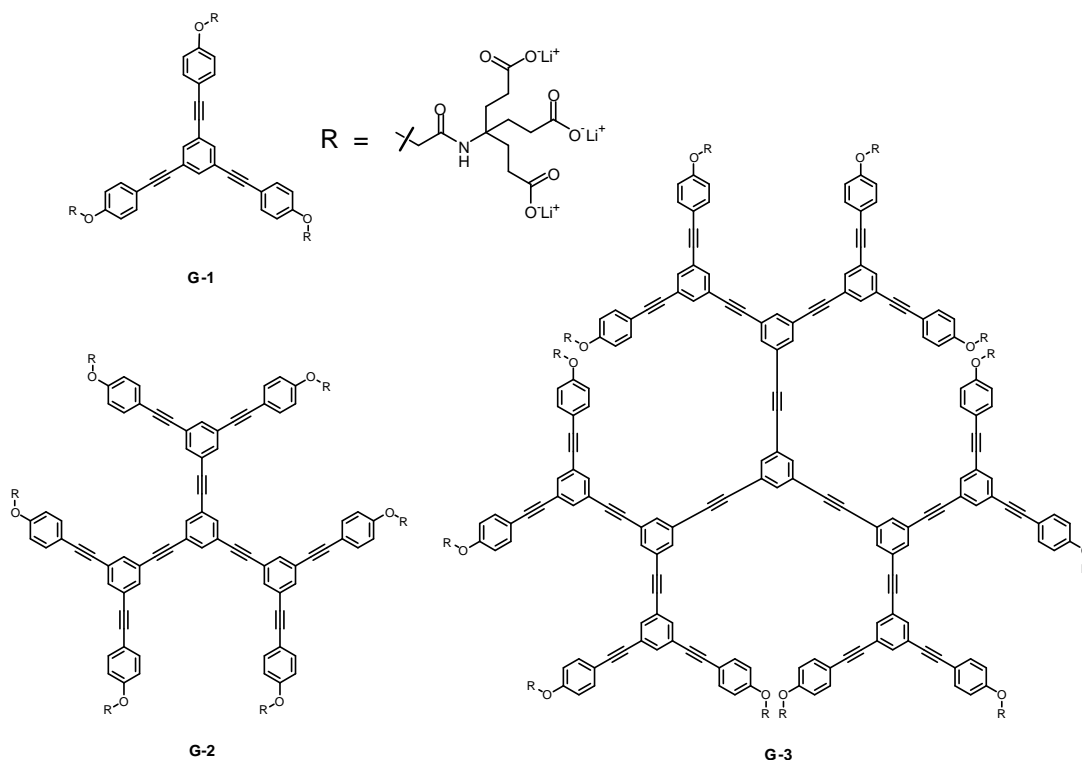


Figure 5-1. Structure of CPE-Ds (**G-1**, **G-2** and **G-3**)

In this Chapter, we designed water-soluble conjugated polyelectrolyte dendrimers (CPE-Ds) containing branched carboxylate end-groups and *meta*-conjugated phenylacetylene as a core and branched repeat units. Figure 5-1 shows the structure of the CPE-Ds (**G-1**, **G-2**, and **G-3**). As the generation increases, the interior hydrophobic focal point and branches are surrounded by an increasing number of hydrophilic carboxylate end-groups. Interestingly, the **G-2** and **G-3** systems closely resemble unimolecular micelles. Unlike traditional micelle, all hydrophilic carboxylate end-groups are covalently connected to the hydrophobic inner parts. Consequently, this structure displays unimolecular micelle type formation, which retains its structure in various solvents and over the entire range of concentrations.³³⁻³⁴

Results

Synthesis and Characterization

Synthesis of precursors

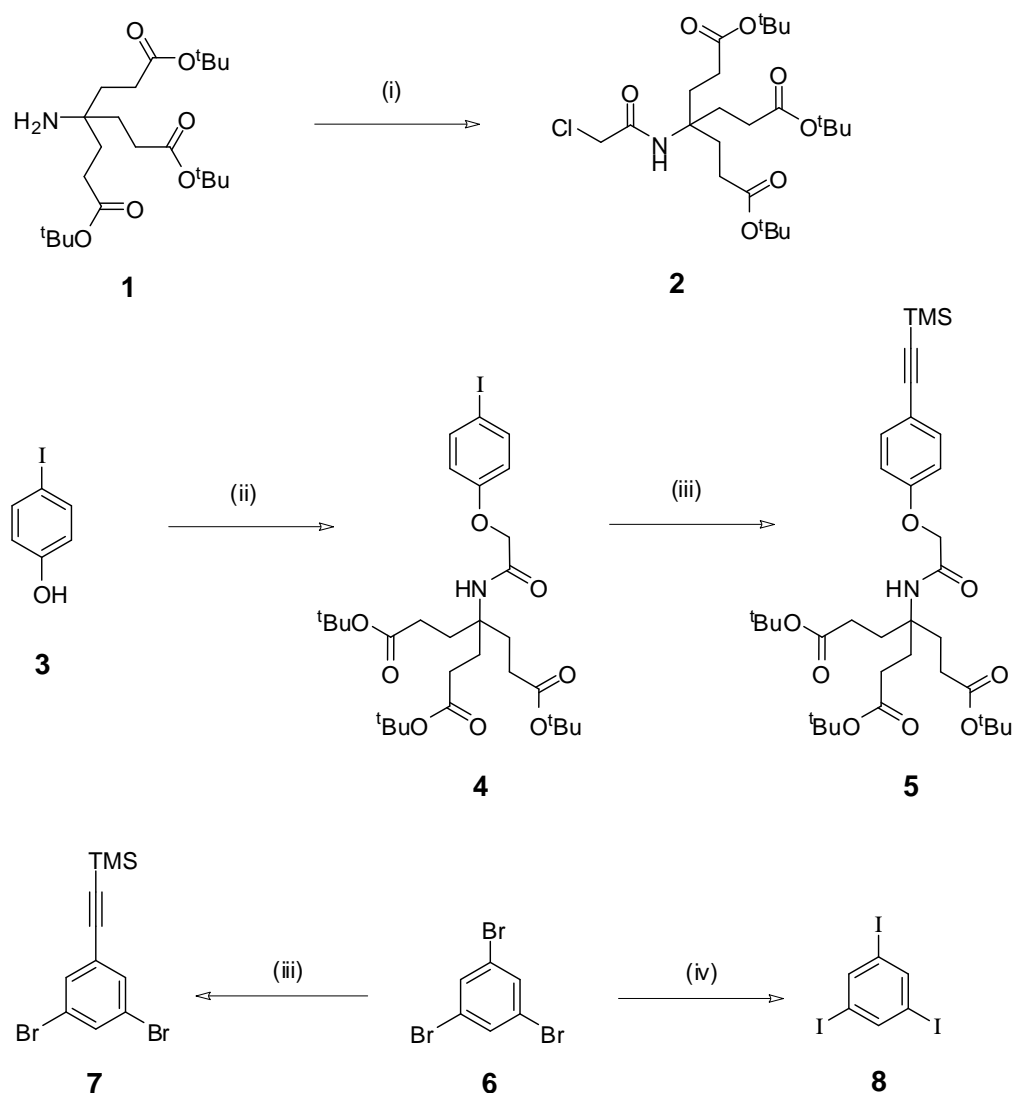


Figure 5-2. Synthesis of **5**, **7**, and **8** (i) chloroacetyl chloride, K_2CO_3 , EtOAc/ H_2O (1/1, v/v), r.t. for 2 hrs.; (ii) **2**, K_2CO_3 , CH_3CN , 80 °C for 12 hrs.; (iii) ethynyltrimethylsilane, THF/DIPA (1/1, v/v), $Pd(PPh_3)_2Cl_2$, CuI , and PPh_3 , r.t. for 12 hrs; (iv) CuI , I_2 , HMPA, reflux.

The preparation of water-soluble conjugated polyelectrolyte dendrimers (CPE-Ds) is described in Figure 5-2~4. Figure 5-2 presents the synthesis of compound **5**. Compound **1** was easily synthesized with an excellent yield as described in the

literature.³⁹ It was converted to di-*tert*-butyl 4-(3-*tert*-butoxy-3-oxopropyl)-4-(2-chloroacetamido)heptanedioate (**2**) with 95.0% yield by the reaction with chloroacetyl chloride in the presence of K₂CO₃ in EtOAc/H₂O (1/1, v/v) solution. Then, 4-iodophenol was (**3**) reacted with **2** to give **4** in 72.0% yield. The coupling reaction of **4** with commercially available ethynyltrimethylsilane in the presence of Pd(PPh₃)₄ and CuI in THF/DIPA (1/3, v/v) afforded **5** in 62.8% yield. Compound **7** was readily synthesized from 1,3,5-tribromobenzene (**6**) by Sonogashira coupling reaction. Also, the bromine group of compound **6** was effectively converted to iodine group in the presence of CuI and I₂.¹²²⁻¹²³

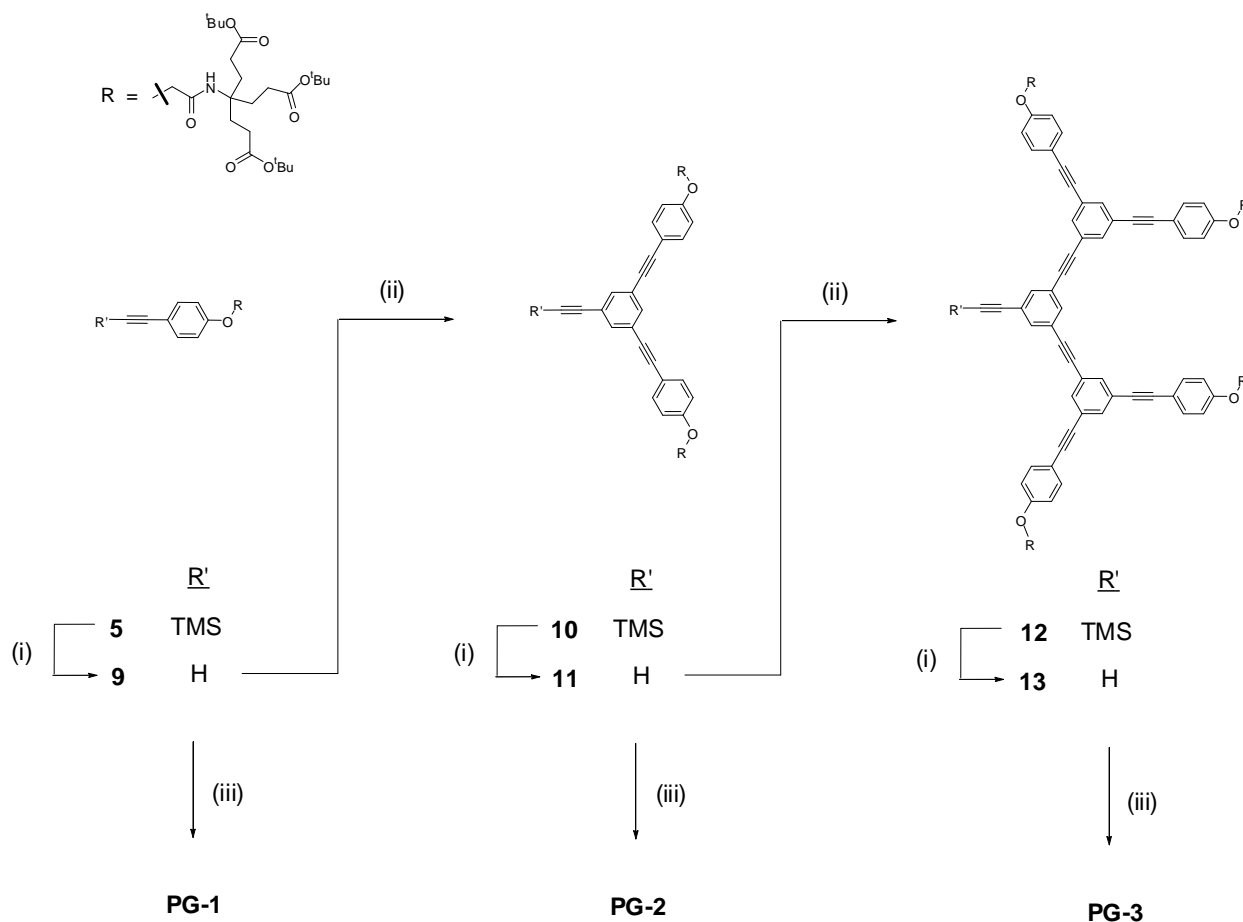


Figure 5-3. Synthesis of **PG-1**, **PG-2**, and **PG-3** (i) K₂CO₃, DCM/CH₃OH (1/1, v/v), r.t. for 2 hrs.; (ii) **7**, THF/DIPA (1/4, v/v), Pd(dba)₂, PPh₃, CuI, 80 °C for 12 hrs.; (iii) **8**, THF/DIPA (1/4, v/v), Pd(dba)₂, PPh₃, CuI, 80 °C for 12 hrs.

Figure 5-3 shows the synthesis of precursor **G-1**, **G-2** and **G-3** (**PG-1**, **PG-2** and **PG-3**). De-protection of trimethylsilyl group of **5** was accomplished by using K_2CO_3 , giving compound **9** in 95% yield. Convergent approach³⁷ was used to extend the size of the dendrimers, and compound **7** was used as a focal point monomer. Coupling of **7** with 2.4 equiv of **9** in the presence of $Pd(dba)_2$ as a catalyst resulted in the dendron **10**. The repeat of de-protection of dendron **10** and accumulation processes of dendron **11** with a focal point monomer **7** gives a more accumulated dendron **12**. Compound **13** was obtained for further reaction by de-protection of the trimethylsilyl group. The coupling reaction of **9** with 1,3,5-triiodobenzene (**8**) in the presence of CuI and $Pd(dba)_2$ as catalysts in THF/DIPA(1/3, v/v) gives **PG-1** (35% yield). **PG-2** and **PG-3** were also obtained in 20-30% yield by the coupling reaction of dendron **11** or **13** with 1,3,5-triiodobenzene (**8**) in the presence of $Pd(dba)_2$, respectively. Further iteration of Dendron **13** leads to a highly congested dendron for the next generation (**PG-4**). Unfortunately, however, sterically dense **PG-4** was not synthesized. It is possible that sterically congested carboxylate end groups prevent formation of the next generation (**PG-4**) as physical limitation on dendrimer size.

Hydrolysis of precursor

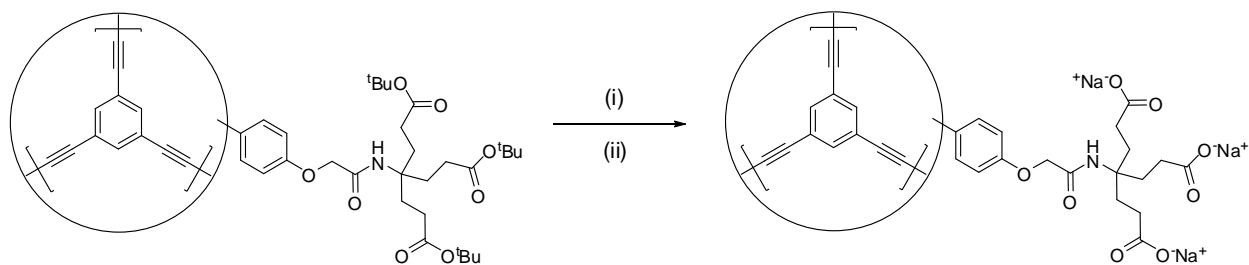


Figure 5-4. Hydrolysis of branched side chains (i) TFA/DCM, r.t. for 2 hrs.; (ii) sat. Na_2CO_3 aqueous solution.

Hydrolysis process of organic soluble dendrimers is well described in Figure 5-4. Hydrolysis was easily accomplished in acidic conditions (TFA/DCM) for 12 hours. The residues were treated with saturated Na_2CO_3 solution and then purified by dialysis method using 1000 D molecular-weight-cutoff (MWCO) dialysis membranes. The water soluble anionic conjugated polyelectrolyte dendrimers (CPE-Ds: **G1**, **G2** and **G3**) were obtained as solids in 80-90% yield. The purity of all compounds was proven by ^1H and ^{13}C NMR spectroscopy, and mass spectroscopy.

Geometric structure of CPE-Ds

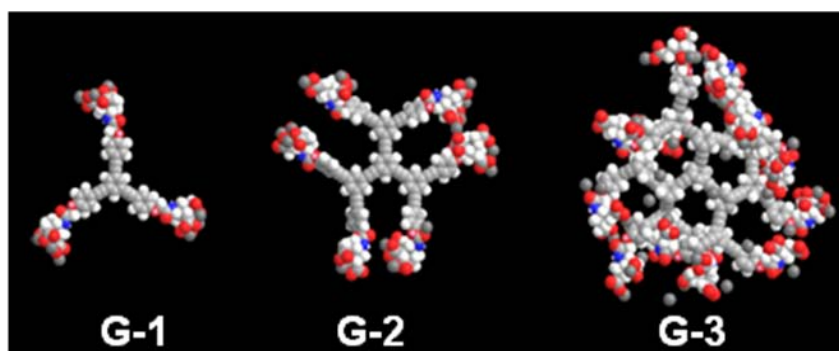


Figure 5-5. Space-filling model of **G-1**, **G-2**, and **G-3** generated by using MM2 molecular mechanics in Chem 3D Pro (version 10.0).

The structure of CPE-Ds presents fully conjugated phenylacetylene branches at *meta*-position with branched carboxylate end-groups. The number of end-groups geometrically increases with generation, in which **G-1**, **G-2**, and **G-3** possess 9, 18, and 36 carboxylate groups, respectively. It is noted that poor intrinsic solubility of dendrimers especially in higher generation is one of the factors that make dendrimer synthesis difficult. Attaching ample carboxylate end-groups into CPE-Ds not only solves such solubility issue, but also affords the sufficient volume to overspread the inside core and branches. It is evident from space-filling models that CPE-Ds take on a more three-dimensional spherical shape as the generation increases (Figure 5-5). Another

distinctive character in the dendrimer chemistry is that they are perfect monodisperse macromolecules.³⁷ In a series of CPE-Ds, GPC data provide information on relative size of the precursor CPE-Ds (**PG-1**, **PG-2** and **PG-3**) as seen in Figure 5-6, in which the polydispersities are close to one.

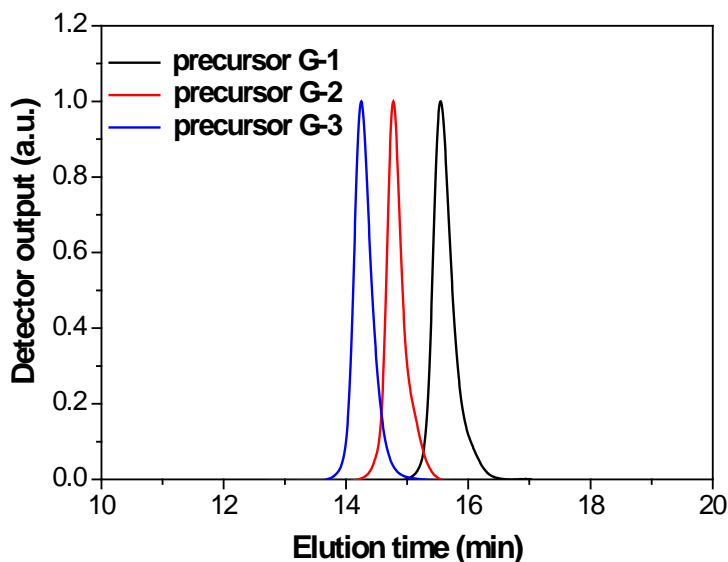


Figure 5-6. GPC data of precursor of CPE-Ds (**PG-1**, **PG-2**, and **PG-3**); polystyrene standards in THF.

Geometric Properties: CPE-Ds' Size

Dynamic light scattering (DLS)

The solution state of the CPE-Ds was studied by dynamic light scattering (DLS) measurements. This study provides information for the hydrodynamic radius of the molecules in different solvent environments and goes insight to state of aggregation.⁶⁷ Figure 5-7 shows the distribution profiles for the populations of scatterers with the hydrodynamic radii in CH₃OH and H₂O solution. In CH₃OH, DLS on **G-1**, **G-2**, and **G-3** shows 1.61, 1.56 and 1.47 nm as an average size, respectively. Although their average sizes were opposite of the dendrimer generation, the distribution profiles are consider to

be the single dendrimer. As expected, DLS of **G-1** in H₂O shows a relatively larger size (3.26 nm), and the distribution profile shows a maximum size of approximately 5.5 nm. Thus, based on DLS studies, we believe that **G-1** undergoes *inter-dendrimer* aggregation in H₂O, but its accumulation is restricted within narrow limits. For **G-2** and **G-3**, DLS data in H₂O present 1.04 and 1.03 nm respectively. The single dendrimer structures of **G-2** and **G-3** retained even in H₂O solution. Interestingly, the smaller hydrodynamic radius than those in CH₃OH was observed for **G-2** and **G-3**. For this observation, we suggest that intra-dendrimer self-aggregation process caused by hydrophobic interaction leads to the contraction of the dendrimer in H₂O.

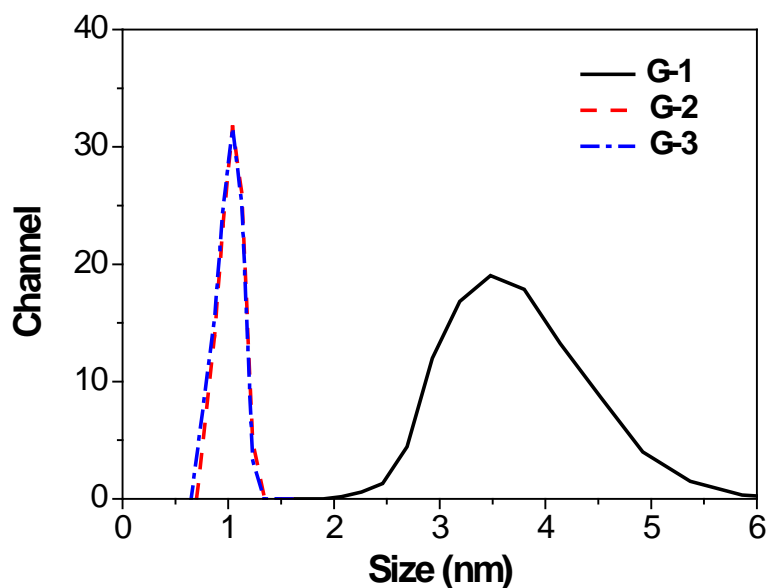


Figure 5-7. Hydrodynamic radii obtained from dynamic light scattering (DLS) for **G-1** (black), **G-2** (red), and **G-3** (blue) in H₂O; [**G-n**] = 1.0 μ M; average size: 1.61 nm (**G-1**), 1.56 nm (**G-2**), and 1.47 nm (**G-3**).

Atomic force microscopy (AFM)

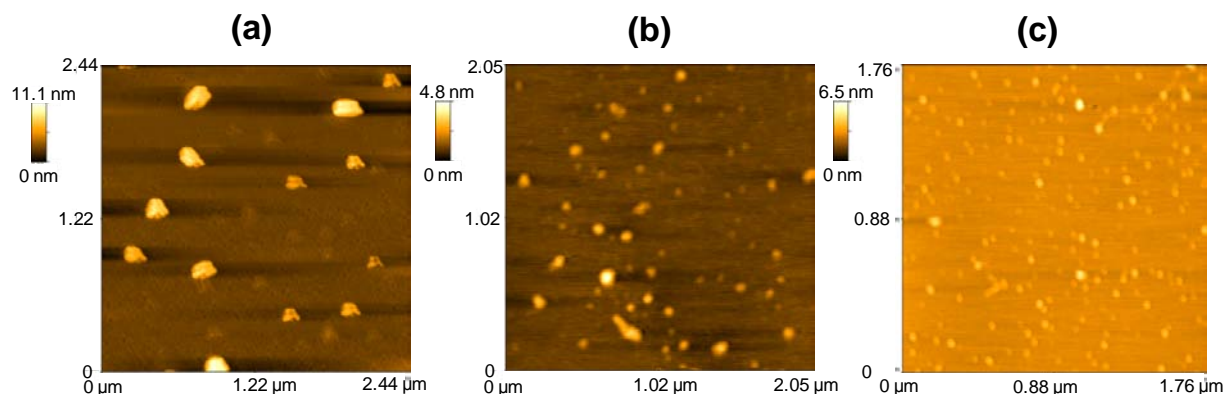


Figure 5-8. AFM images of (a) **G-1**, (b) **G-2**, and (c) **G-3**.

To further elucidate the intra or intermolecular aggregation of CPE-Ds, the CPE-Ds were visualized by AFM (Atomic Force Microscope). Figure 5-8 shows the topographic images of CPE-Ds, which were deposited on mica substrates from 1 mM solution in H₂O solvent. This confirms the dendrimer shape and size on the Mica surface. As seen in Figure 5-8a, the **G-1** exhibits the round-type dendrimers, and their size are analogous (approximately 4.56 nm). Figure 5-8b and 5-8c show a large number of dendrimers (**G-2** and **G-3**) with consistent sizes, respectively. Interestingly, even smaller size of **G-2** (approximately 1.32 nm) and **G-3** (approximately 0.98 nm) than that of **G-1** was observed. The relatively small and constant size of **G-2** and **G-3** supports that their geometric structures disfavor mutual approaches, resulting in little or no inter-dendrimer aggregate formation. On the other hand, the relatively larger size of **G-1** reflects inter-dendrimer aggregation in the ground state. Also, consistency in aggregate size supports that spatially crowded carboxylate anions in **G-1** aggregates prevent additional aggregation. The smaller size of **G-3** compared to **G-2** is explained by the fact that strong electrostatic interactions between the terminal end-groups and substrate causes compression, resulting in deformation of surface-bound dendrimers. It is

possible that more end-group substitution provides better interaction with substrate, resulting in smaller size in AFM images.⁴⁵

Optical Properties

UV-Vis & fluorescence spectroscopy

Table 5-1. UV-Vis absorption and photoluminescent properties of CPE-Ds (CH₃OH and H₂O) and their precursors (THF) .

CDs	THF			CPE-Ds	CH ₃ OH			H ₂ O		
	$\lambda_{\max}^{\text{abs}}$ (nm)	$\lambda_{\max}^{\text{em}}$ (nm)	Φ_{PL}^a		$\lambda_{\max}^{\text{abs}}$ (nm)	$\lambda_{\max}^{\text{em}}$ (nm)	Φ_{PL}^a	$\lambda_{\max}^{\text{abs}}$ (nm)	$\lambda_{\max}^{\text{em}}$ (nm)	Φ_{PL}^a
PG-1	316	373	0.34	G-1	277	373	0.025	283	390	0.011
PG-2	314	374	0.38	G-2	291	374	0.024	291	416	0.008
PG-3	313	376	0.36	G-3	294	404	0.018	294	435	0.004

^a 9,10-Diphenylanthracene in EtOH as the standard, $\Phi_{\text{FL}}=0.90$.

The UV-Vis absorption and fluorescence spectra of the CPE-Ds (**G-1**, **G-2**, and **G-3**) and their precursors (**PG-1**, **PG-2**, and **PG-3**) are shown in Figure 5-9, and their wavelength maxima are collected in Table 5-1. The UV-Vis absorption spectra of **PG-1**, **PG-2**, and **PG-3** in THF show the two peaks around 303 and 313 nm, respectively. The water-soluble CPE-Ds (**G-1**, **G-2**, and **G-3**) exhibit blue-shifted UV-Vis absorption spectra compared to their precursor dendrimers (**PG-n** series) by around 10 ~ 20 nm in both CH₃OH and H₂O solutions. We believe that these hypsochromic shifts of CPE-Ds in UV-Vis absorption spectra are attributed to more twisted states of the branches induced by their hydrophobic effect and electrostatic repulsion between bulky carboxylate end-groups. It is possible that the contraction of interior branches caused by the hydrophobic effect in CH₃OH and H₂O solutions induces their twist, and the electrostatic repulsions between negatively charged terminal end-groups give rise to the

rotation of single bonds in the branches to minimize the resistance. Such distortion of the CPE-D's branches can also be supported by blue-shifted absorption spectrum of the monomer unit (**8**) compared to those of **PG-n** series, in which the absorption maximum showed at 250 nm in THF. Interestingly, for only **G-1**, absorption spectra in H₂O was bathochromically shifted by 6 nm compared to that in CH₃OH, showing narrow absorption spectra (Figure 5-10). This observation is distinguished from that of **G-2** or **G-3** which shows negligible spectral difference between CH₃OH and in H₂O solutions. The spectral change of **G-1** in CH₃OH and in H₂O solutions can be ascribed to the ground state aggregation in H₂O solution. Also, it should be noted that, for **G-2** and **G-3**, such spectral similarity in CH₃OH and H₂O solutions implies that solvent polarity does not much affect to photophysical changes in the ground state.

As can be seen from Figure 5-11 the absorbance of CPE-Ds and their precursors increases with increasing generation. In THF for **PG-n** series, their absorption maxima in the UV-Vis absorption spectra are retained for all generations. In other words, the dendrimer size of **PG-n** series in THF does not affect to their wavelength change in the UV-Vis absorption spectra. On the other hand, **G-n** series were gradually red-shifted with increasing generation in CH₃OH ($\Delta\lambda = 7$ nm from **G-1** to **G-3**) and H₂O ($\Delta\lambda = 10$ nm from **G-1** to **G-3**) solutions as seen in Figure 5-11. Besides, the wavelength maxima with increasing generation of **G-n** series approach that of **PG-n** series. For this observation, we propose that the red shift is likely a result of the geometrical changes of CPE-Ds toward decreased torsional conformation of each phenylacetylene unit when branches approach closely: the approaching is due to the increased number of branches and end-groups with increasing generation, and outer hydrophilic solvents

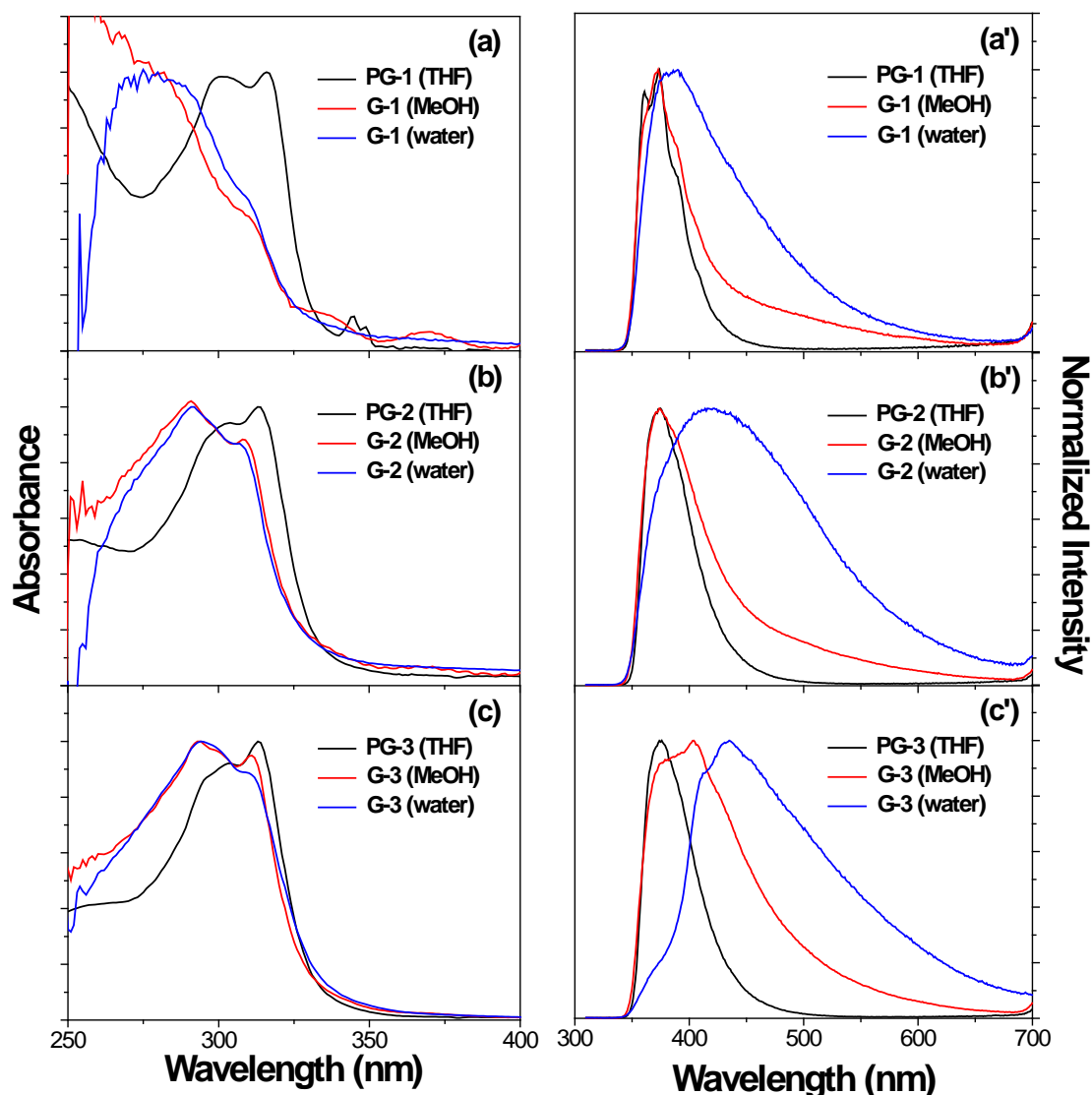


Figure 5-9. UV-Vis absorption and fluorescence spectra of CPE-Ds (**G-1**, **G-2**, and **G-3**) and their precursors (**PG-1**, **PG-2**, and **PG-3**) in CH₃OH, H₂O, and THF, respectively; (a, a') first generation, (b, b') second generation, and (c, c') third generation; Excitation wavelength is 300 nm; [**G-n**] = [**PG-n**] = 1 μ M.

lead to approaching phenylene units to the adjacent moieties. It is not expected that such approaching occurs in well-dissolved organic soluble **PG-n** series in THF. On the other hand, it is likely that the conformational changes of CPE-Ds having two different properties (hydrophobic interior and hydrophilic exterior) in one molecule are correlated

with solvent effects. This effectiveness is more pronounced as the generation increases, resulting in further bathochromic shift in the UV-Vis spectra.

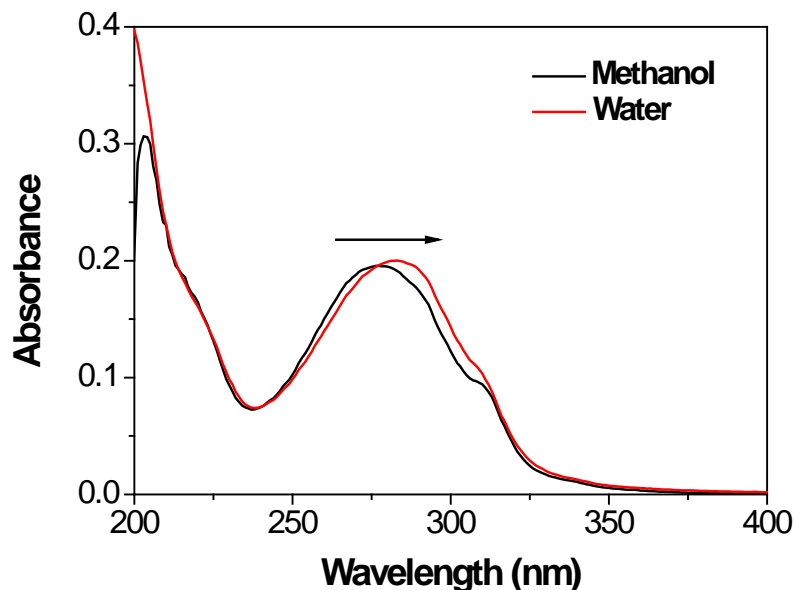


Figure 5-10. UV-Vis absorption spectra of **G-1** in CH₃OH and H₂O; [**G-1**] = 5.0 μ M.

In contrast to the UV-Vis absorption spectra, CPE-Ds (**G-1**, **G-2**, and **G-3**) in the fluorescence spectra exhibit bathochromic shift compared to their precursors (**G-1**: $\Delta\lambda = 0$ nm/CH₃OH, $\Delta\lambda = 17$ nm/water; **G-2**: $\Delta\lambda = 0$ nm/CH₃OH, $\Delta\lambda = 42$ nm/water; **G-3**: $\Delta\lambda = 28$ nm/CH₃OH, $\Delta\lambda = 59$ nm/water), and the spectra become more shifted to red region and broadened as the solvent polarity increases. Furthermore, such spectral shifts were more significant at higher generation. The red shift and broad spectra of **G-1**, **G-2**, and **G-3** in fluorescence emission might be ascribed to both the solvent effect and excited state dimer formation (excimer) in water solution. It is well known that solvent effect becomes larger as the solvent polarity is increased, resulting in emission at lower energy.¹²⁴⁻¹²⁵ Also, the broad long-wavelength emission can be the results of ground state and/or excited state complexes of two or more chromophores. For **G-2** and **G-3**,

however, no considerable UV-Vis absorption changes were observed in water solution, suggesting that ground state strong dendrimer aggregation can be exclusive.

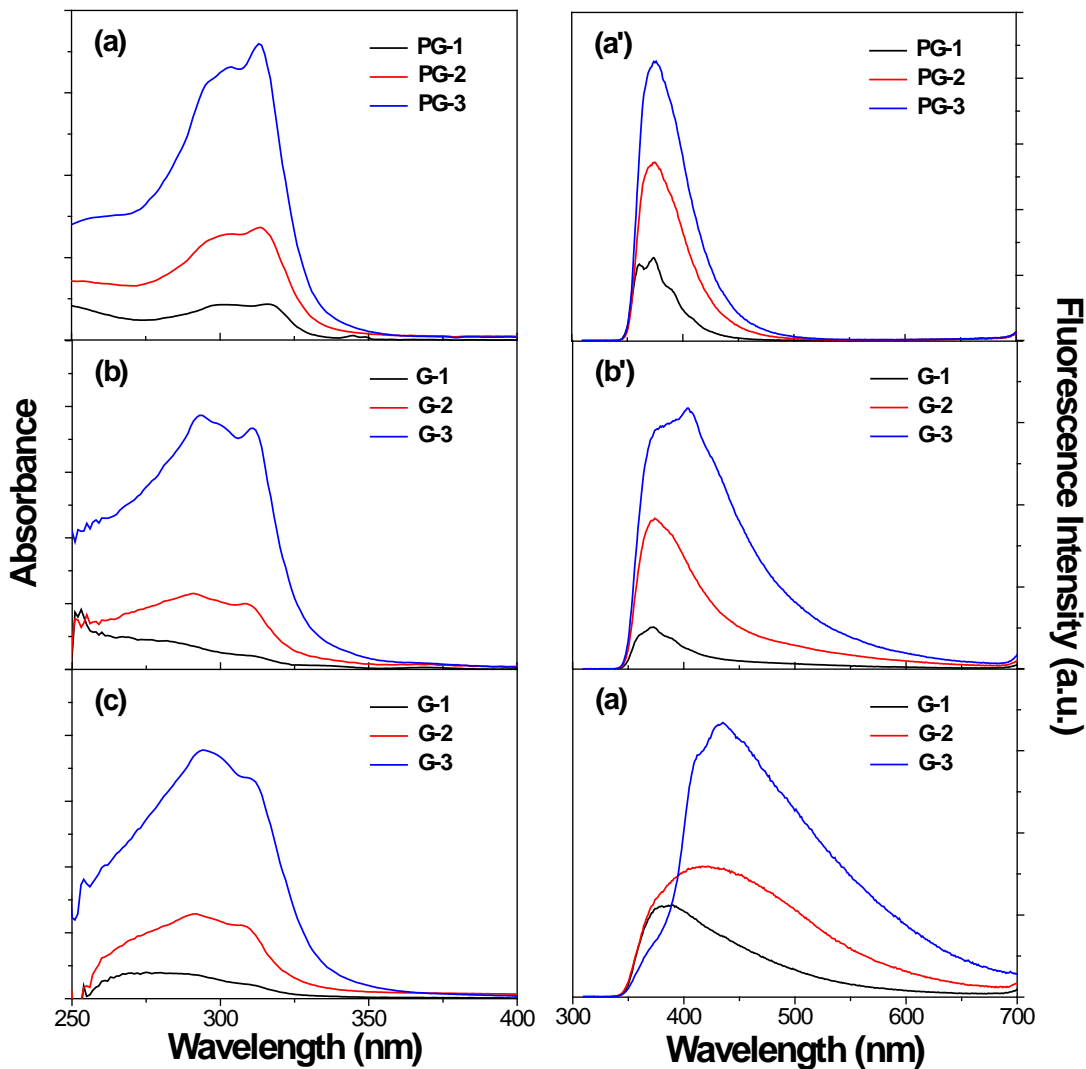


Figure 5-11. UV-Vis absorption and fluorescence spectra of CPE-Ds (**G-1**, **G-2**, and **G-3**) and their precursors (**PG-1**, **PG-2**, and **PG-3**) with increasing generation in (a, a') THF, (b, b') CH₃OH, and (c, c') H₂O, respectively; Excitation wavelength is 300 nm; [**G-n**] = [**PG-n**] = 1 μ M.

Similar to the UV-Vis absorbance, the fluorescence emission intensities increase with the generation as seen in Figure 5-11. For **PG-n** series ($\lambda_{\text{max}} = 373\sim 376$ nm), wavelength changes were not observed with increasing generation in THF, but for the

water-soluble **G-n** series, the UV-Vis absorption is bathochromically shifted in CH₃OH ($\Delta\lambda = 31$ nm from **G-1** to **G-3**) and H₂O ($\Delta\lambda = 45$ nm from **G-1** to **G-3**) solutions, respectively. Notably, the photophysical properties of **PG-n** series in the excited state as well as the ground state are unrelated to the dendrimer size in terms of wavelength changes. As expected, meta-linked phenylacetylene system does not vary with conjugation lengths. Nevertheless, in the fluorescence spectra, more significant red-shifts of **G-n** series were observed in more polar solvents (CH₃OH < H₂O): some bathochromic shift as seen in the UV-Vis absorption spectra were observed in CH₃OH while more significant red-shift compared to those in UV-Vis absorption spectra were observed in H₂O. Such remarkable change in highly polar solvent (H₂O) with increasing generation compared to that in UV-Vis absorption spectra is ascribed to excited state aggregation of CPE-Ds in water solution; the aggregation is more pronounced in higher generation. Consequently, the excited state π - π stacking of interior branches is more pronounced in the higher generation dendrimers (**G-1** < **G-2** < **G-3**) and in the more polar solvent.

Fluorescence quantum yield

The fluorescence quantum yields for **PG-n** series in THF and **G-n** series in CH₃OH and under various pH conditions were obtained as seen in Table 5-1 and Figure 5-12. In spite of different size of **PG-n**, similar quantum yields for **PG-1**, **PG-2**, and **PG-3** were observed ($\Phi_{FL} = 0.34/\mathbf{PG-1}$, $0.38/\mathbf{PG-2}$ and $0.36/\mathbf{PG-3}$). Such similarity in quantum yield of **PG-n** series confirms that because of their *meta*-linked system, each chromophore acts independently even in **PG-3** as it shows in **PG-1**. Furthermore, formation of aggregates which can act as an exciton trap is negligible. On the other hand, for **G-n**

series the higher generation dendrimers have lower quantum yield in both CH₃OH and H₂O, which follow the order **G-1** > **G-2** > **G-3** (Table 5-1 and Figure 5-12).

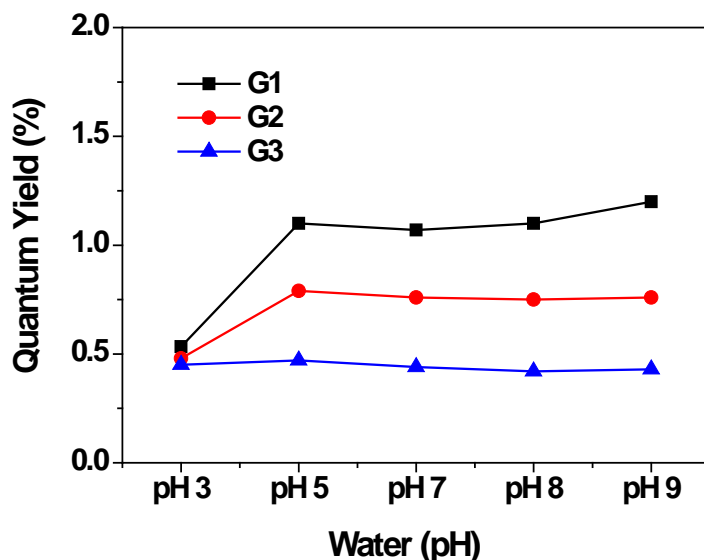


Figure 5-12. Fluorescence quantum yields changes of **G-1**, **G-2**, and **G-3** at the pH 3~9; 9,10-diphenylanthracene in EtOH as the standard, $\Phi_{FL}=0.90$.

In addition, **G-n** series showed the consistent quantum yield in various pH ranges (pH 5 ~ 9). These results support that aggregates are more pronounced in the higher generation and H₂O, but they are not dependent on pH changes (pH 5 ~ 9). At pH 3, the quantum yield of **G-1** and **G-2** decreased, but it was retained in **G-3**; this decrease displayed higher rate in lower generation (**G-1** > **G-2** > **G-3**). After all, the degree of aggregation of **G-1** was maintained in the range of pH 5 ~ 9. However, highly acidic condition (pH 3) caused more aggregation of **G-1**, in which hydrogenated carboxylates probably induce hydrogen bonding with adjacent terminal groups. Nevertheless, the quantum yield of **G-3** at pH 3 is similar to those at other pH ranges. Probably more intra-dendrimer aggregation is not allowed because of highly dense branched carboxylate side chains. Relatively less branched **G-2** might be inter-molecularly aggregated in pH 3.

Fluorescence lifetime studies

Table 5-2. Fluorescence lifetimes (τ_i , ns)^a and relative amplitudes (RA, %) for CPE-Ds (CH₃OH and H₂O) and their precursors (THF).

CDs	THF		CPE-Ds	CH ₃ OH			H ₂ O		
	τ (ns)	RA (%)		τ (ns)	RA (%)	τ_{av} (ns)	τ (ns)	RA (%)	τ_{av} (ns)
PG-1	9.08	100	G-1	$\tau_1 = 0.62$ $\tau_2 = 5.57$	32 68	4.00	$\tau_1 = 1.21$ $\tau_2 = 3.23$	22 78	2.92
PG-2	8.05	100	G-2	$\tau_1 = 1.54$ $\tau_2 = 6.54$	72 28	2.93	$\tau_1 = 0.94$ $\tau_2 = 4.33$	43 57	2.88
PG-3	8.20	100	G-3	$\tau_1 = 1.59$ $\tau_2 = 5.63$	66 34	2.96	$\tau_1 = 0.88$ $\tau_2 = 4.16$	47 53	2.39

^a Typical limits of error on τ_i are less than $\pm 3\%$.

Fluorescence lifetimes of **G-n** series and their precursors (**PG-n** series) were measured in CH₃OH, H₂O and THF, respectively. The values of the fluorescence lifetime are given in Table 5-2. The excitation wavelength is 300 nm and emission decays were monitored over 320 nm. Like fluorescence quantum yield, each **PG-n** showed similarity in fluorescence lifetimes in THF. Also, relatively longer lifetimes with single exponential decay were measured ($\tau = 9.08$, 8.05 and 8.20 for **PG-1**, **PG-2** and **PG-3**, respectively) and these are not dependent on dendrimer size. These features indicate that only one component exists in both ground and excited states and both intra and inter dendrimer aggregation of **PG-n** series does not occur in THF.

On the other hand, the **G-n** series showed two decay constants in CH₃OH and H₂O solutions, respectively (Table 5-2). The emission decay of **G-1** in CH₃OH features 32% of fast decay ($\tau_1 = 0.62$ ns) and 68% of relatively long-lived decay ($\tau_2 = 5.57$ ns). Similar results are obtained in H₂O solution, where 22% of fast decay ($\tau_1 = 1.21$) and 78% of long-lived one ($\tau_2 = 3.23$ ns) are observed. This suggests that there are two emissive pathways in this condition. We suggested that the slow decay component is a

similar state with long-lived component seen in **PG-1** in THF; faster decay is due to the geometrical change caused by electrostatic repulsion between bulky end-groups. It is noted that high polar solvent allows the long-lived charge separation state in the excited state. Nevertheless, the average lifetime in more polar solvent (H₂O) is about 1.5 times shorter than that in less polar solvent (CH₃OH). It is found that energy transfer or quenching lead to changes on the emission decay times.^{53,73} The decrease of average lifetime in this case is mainly due to two issues: first, aggregated states exist in H₂O, and so it acts as an exciton or energy trap; second, the direct contact of less shield branches of **G-1** with water molecules causes enhanced non-radiative deactivation.

For **G-2** and **G-3** in CH₃OH, long-lived components ($\tau_2^{G-2} = 6.54$ ns and $\tau_2^{G-3} = 5.63$ ns) were observed with around 30% amplitude, while fast decay components are predominant with $\tau_1 = 1.54$ ns (72%) and 1.59 ns (66%) concomitant with the faster average lifetimes ($\tau_{av.}^{G-2} = 2.93$ ns and $\tau_{av.}^{G-3} = 2.96$ ns) than **G-1** ($\tau_{av.} = 4.00$ ns). The more twisted states of the branches allows a larger contribution from the fast decay. In H₂O, however, the contribution of fast decay components ($\tau_1^{G-2} = 0.94$ and $\tau_1^{G-3} = 0.88$ ns) decreased and long-lived components ($\tau_2^{G-2} = 4.33$ ns and $\tau_2^{G-3} = 4.16$ ns) are more dominant, contributing to 57% (**G-2**) and 53% (**G-3**). The increased contribution of long-lived decay supports that torsional conformation of interior branches is reduced where the branches are more like that in **PG-n** series. Interestingly, the faster decay in the average lifetime of **G-3** ($\tau_{av.} = 2.39$) compared to that of **G-2** ($\tau_{av.} = 2.88$) was observed in H₂O. This decrease implies that more interaction between phenylacetylene units occurs in **G-3** rather than **G-2**. Thus, *intra-dendrimer* aggregation is more pronounced at the higher generation.

Fluorescence excitation spectroscopy

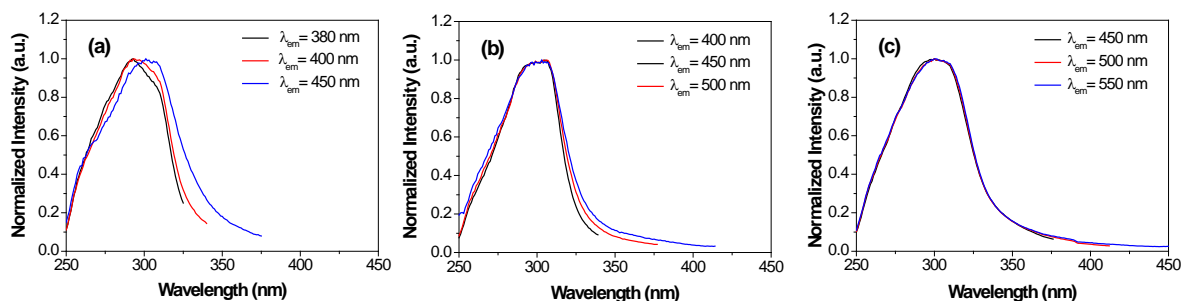


Figure 5-13. Fluorescence excitation spectra of (a) **G-1** at 380, 400, and 450 nm, (b) **G-2** at 400, 450, and 500 nm, and (c) **G-3** at 450, 500, and 550 nm; [**G-n**] = 1.0 μM in H_2O .

The excitation spectra of **G-1** ($\lambda_{\text{em}} = 380, 400, \text{ and } 450 \text{ nm}$) clearly showed that aggregates exist in the ground state in water solution, in which distinctive excitation spectra were observed (Figure 5-13a). On the other hand, little difference was observed in the excitation spectra of **G-2** ($\lambda_{\text{em}} = 400, 450, \text{ and } 500 \text{ nm}$) and **G-3** ($\lambda_{\text{em}} = 450, 500, \text{ and } 550 \text{ nm}$) in the same media as seen in Figure 5-13b and 13c. This implies that the ground state aggregates of **G-1** exist in H_2O . In the cases of **G-2** and **G-3**, however, little aggregation occurs in the ground state; excited state complexes are dominant.

Concentration dependent fluorescence studies

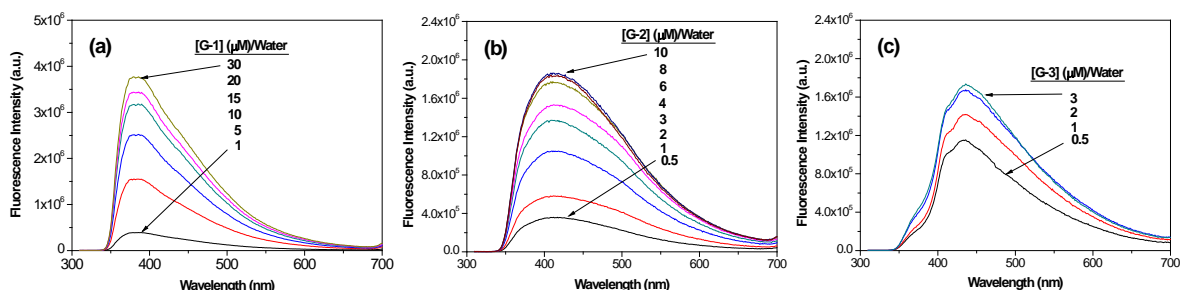


Figure 5-14. Fluorescence emission spectra of (a) **G-1**, (b) **G-2**, and (c) **G-3** with increasing concentration in H_2O ; [**G-n**] = 1.0 μM .

As shown in Figure 5-14, the fluorescence spectra ($\lambda_{\text{ex}} = 300 \text{ nm}$) of all CPE-Ds display little change in wavelength and band-shape with increasing concentration in water solution, indicating that their state of aggregation is independent of the concentration of CPE-Ds. This indicates that the spectral shifts seen in the UV-Vis absorption and fluorescence spectra are potentially due to *intra-dendrimer* aggregation. It is reported that Intra-molecular self association is predominant especially at sterically highly crowded dendrimers.³³ As discussed above in UV-Vis spectra and fluorescence excitation spectra of **G-1**, its ground state aggregates exist in H_2O . Also, it should be noted that it is difficult to form intra-dendrimer aggregates in the case of spatially less crowded CPE-D (**G-1**). Nevertheless, for **G-1**, the fluorescence spectra do not vary as the concentration increases (Figure 5-14a). For this observation, we propose that inter-dendrimer π - π aggregates of **G-1** can be formed, but its size is limited by the proportion of aggregation. The certain degree of aggregation seems to produce another spherical type of dendrimer in which external surface is fully charged, which prevents additional π - π aggregation. This would be analogous to micelle formation.

Fluorescence Quenching of CPE-Ds by DOC, DODC, and DOTC

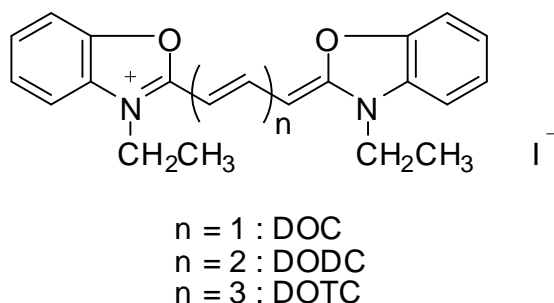


Figure 5-15. Structure of cyanine dyes (DOC, DODC, and DOTC).

Table 5-3. K_{SV} ^a and $[Q]_{90}$ ^b of CPE-Ds with cyanine dyes in H₂O.

CPE-Ds	K_{SV}/M^{-1}		
	DOC	DODC	DOTC
G-3	1.84×10^6	1.67×10^6	7.03×10^5

^a Computed from linear fit at low quencher concentration (0~1.0 μ M).

Fluorescence quenching of **G-3** series in H₂O was investigated upon the addition of cyanine dyes (DOC, DODC, and DOTC), in which the quenching occurs via energy transfer. Figure 5-15 shows the structure of DOC, DODC, and DOTC, in which conjugation chain length are only in difference. As seen in Figure 5-16, the addition of cyanine dyes causes the overall emission intensity of **G-3** to decrease. Their Stern-Volmer¹⁹ plots and K_{SV} values present in Table 5-3 and Figure 5-17, respectively. Figure 5-16 shows the fluorescence intensity changes of **G-3** upon addition of DOC. It is reported in CPEs' research areas where the fluorescence quenching is more amplified in interchain aggregates or aggregation-induced coplanarized conjugated backbones because singlet excitons migrate more efficiently, leading to upward SV plots.^{53,67-68} Similarly, the addition of cyanine dyes causes the amplified fluorescence quenching **G-3**, resulting in upward curves (Figure 5-17). As the chain length of cyanine dyes increases, quenching efficiency of **G-3** decreases: SV plots displayed upward curves and K_{SV} values were significant in the sequence DOC > DODC > DOTC (see Table 5-3 and Figure 5-17). These observations conflict with our previous work in which quenching efficiency increased with expanding chain length of cyanine dyes (DOC < DODC < DOTC).⁵³ Such efficient quenching with increasing chain length is due to stabilization of complexes by the solvophobic and π - π interactions in polymer-dye electrostatic interaction. Unlike polymers, FRET (Fluorescence Resonance Energy

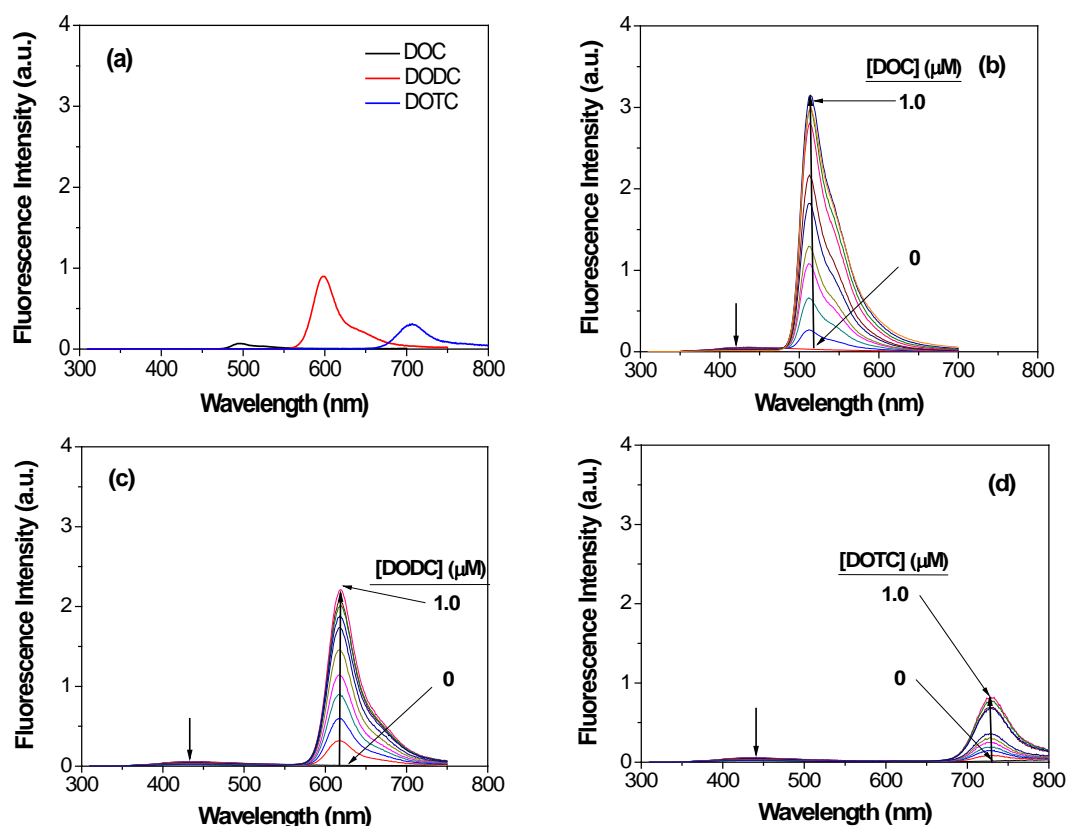


Figure 5-16. Fluorescence emission spectra of (a) cyanine dyes only (DOC, DODC, and DOTC: 1.0 μM) and **G-3** titrated with (b) DOC, (c) DODC, and (d) DOTC in H_2O , pH 8.0; [**G-3**] = 1.0 μM ; [dye quencher] = 0 ~ 1.0 μM ; excitation wavelength = 300 nm.

Transfer) effect related to chain length is involved in the quenching mechanism. It is well known that the FRET efficiency depends on many parameters such as the distance between donor and acceptor and the spectral overlap of the donor emission and the acceptor absorption spectra. In **G-3**, we observed that degree of spectral overlap increases as the chain length of cyanine dyes decreases. Furthermore, most significant fluorescence enhancement was observed upon the addition of DOC (Figure 16-b). Only subtle fluorescence increase was observed for the largest dye, DOTC (Figure 5-16d). These observations clearly indicate that the degree of FRET determines quenching efficiency of **G-3**.

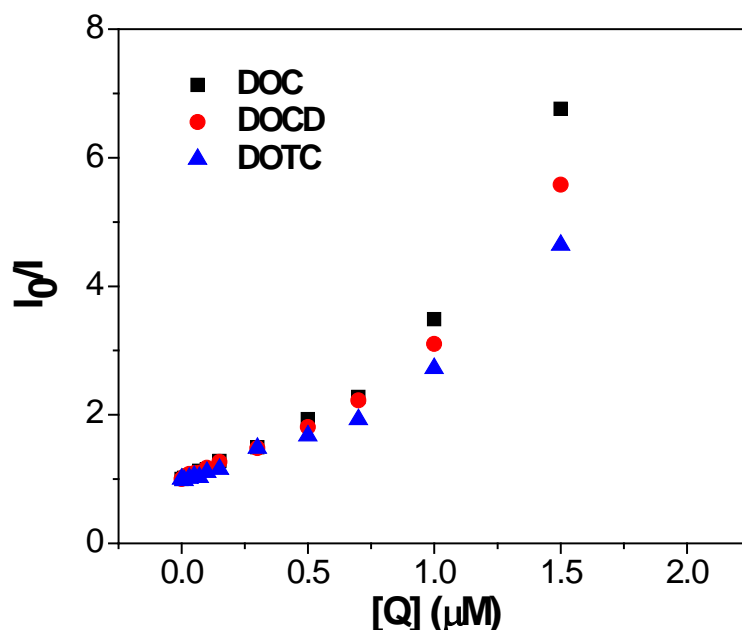


Figure 5-17. Stern-Volmer plots of **G-3**; fluorescence quenched by cyanine dyes in H₂O; [CPE-Ds] = 1.0 μM; DOC (■), DODC (●), and DOTC (▲) .

Summary and Conclusions

In this Chapter, we have prepared conjugated polyelectrolyte dendrimers (CPE-Ds) **G-1**, **G-2**, and **G-3** with branched carboxylate side chains, providing globular architecture with increasing generation. Both AFM and DLS results suggested that the aggregate state of **G-2** and **G-3** in H₂O is likely due to *intra-dendrimer* interactions rather than *inter-dendrimer* aggregation while inter-dendrimer aggregation occurs in **G-1**. The absorption and fluorescence intensities of CPE-Ds increase as the generation increases. In MeOH, absorption and fluorescence spectral bandshape of **G-n** does not change significantly, suggesting that the state of the chromophores does not change much with generation. By contrast, in H₂O there is a considerable change in the fluorescence wavelength and band shape with increasing generation. This observation suggests that an aggregate state of CPE-Ds develops in the poor solvent environment.

Both comparison of fluorescence spectra in CH₃OH and H₂O and the excitation spectra in H₂O revealed that **G-1** shows *inter-dendrimer* aggregation in the ground state while **G-2** and **G-3** display *intra-dendrimer* aggregates in the excited state in aqueous solution. Also, the same quantum yields of **G-3** at various pH condition (pH 3 ~ 9) support *inter-dendrimer* aggregates do not exist. Fluorescence lifetime also support the aggregation features of CPE-Ds. The quenching from **G-3** to cyanine dyes is independent on the chain length of cyanine dyes and is due to primarily energy transfer effects.

Experimental

Materials

All chemicals used for the synthesis were of reagent grade and used without further purification. Nitromethane, *tert*-butylacrylate, T-1 Raney nickel, diisopropylamine, chloroacetyl chloride, 4-iodophenol, palladium (0) bis(dibenzylideneacetone), tetrakis(triphenylphosphine)palladium, 1,3,5-tribromobenzene, and triphenylphosphine were purchased from Sigma-Aldrich Chemical Company. Sodium carbonate, and copper iodide were obtained from Acros Chemical Company. Ethynyltrimethylsilane was obtained from GFC Chemical Company. *trans*-Dichlorobis(triphenylphosphine)palladium (II) was purchased from Strem Chemical Company. Potassium carbonate and trifluoroacetic acid were obtained from Fisher Scientific Company. THF and DMF were purified by solvent dispensing system. Silica gel (Merck, 230-400 mesh) was used for chromatographic purification of all of intermediates and target molecules. All other chemicals and solvents were purchased from either Sigma-Aldrich or Acros Chemical Company and used as received.

Instrumentation and Methods

NMR spectra were recorded using a Varian VXR-300 FT NMR, operating at 300 MHz for ^1H NMR and at 75 MHz for ^{13}C NMR. Gel permeation chromatography (GPC) analyses were carried out on a system comprised of a Rainin Dynamax SD-200 pump, Polymer Laboratories PL gel mixed D columns, and a Beckman Instruments Spectroflow 757 absorbance detector. Molecular weight calibration was effected by using polystyrene standards. UV/Vis absorption spectra were recorded using a Varian Cary 50 Spectrophotometer. Steady-state fluorescence spectra were obtained with a PTI fluorometer. Lifetime measurements were carried out using a PicoQuant FluoTime 100 Compact Fluorescence Lifetime Spectrometer. A 1 cm quartz cuvette was used for all spectral measurements. Dynamic light scattering (DLS) experiments were performed with Zeta PALS from Brookhaven Instrument Corporation. Atomic Force Microscopy (AFM) images were obtained with a Veeco Innova Scanning Probe Microscope.

Stock solutions (1.0 mM) of all of the CPE-Ds were prepared in H_2O and were stored at $0\text{ }^\circ\text{C}$. The solutions were maintained at room temperature for one hour before use. Fluorescence quantum yields are reported relative to known standards (9,10-diphenyl anthracene, $\Phi = 0.90$ in EtOH). The pH of aqueous solution was adjusted with HCl and/or NaOH using a corning pH meter 320.

Synthetic Procedures

Compounds **1**, **7** and **8** were prepared in a good yield as described in the literature.^{39,122-123}

Compound 2. To a suspension of **1** (30.0 g, 72.2 mmol) and anhydrous K_2CO_3 (40.1 g, 296.0 mmol) in a mixture of water (200 mL) and ethyl acetate (200 mL), a solution of chloroacetyl chloride (7.30 mL, 91.7 mmol) in ethyl acetate (50 mL) was

added dropwise. The reaction mixture was then stirred at room temperature for 2 hours, after which the organic phase was separated from the aqueous phase, and dried over anhydrous MgSO_4 . The solvent was evaporated to give the crude product. Column chromatography using EtOAc:hexane (2:1) as eluent ($R_f = 0.80$) on silica gel gave **2** as a white solid in a 95.0% yield. mp: 73-74 °C; ^1H NMR (300 MHz, CDCl_3 , δ_{ppm}): 6.45 (s, 1H, CON-H), 3.87 (s, 2H, $\text{ArOCH}_2\text{CO}_2$), 2.15 (m, 6H, $\text{NHC}(\text{CH}_2\text{CH}_2\text{CO}_2^t\text{Bu})_3$), 1.93 (m, 6H, $\text{NHC}(\text{CH}_2\text{CH}_2\text{CO}_2^t\text{Bu})_3$), 1.36 (s, 27H, CO_2^tBu); ^{13}C NMR (75 MHz, CDCl_3 , δ_{ppm}): 172.5, 165.2, 80.8, 60.5, 58.1, 42.5, 34.5, 29.8, 28.2; LC-MS (m/z): $[\text{M}+\text{Na}]^+$ calcd for $\text{C}_{22}\text{H}_{42}\text{ClNO}_7$, 514.3; found, 514.1.

Compound 4. To a solution of 4-iodophenol (**3**) (11.6 g, 52.8 mmol) in dried CH_3CN (50 mL), anhydrous K_2CO_3 (8.03 g, 58.1 mmol) was added. After stirring for 30 min, compound **2** (26.0 g, 52.8 mmol) was added to the reaction mixture. The resulting mixture was vigorously stirred at 80 °C for 12 hours under argon gas. After the reaction mixture was cooled to room temperature, the solvent was removed *in vacuo*. The reaction mixture was acidified with 5% aqueous HCl solution (200 mL), and then extracted with CH_2Cl_2 (200 mL). The organic layer was separated and washed with water (200 mL) and dried over anhydrous MgSO_4 , and the solvent was evaporated to yield a white solid. The crude product was isolated by column chromatography on silica gel using ethyl acetate:hexane (1:2) as the eluent. 72.0% yield; mp 114-116 °C; ^1H NMR (300 MHz, CDCl_3 , δ_{ppm}): 7.62 (d, 2H, $\text{IAr-}H_{\text{ortho}}$, $J=9.0$ Hz), 6.75 (d, 2H, $\text{IAr-}H_{\text{meta}}$, $J=9.0$ Hz), 6.57 (s, 1H, CON-H), 4.35 (s, 2H, $\text{ArOCH}_2\text{CO}_2$), 2.20 (m, 6H, $\text{NHC}(\text{CH}_2\text{CH}_2\text{CO}_2^t\text{Bu})_3$), 2.00 (m, 6H, $\text{NHC}(\text{CH}_2\text{CH}_2\text{CO}_2^t\text{Bu})_3$), 1.44 (s, 27H, CO_2^tBu);

^{13}C NMR (75 MHz, CDCl_3 , δ_{ppm}): 172.7, 167.2, 157.0, 138.7, 117.2, 82.5, 80.9, 67.8, 57.9, 30.1, 29.8, 28.3; LC-MS (m/z): $[\text{M}+\text{Na}]^+$ calcd for $\text{C}_{30}\text{H}_{46}\text{INO}_8$, 698.0; found, 698.1.

Compound 5. To a solution of compound **4** (25.0 g, 37.0 mmol) in degased 100 mL THF/DIPA (1/3, v/v), $\text{Pd}(\text{PPh}_3)_2\text{Cl}_2$ (0.52 g, 0.74 mmol) and CuI (0.28 g, 1.48 mmol) were added. Then, ethynyltrimethylsilane (6.32 mL, 44.4 mmol) was added to the reaction mixture. The resulting mixture was vigorously stirred at 70 ~ 75 °C for 12 hours under argon gas. After the reaction mixture was cooled to room temperature, the solvent was removed *in vacuo*. The crude product was isolated by column chromatography on silica gel using methylene chloride:acetone (10:1) as the eluent. 62.8% yield; mp 148-150 °C; ^1H NMR (300 MHz, CDCl_3 , δ_{ppm}): 7.45 (d, 2H, $\text{IAr-}H_{\text{ortho}}$, $J=9.0$ Hz), 6.89 (d, 2H, $\text{IAr-}H_{\text{meta}}$, $J=9.0$ Hz), 6.51 (s, 1H, $\text{CON-}H$), 4.39 (s, 2H, $\text{ArOCH}_2\text{CO}_2$), 2.20 (m, 6H, $\text{NHC}(\text{CH}_2\text{CH}_2\text{CO}_2^t\text{Bu})_3$), 2.00 (m, 6H, $\text{NHC}(\text{CH}_2\text{CH}_2\text{CO}_2^t\text{Bu})_3$), 1.43 (s, 27H, CO_2^tBu), 0.24 (s, 9H, $(\text{CH}_3)_3\text{Si}$); ^{13}C NMR (75 MHz, CDCl_3 , δ_{ppm}): 172.7, 167.5, 157.5, 133.9, 117.0, 114.8, 105.1, 93.8, 80.9, 67.6, 57.9, 30.1, 29.8, 28.3, 0.2; LC-MS (m/z): $[\text{M}+\text{Na}]^+$ calcd for $\text{C}_{35}\text{H}_{55}\text{NO}_8\text{Si}$, 668.0; found, 668.2.

General deprotection process of trimethylsilyl group. A mixture of compound **5**, **10**, or **12** (1.0 mmol) and K_2CO_3 (5.0 equiv.) in a solution mixture of dichloromethane (20 mL) and methanol (20 mL) was stirred at room temperature for 2 hours. The mixture was washed with water (20 mL \times 3), and dried over anhydrous magnesium sulfate, then the solvent was removed *in vacuo*. The product was used in the coupling reaction without further purification. 80 ~ 90% yield.

9: mp 126-128 °C; ^1H NMR (300 MHz, CDCl_3 , δ_{ppm}): 7.47 (d, 2H, $\text{IAr-}H_{\text{ortho}}$, $J=9.0$ Hz), 6.92 (d, 2H, $\text{IAr-}H_{\text{meta}}$, $J=9.0$ Hz), 6.55 (s, 1H, $\text{CON-}H$), 4.39 (s, 2H, $\text{ArOCH}_2\text{CO}_2$), 3.03 (s, 1H, $H\text{-CC-Ar}$), 2.20 (m, 6H, $\text{NHC}(\text{CH}_2\text{CH}_2\text{CO}_2^t\text{Bu})_3$), 2.00 (m, 6H, $\text{NHC}(\text{CH}_2\text{CH}_2\text{CO}_2^t\text{Bu})_3$), 1.43 (s, 27H, CO_2^tBu); ^{13}C NMR (75 MHz, CDCl_3 , δ_{ppm}): 172.7, 167.2, 157.5, 134.0, 116.0, 114.9, 83.8, 80.9, 67.5, 57.8, 30.1, 29.8, 28.3; LC-MS (m/z): $[\text{M}+\text{Na}]^+$ calcd for $\text{C}_{32}\text{H}_{47}\text{NO}_8$, 596.0; found, 596.2.

11: mp 74-76 °C; ^1H NMR (300 MHz, CDCl_3 , δ_{ppm}): 7.58 (s, 1H, $\text{phenyl-}H$), 7.54 (s, 2H, $\text{phenyl-}H$), 7.48 (d, 4H, $\text{CH}_2\text{OAr-}H_{\text{meta}}$, $J=9.0$ Hz), 6.94 (d, 4H, $\text{CH}_2\text{OAr-}H_{\text{ortho}}$, $J=9.0$ Hz), 6.56 (s, 2H, $\text{CON-}H$), 4.39 (s, 4H, $\text{ArOCH}_2\text{CO}_2$), 3.09 (s, 1H, $H\text{-CC-Ar}$), 2.20 (m, 12H, $\text{NHC}(\text{CH}_2\text{CH}_2\text{CO}_2^t\text{Bu})_3$), 2.00 (m, 12H, $\text{NHC}(\text{CH}_2\text{CH}_2\text{CO}_2^t\text{Bu})_3$), 1.41 (s, 54H, CO_2^tBu); ^{13}C NMR (75 MHz, CDCl_3 , δ_{ppm}): 172.4, 166.6, 156.7, 132.2, 131.8, 124.2, 116.3, 115.0, 90.3, 87.2, 80.9, 67.5, 57.9, 30.1, 29.8, 28.3; LC-MS (m/z): $[\text{M}+\text{Na}]^+$ calcd for $\text{C}_{72}\text{H}_{96}\text{N}_2\text{O}_{16}$, 1267.0; found, 1267.4.

13: mp 102-104 °C; ^1H NMR (300 MHz, CDCl_3 , δ_{ppm}): ^1H NMR (300 MHz, CDCl_3 , δ_{ppm}): 7.60 (m, 9H, $\text{phenyl-}H$), 7.55 (d, 8H, $\text{CH}_2\text{OAr-}H_{\text{meta}}$, $J=9.0$ Hz), 6.98 (d, 8H, $\text{CH}_2\text{OAr-}H_{\text{ortho}}$, $J=9.0$ Hz), 6.58 (s, 4H, $\text{CON-}H$), 4.41 (s, 8H, $\text{ArOCH}_2\text{CO}_2$), 3.12 (s, 1H, $H\text{-CC-Ar}$), 2.20 (m, 24H, $\text{NHC}(\text{CH}_2\text{CH}_2\text{CO}_2^t\text{Bu})_3$), 2.00 (m, 24H, $\text{NHC}(\text{CH}_2\text{CH}_2\text{CO}_2^t\text{Bu})_3$), 1.42 (s, 108H, CO_2^tBu); ^{13}C NMR (75 MHz, CDCl_3 , δ_{ppm}): 172.7, 167.1, 157.5, 133.8, 124.5, 116.5, 115.2, 90.3, 87.2, 80.9, 67.7, 57.8, 30.0, 29.9, 28.3; LC-MS (m/z): $[\text{M}+2\text{Na}]^{2+}$ calcd for $\text{C}_{152}\text{H}_{194}\text{N}_4\text{O}_{32}$, 1316.7; found, 1316.8.

General coupling reaction procedure. Dendron **9**, **11**, or **13** (2.2 or 3.3 equiv.) and 0.2 mmol of compound 3,5-dibromo-1-trimethylsilylethynylbenzene (**7**) or 1,3,5-triiodobenzene (**8**) were dissolved in 20 mL of THF/ Et_3N (1/3, v/v). The resulting solution

was deoxygenated with argon for 30 minutes. Then Pd(dba)₂ (5.8 mg, 10.0 μmol), PPh₃ (5.2 mg, 20.0 μmol) and CuI (1.9 mg, 10.0 μmol) were added to the stirred solution under the protection of argon. The reaction mixture was then heated up to 70 ~ 75 °C and stirred for 12 hours. The reaction mixture was cooled down to the room temperature and the solvent was removed *in vacuo*, affording a pale yellow solid. The crude product was isolated by column chromatography on silica gel using methylene chloride:acetone (10:1) as the eluent. 30 ~ 40% yield.

10: mp 86-88 °C; ¹H NMR (300 MHz, CDCl₃, δ_{ppm}): 7.55 (s, 1H, TMS-C₂-Ar-*H*_{para}), 7.52 (s, 2H, TMS-C₂-Ar-*H*_{ortho}), 7.46 (d, 4H, CH₂OAr-*H*_{meta}, *J*=9.1 Hz), 6.92 (d, 4H, CH₂OAr-*H*_{ortho}, *J*=9.2 Hz), 6.54 (s, 2H, CON-*H*), 4.39 (s, 4H, ArOCH₂CO₂), 2.15 (m, 12H, NHC(CH₂CH₂CO₂^{*t*}Bu)₃), 2.00 (m, 12H, NHC(CH₂CH₂CO₂^{*t*}Bu)₃), 1.41 (s, 54H, CO₂^{*t*}Bu), 0.23 (s, 9H, (CH₃)₃Si); ¹³C NMR (75 MHz, CDCl₃, δ_{ppm}): 172.5, 167.1, 157.9, 134.0, 124.0, 116.0, 114.0, 92.0, 86.5, 81.0, 67.5, 57.8, 30.1, 29.9, 28.0, 0.1; LC-MS (*m/z*): [M+Na]⁺ calcd for C₇₅H₁₀₄N₂O₁₆Si, 1339.0; found, 1339.7.

12: mp 108-110 °C; ¹H NMR (300 MHz, CDCl₃, δ_{ppm}): 7.62 (m, 9H, phenyl-*H*), 7.53 (d, 8H, CH₂OAr-*H*_{meta}, *J*=9.0 Hz), 6.98 (d, 8H, CH₂OAr-*H*_{ortho}, *J*=9.0 Hz), 6.58 (s, 4H, CON-*H*), 4.42 (s, 8H, ArOCH₂CO₂), 2.20 (m, 24H, NHC(CH₂CH₂CO₂^{*t*}Bu)₃), 2.00 (m, 24H, NHC(CH₂CH₂CO₂^{*t*}Bu)₃), 1.43 (s, 108H, CO₂^{*t*}Bu), 0.27 (s, 9H, (CH₃)₃Si); ¹³C NMR (75 MHz, CDCl₃, δ_{ppm}): 172.7, 167.2, 157.5, 133.8, 124.6, 116.7, 114.9, 90.5, 87.3, 80.9, 67.7, 57.9, 30.2, 29.8, 28.3, 0.2; LC-MS (*m/z*): [M+2Na]²⁺ calcd for C₁₅₅H₂₀₂N₄O₃₂Si, 1352.7; found, 1352.7.

PG-1: mp 175-177 °C; ¹H NMR (300 MHz, CDCl₃, δ_{ppm}): 7.57 (s, 3H, phenyl-*H*), 7.50 (d, 6H, CH₂OAr-*H*_{meta}, *J*=9.0 Hz), 6.93 (d, 6H, CH₂OAr-*H*_{ortho}, *J*=9.0 Hz), 6.55 (s,

3H, CON-*H*), 4.40 (s, 6H, ArOCH₂CO₂), 2.20 (m, 18H, NHC(CH₂CH₂CO₂^{*t*}Bu)₃), 2.00 (m, 18H, NHC(CH₂CH₂CO₂^{*t*}Bu)₃), 1.42 (s, 81H, CO₂^{*t*}Bu); ¹³C NMR (75 MHz, CDCl₃, δ_{ppm}): 172.6, 167.3, 157.5, 133.8, 130.0, 124.2, 116.7, 115.0, 90.2, 87.5, 80.9, 67.5, 57.8, 30.2, 29.9, 28.3; MALDI-MS (*m/z*): calcd for C₁₀₁H₁₄₁N₃O₂₄, 1793.22; found, 1792.30.

PG-2: mp 152-154 °C; ¹H NMR (300 MHz, CDCl₃, δ_{ppm}): 7.68 (s, 3H, phenyl-*H*), 7.63 (m, 9H, phenyl-*H*) 7.50 (d, 12H, CH₂OAr-*H*_{meta}, *J*=9.0 Hz), 6.96 (d, 12H, CH₂OAr-*H*_{ortho}, *J*=9.0 Hz), 6.58 (s, 6H, CON-*H*), 4.41 (s, 12H, ArOCH₂CO₂), 2.20 (m, 36H, NHC(CH₂CH₂CO₂^{*t*}Bu)₃), 2.00 (m, 36H, NHC(CH₂CH₂CO₂^{*t*}Bu)₃), 1.42 (s, 162H, CO₂^{*t*}Bu); ¹³C NMR (75 MHz, CDCl₃, δ_{ppm}): 172.6, 167.2, 154.4, 133.5, 130.0, 124.4, 116.3, 114.9, 90.3, 87.2, 80.8, 67.5, 57.8, 30.1, 29.7, 28.2; MALDI-MS (*m/z*): M⁺ calcd for C₂₂₂H₂₈₈N₆O₄₈, 3808.67; found, 3809.15.

PG-3: mp 90-92 °C; ¹H NMR (300 MHz, CDCl₃, δ_{ppm}): 7.71 (s, 3H, phenyl-*H*), 7.68 (s, 9H, phenyl-*H*), 7.62 (s, 18H, phenyl-*H*), 7.49 (d, 24H, CH₂OAr-*H*_{meta}, *J*=9.0 Hz), 6.94 (d, 24H, CH₂OAr-*H*_{ortho}, *J*=9.0 Hz), 6.55 (s, 12H, CON-*H*), 4.39 (s, 24H, ArOCH₂CO₂), 2.20 (m, 72H, NHC(CH₂CH₂CO₂^{*t*}Bu)₃), 2.00 (m, 72H, NHC(CH₂CH₂CO₂^{*t*}Bu)₃), 1.42 (s, 324H, CO₂^{*t*}Bu); ¹³C NMR (75 MHz, CDCl₃, δ_{ppm}): 172.7, 167.2, 157.5, 133.8, 130.0, 124.2, 116.3, 114.9, 90.6, 87.5, 80.9, 67.6, 57.9, 30.1, 29.8, 28.2; MALDI-MS (*m/z*): M⁺ calcd for C₄₆₂H₅₈₂N₁₂O₉₆, 7839.59; found, 7839.50.

Hydrolysis for CPE-Ds with branched anionic side chains. Precursors (0.2 g) of **G-1**, **G-2**, and **G-3** (**PG-1**, **PG-2**, and **PG-3**) were dissolved in 20 mL CH₂Cl₂ and cooled in an ice/water bath. 20 mL of trifluoroacetic acid (TFA) was added to the dendrimer solution drop-wise. Upon the completion of the addition, the reaction mixture was allowed to warm to room temperature and stirred for another 12 hours. The excess

TFA and the solvent were removed *in vacuo*. The residue was treated with saturated aqueous Na₂CO₃ solution (10 mL) and stirred at room temperature for 3 hours. The solution was then poured into 50 mL of methanol. The dendrimer precipitate was then dissolved in water and purified by dialysis using 1000 D MWCO regenerated cellulose membranes (yield: 90~100%). The water-soluble conjugated polyelectrolyte dendrimers could be either stored as aqueous solutions or as solid powders.

G-1. ¹H NMR (300 MHz, D₂O/DMSO-*d*₆ (v/v, 1/1), δ_{ppm}): 8.1-7.2 (br, 18H), 4.65 (br, 6H, ArOCH₂CO₂), 2.19 (br, 18H, NHC(CH₂CH₂CO₂[†]Na)₃), 1.98 (br, 18H, NHC(CH₂CH₂CO₂[†]Na)₃); ¹³C NMR (75 MHz, CDCl₃, δ_{ppm}): 182.9, 170.0, 162.0, 131.5, 115.0, 67.9, 58.6, 31.8, 30.1; ESI-MS (*m/z*): [M-H]⁻ calcd for C₆₆H₆₉N₃O₂₄, 1286.0; found, 1286.2.

G-2. ¹H NMR (300 MHz, D₂O/DMSO-*d*₆ (v/v, 1/1), δ_{ppm}): 8.15-7.05 (br, 42H) 4.65 (br, 12H, ArOCH₂CO₂), 2.18 (br, 36H, NHC(CH₂CH₂CO₂[†]Na)₃), 1.98 (m, 36H, NHC(CH₂CH₂CO₂[†]Na)₃); ¹³C NMR (75 MHz, CDCl₃, δ_{ppm}): 183.2, 170.0, 162.1, 151.0, 132.0, 112.0, 100.3, 66.5, 59.0, 32.0, 31.0; ESI-MS (*m/z*): [M-H]⁻ calcd for C₁₅₀H₁₄₄N₆O₄₈, 2796.0; found, 2800.0-2900.0: With both C8 HPLC analysis and flow injection analyses, numerous compounds were detected. A number of compounds yielded ions consistent with molecular weights in the 2800-2900 u range. None yielded ions consistent with the fully protonated or fully sodiated forms of the expected compound.

G-3. ¹H NMR (300 MHz, D₂O/DMSO-*d*₆ (v/v, 1/1), δ_{ppm}): 8.20-7.0 (br, 90H) 4.70 (br, 24H, ArOCH₂CO₂), 2.10 (br, 144H, NHC(CH₂CH₂CO₂[†]Na)₃).

CHAPTER 6

DESIGN, SYNTHESIS, AND PHOTOPHYSICAL STUDIES OF THIENYL GROUP EXTENDED CONJUGATED POLYELECTROLYTE DENDRIMERS

Conjugated polyelectrolytes (CPEs) have attracted considerable attention because of their remarkable materials properties. In particular, the CPEs are water soluble and retain the optical and electronic properties characteristic of the π -conjugated backbone in polar solvents.¹⁰ However, the CPEs have a strong propensity to self-assemble into aggregates in solution because of their amphiphilic feature. For this reason, much effort has been devoted to retaining non-aggregated state in aqueous media.⁵⁶⁻⁵⁸ For instance, in our previous work, CPEs with branched polyionic side chains shows little or no aggregation because of the electrostatic repulsion between branched polyionic side chains. Nevertheless, the problems including the polydisperse and structure defect of CPEs which can affect to the photophysical studies are still remained.

Dendrimer chemistry is a fast-growing field and its numerous applications ranging from medicine to nano-engineering have led to a great interest in the development of novel domain in dendrimer field.^{37,41-42,44-45} Conjugated polyelectrolyte dendrimers (CPE-Ds) are a new class of water-soluble dendrimer and mono-disperse macromolecules. The CPE-Ds include π -conjugated backbone at the inner part and ionic-solubilizing groups at the periphery, preserving the intrinsic optical and electronic features of the π -conjugated backbone in aqueous media.³⁸ Also, the large number of ionic peripheries prevents inter-dendrimer aggregation in polar solvents as well as such sufficient side chains is related to the solubility of conjugated dendrimers. Unlike ordinary non-conjugated dendrimers, the CPE-Ds are structurally rigid because of the fully conjugated backbone, and have globular structure with increasing generation. Such

unique characteristics of CPE-Ds enable various photophysical studies and provide possibilities for the applications to the solar cells, electrochromic devices, and sensors.⁴⁴

The low band gap conjugated molecules exhibit many useful photophysical properties, including broad and long wavelength absorption and fluorescence.¹²⁶ The absorption of conjugate dendrimer can be tuned via structural modification; one of the synthetic strategies is to introduce electron donor and acceptor units into the conjugated backbone.^{1,119} Also, One characteristic of dendritic molecules is the presence of numerous peripheral end groups that all converge to a single core. One particular design is the so-called “extended” dendrimer that possesses consecutively increasing conjugation length toward the center of the molecule.¹¹⁹ Such a structure naturally creates energy gradient from the outside branches to the inside branches. Thus, efficient energy transfer can be achieved in the donor-acceptor type dendrimer.

In the present Chapter, as a D- π -A system, a series of CPE-Ds having thienyl (Th) groups in the conjugated backbone was synthesized and characterized. Figure 6-1 shows the structures of the series of CPE-Ds having thienyl (Th) groups (**Th-G-1**, **Th-G-1**, and **Th-G-3**). Branched polyionic side chains were substituted at the peripheries, which provide more abundant ionic units with increasing the generation. Utilizing both divergent and convergent synthetic approaches allows relatively facile preparation of CPE-Ds. The geometric characteristic of the series of CPE-Ds was studied via dynamic light scattering (DLS), and their photophysical properties were compared to their organic soluble precursors and also studied in methanol and aqueous solutions. To the end, the quenching or energy transfer effects from CPE-Ds to methyl viologen or cyanine dyes

were studied using UV-Vis absorption, steady-state fluorescence, and lifetime spectroscopy.

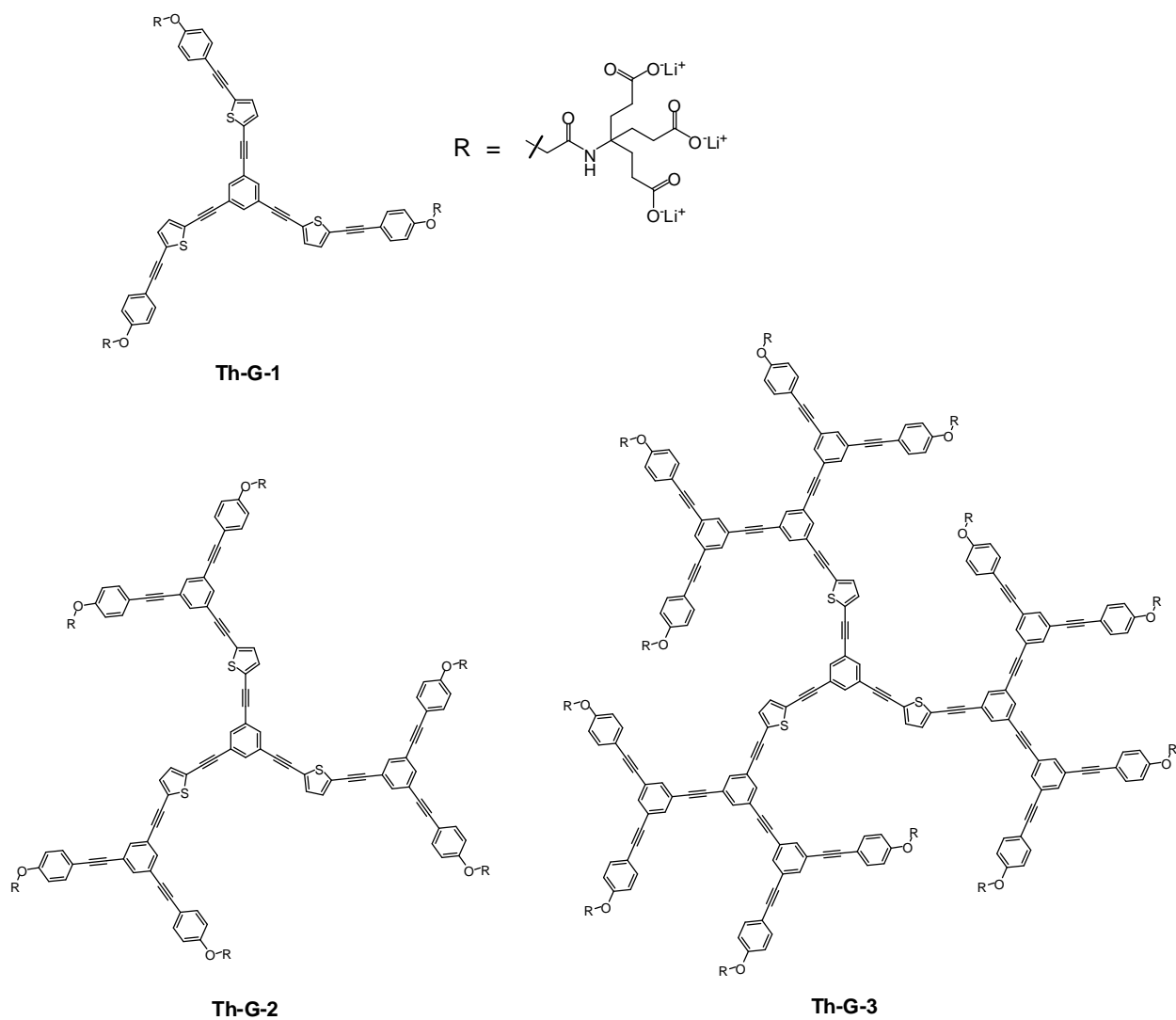


Figure 6-1. Structure of CPE-Ds (**Th-G-1**, **Th-G-2**, and **Th-G-3**).

Results and Discussion

Synthesis and Characterization

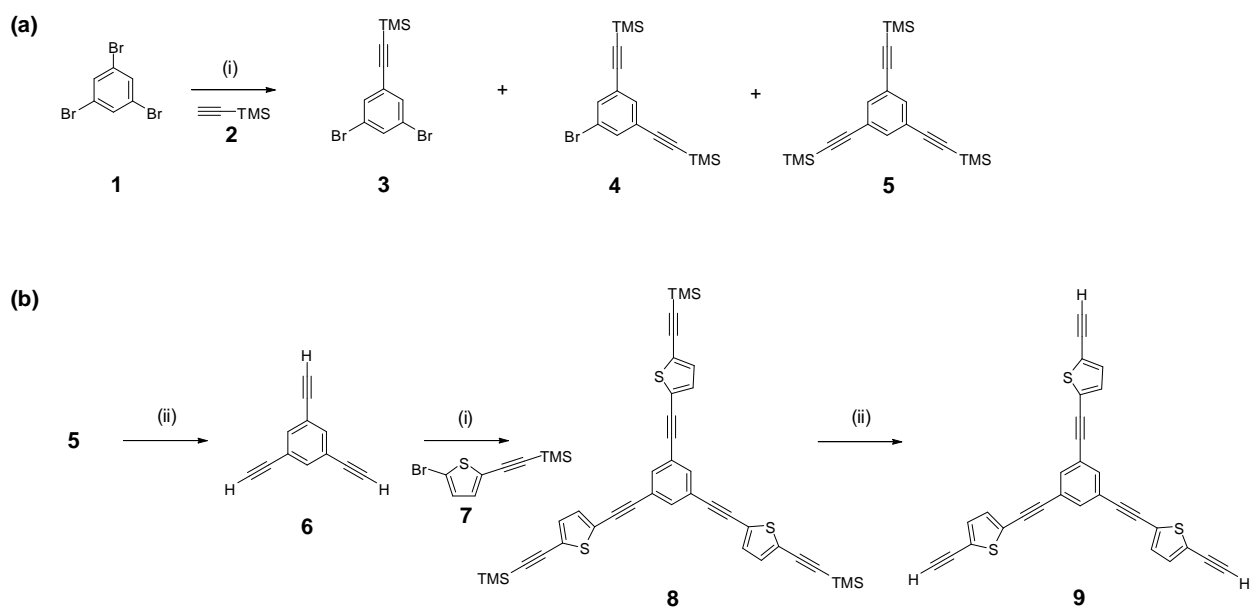


Figure 6-2. Synthesis of (a) focal points and (b) a core unit (i) $\text{Pd}(\text{PPh}_3)_2\text{Cl}_2$, CuI , THF/DIPA (1/1, v/v), 80°C for 12 hrs.; (ii) K_2CO_3 , MeOH/DCM (1/1, v/v) r.t. for 2 hrs

Both convergent and divergent methods³⁷ have been used in the synthesis of dendrimers. However, it should be noted that a conventional divergent or convergent approach is restrictive in the CPE-Ds' synthesis because of the intrinsic poor solubility of conjugated backbone and highly congested branched polyionic side chains. Thus, the combined approach of both methods should be considered in the synthesis of CPE-Ds, where a divergent method was used in the core synthesis; dendrons were prepared by two-stage convergent methods. As a focal point, mono- (**3**), bis- (**4**), and tris(trimethylsilylethynyl) group substituted benzene (**5**) were prepared by the coupling reaction using commercially available 1,3,5-tribromobenzene (**1**) and trimethylsilylethylene (**2**) in the presence of a catalytic amount of $\text{Pd}(\text{PPh}_3)_2\text{Cl}_2$ and CuI (Figure 6-2a). The compounds

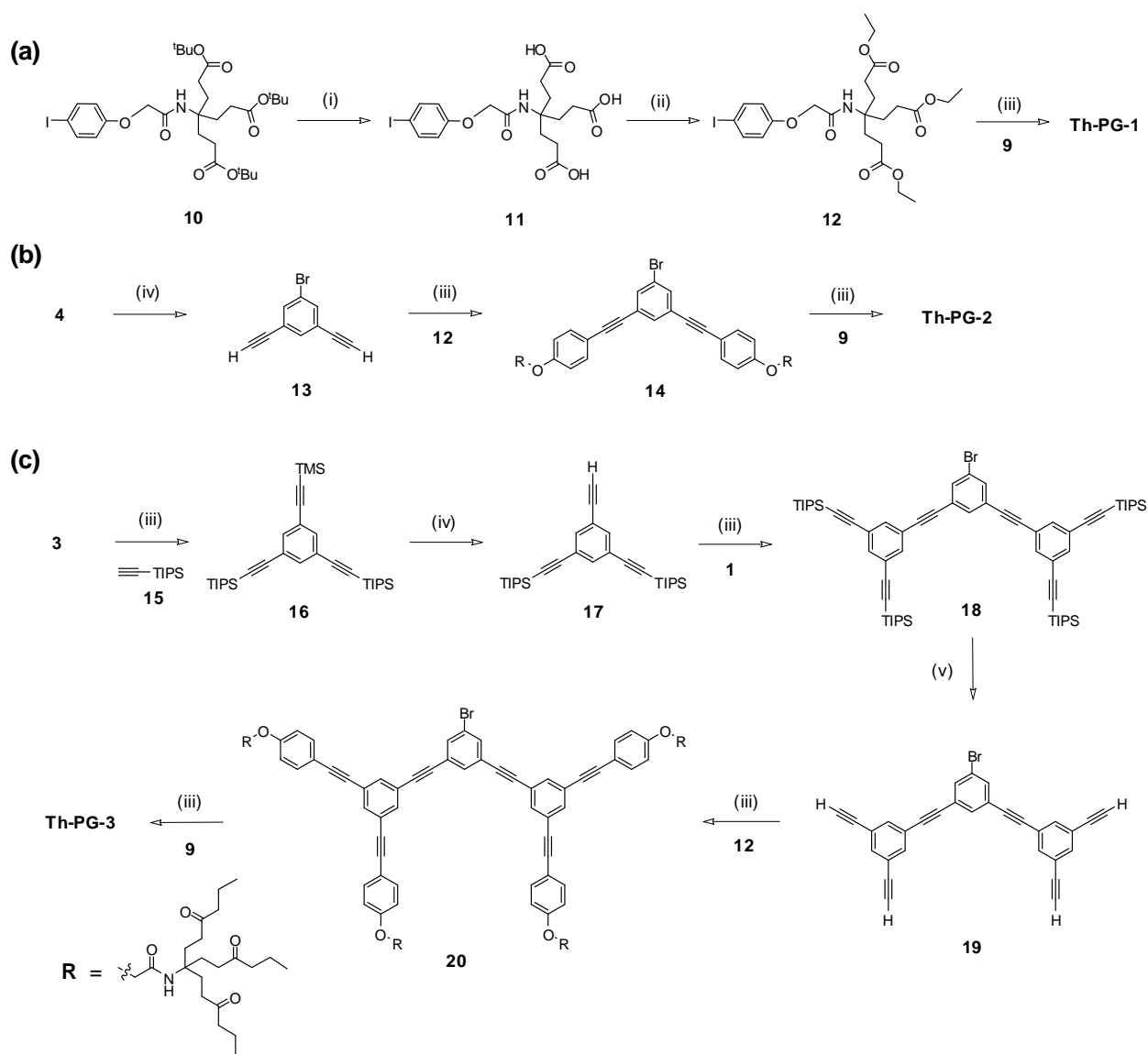


Figure 6-3. Synthesis of precursors of CPE-Ds ((a) **Th-PG-1**, (b) **Th-PG-2**, and (c) **Th-PG-3**) (i) TFA, DCM, r.t. for 3 hrs.; (ii) H₂SO₄, EtOH, 80 °C for 12 hrs.; (iii) Pd(PPh₃)₂Cl₂, CuI, THF/DIPA (1/1, v/v), 80 °C for 12 hrs.; (iv) K₂CO₃, MeOH/DCM (1/1, v/v) r.t. for 2 hrs.; (v) TBAF, THF, r.t. for 1 hr.

3, **4**, and **5** were isolated using column chromatography as solids in 20~35% yield.

Figure 6-2b illustrates the synthesis of a core having thienyl (Th) units. Trimethylsilyl groups of **5** were readily deprotected by using K₂CO₃ in CH₃OH/H₂O (1/1, v/v) to produce 1,3,5-triethynylbenzene (**6**). Then deactivated compound **8** was synthesized by the reaction of **6** with mono-substituted ((5-bromothiophen-2-yl)ethynyl)trimethylsilane

(7)¹²⁷ which is previously prepared by the quantitative use of ethynyltrimethylsilane. Finally, core (9) was obtained by deprotection of TMS (trimethylsilyl) protected ethynyl terminal groups.

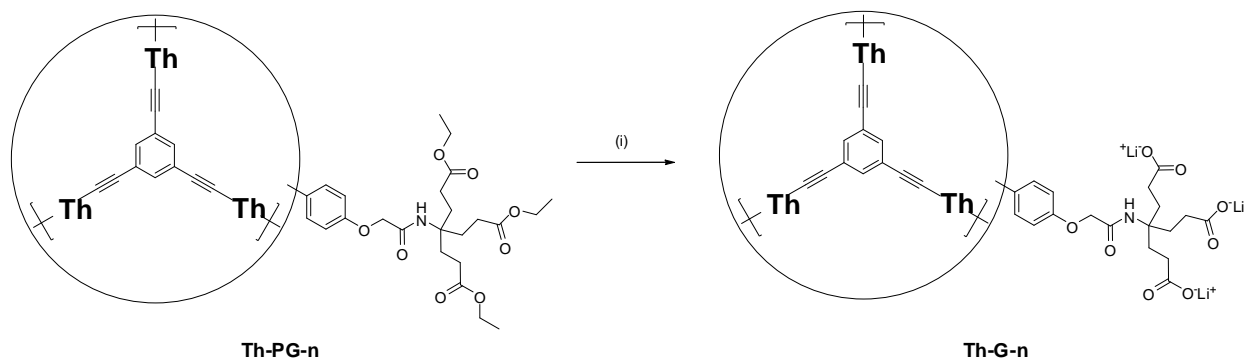


Figure 6-4. Hydrolysis of branched side chains (i) LiOH, THF/water.

Compound **10** was prepared in good yield as described in our previous work (see Chapter 5). To convert organic side chains to ionic side chains, the stability of the conjugated backbone should be considered in the final hydrolysis step. Unfortunately, thienyl units in the conjugated backbone undergo reaction under the acidic conditions used in the hydrolysis process of the *tert*-butyl ester group. Therefore, the *tert*-butyl ester group was modified to the *n*-alkyl ester group which can be hydrolyzed in basic conditions. To change the *tert*-butyl ester group to *n*-alkyl ester group, the *tert*-butyl ester of **10** was first hydrolyzed to carboxylic acid, and then it was converted to the ethyl ester, affording **12** (Figure 6-3a). As seen in Figure 6-3b, after deprotection of TMS group of **4**, two activated ethyl terminal groups of **13** were reacted with the first dendron (**12**), which produced the second dendron (**14**) in moderate yield. As seen in Figure 6-3c, for the third dendron, **3** was used as an intermediary compound, which was reacted with ethynyltriisopropylsilane (**15**) to prepare **16**, and then its TMS group was deprotected by K₂CO₃ in the mixture of MeOH and DCM. The main framework (**18**) for

the third dendron was successfully synthesized by the coupling reaction of **17** with 1,3,5-tribromobenzene (**1**), and its terminal TIPS protected ethynyl groups were readily activated by TBAF in THF solution. Then, the coupling reaction of **19** with **12** produced the third dendron (**20**). As precursor dendrimers, **Th-PG-1**, **Th-PG-2**, and **Th-PG-3** were prepared in 20-30% yield by the coupling reaction of dendron **12**, **14**, or **20** with a core unit (**9**), respectively. Finally, we successfully obtained water-soluble **Th-G-1**, **Th-G-2**, and **Th-G-3** by hydrolysis of the ethyl ester groups of each precursor in the presence of LiOH in the solution of THF and water. The structure of all intermediates, CPE-Ds, and their precursors were characterized and confirmed by ^1H NMR, ^{13}C NMR, and Mass spectroscopy.

Optical Properties

UV-Vis absorption spectroscopy

Figure 6-5 shows the UV-Vis absorption and fluorescence spectra of CPE-Ds (**Th-G-1**, **Th-G-2**, and **Th-G-3**) and their precursors (**Th-PG-1**, **Th-PG-2**, and **Th-PG-3**), and their wavelength maxima were displayed in Table 6-1. As seen in Figure 6-5, both **Th-PG-2** and **Th-PG-3** showed strong absorption at 302 nm and shoulder band at 360 nm in THF (Figure 6-5a). The absorption at 302 nm increased with increasing generation while the long-wavelength absorption remains approximately constant intensity. We believe that the enhanced absorption intensity at short wavelength is attributed to exponentially increased conjugated branches with increasing generation. Also, the same number of thienyl groups in all CPE-Ds induced spectral similarity in the wavelength and absorption intensity. Nevertheless, thienyl moieties of **Th-PG-1** showed slightly higher intensity and red-shifted UV-Vis absorption spectrum ($\lambda_{\text{max}} = 364 \text{ nm}$).

Unlike **Th-PG-2** and **Th-PG-3**, the alkoxy group at the para-position of the periphery phenyl groups is believed to the electron density on the thienyl group of the core,

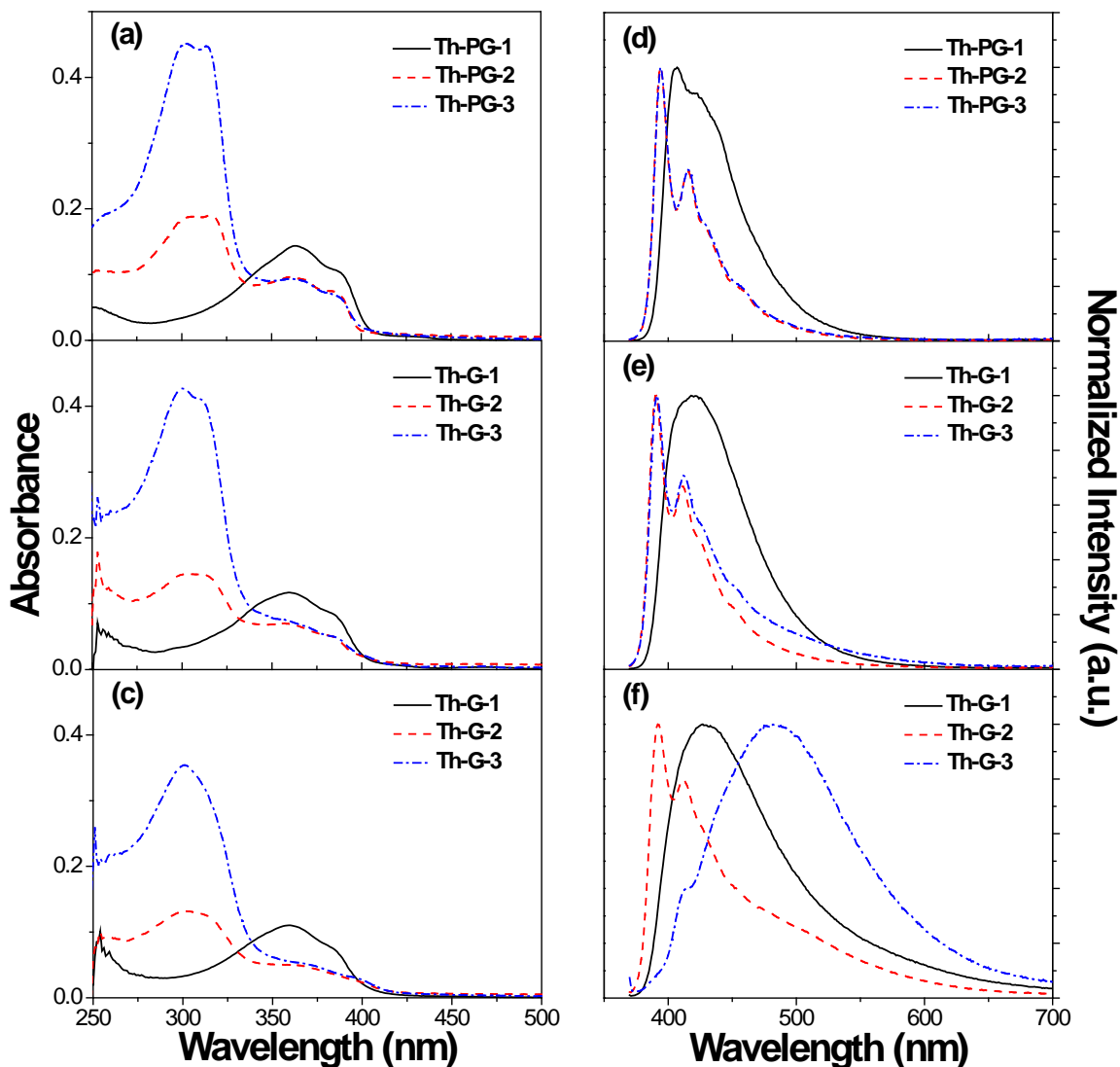


Figure 6-5. UV-Vis absorption and Fluorescence spectra of CPE-Ds (**Th-G-1**, **Th-G-2**, and **Th-G-3**) and their precursors (**Th-PG-1**, **Th-PG-2**, and **Th-PG-3**) in (a, d) THF, (b, e) CH₃OH, and (c, f) H₂O, respectively; excitation wavelength is 360 nm; [**Th-G-n**] = [**Th-PG-n**] = 1.0 μ M.

inducing increased intensity and bothochromic shift in the UV-Vis absorption of **Th-PG-**

1. The water-soluble **Th-G-n** showed negligible spectral changes compared to their organic-soluble precursors in the UV-Vis absorption spectra (Figure 6-5b and 5c).

Table 6-1. UV-Vis absorption and photoluminescent properties of **Th-G-n** (CH₃OH and H₂O(pH 8.0)) and their precursors (THF) .

CDs	THF			CPE-Ds	CH ₃ OH			H ₂ O, pH 8.0		
	$\lambda_{\max}^{\text{abs}}$ (nm)	$\lambda_{\max}^{\text{em}}$ (nm)	Φ_{PL}^a (%)		$\lambda_{\max}^{\text{abs}}$ (nm)	$\lambda_{\max}^{\text{em}}$ (nm)	Φ_{PL} (%)	$\lambda_{\max}^{\text{abs}}$ (nm)	$\lambda_{\max}^{\text{em}}$ (nm)	Φ_{PL} (%)
Th-PG-1	364	407	31.2	Th-G-1	360	418	23.4	359	427	2.4
Th-PG-2	302 360	394	37.9	Th-G-2	301 359	390	13.8	302 364	392	2.7
Th-PG-3	302 360	394	27.0	Th-G-3	300 362	390	9.6	301 370	480	1.7

^a 9,10-Diphenylanthracene in EtOH as the standard, $\Phi_{\text{FL}}=0.90$.

Fluorescence spectroscopy

Figure 6-5d, 5e, and 5f show the fluorescence emission spectra of **Th-PG-n** and **Th-G-n** in THF, CH₃OH, and H₂O (pH 8.0) solutions, respectively (excitation wavelength is 360 nm). Similar to the UV-Vis absorption spectra, the fluorescence spectra of **Th-PG-2** ($\lambda_{\max} = 394$ nm) and **Th-PG-3** ($\lambda_{\max} = 394$ nm) are similar while that of **Th-PG-1** ($\lambda_{\max} = 407$ nm) is broader and red-shifted compared to the higher generation dendrimer in THF. The similar fluorescence spectra in **Th-PG-2** and **Th-PG-3** imply that the dendrimer size does not affect to photophysical characteristics of thienyl groups. However, the effect of the alkoxy substituent to the thienyl groups in **Th-PG-1** is more pronounced in the excited state, resulting in larger bathochromic shift compared to that in the UV-Vis absorption spectra. Similar to the fluorescence of the precursors **Th-PG-n**, the **Th-G-n** series showed negligible fluorescence spectral changes in CH₃OH. On the other hand, relatively significant spectral changes were observed in water solution. **Th-G-1** showed a slightly bathochromic shift and broader spectrum as the solvent polarity increases ($\lambda_{\max} = 418$ nm/CH₃OH and 427 nm/H₂O, pH 8.0). It is noted that the more polar solvent induces more positive solvatochromic effect, resulting in variation in position, intensity and shape of the fluorescence spectra.¹²⁴⁻¹²⁵ In MeOH, **Th-G-2**

exhibits the well-defined structure in the fluorescence spectra, and a new emission band at 475 nm appeared in H₂O (pH 8.0). For **Th-G-3**, a similar emission band at 480 nm was observed in MeOH, and it became significant in H₂O (pH 8.0). It is proposed that such strong fluorescence at lower energy is ascribed to the intra-dendrimer aggregation between thienyl groups and phenylethynylene moieties in the excited state. This phenomenon was also found in our previous work for compact type CPE-Ds, in which the phenylethynylene units were intra-molecularly aggregated in the excited state, and their aggregation effect was more significant at higher generation (see Chapter 5).

Fluorescence quantum yield

The fluorescence quantum yields of the precursors (**Th-PG-n**) and **Th-G-n** were obtained in THF, CH₃OH, and H₂O (pH 8.0) solutions (Table 6-1). The excitation wavelength was 360 nm which corresponds to the thienyl unit. The quantum yields of **Th-G-n** in H₂O are similar and significantly lowered (approximately 5~10 folds) compared to CH₃OH. This decrease of the fluorescence quantum yield is attributed to the solvent effect rather than the aggregate formation.

Fluorescence lifetimes

Table 6-2 and Figure 6-6 show the fluorescence lifetimes and their fractional amplitude changes of **Th-PG-n** (precursors) in THF and **Th-G-n** in CH₃OH, and H₂O (pH 8.0), respectively. The excitation wavelength is 370 nm and emission decays of **Th-PG-n** were monitored over 380 nm. **Th-G-n**'s decays were obtained at 400, 450, and 500 nm where the data were collected by global fitting algorithm. Relatively fast decays were observed for **Th-PG-1** ($\tau = 0.36$ ns), **Th-PG-2** ($\tau = 0.30$ ns), and **Th-PG-3** ($\tau = 0.39$ ns), and these are predominant (>94%) and independent from dendrimer size. For this observation, we propose that a single molecular species is predominant in both ground

Table 6-2. Fluorescence lifetimes (τ_i , ns) and relative amplitudes (RA, %) for **Th-PG-n** and **Th-G-n** in THF, CH₃OH, and H₂O (pH = 8.0) solutions.^a

THF			CH ₃ OH				H ₂ O, pH 8.0					
RA (%)			RA (%)				RA (%)					
Th-PG-1	τ_i (ns) ^b	>380 nm	Th-G-1	τ_i (ns)	400 nm	450 nm	500 nm	τ_i (ns)	400 nm	450 nm	500 nm	
	$\tau_1 = 0.36$	100		$\tau_1 = 0.39$	100	>99	99		$\tau_1 = 0.37$	>99	>99	93
				$\tau_2 = 1.30$	0	<1	1		$\tau_2 = 1.57$	<1	<1	7
	χ^2	1.062		χ^2	1.010	0.953	1.031		χ^2	1.067	1.009	0.995
Th-PG-2	τ_i (ns)	>380 nm	Th-G-2	τ_i (ns)	400 nm	450 nm	500 nm	τ_i (ns)	400 nm	450 nm	500 nm	
	$\tau_1 = 0.30$	28		$\tau_1 = 0.32$	99	91	63		$\tau_1 = 0.32$	13	24	33
	$\tau_2 = 0.66$	6		$\tau_2 = 0.98$	1	8	30		$\tau_2 = 1.04$	86	74	60
				$\tau_3 = 3.06$	0	1	7		$\tau_3 = 3.61$	<1	2	7
	χ^2	0.968		χ^2	1.160	1.162	1.084		χ^2	1.035	1.241	1.074
Th-PG-3	τ_i (ns)	>380 nm	Th-G-3	τ_i (ns)	400 nm	450 nm	500 nm	τ_i (ns)	400 nm	450 nm	500 nm	
	$\tau_1 = 0.39$	68		$\tau_1 = 0.32$	99	82	42		$\tau_1 = 0.44$	66	47	32
	$\tau_2 = 0.78$	5		$\tau_2 = 1.19$	<1	15	39		$\tau_2 = 1.65$	27	48	56
				$\tau_3 = 3.64$	<1	3	19		$\tau_3 = 5.35$	6	5	12
	χ^2	1.029		χ^2	1.167	0.973	0.921		χ^2	1.123	1.172	0.979

^aData were collected by global fitting Algorithm. ^bTypical limits of error on τ_i are less than $\pm 3\%$.

and excited states. Such simplicity in the emission decays implies absence of inter or intra dendrimer aggregation of **Th-PG-n** in THF.

Unlike **Th-PG-n**, **Th-G-n** showed two or three emission decays in CH₃OH and H₂O (pH 8.0) solutions (Table 6-2). The emission decay of **Th-G-1** features two pathways ($\tau_1 = 0.39$ ns, $\tau_2 = 1.30$ ns in CH₃OH and $\tau_1 = 0.37$ ns, $\tau_2 = 1.57$ ns in H₂O, pH 8.0). One faster component is predominant in both solutions (τ_1 at $\lambda = 400$ nm > 99% in CH₃OH and τ_1 at $\lambda = 400$ nm > 98%, in H₂O. pH8.0). The amplitude of $\tau_2 = 1.57$ ns in H₂O (pH 8.0) showed slightly increased aspect at 500 nm ($\tau_2 > 6\%$) (Figure 6-6d). We suggest that fast decay component is a similar state with short-lived component as seen in its precursor in THF. In CH₃OH, the similar results are obtained for **Th-G-2** and **Th-G-3**, where the fast decays are predominant ($\tau_1^{\text{Th-G-2}} = 0.32$ ns > 99% and $\tau_1^{\text{Th-G-3}} = 0.32$ ns > 99%) at 400 nm. These observations imply that both dendrimer states are very similar to their precursors in THF. These fast components showed decreased contribution at 500 nm, where the amplitudes of **Th-G-2** and **Th-G-3** are 63% and 42%, respectively (Figure 6-6b and 6c). On the other hand, relatively slow decays ($\tau_2^{\text{Th-G-2}} = 0.98$ ns and $\tau_3^{\text{Th-G-2}} = 3.06$ ns; $\tau_2^{\text{Th-G-3}} = 1.19$ ns and $\tau_3^{\text{Th-G-3}} = 3.64$ ns) showed increased amplitudes. Also, it is found that such decrease or increase of the fast or slow decays becomes more significant with increasing generation. Based on above observation in CH₃OH, we propose that **Th-G-2** and **Th-G-3** retain the characteristics of their precursors. However, small fractions of intra-dendrimer aggregates exist, but these are only detectable at longer wavelength.

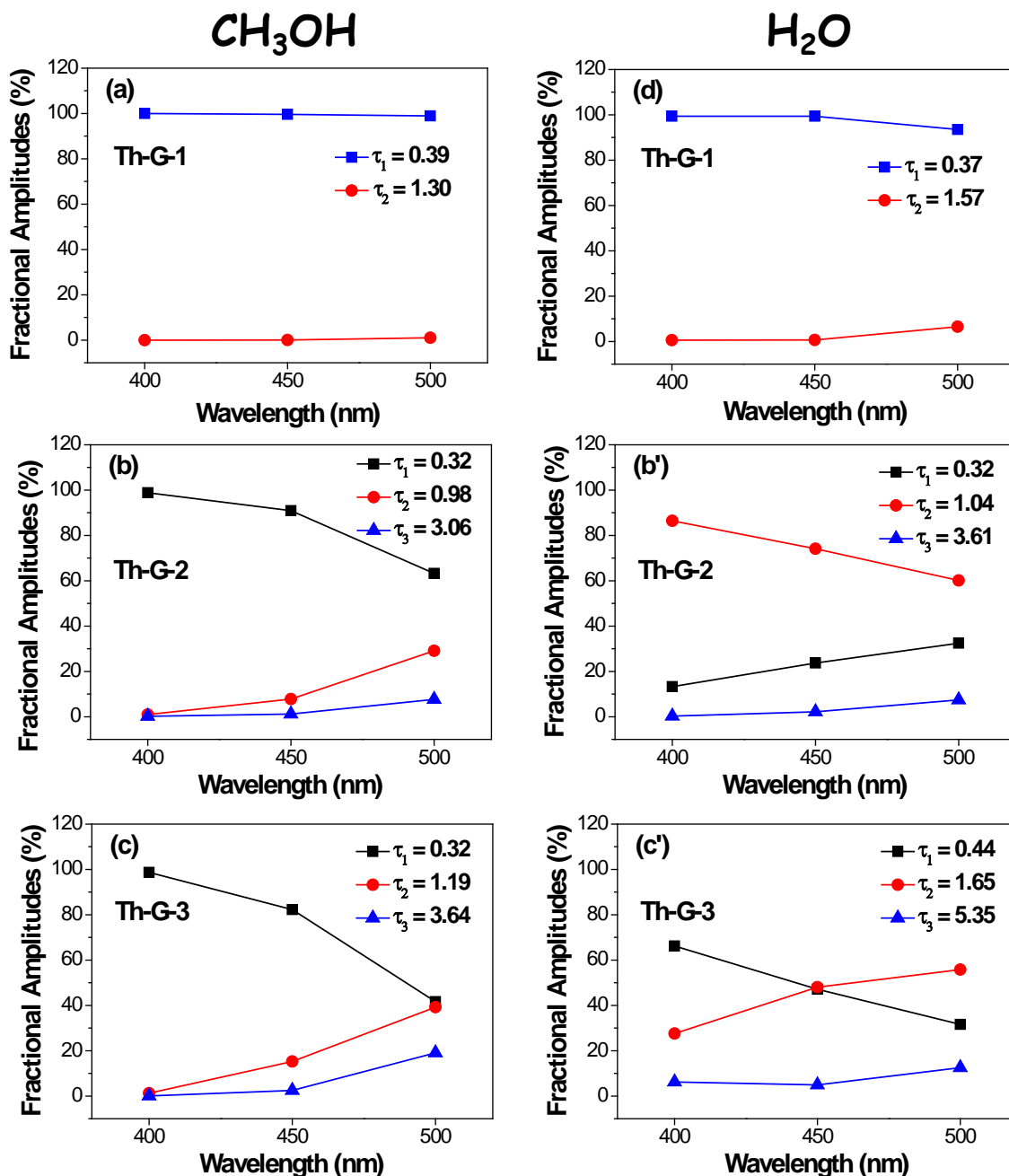


Figure 6-6. Fractional amplitude changes of fluorescence lifetimes of **Th-G-1** in (a) CH₃OH and (d) H₂O, **Th-G-2** in (b) CH₃OH and (e) H₂O, and **Th-G-3** in (c) CH₃OH and (f) H₂O; excitation wavelength is 370 nm and life time decays were monitored at 400, 450, and 500 nm; Data were collected by global fitting algorithm.

More contributions of the decays at 400 nm corresponding to the slow component of **Th-G-1** were observed in **Th-G-2** ($\tau_2 = 1.04$ ns > 86%) in H₂O while the fast ($\tau_1 = 0.32$

ns) and long-lived decay ($\tau_3 = 3.61$ ns) showed relatively lower contributions (Figure 6-6e). At 500 nm, however, the contribution of $\tau_2 = 1.04$ ns decrease to around 60% and 32% of the fast decay ($\tau_1 = 0.32$ ns) was observed with 7% new long-lived decay ($\tau_1 = 3.61$ ns). The moderate increase of both a fast decay and a slow decay is ascribed to the slight intra-dendrimer aggregation, which also induced decrease of the component of $\tau_2 = 1.04$ ns. For **Th-G-3**, although the amplitude of $\tau_2 = 1.65$ ns is relatively small ($\tau_2 > 27\%$) at 400 nm, that of the fast component ($\tau_1 = 0.44$ ns) decreased to around 66%. As seen in Figure 6-5f, the emission of **Th-G-3** at 400 nm in H₂O is fully quenched because of intra-dendrimer aggregation. It is noted that energy transfer or quenching lead to changes on the emission decay times.^{53,73} In this case of **Th-G-3** in H₂O, the relatively large contribution of fast decay ($\tau_1 = 0.44$ ns > 66%) at 400 nm is possibly due to two issues: first, the electron or energy trap caused by intra-dendrimer aggregation lead to fast decay; second, the direct contact of thienyl moieties with H₂O caused nonradiative decay. On the other hand, at 500 nm, the fast component ($\tau_1 = 0.44$ ns) of **Th-G-3** showed decreased contribution (32%), and the component of $\tau_2 = 1.65$ ns and $\tau_3 = 5.35$ ns increased to around 56% and 13%, respectively. **Th-G-3** shows strong exciplex type fluorescence for intra-dendrimer aggregated state at 500 nm. As a result, the increased contribution of fast decay ($\tau_1 = 0.44$ ns) and long-lived component ($\tau_3 = 5.35$) ns at 500 nm is due to the aggregation effect. Also, it is possible that structure changes induced by the intra-dendrimer aggregation give rise to the increase of contribution of the decay ($\tau_2 = 1.65$ ns).

Chromophore/Dendrimer Aggregation

Concentration dependent fluorescence

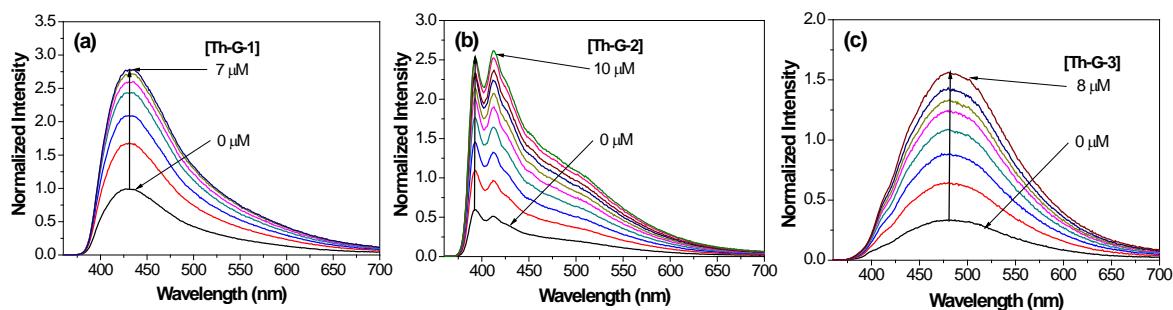


Figure 6-7. Fluorescence emission spectra of (a) **Th-G-1**, (b) **Th-G-2**, and (c) **Th-G-3** with increasing concentration in H_2O ; [**Th-G-n**] = 1.0 μM .

Aggregation of **Th-G-n** in aqueous solution is further studied by the concentration dependent fluorescence and excitation spectral changes. As the concentration of **Th-G-n** increases, the fluorescence spectra ($\lambda_{\text{ex}} = 360 \text{ nm}$) exhibit no change in the wavelength and band-shape in H_2O (pH 8.0) (Figure 6-7). This observation suggests that inter-dendrimer aggregation does not occur in **Th-G-n**.

Fluorescence excitation spectroscopy

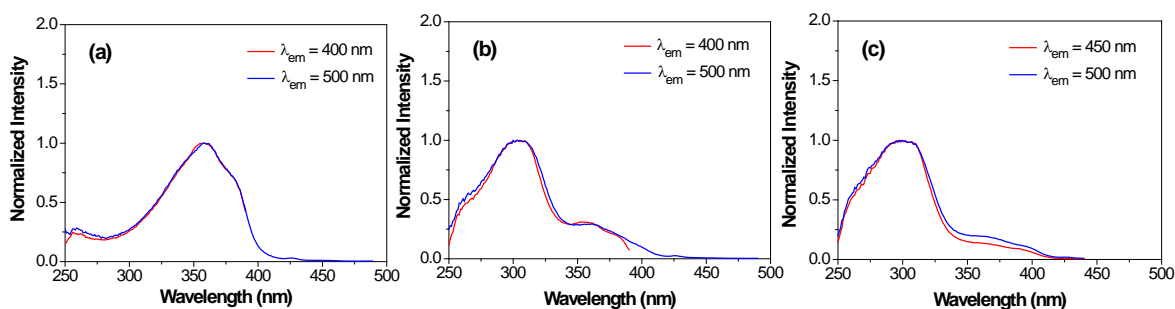


Figure 6-8. Fluorescence excitation spectra of (a) **Th-G-1** at 400 and 500 nm, (b) **Th-G-2** at 400 and 500 nm, and (c) **Th-G-3** at 450 and 500 nm; [**Th-G-n**] = 1.0 μM in H_2O .

As seen in Figure 6-8, the excitation spectra ($\lambda_{\text{em}} = 400, 450$ or 500 nm) of all **Th-G-n** do not display any changes in the excitation spectra. Although **Th-G-1** showed

slightly broader fluorescence spectra in water solution, the wavelength independent excitation spectra and constant fluorescence spectra as a function of concentration suggest that it does not aggregate. In addition, excitation spectral results of **Th-G-2** and **Th-G-3** illustrate that their *inter-dendrimer* aggregation is negligible. Nevertheless, aggregation seen in fluorescence spectra is attributed to the excited state *intra-dendrimer* aggregation. For **Th-G-1**, it is possible that its inter-dendrimer interaction can be fairly minimized by the geometrical peculiarity of the thienyl group.

Dynamic light scattering (DLS)

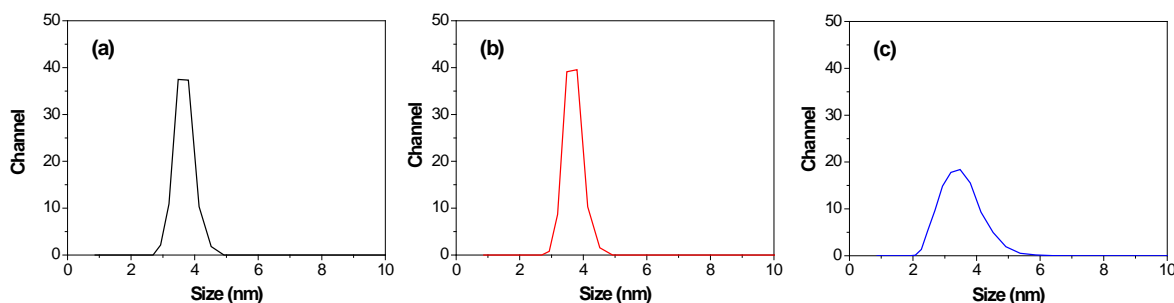


Figure 6-9. Hydrodynamic radii obtained from dynamic light scattering (DLS) for (a) **Th-G-1**, (b) **Th-G-2**, and (c) **Th-G-3** in H₂O; [**G-n**] = 1.0 μ M.

Dynamic light scattering (DLS) provide further evidence for the state of aggregation of **Th-G-n** in H₂O (pH 8.0). Figure 6-9 shows the distribution profiles of the populations for hydrodynamic radius of **Th-G-n** in aqueous solution. DLS on **Th-G-1**, **Th-G-2**, and **Th-G-3** shows 3.42, 3.45, and 2.86 nm as an average size, respectively. Their average sizes are relatively larger than compact type **G-n**, which is probably ascribed to the extended size of inner part by incorporating thienyl groups into the conjugated backbone. The physical size increases with the generation but smaller size of **Th-G-3** than the other two dendrimers was observed. It is possible that more hydrophobic conjugated backbones induce stronger contraction. In fact, a strong

correlation was established between the solvent polarity and the mean radius of gyration.^{44,128} For example, the simulations with branched polyelectrolytes showed a drastic contraction as the ionic strength of the solvent increases.¹²⁹ Also, unlike compact type **G-1** in aqueous solution, DLS result showed narrow and regular size of hydrodynamic radius for **Th-G-1**. This implies the absence of aggregation of **Th-G-1** in aqueous solution. For **Th-G-3**, although its distribution profile is very broad compared to **Th-G-1** and **Th-G-2**, the maximum size does not exceed around 5.8 in aqueous solution. Thus, it is concluded that ground state inter-dendrimer aggregation of **Th-G-n** does not occur but intra-dendrimer interaction is more pronounced with increasing generation in more polar solvent.

Fluorescence Quenching of **Th-G-n** with MV^{2+}

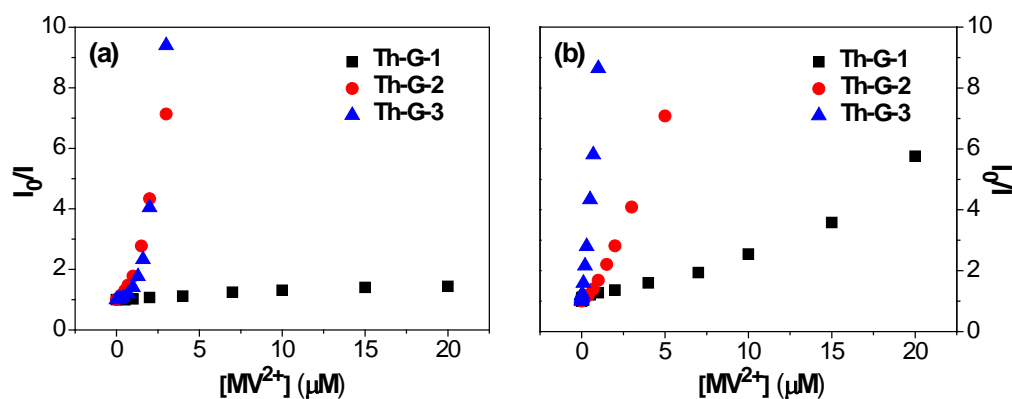


Figure 6-10. Stern-Volmer plots of **Th-G-n** (a) CH_3OH and (b) H_2O ; fluorescence was quenched by methyl viologen (MV^{2+}); **Th-G-1** (■), **Th-G-2** (●), and **Th-G-3** (▲); $[Th-G-n] = 1.0 \mu M$.

Table 6-3. K_{sv}^a of **Th-G-n** with methyl viologen (MV^{2+}) in CH_3OH and H_2O .

CPE-Ds	CH_3OH	H_2O
	K_{sv}/M^{-1}	K_{sv}/M^{-1}
Th-G-1	2.4×10^4	1.4×10^5
Th-G-2	7.8×10^5	6.1×10^5
Th-G-3	4.0×10^5	7.3×10^6

^a Computed from linear fit at low quencher concentration (0~2.5 μM).

The fluorescence quenching of **Th-G-n** was investigated with methyl viologen (MV^{2+}) in CH_3OH and H_2O solutions. Their Stern-Volmer (SV) plots and K_{SV} values present in Figure 6-10 and Table 6-3, respectively. The SV plots were obtained at the wavelength of maximum fluorescence intensity. As seen in Figure 6-10, the typical SV plots of **Th-G-n** were observed: at very low quencher concentration ($< 2.5 \mu M$) SV plot is linear and it becomes upward curved at high concentration ($> 5.0 \mu M$). In CH_3OH , **Th-G-1** showed much less efficient quenching with a low K_{SV} value ($K_{SV} = 2.4 \times 10^4 M^{-1}$) while very similar quenching features were observed in **Th-G-2** ($K_{SV} = 7.8 \times 10^5 M^{-1}$) and **Th-G-3** ($K_{SV} = 4.0 \times 10^5 M^{-1}$). Based on the similarity in the results of both fluorescence and lifetime decays, we suggest that the quenching effect in **Th-G-2** and **Th-G-3** is not related to the dendrimer size.

Interestingly, the fluorescence quenching efficiency increased with the generation (**Th-G-1** < **Th-G-2** < **Th-G-3**) in H_2O (Figure 6-10b), and the most efficient quenching was observed in **Th-G-3** ($K_{SV} = 7.3 \times 10^6 M^{-1}$). The K_{SV} value ($K_{SV} = 1.4 \times 10^5 M^{-1}$) of **Th-G-1** in H_2O showed slightly higher value than that in CH_3OH , and similar K_{SV} values ($K_{SV} = 7.8 \times 10^5 M^{-1}/H_2O$ and $K_{SV} = 6.1 \times 10^5 M^{-1}$) of **Th-G-2** were observed in CH_3OH and H_2O solutions. The highest K_{SV} value of **Th-G-3** is ascribed to intra-dendrimer aggregation effect, which is supported by the fact that the quenching is amplified in aggregate states by effective energy or exciton migration between chromophores.^{1,68} We also propose that static quenching is dominant in all processes based on the results of SV quenching.

FRET from Th-G-3 to Cyanine Dyes

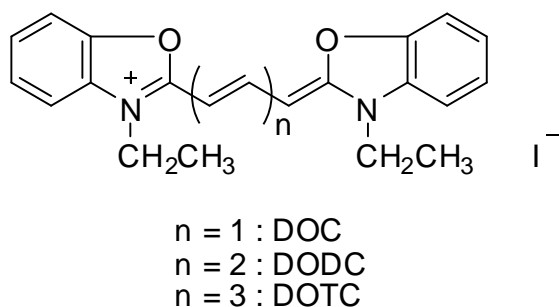


Figure 6-11. Structure of cyanine dyes (DOC, DODC, and DOTC).

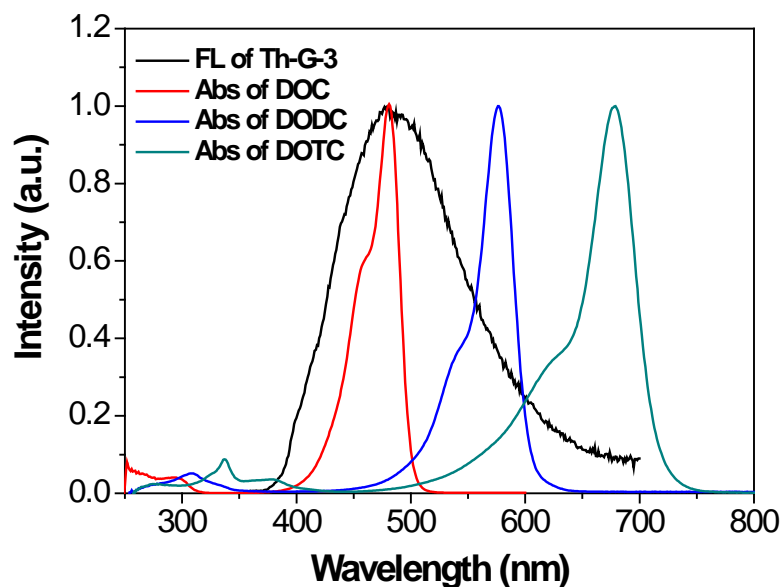


Figure 6-12. Fluorescence of FRET donor (**Th-G-3**) and absorption of FRET acceptors (cyanine dyes).

Fluorescence quenching of **Th-G-3** with cyanine dyes (DOC, DODC, and DOTC) was studied in H₂O (excitation wavelength is 360 nm). The structures of DOC, DODC, and DOTC are presented in Figure 6-11. These cyanine dyes are different in conjugation length, showing the variation of the absorption (Figure 6-12). Figure 6-13 shows the overall fluorescence intensity changes upon the addition of DOC, DODC, and DOTC. As seen in Figure 6-13, all cyanine dyes are nearly non-fluorescent in 0.2~0.3

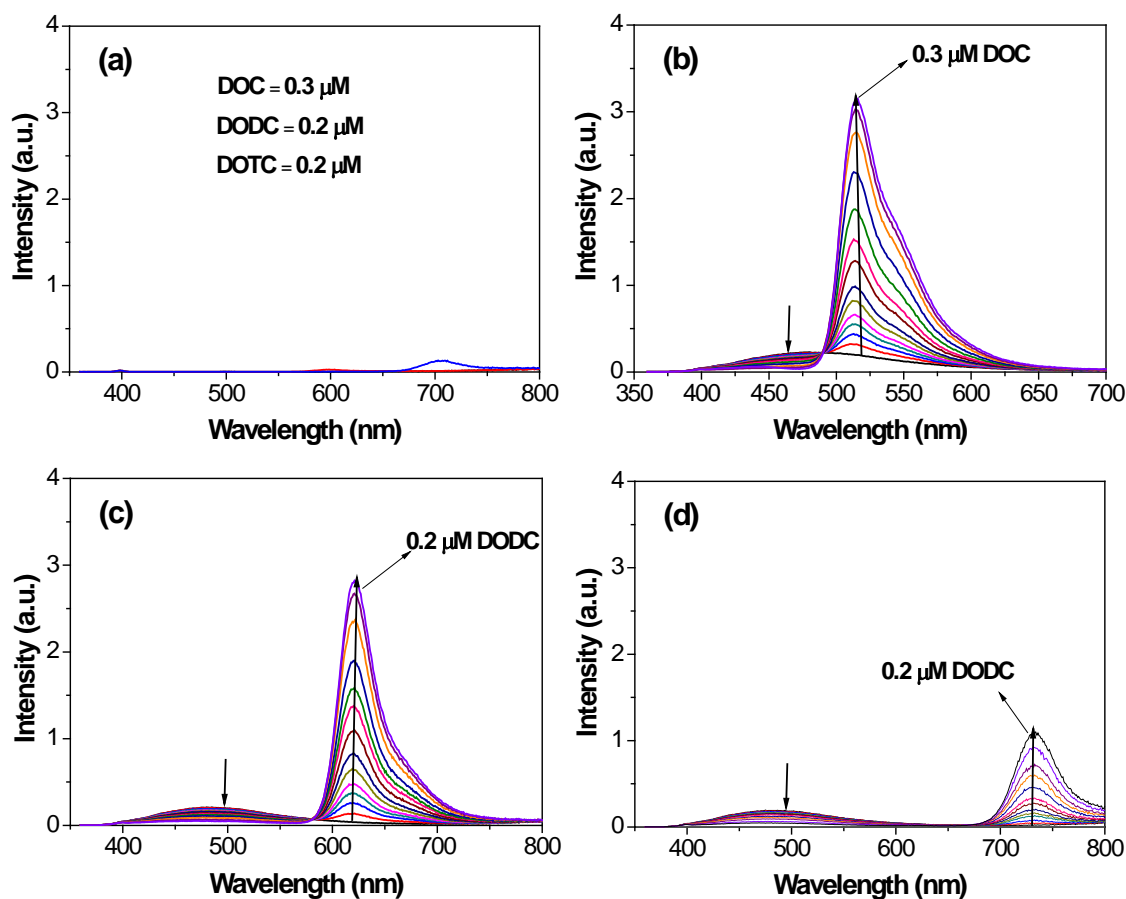


Figure 6-13. Fluorescence emission spectra of (a) cyanine dyes only (DOC, DODC, and DOTC) and **Th-G-3** titrated with (b) DOC, (c) DODC, and (d) DOTC in H₂O pH 8; [**Th-G-3**] = 1.0 μ M; [dye quencher] = 0 ~ 0.3 μ M; excitation wavelength is 360 nm.

μ M concentration range. The fluorescence intensity of **Th-G-3** was efficiently quenched, which was concomitant with a significant fluorescence enhancement of cyanine dyes via fluorescence energy transfer. Figure 6-12 shows the spectral overlap between donor fluorescence (**Th-G-3**) and acceptor absorption (DOC, DODC, or DOTC), in which the degree of overlap is in the order DOC>DODC>DOTC. The more overlap between donor fluorescence and acceptor absorption gives rise to efficient energy transfer from **Th-G-3** to cyanine dyes.

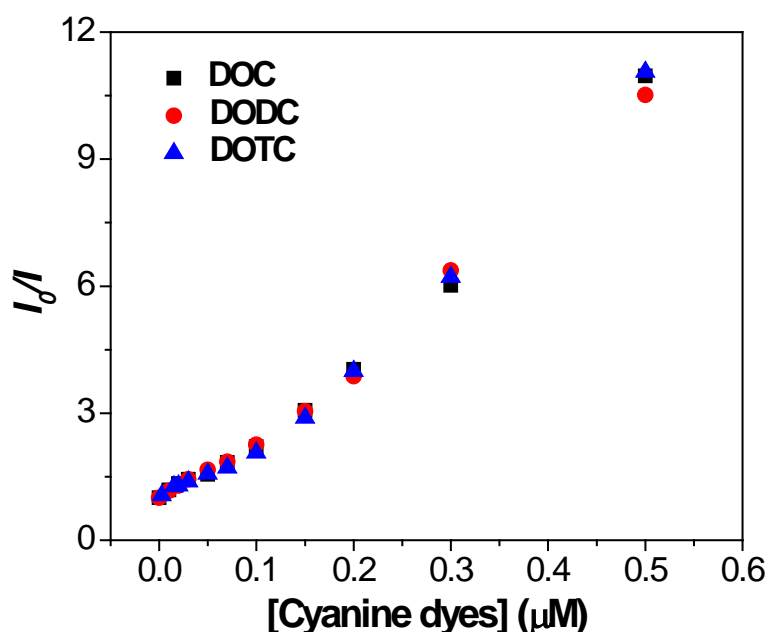


Figure 6-14. Stern-Volmer plots of **Th-G-3** in H₂O; fluorescence quenched by cyanine dyes; DOC (■), DODC (●), and DOTC (▲); [**Th-G-3**] = 1.0 μM.

Table 6-4. K_{sv} ^a of CPE-Ds with cyanine dyes in H₂O.

CPE-D	K_{sv}/M^{-1} (H ₂ O, pH 8)		
	DOC	DODC	DOTC
Th-G-3	1.43×10^7	1.39×10^7	1.35×10^7

^a Computed from linear fit at low quencher concentration.

Interestingly, the similar the quenching efficiency of **Th-G-3** for all cyanine dyes was observed. As seen in Figure 6-14 and Table 6-4, the Stern-Volmer (SV) plots of **Th-G-3** are very similar and their K_{sv} values are the same ($K_{sv} \approx 1.35 \times 10^7$). We could not clearly explain the interesting results. However, one possible reason is that the charge transfer effect participates in their quenching and its efficiency is compatible with energy transfer effect. Thus, although the energy transfer effect from **Th-G-3** to DOTC is less

effective than other cyanine dyes, the further fluorescence can be quenched by charge transfer effect.

Summary and Conclusions

In this Chapter, a series of CPE-Ds having thienyl (Th) groups in the conjugated backbone was systemically prepared via precursor route. In CH₃OH, all **Th-G-1**, **Th-G-2**, and **Th-G-3** showed well-defined UV-Vis absorption and fluorescence spectra, implying non-aggregated states in CH₃OH. On the other hand, the UV-Vis absorption and fluorescence spectra were red-shifted in H₂O, which was more significant with increasing generation. It was proposed that such red-shift with generation is due to *intra-dendrimer* aggregation. Also, fluorescence lifetime decays provide the information for the *intra-dendrimer* aggregation of **Th-G-n** in H₂O. Methyl viologen and cyanine dyes (DOC, DODC, and DOTC) efficiently quenched the fluorescence of **Th-G-3** rather than the other generation in H₂O, which is due to more efficient energy or charge transfer effect in aggregated state. The similar quenching results for all cyanine dyes illustrated that both energy and charge transfer effects complementarily participate in entire quenching mechanism.

Experimental

Materials

All chemicals used for the synthesis were of reagent grade and used without further purification. Nitromethane, *tert*-butylacrylate, T-1 Raney nickel, diisopropylamine, chloroacetyl chloride, 4-iodophenol, 1,3,5-tribromobenzene, 2,5-dibromothiophene, and triphenylphosphine were purchased from Sigma-Aldrich Chemical Company. Sodium carbonate, and copper iodide were obtained from Acros Chemical Company. *trans*-Dichlorobis(triphenylphosphine)palladium (II) was purchased from Sterm Chemical

Company. Ethynyltrimethylsilane and ethynyltriisopropylsilane were bought from GFC Chemical Company. Potassium carbonate, ethanol, sulfuric acid, and trifluoroacetic acid were obtained from Fisher Scientific Company. THF was purified by Solvent Dispensing System (SDS). Silica gel (Merck, 230-400 mesh) was used for chromatographic purification of all of intermediate and target molecules. All other chemicals and solvents were purchased from either Sigma-Aldrich or Acros Chemical Company and used as received.

Instrumentation and Methods

NMR spectra were recorded using a Varian VXR-300 FT NMR, operating at 300 MHz for ^1H NMR and at 75 MHz for ^{13}C NMR. Gel permeation chromatography (GPC) analyses were carried out on a system comprised of a Rainin Dynamax SD-200 pump, Polymer Laboratories PL gel mixed D columns, and a Beckman Instruments Spectroflow 757 absorbance detector. Molecular weight calibration was effected by using polystyrene standards. UV/Vis absorption spectra were recorded using a Varian Cary 50 Spectrophotometer. Steady-state fluorescence spectra were obtained with a PTI fluorometer. Lifetime measurements were carried out using a PicoQuant FluoTime 100 Compact Fluorescence Lifetime Spectrometer. A 1 cm quartz cuvette was used for all spectral measurements. Dynamic light scattering (DLS) experiments were performed with Zeta PALS from Brookhaven Instrument Corporation.

Stock solutions (1.0 mM) of all of the CPE-Ds were prepared in H_2O and have been stored at 0 °C. The solutions have been kept at the room temperature for one hour before use. Fluorescence quantum yield are reported relative to known standards (9,10-

diphenyl anthracene, $\Phi = 0.90$ in EtOH). The pH of aqueous solution was adjusted with HCl and/or NaOH using a Corning pH meter 320.

Synthetic Procedures

Compounds **7** and **10** were prepared in a good yield as described in literature and Chapter 5, respectively.

4-(2-carboxyethyl)-4-(2-(4-iodophenoxy)acetamido)heptanedioic acid (11). To a solution of **10** (50.0 g, 74.0 mmol) in 500 mL of CH_2Cl_2 , 200 mL of trifluoroacetic acid (TFA) was added dropwise. Upon completion of the addition, the reaction mixture was stirred at room temperature for 3 hours. excess TFA and the solvent were removed *in vacuo*. The crude product was used in the next esterification reaction without further purification. Yield: 98%.

Dendron 1 (12). To a solution of compound **11** (30.0 g, 59.1 mmol) in EtOH (300 mL), 5 mL of H_2SO_4 was added. The mixture was vigorously stirred at 80 °C for 12 hours under argon gas. After the reaction mixture was cooled to room temperature, the solvent was removed *in vacuo*. The reaction mixture was washed with water (200 mL), and then extracted with CH_2Cl_2 (200 mL). The organic layer was separated and dried over anhydrous MgSO_4 , and the solvent was evaporated to yield a white solid. The crude product was isolated by column chromatography on silica gel using ethyl acetate:hexane (1:2) as the eluent. 86% yield; mp 120-122 °C; ^1H NMR (300 MHz, CDCl_3 , δ_{ppm}): 7.42 (d, 2H, $\text{IAr-}H_{\text{ortho}}$, $J=8.9$ Hz), 6.85 (d, 2H, $\text{IAr-}H_{\text{meta}}$, $J=8.9$ Hz), 6.50 (s, 1H, CON-H), 4.37 (s, 2H, $\text{ArOCH}_2\text{CO}_2$), 4.10 (q, 6H, $\text{CO}_2\text{CH}_2\text{CH}_3$) 2.25 (m, 6H, $\text{NHC}(\text{CH}_2\text{CH}_2\text{CO}_2^t\text{Et})_3$), 2.05 (m, 6H, $\text{NHC}(\text{CH}_2\text{CH}_2\text{CO}_2^t\text{Et})_3$), 1.23 (t, 9H, $\text{CO}_2\text{CH}_2\text{CH}_3$).

General coupling reaction procedure. Terminal alkynes and aryl halides were dissolved in 20 mL of THF/DIPA (1/3, v/v). The resulting solution was deoxygenated with argon for 1 hour. Then Pd(PPh₃)₂Cl₂ (2 mol%) and CuI (1.9 mg, 10.0 μmol) were added to the stirred solution under the protection of argon. The reaction mixture was then heated up to 70 ~ 75 °C and stirred for 12 hours. The reaction mixture was cooled down to the room temperature and the solvent was removed *in vacuo*. The crude product was isolated by column chromatography on silica gel using methylene chloride:acetone as the eluent.

Mono-, di-, or tri-substitution of trimethylsilylethynyl group onto 1,3,5-tribromobenzene. 1,3,5-tribromobenzene (**1**) (30.0 g, 95.3 mmol) and two equivalents of ethynyltrimethylsilane (**2**) (18.7 g, 190.6 mmol) were used as an aryl halide and terminal alkynes, respectively. The mixture of mono-, di-, or tri- trimethylsilylethynyl substituted benzenes was separated by column chromatography on silica gel using ethyl acetate:hexane as the eluent.

((3,5-dibromophenyl)ethynyl)trimethylsilane (3): Yield: 22%; mp 105-106 °C; ¹H NMR (300 MHz, CDCl₃, δ_{ppm}): 7.56 (s, 1H, TMS-C₂-Ar-*H*_{para}), 7.53 (s, 2H, TMS-C₂-Ar-*H*_{ortho}), 0.25 (s, 9H, (CH₃)₃Si).

(5-bromo-1,3-phenylene)bis(ethyne-2,1-diyl)bis(trimethylsilane) (4): Yield: 35%; mp 125-126 °C; ¹H NMR (300 MHz, CDCl₃, δ_{ppm}): 7.54 (s, 2H, Br-Ar-*H*_{ortho}), 7.53 (s, 1H, Br-Ar-*H*_{para}), 0.25 (s, 18H, (CH₃)₃Si).

1,3,5-tris(trimethylsilyl)ethynylbenzene (5): Yield: 31%; mp 129-130 °C; ¹H NMR (300 MHz, CDCl₃, δ_{ppm}): 7.48 (s, 3H, benzene-*H*), 0.25 (s, 27H, (CH₃)₃Si); ¹³C NMR (75 MHz, CDCl₃, δ_{ppm}): 135.0, 124.2, 105.5, 92.5, 11.5.

1,3,5-tris((5-((trimethylsilyl)ethynyl)thiophen-2-yl)ethynyl)benzene (8): ((5-bromothiophen-2-yl)ethynyl)trimethylsilane (**7**) (11.4 g, 43.9 mmol) and 1,3,5-triethynylbenzene (**6**) (2.0 g, 13.3 mmol) were used as an aryl halide and terminal alkynes, respectively. Yield: 54%; mp 132-133 °C; ¹H NMR (300 MHz, CDCl₃, δ_{ppm}): 7.61 (s, 3H, benzene-*H*), 7.12 (s, 6H, thiophene-*H*), 0.26 (s, 27H, (CH₃)₃Si); ¹³C NMR (75 MHz, CDCl₃, δ_{ppm}): 134.1, 132.2, 132.1, 125.6, 123.9, 123.8, 100.5, 96.8, 92.0, 84.0, 0.1.

Dendron 2 (14): Dendron 1 (**12**) (6.4 g, 10.7 mmol) and 1-bromo-3,5-diethynylbenzene (**13**) (2.0 g, 4.9 mmol) were used as an aryl halide and terminal alkynes, respectively. Yield: 45%; mp 145-146 °C; ¹H NMR (300 MHz, CDCl₃, δ_{ppm}): 7.60 (s, 2H, Br-Ar-*H*_{ortho}), 7.58 (s, 1H, Br-Ar-*H*_{para}), 7.50 (d, 4H, CH₂OAr-*H*_{meta}, *J*=9.0 Hz), 6.98 (d, 4H, CH₂OAr-*H*_{ortho}, *J*=9.0 Hz), 6.58 (s, 2H, CON-*H*), 4.42 (s, 4H, ArOCH₂CO₂), 4.12 (q, 12H, CO₂CH₂CH₃), 2.3 (m, 12H, NHC(CH₂CH₂CO₂^tEt)₃), 2.10 (m, 12H, NHC(CH₂CH₂CO₂^tEt)₃), 1.23 (t, 18H, CO₂CH₂CH₃); ¹³C NMR (75 MHz, CDCl₃, δ_{ppm}): 173.5, 167.3, 157.8, 134.0, 133.8, 133.2, 125.9, 122.1, 116.3, 114.9, 90.8, 86.6, 67.5, 61.0, 57.9, 31.0, 30.0, 28.5, 14.2.

(5-((trimethylsilyl)ethynyl)-1,3-phenylene)bis(ethyne-2,1-diyl)bis(triisopropylsilane) (16): ((3,5-dibromophenyl)ethynyl)trimethylsilane (**3**) (10.0 g, 30.1 mmol) and ethynyltriisopropylsilane (**15**) (16.5 g, 90.3 mmol) were used as an aryl halide and terminal alkynes, respectively. The crude product was used in the next deprotection reaction without further purification. Yield: 72%.

(5,5'-(5-bromo-1,3-phenylene)bis(ethyne-2,1-diyl)bis(benzene-5,3,1-triyl))tetrakis(ethyne-2,1-diyl)tetrakis(triisopropylsilane) (18): 1,3,5-

tribromobenzene (**1**) (5.0 g, 15.9 mmol) and (5-ethynyl-1,3-phenylene)bis(ethyne-2,1-diyl)bis(triisopropylsilane) (**17**) (16.2 g, 34.9 mmol) were used as an aryl halide and terminal alkynes, respectively. The crude product was used in the next deprotection reaction without further purification.

Dendron 3 (20): Dendron 1 (**12**) (5.7 g, 9.7 mmol) and 5,5'-(5-bromo-1,3-phenylene)bis(ethyne-2,1-diyl)bis(1,3-diethynylbenzene) (**19**) (1.0 g, 2.2 mmol) were used as an aryl halide and terminal alkynes, respectively. Yield: 32%; mp 165-166 °C; ¹H NMR (300 MHz, CDCl₃, δ_{ppm}): 7.64 (m, 9H, phenyl-*H*), 7.52 (d, 8H, CH₂OAr-*H*_{meta}, *J*=9.1 Hz), 6.96 (d, 8H, CH₂OAr-*H*_{ortho}, *J*=9.0 Hz), 6.58 (s, 4H, CON-*H*), 4.42 (s, 8H, ArOCH₂CO₂), 4.12 (q, 24H, CO₂CH₂CH₃), 2.30 (m, 24H, NHC(CH₂CH₂CO₂^tEt)₃), 2.10 (m, 24H, NHC(CH₂CH₂CO₂^tEt)₃), 1.23 (t, 36H, CO₂CH₂CH₃); ¹³C NMR (75 MHz, CDCl₃, δ_{ppm}): 173.0, 167.5, 157.8, 133.7, 124.4, 116.2, 114.9, 90.2, 87.3, 67.5, 61.0, 57.9, 30.0, 28.6, 14.3.

Th-PG-1: Dendron 1 (**12**) (2.1 g, 3.3 mmol) and 1,3,5-tris((5-ethynylthiophen-2-yl)ethynyl)benzene (**9**) (0.5 g, 1.1 mmol) were used as an aryl halide and terminal alkynes, respectively. Yield: 40%; mp 169-170 °C; ¹H NMR (300 MHz, CDCl₃, δ_{ppm}): 7.61 (s, 3H, phenyl-*H*), 7.52 (d, 6H, CH₂OAr-*H*_{meta}, *J*=9.0 Hz), 7.17 (dd, 6H, thiophene-*H*), 6.95 (d, 6H, CH₂OAr-*H*_{ortho}, *J*=9.0 Hz), 6.56 (s, 3H, CON-*H*), 4.40 (s, 6H, ArOCH₂CO₂), 4.12 (q, 18H, CO₂CH₂CH₃), 2.30 (m, 18H, NHC(CH₂CH₂CO₂^tEt)₃), 2.12 (m, 18H, NHC(CH₂CH₂CO₂^tEt)₃), 1.23 (t, 27H, CO₂CH₂CH₃); ¹³C NMR (75 MHz, CDCl₃, δ_{ppm}): 173.4, 167.3, 159.3, 157.6, 133.5, 114.4, 114.5, 67.5, 61.2, 58.1, 29.8, 28.7, 14.1; MALDI-MS (*m/z*): M⁺ calcd for C₁₀₂H₁₁₁N₃O₂₄S₃, 1858.68; found, 1857.84.

Th-PG-2: Dendron 2 (**14**) (1.6 g, 1.4 mmol) and 1,3,5-tris((5-ethynylthiophen-2-yl)ethynyl)benzene (**9**) (0.2 g, 0.4 mmol) were used as an aryl halide and terminal alkynes, respectively. Yield: 27%; mp 182-184 °C; ¹H NMR (300 MHz, CDCl₃, δ_{ppm}): 7.66 (s, 3H, phenyl-*H*), 7.62 (m, 9H, phenyl-*H*) 7.51 (d, 12H, CH₂OAr-*H*_{meta}, *J*=9.0 Hz), 6.90 (d, 12H, CH₂OAr-*H*_{ortho}, *J*=9.0 Hz), 6.56 (s, 6H, CON-*H*), 4.40 (s, 12H, ArOCH₂CO₂), 4.12 (q, 36H, CO₂CH₂CH₃), 2.30 (m, 36H, NHC(CH₂CH₂CO₂^tEt)₃), 2.11 (m, 36H, NHC(CH₂CH₂CO₂^tEt)₃), 1.24 (t, 64H, CO₂CH₂CH₃); ¹³C NMR (75 MHz, CDCl₃, δ_{ppm}): 173.5, 167.8, 159.5, 157.7, 133.9, 114.8, 114.7, 67.5, 61.0, 58.0, 30.0, 28.7, 14.2; MALDI-MS (*m/z*): M⁺ calcd for C₂₀₄H₂₂₂N₆O₄₈S₃, 3621.43; found, 3622.52.

Th-PG-3: Dendron 3 (**20**) (3.3 g, 1.4 mmol) and 1,3,5-tris((5-ethynylthiophen-2-yl)ethynyl)benzene (**9**) (0.2 g, 0.4 mmol) were used as an aryl halide and terminal alkynes, respectively. Yield: 24%; mp 189-190 °C; ¹H NMR (300 MHz, CDCl₃, δ_{ppm}): 7.80 (s, 3H, phenyl-*H*), 7.72 (s, 9H, phenyl-*H*), 7.65 (s, 18H, phenyl-*H*), 7.50 (d, 24H, CH₂OAr-*H*_{meta}, *J*=9.0 Hz), 6.96 (d, 24H, CH₂OAr-*H*_{ortho}, *J*=9.0 Hz), 6.50 (s, 12H, CON-*H*), 4.39 (s, 24H, ArOCH₂CO₂), 4.15 (q, 72H, CO₂CH₂CH₃), 2.31 (m, 72H, NHC(CH₂CH₂CO₂^tEt)₃), 2.11 (m, 72H, NHC(CH₂CH₂CO₂^tEt)₃), 1.24 (t, 128H, CO₂CH₂CH₃); ¹³C NMR (75 MHz, CDCl₃, δ_{ppm}): 173.8, 167.9, 160.0, 158.2, 134.5, 115.2, 115.0, 105.4, 100.2, 66.5, 61.3, 58.4, 30.6, 28.9, 14.1; MALDI-MS (*m/z*): M⁺ calcd for C₄₀₈H₄₄₄N₁₂O₉₆S₃, 7146.95; found, 7145.89.

General deprotection process of trimethylsilyl group. A mixture of TMS protected compounds (**3**, **4**, **8**, or **16**) and K₂CO₃ (5.0 equiv.) in a solution mixture of CH₂Cl₂ (20 mL) and CH₃OH (20 mL) was stirred at room temperature for 2 hours. The mixture was washed with water (20 mL × 3), and organic layer was separated. It was

dried over anhydrous magnesium sulfate, and then the solvent was removed in *vacuo*. The product was used in the coupling reaction without further purification. 80 ~ 90% yield.

1,3,5-triethynylbenzene (6): Yield: 90%; mp 127-128 °C; ¹H NMR (300 MHz, CDCl₃, δ_{ppm}): 7.45 (s, 3H, benzene-*H*), 3.76 (s, 3H, Ar-C₂-*H*).

1,3,5-tris((5-ethynylthiophen-2-yl)ethynyl)benzene (9): Yield: 85%; mp 132-133 °C; ¹H NMR (300 MHz, CDCl₃, δ_{ppm}): 7.62 (s, 3H, benzene-*H*), 7.15 (dd, 6H, thiophene-*H*), 3.41 (s, 3H, thiophene-C2-*H*); ¹³C NMR (75 MHz, CDCl₃, δ_{ppm}): 134.0, 133.5, 132.6, 124.1, 124.0, 123.8, 92.2, 83.8, 83.0, 76.3.

1-bromo-3,5-diethynylbenzene (13): Yield: 93%; mp 140-141 °C; ¹H NMR (300 MHz, CDCl₃, δ_{ppm}): 7.55(s, 2H, Br-Ar-*H*_{ortho}), 7.53 (s, 1H, Br-Ar-*H*_{para}), 3.05 (s, 2H, Ar-C₂-*H*).

(5-ethynyl-1,3-phenylene)bis(ethyne-2,1-diyl)bis(triisopropylsilane) (17): Yield: 87%; mp 146-147 °C; ¹H NMR (300 MHz, CDCl₃, δ_{ppm}): 7.52 (s, 3H, benzene-*H*), 3.05 (s, 1H, Ar-C₂-*H*), 1.10 (m, 42H, SiCH(CH₃)₂).

5,5'-(5-bromo-1,3-phenylene)bis(ethyne-2,1-diyl)bis(1,3-diethynylbenzene) (19). TIPS protected compound (**18**) (5.0 g, 4.6 mmol) was dissolved in THF, and *tetrabutylammonium* fluoride (4.6 mL, 4.6 mmol) was added dropwise. Upon the completion of the addition, the reaction mixture stirred for another 30 minutes, and then the solvent was removed *in vacuo*. The crude product was isolated by flash column chromatography on silica gel using THF as the eluent. Yield: 89%; mp 186-187 °C; ¹H NMR (300 MHz, THF-*d*₈, δ_{ppm}): 7.76 (s, 2H, Br-Ar-*H*_{ortho}), 7.70, (s, 1H, Br-Ar-*H*_{para}), 7.64

(s, 4H, Br-Ar-C₂-Ar-*H*_{ortho}), (s, 2H, Br-Ar-C₂-Ar-*H*_{para}); ¹³C NMR (75 MHz, CDCl₃, δ_{ppm}): 136.0, 135.8, 135.7, 134.2, 133.2, 126.0, 124.2, 123.8, 122.5, 82.0, 81.0.

Hydrolysis of ethyl ester groups on precursor of CPE-Ds. To a solution of ester precursors **Th-PG-1**, **Th-PG-2**, and **Th-PG-3** in THF (20 mL), LiOH in H₂O (1 mL) was added dropwise. The reaction mixture was vigorously stirred at 80 °C for 12 hours. The reaction mixture was cooled to room temperature, and then poured into a solution of methanol (100 mL) to give the yellowish precipitate. Further purification of CPE-Ds was accomplished by dialysis using nanopure water (Millipore Simplicity water system) and a 500 D MWCO cellulose membrane. After dialysis, the water was removed *in vacuo*, which gave the pale yellow solid powder. 85~90% yield.

Th-G-1: ¹H NMR (300 MHz, D₂O/DMSO-*d*₆ (v/v, 1/1), δ_{ppm}): 7.50-6.80 (br, 22H), 4.75 (br, 6H, ArOCH₂CO₂), 2.18 (br, 36H, NHC(CH₂CH₂CO₂Na)₃).

Th-G-2: ¹H NMR (300 MHz, D₂O/DMSO-*d*₆ (v/v, 1/1), δ_{ppm}): 7.80-6.90 (br, 60H), 4.77 (br, 12H, ArOCH₂CO₂), 2.19 (br, 72H, NHC(CH₂CH₂CO₂Na)₃).

Th-G-3: ¹H NMR (300 MHz, D₂O/DMSO-*d*₆ (v/v, 1/1), δ_{ppm}): 8.10-6.95 (br, 96H), 4.75 (br, 24H, ArOCH₂CO₂), 2.18 (br, 144H, NHC(CH₂CH₂CO₂Na)₃).

CHAPTER 7 CONCLUSIONS

In conclusions, we have seen a tremendous amount of growth in polymer and dendrimer field. Nevertheless, many scientists are still looking for the new domains in the polymer and dendrimer field in order to overcome the inveterate drawbacks or to discover potential possibility to advanced application. In this dissertation, newly designed conjugated polyelectrolytes (CPEs) and conjugated polyelectrolyte dendrimers (CPE-Ds) were studied and described. In Chapter 2, a series of CPEs having branched polyionic side chains were synthesized and their non-aggregation effects by electrostatic repulsions of side chains were investigated. In Chapter 3, a highly selective and sensitive Hg^{2+} ion sensor was studied using CPE and rhodamine combinative system. In Chapter 4, the aggregation of water soluble pyrene derivatives was characterized and such effect was utilized for efficient PPI sensing and to monitor enzyme's activity. In Chapter 5 and 6, two different types (compact and thienyl π -extended types) of CPE-Ds having phenylethylene backbone and branched polyionic side chains were synthesized. The geometric structure and features of these CPE-Ds were investigated, and their photophysical properties, fluorescence quenching, and energy transfer were also explored.

Branched Polyionic Effect on Aggregation

A new series of water soluble PPE-type CPEs (conjugated polyelectrolytes) with branched polyionic side chains featuring less aggregation in aqueous solution have been synthesized and characterized. The branched polyionic side chains in a conjugated polymer caused a less aggregation even in aqueous solution, which resulted in high quantum yields compared to CPEs with linear side chains. The pH dependent

results supported their little aggregation effect in natural aqueous solution. More aggregations were observed as pH decreases while the photophysical properties exhibited by their organic soluble precursors were retained at higher pH. As expected, the CPEs with branched polycationic side chains ($R-^b\text{NH}_3^+\text{Cl}^-$) showed opposite behaviors. At pH 4.5, aggregated **PPE-BTD-^bCO₂⁻** showed a typical feature. On the contrary, both **PPE-BTD-^dCO₂⁻** and **PPE TBT-^dCO₂⁻** exhibit unusually enhanced fluorescence in their aggregated form at pH 4.5. We proposed that the aggregation of these CPEs reduces water contact of conjugated backbone, thereby decreasing of a nonradiative process. Lifetime measurements also supported the aggregation of the anionic and cationic branched polymers at low pH (~4.5) and high pH (~10.5), respectively. The emission lifetime ($\tau < 1$ ns) of CPEs with branched polyanionic side chains are wavelength independent lifetimes in both methanol and aqueous (pH 9.0) solutions. However, it was found that the emission lifetime of **PPE-Ar-^dCO₂⁻** at pH 4.5 consisted of two wavelength dependent lifetimes: long-lived lifetimes ($\tau > 2$ ns) and extremely short-lived lifetimes ($\tau < 250$ ps). Such observation suggested the existence of aggregated polymers.

Mercury (II) ion and Pyrophosphate ion Sensors

Hg^{2+} ion was efficiently detected by using the mixture of **PPE-^dCO₂⁻** and **S-Rho 1**. Rhodamine derivatives (**S-Rho1**) have been synthesized and used as a Hg^{2+} ion receptor. The strong thiophilic affinity of mercury ion induced complex formation between **S-Rho 1** and Hg^{2+} ion, which induced ring-opening of spiro structure. Its complex sensitively quenched **PPE-^bCO₂⁻** through the fluorescence resonance energy transfer, where hydrogen bonding between terminal **^bCO₂⁻** groups and hydrogen on

nitrogen atom of **S-Rho-1** act as an important role for their complex formation. This combination system showed improved sensory response compared to **S-Rho 1** alone.

We synthesized a **PyA4** that displays self-assembly with strong excimer emission in HEPES buffer solution. The fluorescence intensity of **PyA4** was most efficiently quenched with the Cu^{2+} ion and the efficient quenching effect of **PyA4** can be explained by intermolecular energy migration in aggregated **PyA4**. Taking advantage of the efficient fluorescence quenching of **PyA4** by Cu^{2+} , **PyA4**- Cu^{2+} complex was used as a fluorescence turn-on sensor and it sensitively and selectively recognizes PPI over other anions. It is believed that efficient chelation of the diphosphate anion to Cu^{2+} ion induced higher selectivity.

Conjugated Polyelectrolyte Dendrimers

Three generation of water soluble conjugated polyelectrolyte dendrimers (CPE-Ds) with branched polyionic side chains have been synthesized and characterized. Compact type CPE-Ds and CPE-Ds having thienyl (Th) groups in the conjugated backbone were systemically prepared via precursor route. The geometric structure of CPE-Ds based on computational modeling, GPC, and AFM studies showed three-dimensional globular architectures and mono-disperse macromolecules. Photophysical studies of CPDs revealed that intra-dendrimer interaction becomes stronger in aqueous solution with generation. Incorporation of thienyl groups induced enhanced optical properties compared to the compact type CPE-Ds without thienyl groups. The fluorescence lifetime decays provide information for intra-dendrimer aggregation in H_2O . Methyl viologen and cyanine dyes (DOC, DODC, and DOTC) efficiently quenched the fluorescence of the third generation CPE-D rather than the other generation in H_2O , which is due to more efficient energy or charge transfer effect in aggregated state.

APPENDIX A
CONJUGATED POLYELECTROLYTES WITH BRANCHED POLYCATIONIC SIDE CHAINS

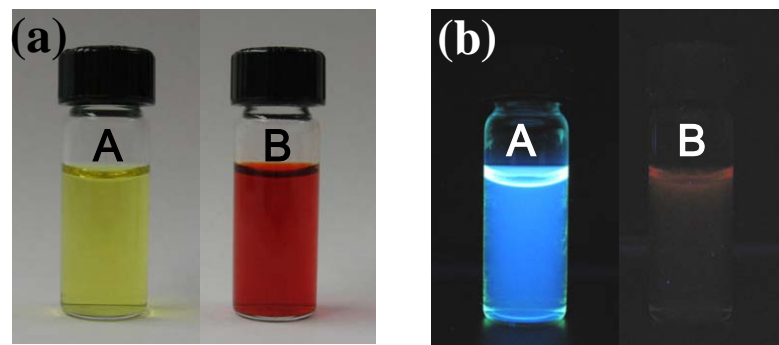


Figure A-1. (a) Visual and (b) Fluorescence colors of A: **PPE-Ph-^bNH₃⁺** and B: **PPE-BTD-^bNH₃⁺**; [**PPE-Ar-^bNH₃⁺**] = 30 μM in H₂O.

Table A-1. Fluorescence lifetimes (τ_i , ns) and relative amplitudes (RA, %) for **PPE-Ar-^bNH₃⁺** in MeOH, basic (pH = 9.5), and acidic (pH = 4.5) conditions^a

Compd.	MeOH			H ₂ O, pH 9.5			H ₂ O, pH 4.5		
	RA (%)			RA (%)			RA (%)		
PPE-Ph- ^b NH ₃ ⁺	τ_i (ns) ^b	430 nm	500 nm	τ_i (ns)	430 nm	500 nm	τ_i (ns)	430 nm	500 nm
	$\tau_1 = 0.20$	35	14	$\tau_1 = 0.38$	50	18	$\tau_1 = 0.20$	92	58
	$\tau_2 = 0.47$	64	66	$\tau_2 = 1.72$	30	41	$\tau_2 = 0.87$	6	17
	$\tau_3 = 1.59$	<1	13	$\tau_3 = 4.52$	20	41	$\tau_3 = 3.71$	2	25
	$\tau_4 = 3.97$	<1	<7						
	χ^2	1.183	1.043	χ^2	1.133	1.128	χ^2	1.211	1.108
PPE-BTD- ^b NH ₃ ⁺	τ_i (ns)	600 nm	650 nm	τ_i (ns)	600 nm	650 nm	τ_i (ns)	600 nm	650 nm
	$\tau_1 = 0.31$	35	33	$\tau_1 = 0.22$	48	48	$\tau_1 = 0.17$	92	90
	$\tau_2 = 0.87$	44	46	$\tau_2 = 0.64$	39	39	$\tau_2 = 0.73$	7	8
	$\tau_3 = 1.71$	21	21	$\tau_3 = 1.41$	12	12	$\tau_3 = 2.24$	<1	<2
				$\tau_4 = 5.34$	<1	<1			
	χ^2	1.128	1.109	χ^2	1.179	1.014	χ^2	1.066	1.262

^aData were collected by global fitting Algorithm. ^bTypical limits of error on τ_i are less than $\pm 3\%$.

APPENDIX B
NMR SPECTRA

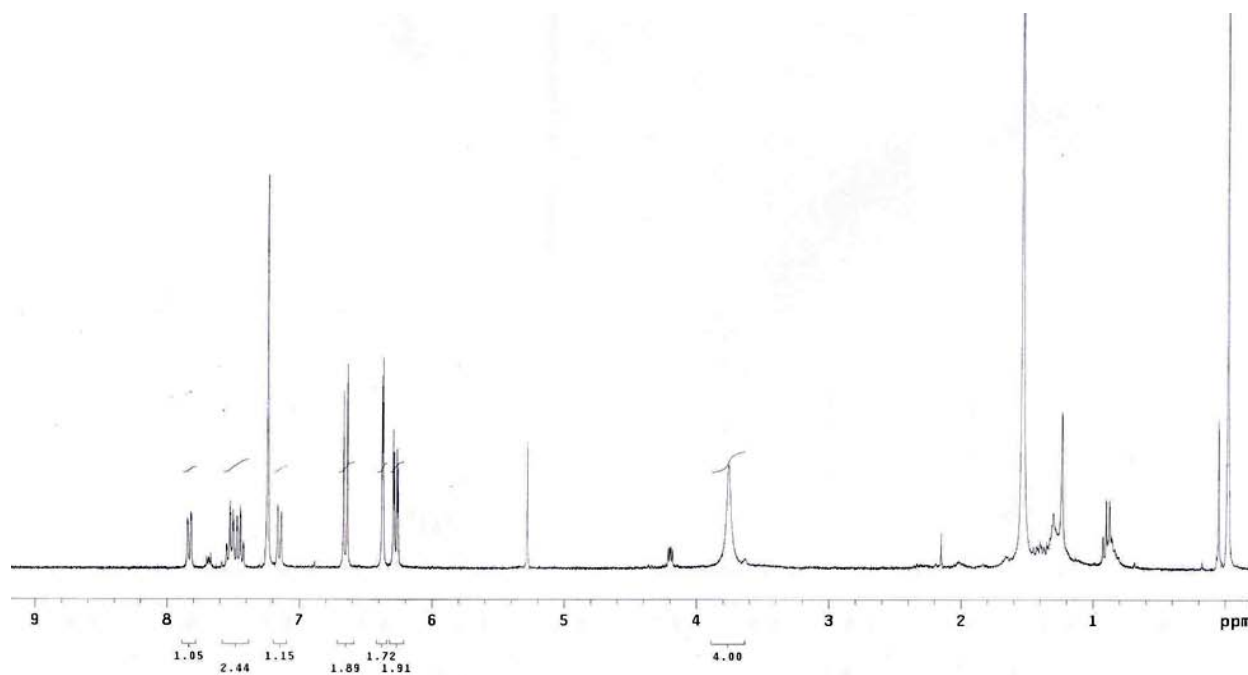


Figure B-1. ¹H NMR (300 MHz, CDCl₃) spectrum of **S-Rho 1** (chapter 3).

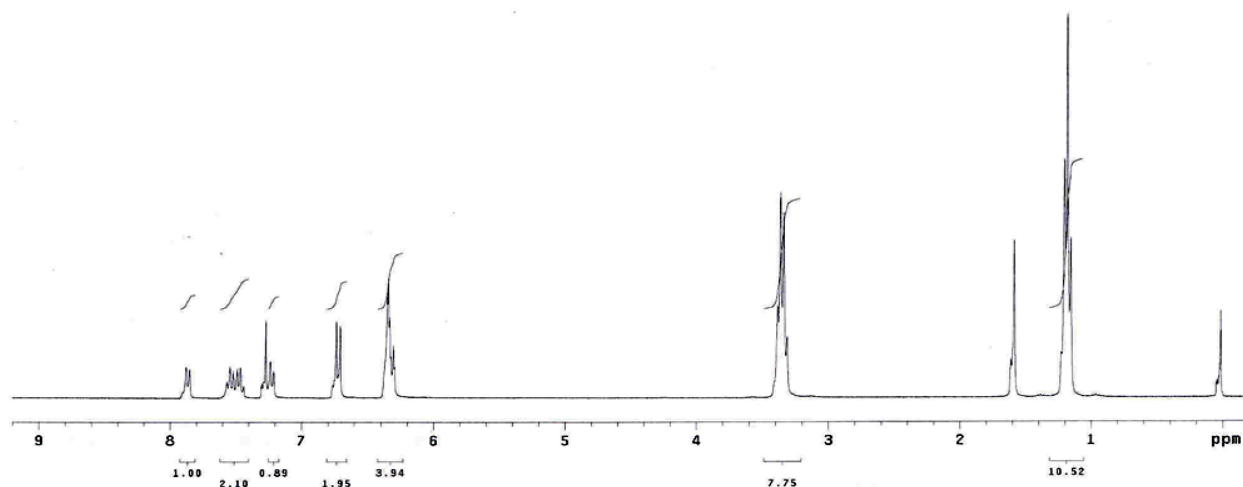


Figure B-2. ¹H NMR (300 MHz, CDCl₃) spectrum of **S-Rho 2** (chapter 3).

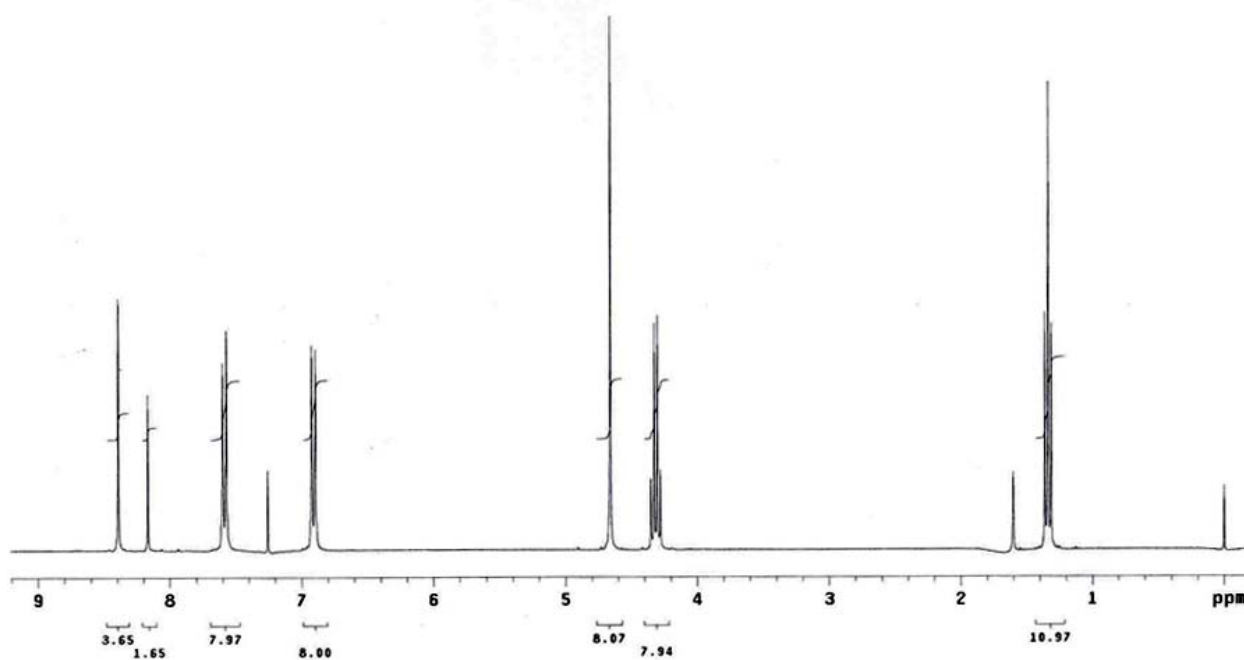


Figure B-3. ^1H NMR (300 MHz, CDCl_3) spectrum of **PyE4** (chapter 4).

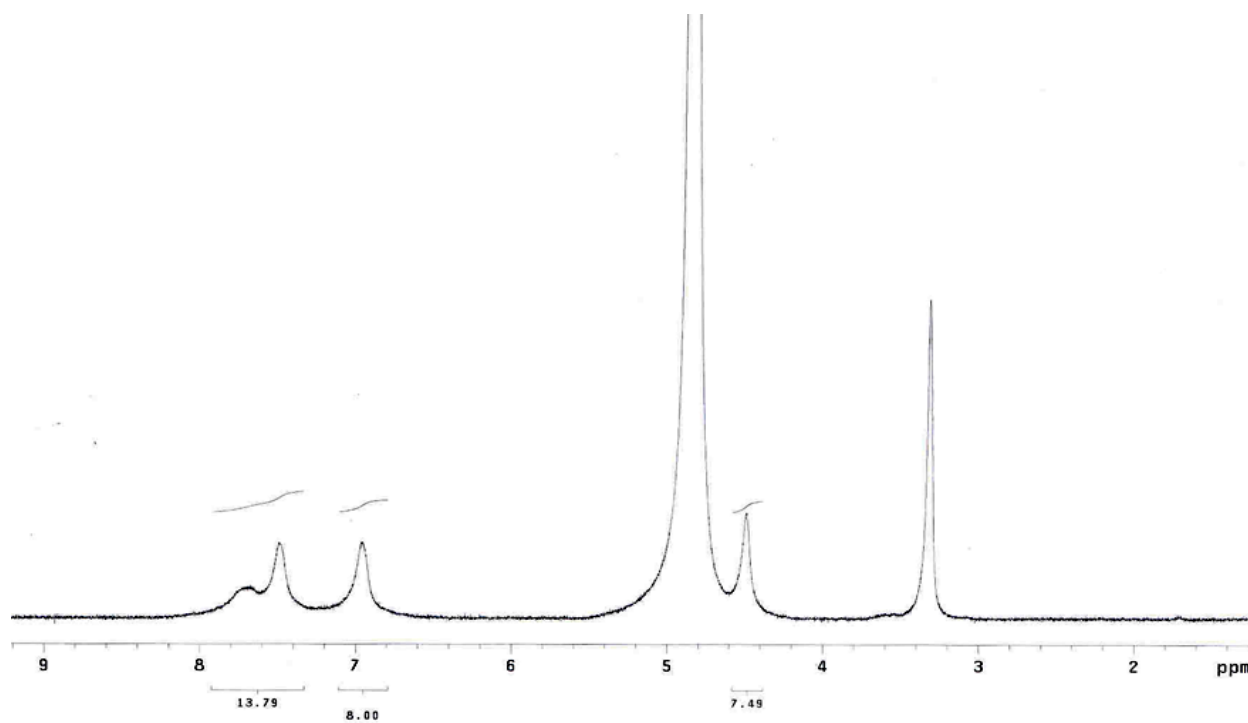


Figure B-4. ^1H NMR (300 MHz, $\text{D}_2\text{O}/\text{CD}_3\text{OD}$ (3/1, v/v)) spectrum of **PyA4** (chapter 4).

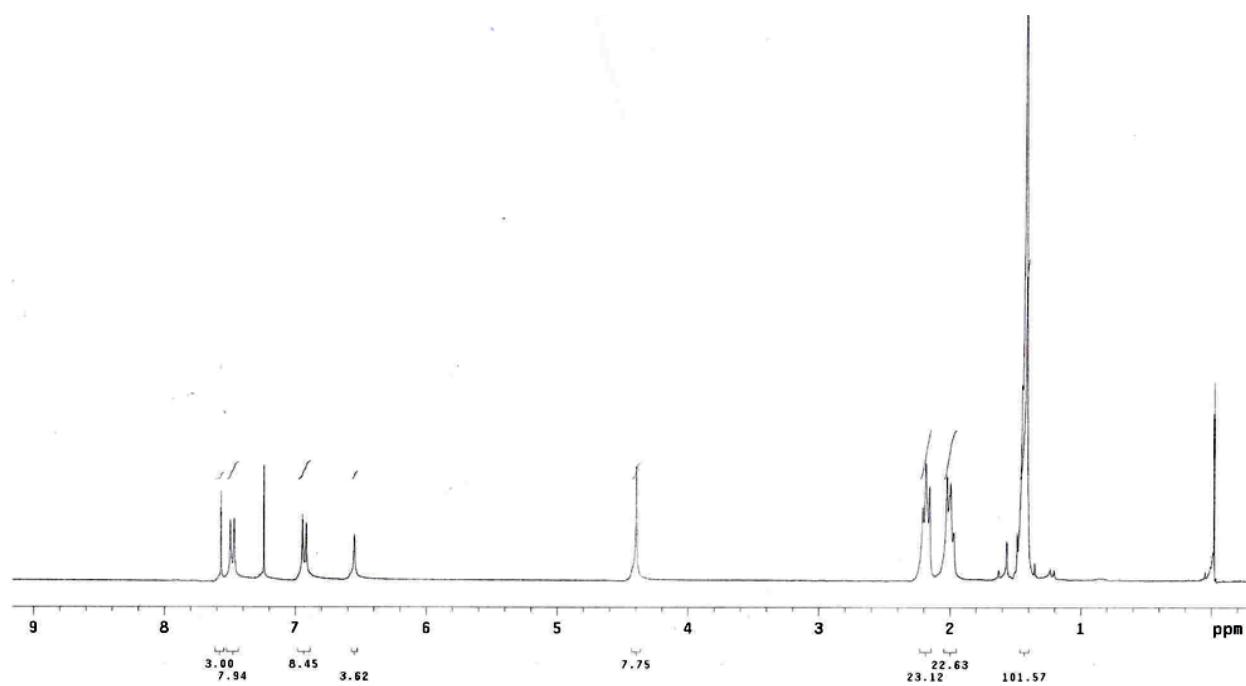


Figure B-5. ^1H NMR (300 MHz, CDCl_3) spectrum of **PG-1** (chapter 5).

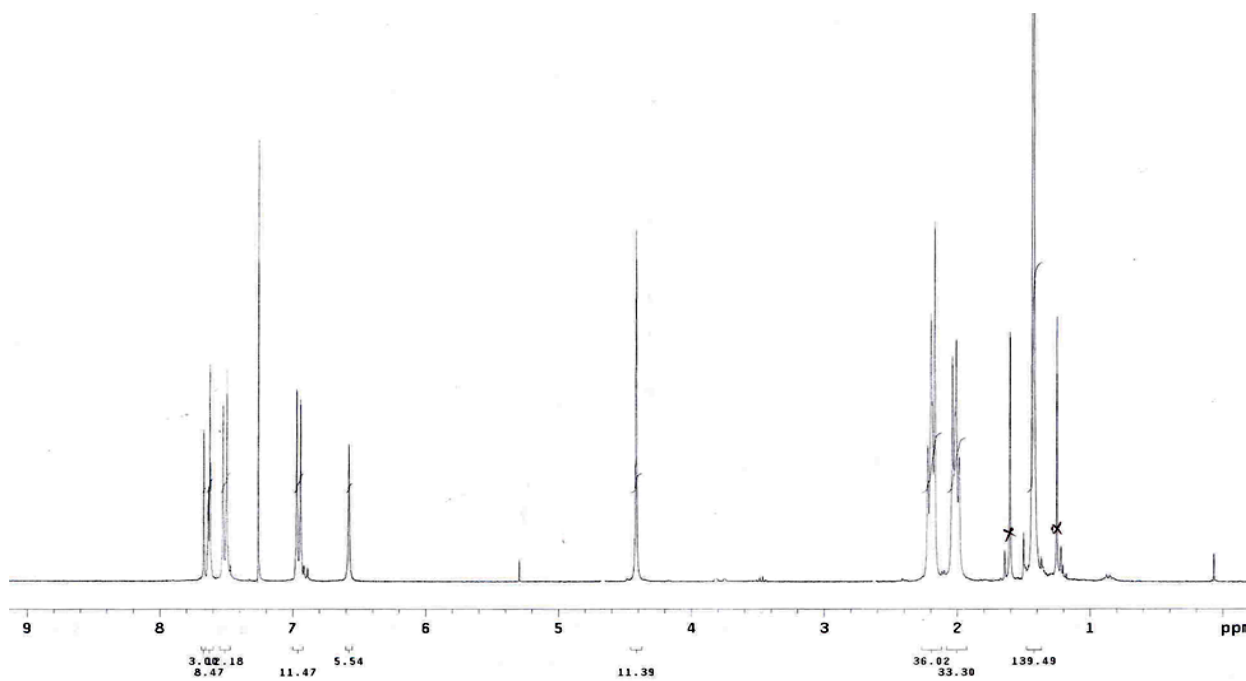


Figure B-6. ^1H NMR (300 MHz, CDCl_3) spectrum of **PG-2** (chapter 5).

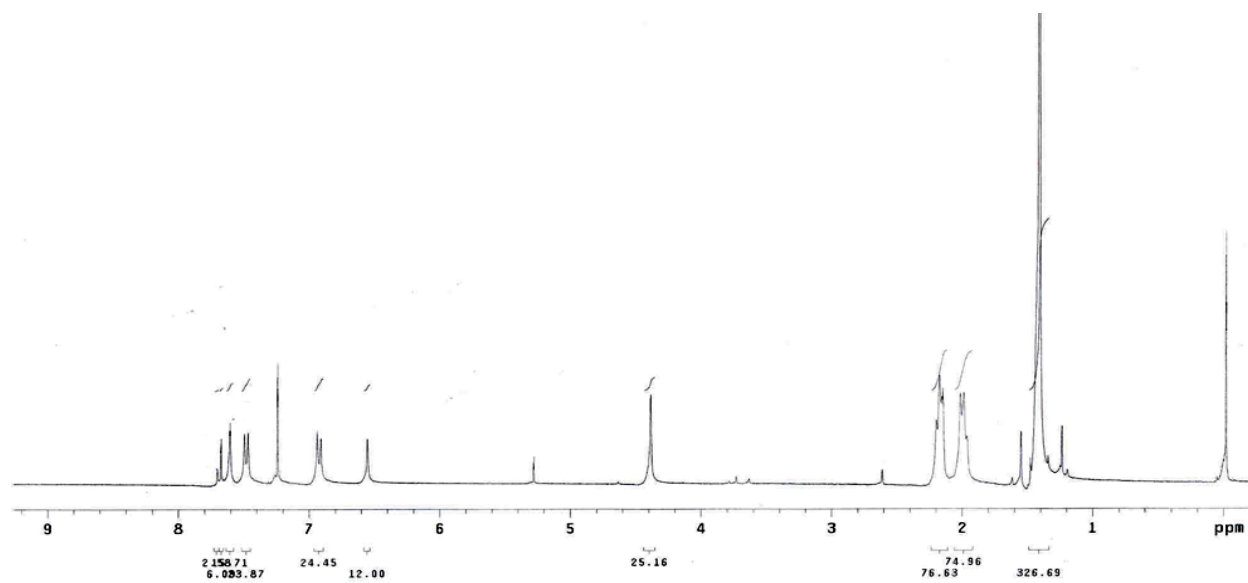


Figure B-7. ^1H NMR (300 MHz, CDCl_3) spectrum of **PG-3** (chapter 5).

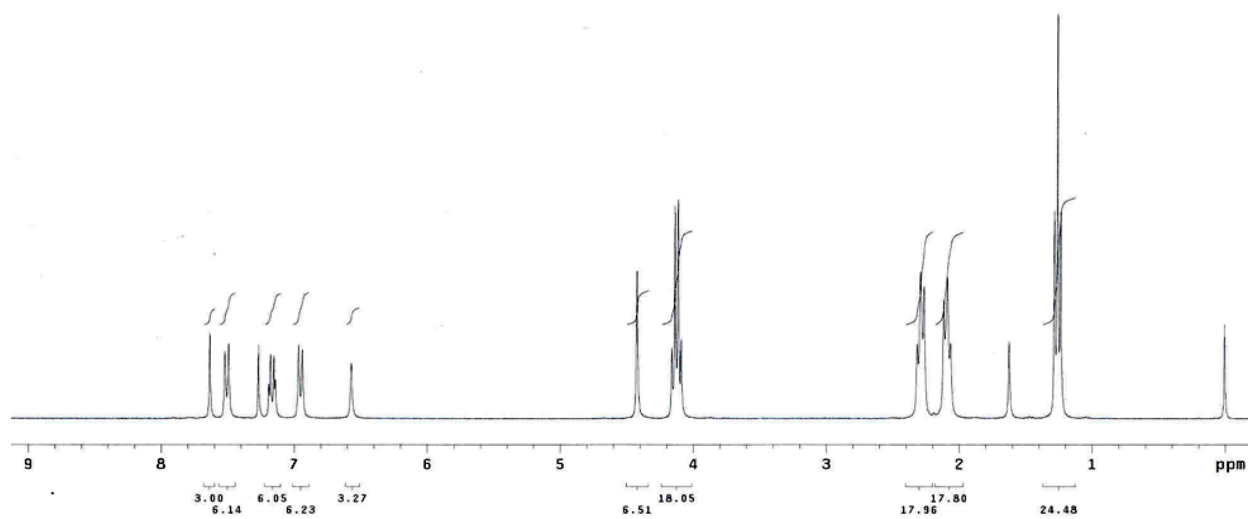


Figure B-8. ^1H NMR (300 MHz, CDCl_3) spectrum of **Th-PG-1** (chapter 6).

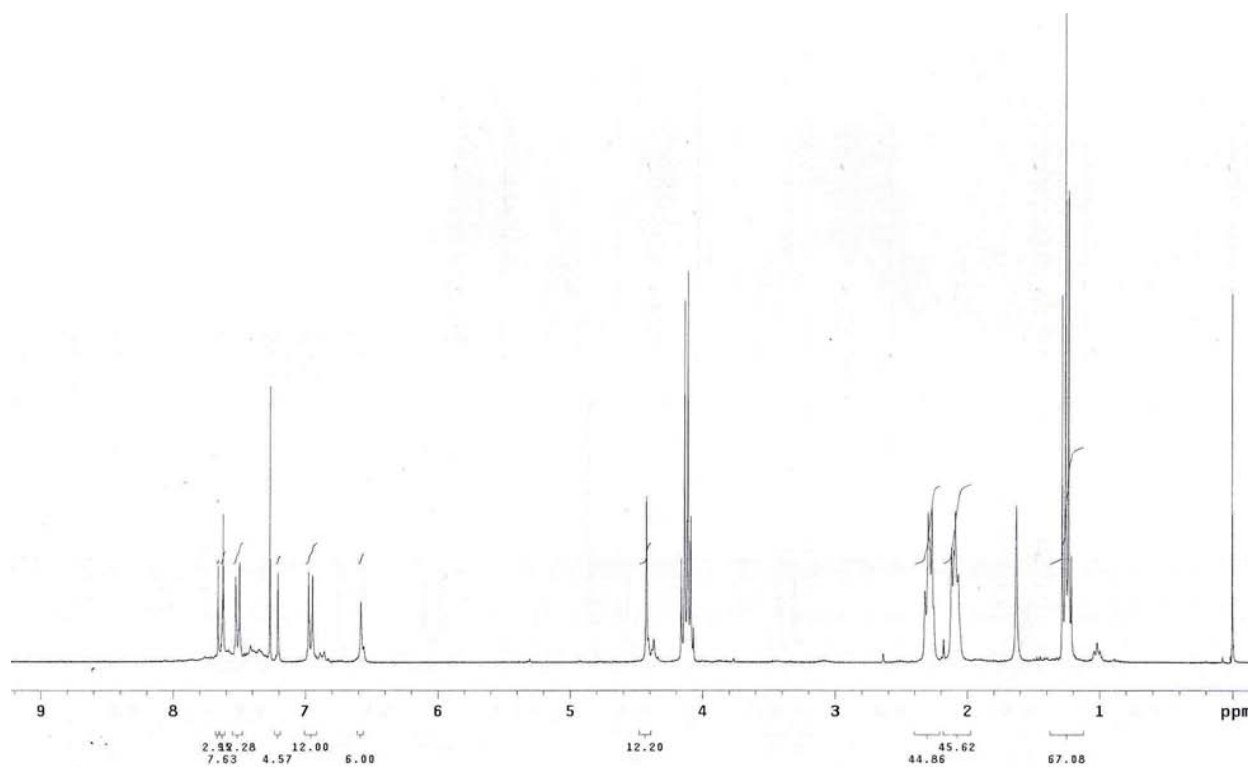


Figure B-9. ¹H NMR (300 MHz, CDCl₃) spectrum of **Th-PG-2** (chapter 6).

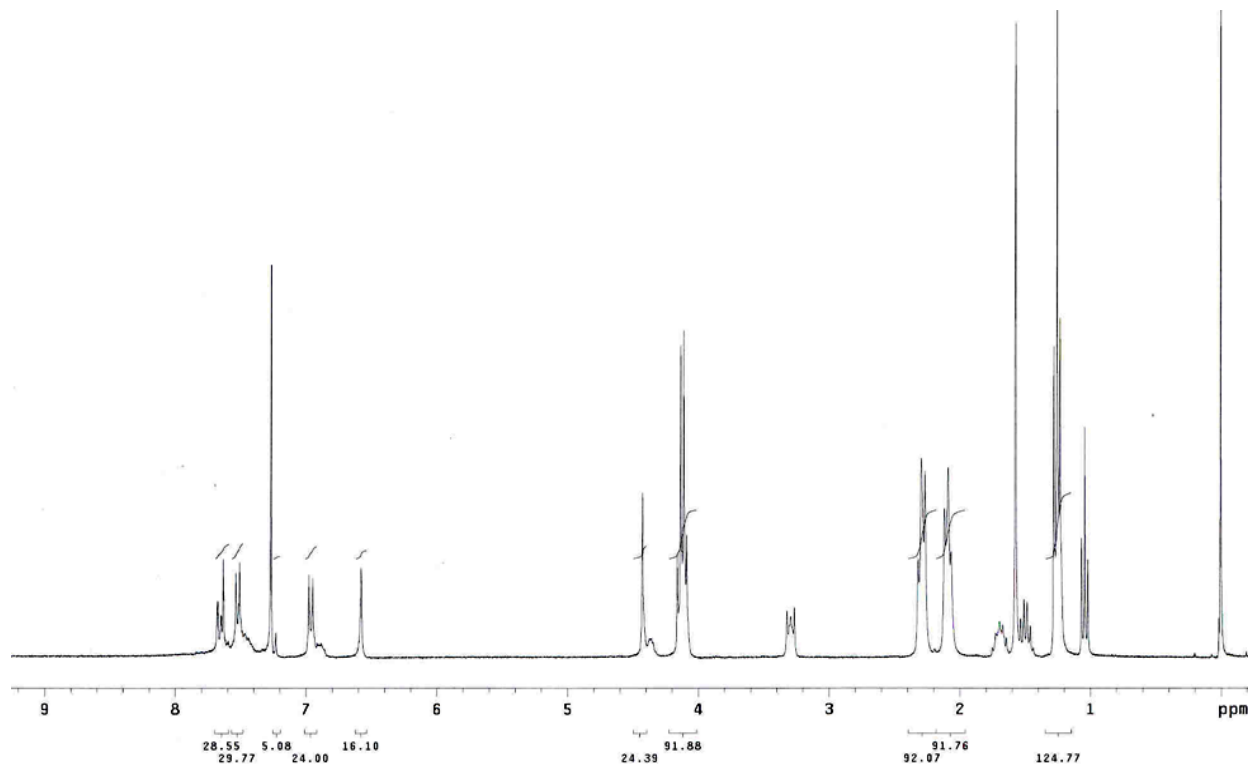


Figure B-10. ¹H NMR (300 MHz, CDCl₃) spectrum of **Th-PG-3** (chapter 6).

LIST OF REFERENCES

- (1) Jiang, H.; Taranekar, P.; Reynolds, John R.; Schanze, Kirk S. *Angew. Chem. Int. Ed.* **2009**, *48*, 4300.
- (2) Pinto, M. R.; Schanze, K. S. *Synthesis* **2002**, 1293.
- (3) Lin, C.-Y.; Garcia, A.; Zalar, P.; Brzezinski, J. Z.; Nguyen, T.-Q. *J. Phys. Chem. C* **2010**, *114*, 15786.
- (4) Ding, L.; Chi, E. Y.; Schanze, K. S.; Lopez, G. P.; Whitten, D. G. *Langmuir* **2009**, *26*, 5544.
- (5) Wigenius, J. A.; Magnusson, K.; Björk P.; Andersson, O.; Inganäs O. *Langmuir* **2009**, *26*, 3753.
- (6) Pecher, J.; Mecking, S. *Chem. Rev.* **2010**, *110*, 6260.
- (7) Seo, J. H.; Gutacker, A.; Walker, B.; Cho, S.; Garcia, A.; Yang, R.; Nguyen, T.-Q.; Heeger, A. J.; Bazan, G. C. *J. Am. Chem. Soc.* **2009**, *131*, 18220.
- (8) Patil, A. O.; Ikenoue, Y.; Wudl, F.; Heeger, A. J. *J. Am. Chem. Soc.* **1987**, *109*, 1858.
- (9) Huang, F.; Wu, H.; Wang, D.; Yang, W.; Cao, Y. *Chem. Mater.* **2004**, *16*, 708.
- (10) Zhao, X.; Pinto, M. R.; Hardison, L. M.; Mwaura, J.; Muller, J.; Jiang, H.; Witker, D.; Kleiman, V. D.; Reynolds, J. R.; Schanze, K. S. *Macromolecules* **2006**, *39*, 6355.
- (11) Zhu, B.; Han, Y.; Sun, M.; Bo, Z. *Macromolecules* **2007**, *40*, 4494.
- (12) Milstein, D.; Stille, J. K. *J. Am. Chem. Soc.* **1978**, *100*, 3636.
- (13) Heck, R. F. *J. Am. Chem. Soc.* **1969**, *91*, 6707.
- (14) Miyaura, N.; Suzuki, A. *Chem. Rev.* **1995**, *95*, 2457.
- (15) Sonogashira, K.; Tohda, Y.; Hagihara, N. *Tetrahedron Lett.* **1975**, *16*, 4467.
- (16) Tan, C.; Pinto, M. R.; Schnaze, K. S. *Chem. Commun.* **2002**, 446.
- (17) Bunz, U. H. F. *Chem. Rev.* **2000**, *100*, 1605.
- (18) Huang, Y.-Q.; Fan, Q.-L.; Lu, X.-M.; Fang, C.; Liu, S.-J.; Yu-Wen, L.-H.; Wang, L.-H.; Huang, W. *"J. Polym. Sci., Part A: Polym. Chem."* **2006**, *44*, 5778.

- (19) *Chemosensors of Ion and Molecule Recognition*; Desvergne, J. P.; Czarnik, A. W., Eds.; Kluwer Academic Publishers: Dordrecht, The Netherlands, 1997.
- (20) Zhou, Q.; Swager, T. M. *J. Am. Chem. Soc.* **1995**, *117*, 7017.
- (21) Zhou, Q.; Swager, T. M. *J. Am. Chem. Soc.* **1995**, *117*, 12593.
- (22) Duan, X.; Liu, L.; Feng, F.; Wang, S. *Acc. Chem. Res.* **2009**, *43*, 260.
- (23) Ho, H.-A.; Najari, A.; Leclerc, M. *Acc. Chem. Res.* **2008**, *41*, 168.
- (24) Fang, Z.; Pu, K.-Y.; Liu, B. *Macromolecules* **2008**, *41*, 8380.
- (25) An, L.; Liu, L.; Wang, S. *Biomacromolecules* **2008**, *10*, 454.
- (26) Thomas, S. W.; Joly, G. D.; Swager, T. M. *Chem. Rev.* **2007**, *107*, 1339.
- (27) Gaylord, B. S.; Heeger, A. J.; Bazan, G. C. *Proc. Natl. Acad. Sci. USA* **2002**, *99*, 10954.
- (28) Kim, I.-B.; Bunz, U. H. F. *J. Am. Chem. Soc.* **2006**, *128*, 2818.
- (29) Buhleier Egon ; Wehner, W.; Vögtle, F. *Synthesis* **1978**, 155.
- (30) Tomalia, D. A.; Baker, H.; Dewald, J.; Hall, M.; Kallos, G.; Martin, S.; Roeck, J.; Ryder, J.; Smith, P. *Polym. J.* **1985**, *17*.
- (31) Newkome, G. R.; Yao, Z.; Baker, G. R.; Gupta, V. K. *J. Org. Chem.* **1985**, *50*, 2003.
- (32) Hawker, C. J.; Fréchet, J. M. J. *J. Am. Chem. Soc.* **1990**, *112*, 7638.
- (33) Wang, B.-B.; Zhang, X.; Jia, X.-R.; Li, Z.-C.; Ji, Y.; Yang, L.; Wei, Y. *J. Am. Chem. Soc.* **2004**, *126*, 15180.
- (34) Hawker, C. J.; Wooley, K. L.; Fréchet, J. M. J. *J. Chem. Soc. Perkin Trans. 1* **1993**, 1287.
- (35) Moore, J. S. *Acc. Chem. Res.* **1997**, *30*, 402.
- (36) Xu, Z.; Kahr, M.; Walker, K. L.; Wilkins, C. L.; Moore, J. S. *J. Am. Chem. Soc.* **1994**, *116*, 4537.
- (37) Grayson, S. M.; Fréchet, J. M. J. *Chem. Rev.* **2001**, *101*, 3819.
- (38) Pesak, D. J.; Moore, J. S.; Wheat, T. E. *Macromolecules* **1997**, *30*, 6467.

- (39) Newkome, G. R.; Behera, R. K.; Moorefield, C. N.; Baker, G. R. *J. Org. Chem.* **1991**, *56*, 7162.
- (40) Zhang, L.; Nguyen, T. L. U.; Bernard, J.; Davis, T. P.; Barner-Kowollik, C.; Stenzel, M. H. *Biomacromolecules* **2007**, *8*, 2890.
- (41) Li, W.-S.; Aida, T. *Chem. Rev.* **2009**, *109*, 6047.
- (42) Newkome, G. R.; Shreiner, C. *Chem. Rev.* **2010**, *110*, 6338.
- (43) Nobuyuki, T.; Daisuke, T.; Toshie, T.; Takuzo, A. *Angew. Chem. Int. Ed.* **1998**, *37*, 1531.
- (44) Astruc, D.; Boisselier, E.; Ornelas, C. t. *Chem. Rev.* **2010**, *110*, 1857.
- (45) Bosman, A. W.; Janssen, H. M.; Meijer, E. W. *Chem. Rev.* **1999**, *99*, 1665.
- (46) van Dongen, S. F. M.; de Hoog, H.-P. M.; Peters, R. J. R. W.; Nallani, M.; Nolte, R. J. M.; van Hest, J. C. M. *Chem. Rev.* **2009**, *109*, 6212.
- (47) Carter, F. L. *Molecular Electronic Devices, II*; ed.; Marcel Dekker: New York, 1987.
- (48) Liu, B.; Bazan, G. C. *Chem. Mater.* **2004**, *16*, 4467.
- (49) Feng, F.; He, F.; An, L.; Wang, S.; Li, Y.; Zhu, D. *Adv. Mater.* **2008**, *20*, 2959.
- (50) Ortony, J.; Yang, R.; Brzezinski, J.; Edman, L.; Nguyen, T. Q.; Bazan, G. *Adv. Mater.* **2008**, *20*, 298.
- (51) Woo, H.; Vak, D.; Korystov, D.; Mikhailovsky, A.; Bazan, G.; Kim, D. Y. *Adv. Funct. Mater.* **2007**, *17*, 290.
- (52) Pinto, M. R.; Kristal, B. M.; Schanze, K. S. *Langmuir* **2003**, *19*, 6523.
- (53) Tan, C.; Atas, E.; Muller, J. G.; Pinto, M. R.; Kleiman, V. D.; Schanze, K. S. *J. Am. Chem. Soc.* **2004**, *126*, 13685.
- (54) Swager, T. M. *Acc. Chem. Res.* **2008**, *41*, 1181.
- (55) Jiang, D.-L.; Choi, C.-K.; Honda, K.; Li, W.-S.; Yuzawa, T.; Aida, T. *J. Am. Chem. Soc.* **2004**, *126*, 12084.
- (56) Xu, Q.; An, L.; Yu, M.; Wang, S. *Macromol. Rapid Commun.* **2008**, *29*, 390.

- (57) Wu, M.; Kaur, P.; Yue, H.; Clemmens, A. M.; Waldeck, D. H.; Xue, C.; Liu, H. *J. Phys. Chem. B* **2008**, *112*, 3300.
- (58) Haskins-Glusac, K.; Pinto, M. R.; Tan, C.; Schanze, K. S. *J. Am. Chem. Soc.* **2004**, *126*, 14964.
- (59) Tan, C.; Pinto, M.; Kose, M.; Ghiviriga, I.; Schanze, K. *Adv. Mater.* **2004**, *16*, 1208.
- (60) An, L.; Wang, S.; Zhu, D. *Chemistry – An Asian Journal* **2008**, *3*, 1601.
- (61) Garcia, A.; Nguyen, T.-Q. *J. Phys. Chem. C* **2008**, *112*, 7054.
- (62) Wang, F.; Bazan, G. C. *J. Am. Chem. Soc.* **2006**, *128*, 15786.
- (63) Kido, J.; Okamoto, Y. *Chem. Rev.* **2002**, *102*, 2357.
- (64) Kirby, J. P.; Cable, M. L.; Levine, D. J.; Gray, H. B.; Ponce, A. *Anal. Chem.* **2008**, *80*, 5750.
- (65) Dominguez, X.; Lopez, I.; Franco, R. *J. Org. Chem.* **1961**, *26*, 1625.
- (66) Wu, Y.-q.; Limburg, D. C.; Wilkinson, D. E.; Vaal, M. J.; Hamilton, G. S. *Tetrahedron Lett.* **2000**, *41*, 2847.
- (67) Jiang, H.; Zhao, X.; Schanze, K. S. *Langmuir* **2007**, *23*, 9481.
- (68) Jiang, H.; Zhao, X.; Schanze, K. S. *Langmuir* **2006**, *22*, 5541.
- (69) Pschirer, N. G.; Bunz, U. H. F. *Macromolecules* **2000**, *33*, 3961.
- (70) Levitus, M.; Schmieder, K.; Ricks, H.; Shimizu, K. D.; Bunz, U. H. F.; Garcia-Garibay, M. A. *J. Am. Chem. Soc.* **2001**, *123*, 4259.
- (71) Kato, S.-i.; Matsumoto, T.; Ishi-i, T.; Thiemann, T.; Shigeiwa, M.; Gorohmaru, H.; Maeda, S.; Yamashita, Y.; Mataka, S. *Chem. Commun.* **2004**, 2342.
- (72) Wong, W.-Y.; Wang, X.-Z.; He, Z.; Djuricic, A. B.; Yip, C.-T.; Cheung, K.-Y.; Wang, H.; Mak, C. S. K.; Chan, W.-K. *Nat Mater* **2007**, *6*, 521.
- (73) Hardison, L. M.; Zhao, X.; Jiang, H.; Schanze, K. S.; Kleiman, V. D. *J. Phys. Chem. C* **2008**, *112*, 16140.
- (74) Gust, D.; Moore, T. A.; Liddell, P. A.; Nemeth, G. A.; Makings, L. R.; Moore, A. L.; Barrett, D.; Pessiki, P. J.; Bensasson, R. V. *J. Am. Chem. Soc.* **1987**, *109*, 846.

- (75) Jones, G.; Jackson, W. R.; Choi, C. Y.; Bergmark, W. R. *The Journal of Physical Chemistry* **1985**, 89, 294.
- (76) Harriman, A. *Chem. Commun* **1977**, 777.
- (77) Fitzgerald, W. F.; Lamborg, C. H.; Hammerschmidt, C. R. *Chem. Rev.* **2007**, 107, 641.
- (78) Nolan, E. M.; Lippard, S. J. *Chem. Rev.* **2008**, 108, 3443.
- (79) Quang, D. T.; Kim, J. S. *Chem. Rev.* **2010**, null.
- (80) Kim, H. N.; Lee, M. H.; Kim, H. J.; Kim, J. S.; Yoon, J. *Chem. Soc. Rev.* **2008**, 37, 1465.
- (81) Yang, Y.-K.; Yook, K.-J.; Tae, J. *J. Am. Chem. Soc.* **2005**, 127, 16760.
- (82) Kim, I.-B.; Phillips, R.; Bunz, U. H. F. *Macromolecules* **2007**, 40, 814.
- (83) Jiang, H.; Taranekar, P.; Reynolds, J.; Schanze, K. *Angew. Chem. Int. Ed.* **2009**, 48, 4300.
- (84) Santra, M.; Ryu, D.; Chatterjee, A.; Ko, S.-K.; Shin, I.; Ahn, K. H. *Chem. Commun.* **2009**, 2115.
- (85) Ko, S.-K.; Yang, Y.-K.; Tae, J.; Shin, I. *J. Am. Chem. Soc.* **2006**, 128, 14150.
- (86) Shiraishi, Y.; Sumiya, S.; Kohno, Y.; Hirai, T. *J. Org. Chem.* **2008**, 73, 8571.
- (87) Shi, W.; Ma, H. *Chem. Commun.* **2008**, 1856.
- (88) Zhan, X.-Q.; Qian, Z.-H.; Zheng, H.; Su, B.-Y.; Lan, Z.; Xu, J.-G. *Chem. Commun.* **2008**, 1859.
- (89) Wu, J.-S.; Hwang, I.-C.; Kim, K. S.; Kim, J. S. *Org. Lett.* **2007**, 9, 907.
- (90) Chen, X.; Nam, S.-W.; Jou, M. J.; Kim, Y.; Kim, S.-J.; Park, S.; Yoon, J. *Org. Lett.* **2008**, 10, 5235.
- (91) The chloride salts of metal ions (0.1 mM) were tested to evaluate the metal ion binding properties of CPE/S-Rho 1 system. The excitation was 350 nm.
- (92) de Silva, A. P.; Gunaratne, H. Q. N.; Gunnlaugsson, T.; Huxley, A. J. M.; McCoy, C. P.; Rademacher, J. T.; Rice, T. E. *Chem. Rev.* **1997**, 97, 1515.
- (93) Choi, K.; Hamilton, A. D. *Angew. Chem. Int. Ed.* **2001**, 40, 3912.

- (94) Kim, J. S.; Quang, D. T. *Chem. Rev.* **2007**, *107*, 3780.
- (95) Valeur, B.; Leray, I. *Coord. Chem. Rev.* **2000**, *205*, 3.
- (96) Winnik, F. M. *Chem. Rev.* **1993**, *93*, 587.
- (97) Lee, D. H.; Kim, S. Y.; Hong, J. I. *Angew. Chem. Int. Ed.* **2004**, *43*, 4777.
- (98) *Biological Role of Inorganic Pyrophosphate*; Heinonen, J. K., Ed.; Kluwer Academic Publishers: Boston, 2001.
- (99) Martínez-Máñez, R.; Sancenón, F. *Chem. Rev.* **2003**, *103*, 4419.
- (100) Vance, D. H.; Czarnik, A. W. *J. Am. Chem. Soc.* **1994**, *116*, 9397.
- (101) Nation, D. A.; Martell, A. E.; Carroll, R. I.; Clearfield, A. *Inorg. Chem.* **1996**, *35*, 7246.
- (102) Zhao, X.; Liu, Y.; Schanze, K. S. *Chem. Commun.* **2007**, 2914.
- (103) Lee, H. N.; Swamy, K. M. K.; Kim, S. K.; Kwon, J.-Y.; Kim, Y.; Kim, S.-J.; Yoon, Y. J.; Yoon, J. *Org. Lett.* **2006**, *9*, 243.
- (104) Lee, H. N.; Xu, Z.; Kim, S. K.; Swamy, K. M. K.; Kim, Y.; Kim, S.-J.; Yoon, J. *J. Am. Chem. Soc.* **2007**, *129*, 3828.
- (105) McDonough, M. J.; Reynolds, A. J.; Lee, W. Y. G.; Jolliffe, K. A. *Chem. Commun.* **2006**, 2971.
- (106) Jang, Y. J.; Jun, E. J.; Lee, Y. J.; Kim, Y. S.; Kim, J. S.; Yoon, J. *J. Org. Chem.* **2005**, *70*, 9603.
- (107) Cho, H. K.; Lee, D. H.; Hong, J.-I. *Chem. Commun.* **2005**, 1690.
- (108) Fabbrizzi, L.; Marcotte, N.; Stomeo, F.; Taglietti, A. *Angew. Chem. Int. Ed.* **2002**, *41*, 3811.
- (109) Mizukami, S.; Nagano, T.; Urano, Y.; Odani, A.; Kikuchi, K. *J. Am. Chem. Soc.* **2002**, *124*, 3920.
- (110) Wilson, J. N.; Teo, Y. N.; Kool, E. T. *J. Am. Chem. Soc.* **2007**, *129*, 15426.
- (111) Ingle, J. D., Jr.; Crouch, S. R. *Spectrochemical Analysis*; Prentice-Hall: New Jersey, 1988.

- (112) Ponomarenko, S. A.; Kirchmeyer, S.; Elschner, A.; Huisman, B. H.; Karbach, A.; Drechsler, D. *Adv. Funct. Mat.* **2003**, *13*, 591.
- (113) Yamaguchi, Y.; Ochi, T.; Miyamura, S.; Tanaka, T.; Kobayashi, S.; Wakamiya, T.; Matsubara, Y.; Yoshida, Z.-i. *J. Am. Chem. Soc.* **2006**, *128*, 4504.
- (114) Kukowska-Latallo, J. F.; Bielinska, A. U.; Johnson, J.; Spindler, R.; Tomalia, D. A.; Baker, J. R. *Proc. Natl. Acad. Sci. USA* **1996**, *93*, 4897.
- (115) Mukhopadhyay, S.; Ramasesha, S. *J. Chem. Phys.* **2009**, *131*, 074111.
- (116) Hager, M. W.; Gorman, C. B.; Goodson, T. *J. Phys. Chem. B* **2004**, *108*, 8543.
- (117) Devadoss, C.; Bharathi, P.; Moore, J. S. *J. Am. Chem. Soc.* **1996**, *118*, 9635.
- (118) Varnavski, O. P.; Ostrowski, J. C.; Sukhomlinova, L.; Twieg, R. J.; Bazan, G. C.; Goodson, T. *J. Am. Chem. Soc.* **2002**, *124*, 1736.
- (119) Peng, Z.; Pan, Y.; Xu, B.; Zhang, J. *J. Am. Chem. Soc.* **2000**, *122*, 6619.
- (120) Poliakov, E. Y.; Chernyak, V.; Tretiak, S.; Mukamel, S. *J. Chem. Phys.* **1999**, *110*, 8161.
- (121) Thompson, A. L.; Bharathi, P.; Muller, A.; Bardeen, C. J. *J. Phys. Chem. B* **2006**, *110*, 19810.
- (122) Godt, A.; Franzen, C.; Veit, S.; Enkelmann, V.; Pannier, M.; Jeschke, G. *J. Org. Chem.* **2000**, *65*, 7575.
- (123) Moore, J. S.; Xu, Z. *Macromolecules* **1991**, *24*, 5893.
- (124) Woo, H. Y.; Liu, B.; Kohler, B.; Korystov, D.; Mikhailovsky, A.; Bazan, G. C. *J. Am. Chem. Soc.* **2005**, *127*, 14721.
- (125) Lakowicz, J. R. *Principles of Fluorescence Spectroscopy*, 2nd ed.; Kluwer Academic/Plenum Publishers, 1999.
- (126) Choi, S. H.; Frisbie, C. D. *J. Am. Chem. Soc.* **2010**, *132*, 16191.
- (127) Huang, C.; Zhen, C.-G.; Su, S. P.; Loh, K. P.; Chen, Z.-K. *Org. Lett.* **2005**, *7*, 391.
- (128) Murat, M.; Grest, G. S. *Macromolecules* **1996**, *29*, 1278.
- (129) Welch, P.; Muthukumar, M. *Macromolecules* **1998**, *31*, 5892.

BIOGRAPHICAL SKETCH

Seoung Ho Lee was born in Seoul, Korea in 1976, and completed his undergraduate studies at Konyang University in Nonsan. He received his bachelor's degree with honors in 2002. Lee continued his graduate studies at the same university under the supervision of Dr. Jong Seung Kim, where he studied *Host-Guest Chemistry*. He also received the Best Poster Presentation Award in 2004 Fall Meeting of Korean Chemical Society. During his graduate studies, in 2002 he had a research experience as an exchange student at the University of Louis Pasteur de Strasbourg, France under the supervision of Dr. Jacques Vicens. After he received an M.S. degree with honors in 2004, he moved to the Dankook University in Seoul and continued training as a research associate. In 2005, he started his Ph. D. studies at the University of Florida. In the past five years, he carried out the research in the topic of *Photoactive Conjugated Polyelectrolytes and Conjugated Polyelectrolyte Dendrimers* under the supervision of Dr. Kirk S. Schanze. During the Ph. D. degree, he got married with Sangmi Lee in 2006 and had the first son, Junseo Lee, in the summer of 2009. In 2011, Seoung Ho will join the group of Dr. Eric T. Kool as a postdoctoral associate at Stanford University.